

Open access
virtual testing protocols
for enhanced
road user safety

Virtual Testing, Occupant Protection in Future Vehicles

WP number: 3

Deliverable: D3.2





Virtual Testing, Occupant Protection in Future Vehicles

Work package 3, Deliverable D3.2

Please refer to this report as follows:

Jakobsson, L. Putra, I.P.A., Levallois, I., Keller, A., Johansen, T., Salters, E., Genzel, J., Leledakis, A., Svensson, M.Y., Recko, P., Muser, M., Högberg, L., Wenäll, J., El-Mobader, S., Iraeus, J., Kovalik, M., Tummler, L., Linder, A., Wågström, L., John, J. (2022) Virtual Testing, Occupant Protection in Future Vehicles, Deliverable D3.2 of the H2020 project VIRTUAL.

Project details:

Project start date:	01/06/2018
Duration:	54 months
Project name:	Open access virtual testing protocols for enhanced road user safety - VIRTUAL

Coordinator:	Astrid Linder, Prof, Traffic Safety Swedish National Road and Transport Research Institute (VTI) Regnbågsgatan 1, 417 55 Lindholmen, Göteborg, Sweden
--------------	---



This project has received funding from the European Union Horizon 2020 Research and Innovation Programme under Grant Agreement No. 768960.

Deliverable details:

Version:	Final
Dissemination level:	PU (Public)
Due date:	30/10/2022
Submission date:	24/10/2022
Online location:	https://secure.webforum.com/atvirtual/doc?dfrefid=37702321

Lead contractor for this deliverable:

Lotta Jakobsson, Volvo Cars

Report Author(s):

Jakobsson, L., Leledakis, A., El-Mobader, S., Wågström, L. (Volvo Cars), Sweden
Putra, I.P.A., Svensson, M.Y., Iraeus, J., John, J. (Chalmers University of Technology), Sweden
Levallois, I., Recko, P., Kowalik, M. (Faurecia), France and Poland
Keller, A., Muser, M., Tummler, L. (AGU), Switzerland
Johansen, T., Högberg, L. (DYNAmore Nordic), Sweden
Salters E. (Dorel), Netherlands
Genzel, J., Wenäll J., Linder, A. (VTI), Sweden



Legal Disclaimer

All information in this document is provided "as is" and no guarantee or warranty is given that the information is fit for any particular purpose. The user, therefore, uses the information at its sole risk and liability. For the avoidance of all doubts, the European Commission and INEA has no liability in respect of this document, which is merely representing the authors' view.

© 2018 by VIRTUAL Consortium

Revision history

Date	Version	Reviewer	Description
2022-03-28	Preliminary draft 1	Rune Elvik	Review
2022-05-09	Draft report	Elisabet Agar	Language review
2022-10-24	Final deliverable	Astrid Linder – VTI → EC	



Table of contents

Executive summary	2
1 Introduction	3
1.1 Outlook	3
1.2 Objectives	4
1.3 Outline and Responsibilities	4
2 The Virtual Testing Protocol	5
2.1 OS Occupant and Seat Models	5
2.1.1 The VIVA+ Adult Occupant Models.....	5
2.1.2 The PIPER HBM	6
2.1.3 VIRTUAL OS Vehicle Seat Model.....	7
2.1.4 VIRTUAL OS Chalmers Lab Seat Model	8
2.1.5 VIRTUAL OS Booster Seat Model	9
2.2 Other Models developed within the Project	9
2.2.1 Faurecia Concept Seat Models.....	10
3 The Adult Occupant Protection case	11
3.1 Demonstration of VT protocol for Rear-End Impact	11
3.1.1 Validation Tests using the Seat Evaluation Tools	12
3.1.2 Sled Test Series with the Seat Evaluation Tools.....	13
3.1.3 Simulation Series.....	17
3.2 Simulation Series investigating Novel Seating	21
3.2.1 Rear-End Impacts	21
3.2.2 Frontal and Side Impacts	25
4 The Child Occupant Protection Case	30
4.1.1 HIII6y in a Rearward-Facing Vehicle Seat; Sled Tests and Simulations	31
4.1.2 PIPER HBM in Forward-Facing Concept Vehicle Seat Models	38
4.1.3 PIPER HBM in a Forward-Facing Production Vehicle Seat Model	45
4.1.4 Discussion and Conclusion	47
5 Discussion	49
6 Conclusion	51
References	52
Appendix A VIRTUAL OS Vehicle Seat Model	54
Appendix B VIRTUAL OS Booster Seat Model	73
Appendix C Faurecia Concept Seat Models	78
Appendix D Sled Test Series with the Seat Evaluation Tools	87
Appendix E VIVA+ 50F in Chalmers Lab Seat, Rear-End Impacts	109



Appendix F	Input to CBT - Whiplash Accident Reconstruction Simulations.....	117
Appendix G	Novel Seats and Seated Positions in Rear-End Impact.....	131
Appendix H	Rearward-Facing VIVA+ 50F in Vehicle Interior Environment.....	182
Appendix I	Forward-Facing VIVA+ 50M and 50F Simulations in a Variety of Seated Positions, Frontal and Side Impacts.....	187
Appendix J	HIII6y in a Rearward-Facing Vehicle Seat	200
Appendix K	PIPER HBM in Forward-Facing Concept Vehicle Seat Models.....	209



Acronyms and Terms

Abbreviation	Description
AD	Automated Driving
ALP	Aldman Pressure – A whiplash injury criterion developed in VIRTUAL
ATD	Anthropomorphic Test Device, i.e., a crash test dummy
Booster	A belt-positioning child restraint system for child occupant protection. Booster is the collective term of booster seat (with backrest) and booster cushion (without backrest)
CAD	Computer Aided Design
CAE	Computer Aided Engineering
CBT	Cost-Benefit Tool
CoF	Centre of Gravity
CRS	Child Restraint System
DoF	Degree of Freedom
ECE14	UN ECE regulation No. 14
ECE129	UN ECE regulation No. R129
FE	Finite Element
HIII6y	A 6-year-old sized crash test dummy (ATD), from the Hybrid III-series of ATDs
HBM	Human Body Model
IDS	Injury Detection System – a VIRTUAL term
IP	Instrument Panel
ISOFIX	Standardised in-vehicle child restraint anchorages with corresponding attachments on child seats
NIC	Neck Injury Criterion
SET	Seat Evaluation Tool; SET 50F (mid-sized female) and SET 50M (mid-sized male), v0.1
Q6	A 6-year-old sized crash test dummy (ATD), from the Q-series of ATDs
OR	Overall Ratings
OS	Open-Source
V1, V2, V3	Variant 1, 2 and 3 of the Faurecia Concept Seat Models
VT	Virtual Testing
VRU	Vulnerable Road User
WAD	Whiplash Associated Disorder
WP3	Work Package 3 (within the VIRTUAL project)



Executive summary

The overall objective of the VIRTUAL project is to define and demonstrate a virtual testing (VT) protocol targeting enhanced safety assessment by enabling real-world variability. This encompasses demonstration of the tool chain as such, as well as demonstration of the components of the VT protocol, by simulations using different types of simulation models. Another major objective is the development of a cost-benefit tool (CBT), enabling evaluation of different conceptual design proposals. The purpose of the VIRTUAL D3.2 report is to present and summarise the work on the VT protocol for passenger car occupants in some potential future integrated impact scenarios and novel seated positions. The VT protocol for passenger car occupants includes both adult and child occupant protection cases.

For the adult occupant protection case, the specific objectives include demonstration of the whole tool chain for rear-end impacts, demonstration of the VT protocol for novel seated positions and providing input data for the CBT. Eight sub-studies in this report address these objectives: two physical test series and six simulation series. Half of the simulation sub-studies investigated the influence of variations in seat adjustments, novel seats and seated positions when exposed to rear-end impacts. Using vehicle interior models of a front passenger seat environment, the other half explored the influence of seat position and occupant anthropometry when exposed to certain different frontal and side impact configurations. One of the sub-studies also delivered input to the CBT by providing injury risk reduction calculations for a potential countermeasure for whiplash injuries in rear-end impacts.

For the child occupant protection case, three sub-studies were performed with models representing 6-year-olds exposed to frontal impacts. Two of the sub-studies showed that the kinematics and responses of the PIPER human body model (HBM) were influenced by several parameters, such as vehicle seat adjustments, booster design and seatbelt routing when forward-facing. This emphasises that seat design as well as the seatbelt position and routing are essential design parameters for child occupant protection in current and novel seated positions. In a reverse seat position, the importance of the booster seat and vehicle seat interaction was highlighted, using a crash test dummy (ATD) the size of a 6-year-old. In that situation, the headrest of the booster seat also served as a head-restraint in a crash situation, which it was not primarily developed for. This is one of the examples of 'misfit' situations that were evaluated as part of the study. Other 'misfit' situations include deviations from the nominal vehicle seat position in relation to the seatbelt, which are likely to become more common in novel seated positions.

The VT protocol includes the possibility of employing virtual simulation test setups to study a range of parameter variations. Hence, several models were developed within the project and are available as part of the VIRTUAL project. This report includes the development of several seat models, two of which represent vehicle seats (the VIRTUAL open source (OS) Vehicle seat model and the VIRTUAL OS Chalmers lab seat model), as well as one booster seat model (the VIRTUAL OS Booster seat model). They are openly available and can be downloaded from the OpenVT platform developed within the VIRTUAL project, <https://openvt.eu/>. In addition, three concept seat models were developed and used in two of the simulation sub-studies.



1 Introduction

The VIRTUAL project aims to create a safer road transport system by providing improved ready-to-use safety assessment tools. The open source (OS) strategy of this project is a key to ensuring high market penetration of the tools provided. However, first and foremost, VIRTUAL is meant to make a sustainable impact. Therefore, the OpenVT platform featuring results of VIRTUAL, will be continuously available after the project has ended, providing procedures and open access tools to assess the benefit of novel safety systems.

One of the major objectives of the VIRTUAL project is to define and demonstrate the general workflow of a virtual testing (VT) protocol that starts with a physical test, working as a reference for validation of the virtual simulation environment. The virtual simulation setup is then compared to the physical test setup by replicating the physical test conditions. The virtual simulation test setup can then be employed to study a range of parameter variations. This will enable a more robust assessment, taking into account the real-world variability. Another objective is the development of a cost-benefit tool (CBT), enabling the evaluation of different conceptual design proposals.

Three parts of the road transport system are included in VIRTUAL: seated occupants of passenger cars, standing passengers on public transport and protection of vulnerable road users (VRUs) in conflict situations such as car-to-pedestrian, car-to-cyclist and tram-to-pedestrian impacts. Seated occupants in passenger cars include the adult occupant protection case and the child occupant protection case. This report summarises the part on seated passenger car occupants, focusing on the demonstration of the VT protocol, as part of the research of Work Package 3 (WP3) of the VIRTUAL project.

1.1 Outlook

Vehicle safety will remain an important issue for personal mobility in the foreseeable future. The increased degree of automation, including emergence of automated driving (AD), are likely to change the characteristics of crashes compared to prevailing circumstances. In addition, AD opens up new possibilities for in-car activities which may influence the way seats are arranged and positioned.

The VIRTUAL D3.1. report, 'Impact scenarios and pre-crash seated postures for automated driving' summarises the prior work in WP3, by defining the framework for design of crashworthiness in future passenger vehicles (Wågström et al., 2020). It includes a review of the regulations regarding automotive seats and studies on predicted potential future crash scenarios and seated positions. It was stated that current regulations pose challenges and that they may need refining in order to reflect future seated positions and to support occupant protection in crashes (Linder and Svedberg, 2019). Examples include that in the ECE regulations, the average-sized male ATDs represent the whole adult population, while the average-sized female is not considered at all. Using real-world data and active safety simulations in four conflict situations, the VIRTUAL D3.1. report identified that the number of accidents avoided was higher when applying a collision avoidance function. User studies were performed to identify seated positions for further investigation, including 'forward-facing in relaxed seat position', 'face-to-face in upright seat position', 'face-to-face in relaxed seat position', 'inboard swivelled front seats in upright seat position' and 'parallel swivelled seats in face-to-face upright seat position'. Certain positions will be further investigated in this report.



1.2 Objectives

The overall objective of the VIRTUAL project is to define and demonstrate VT protocols targeting enhanced safety assessment by enabling real-world variability. This encompasses demonstration of the tool chain as such, as well as demonstration of the components of the VT protocol, such as simulations using different types of simulation models. Another overall objective is the development of a CBT, enabling the evaluation of different conceptual design proposals.

The purpose of this report, VIRTUAL D3.2, is to summarise the work on the VT protocol for passenger car occupants, including adult as well as child occupants, in a number of potential future integrated impact scenarios and novel seated positions. This includes the OS seat models developed within the project, which are available on the OpenVT platform, in line with the open access strategy of and developed within VIRTUAL.

For the VT adult occupant protection case, the specific objectives include demonstrating the whole tool chain for rear-end impacts, also including physical tests, in addition to demonstrating the VT protocol for novel seated positions, for a variety of impact directions and seat variations using simulations. Another objective is providing input data for the CBT.

For the VT child occupant protection case, the specific objectives include demonstration of the VT protocol for variations in current and novel seating, such as adjustments of seat orientation and restraints, for one size of child occupant in frontal impacts, using simulations and sled tests.

1.3 Outline and Responsibilities

Following the short introduction, a brief reference to prior work in WP3 and the context of the VT protocol, including the models developed, a short summary of each sub-study addressing the VT protocol are presented. The eight sub-studies, involving physical as well as virtual testing, are structured in two main chapters of the adult and child occupant protection case, respectively. The adult occupant protection case includes demonstration of the VT chain for rear-end impact and simulations investigating novel seated positions in rear-end and frontal impacts, while all the sub-studies for the child occupant case consider frontal impacts. A short discussion follows the summaries, whereafter Appendices are included for the sub-studies requiring more in-depth information, in addition to the activities on the seat model developments.

The work presented in this report is a collaborative task between several VIRTUAL beneficiaries.

The development of the OS vehicle seat models and the OS Booster seat model is part of WP3, while the occupant tools, such as the VIVA+ models, were developed in WP2. The development and validation of the VIRTUAL OS Vehicle seat model was done by Faurecia (scanning of physical seat), Volvo (meshing), VTI (physical component tests for validation) and AGU (virtual tests for validation). The VIRTUAL OS Chalmers lab seat model was developed by Chalmers and VTI. The VIRTUAL OS Booster seat model was developed by Dorel France (CAD models and physical test) and Chalmers (meshing and validation). Volvo Cars provided the booster cushion model. The three Concept Seat Models were developed by Faurecia.

Tests and simulations to demonstrate the adult occupant protection case included contributions by Chalmers, VTI, Volvo Cars and Faurecia. The sled test series in Chapter 3.1.1 was planned and analysed by VTI and Chalmers and executed at VTI's crash test facility in Linköping, Sweden. The sled test series in Chapter 3.1.2 was planned and analysed by Volvo Cars and executed at Volvo Cars Safety Centre in Gothenburg, Sweden. VTI developed and provided the Seat Evaluation Tools (SET) and acquired the



Toyota seats, while Chalmers supported with the Chalmers Lab seat and Volvo Cars with the Volvo seats. The rear-end impact simulation series in Chapters 3.1.3.1. and 3.1.3.2. were executed by Chalmers and supported by TU Graz. Faurecia contributed with the rear-end impact simulation series in Chapter 3.2.1 on 'Novel seats and seated positions'. The three simulation-series in Chapters 3.2.2 on seat position and occupant variations exposed to frontal and side impacts were run by Volvo Cars, with PhD supervision support from Chalmers.

The child occupant protection case was a collaborative task between AGU, Dorel, DYNAMore, Faurecia, Volvo Cars and VTI. Several WP3 beneficiaries collaborated in the rearward-facing sub-study in Chapter 4.1.1. VTI executed the sled test series at VTI's crash test facility in Linköping, Sweden. The vehicle seats were acquired from used cars of production vehicles and procured by VTI. The booster seats were provided by Dorel. Volvo Cars contributed with the HIII6y ATD. The corresponding simulation series was executed by DYNAMore, using the VIRTUAL OS Vehicle seat model and the VIRTUAL OS Booster seat model. AGU supported with analysis of the correlation between the physical sled test and the corresponding simulations. The forward-facing simulation study using PIPER in concept vehicle seat models was executed by Faurecia (Chapter 4.1.2). The forward-facing simulation study using PIPER in a production vehicle seat model was executed by Volvo Cars (Chapter 4.1.3).

The report was structured by Lotta Jakobsson, Volvo Cars.

2 The Virtual Testing Protocol

The VT protocol enables virtual simulation test setups to be employed to study a range of parameter variations. This will allow for a more robust assessment taking the real-world variability into account. Hence, the VIRTUAL project includes development of new models and making them available open source to a wider community of users. The models can be downloaded from the OpenVT platform at: <https://openvt.eu/>

Several occupant and seat models were used throughout this study. The OS models are further described in this chapter, as well as the three concept seat models developed and used by Faurecia as part of the project. Other models used are presented in their respective sub-study.

2.1 OS Occupant and Seat Models

In order to be able to set up generic simulations of seated vehicle occupants and to demonstrate virtual testing procedures, implementing OS Finite Element (FE) occupant models and generic seat models represented a vital part of the VIRTUAL project. Two VIRTUAL OS adult occupant models, VIVA+ 50F and VIVA+ 50M, were developed. In addition, an OS child occupant model, PIPER, developed in the prior EU project PIPER, was adapted for the purposes of the project. Two OS vehicle seat models; the VIRTUAL OS Vehicle seat model and the VIRTUAL OS Chalmers lab seat model, were developed within the project, in addition to the VIRTUAL OS Booster seat model. The occupant models were developed in WP2 and will hence only be briefly presented in this chapter, while the VIRTUAL OS seat and booster seat models will be presented in more detail as they are part of WP3.

2.1.1 The VIVA+ Adult Occupant Models

The VIVA+ OS HBMs were developed in WP2 and the seated versions have been reported in D2.2 (John et al., 2021). Figure 2-1 shows the two seated versions of the VIVA+ HBM representing an average sized female (VIVA+ 50F) and an average sized male (VIVA+ 50M). The VIVA+ 50F was used as the

base model. All model development and updates were first implemented in the base model. At given release stages the 50F version was morphed into the 50M, in addition to the different VRU versions.

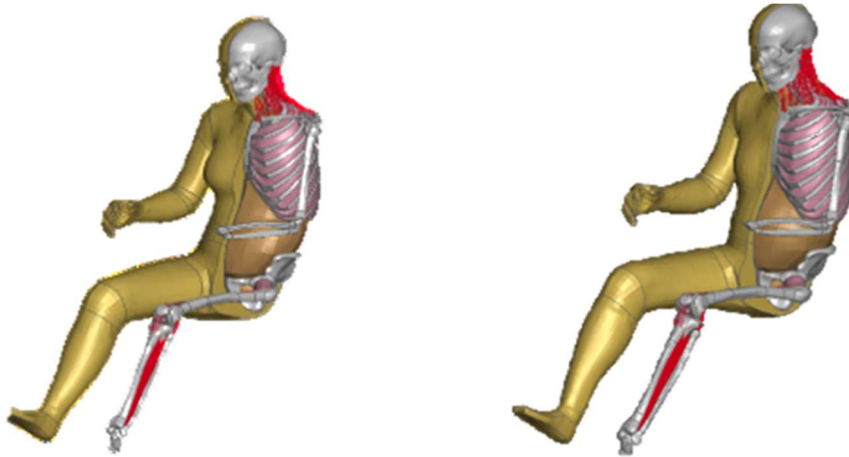


Figure 2-1 VIVA+ 50F (left) and VIVA+ 50M (right)

2.1.2 The PIPER HBM

The PIPER HBM, shown in Figure 2-2, was developed within the EU project PIPER (<http://www.piper-project.org/>) and published in, Beillas et al. (2016) and Giordano et al. (2017), amongst others. The PIPER represents a 6-year-old child occupant.



Figure 2-2 The PIPER HBM

During the VIRTUAL project, Faurecia detected that the spine of the PIPER was not modelled symmetrically, and that the spine behaved differently under moments around the +x versus the -x axis and also around +z and -z axis. This observation was communicated to the PIPER research group for further clarification. The PIPER research group confirmed these issues and rectified them in the PIPER HBM in the beginning of year 2021. The corrected model is available at https://gitlab.com/piper-project.org/child/-/tree/Lspine_update. As the simulation part by Faurecia for the child occupant protection case was almost finalised at the time of the PIPER model update, the new PIPER model was not integrated in the Faurecia study in Chapter 4.1.2.

2.1.3 VIRTUAL OS Vehicle Seat Model

The VIRTUAL OS Vehicle seat model replicates a Toyota Auris driver seat (model year 2010 – 2012), a few of which were acquired from scrap yards and scanned in order to produce CAD data. The VIRTUAL OS Vehicle seat model is shown in Figure 2-3 The VIRTUAL OS Vehicle seat model, including impact locations (a-e) in the validation study Figure 2-3 . The development and validation of the model is described in Appendix A, and a summary is provided in this sub-chapter. The model is available on the VIRTUAL OpenVT platform at <https://openvt.eu/fem/open-access-adult-seat-model>.

As a first validation of the seat model, a series of physical impactor tests were carried out, with four different impactors of masses ranging from 2.8 kg to 22.8 kg. The seat was impacted at five different locations (indicated in Figure 2-3) at impact speeds from 2.21 m/s to 5.42 m/s. In total, 17 test configurations of impactors and impact positions were repeated three times and at three different speeds, resulting in a total of 153 tests. During the impactor tests, the seat was mounted on a custom-made steel plate ('mousetrap'), which could be positioned and tilted relative to the direction of travel of the impactor in order to hit defined locations on the seat (Figure 2-4).



Figure 2-3 The VIRTUAL OS Vehicle seat model, including impact locations (a-e) in the validation study



Figure 2-4 Pendulum test setup for test with Impactor 3. The seat is attached to the 'mousetrap'

The experimental setup was subsequently replicated in a virtual environment, including a model of the mousetrap and rigid body models of the various impactors.

Impactor acceleration was compared for each experimental test to the corresponding numerical test, and overall ratings (OR) were computed according to ISO18571. Mean OR for each configuration and test series were calculated. A mean overall rating of 0.73 was obtained including all impactors, while ranging 0.69-0.89 on average OR per impact location. Impactor 5 was excluded from this analysis due to the fact that this relatively heavy impactor caused displacement of the 'mousetrap', thereby

introducing significant measurement errors. An example of the comparison for Impactor 1 to impact Point B (drop test to seat cushion) at an impact speed of 2.21 m/s is shown in Figure 2-5. Please refer to Appendix A for the other comparisons and rating calculations.

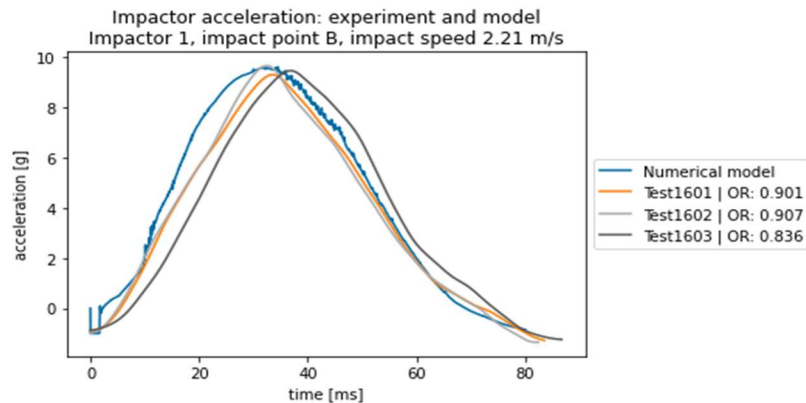


Figure 2-5 Comparison of the numerical model with the physical tests, an example.

Overall, the VIRTUAL OS Vehicle seat model in its current state provides a fairly realistic replication of the corresponding Toyota Auris seat. As the first high-resolution seat model available open access, it closes an important gap in VIRTUAL’s open access tool chain for VT in vehicle safety.

2.1.4 VIRTUAL OS Chalmers Lab Seat Model

The VIRTUAL OS Chalmers lab seat model replicates a generic car seat developed by Chalmers during the 1990s which has been used in several volunteer tests since, such as presented in Carlsson et al. (2011). Originally, the physical seat was based on the characteristics of a Volvo 850 seat, simplified to enable tracking of volunteer kinematics for ATD development, specifically the rear-end impact ATD, BioRID (Davidsson et al., 1998).

Figure 2-6 shows the model and its physical counterpart. VIRTUAL’s FE model of the lab seat was developed and validated as part of the project. The validation includes component tests, in addition to sled tests using BioRID. The model and its validation are further described in Genzel et al. (2022). The model is available on the VIRTUAL OpenVT platform: <https://openvt.eu/fem/open-access-laboratory-seat-model>.

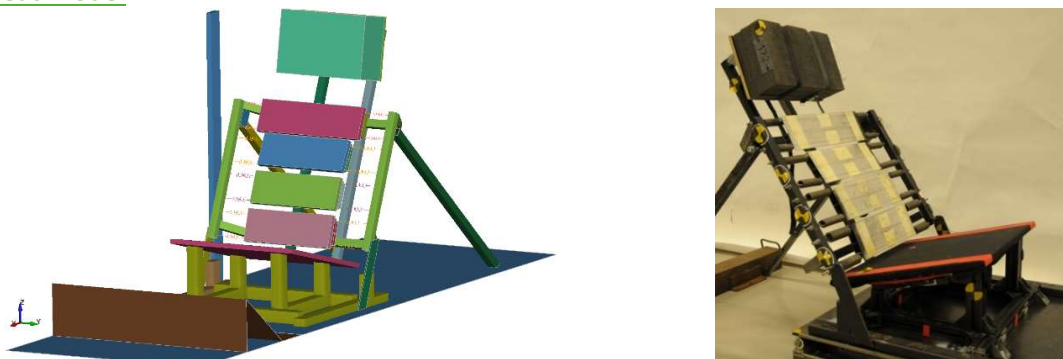


Figure 2-6 OS Chalmers lab seat model (left) developed within the VIRTUAL project and the corresponding physical seat (right)

2.1.5 VIRTUAL OS Booster Seat Model

As part of WP3, an open source child restraint system (CRS) appropriate for use with the PIPER HBM was developed and made available at the VIRTUAL OpenVT platform. Specifically, the aim was to develop a FE model of a representative booster seat.

The VIRTUAL OS Booster seat model (Figure 2-7) was based on the booster seat RodiFix Air Protect (Figure 2-8), a Dorel product sold under the brands Béb e confort and Maxi Cosi. The seat is compliant with the UN ECE R44/04 regulation, Group 2/3 (children 15-36kg, 4-10 years old). The seat is adjustable in two recline positions, the headrest is height adjustable, and the seat can be used with and without attachment to the vehicle ISOFIX anchorages.



Figure 2-7 OS booster seat model developed within the VIRTUAL project



Figure 2-8 The booster seat RodiFix Air Protect on which the OS booster seat model is based on.

The validation included comparison of the numerical and physical tests using the Q6 ATD in the booster seat exposed to the UN ECE R129 (ECE129) frontal impact test configuration. The booster seat was attached to the ISOFIX anchorages in the rig and the Q6 was restrained, together with the booster, using the seatbelt (Figure 2-9). The FE model of the ECE129 sled and the child seat showed a close match to the physical test.

The VIRTUAL OS Booster seat model is available on the VIRTUAL OpenVT platform. The model and the validation is further described in Appendix B.

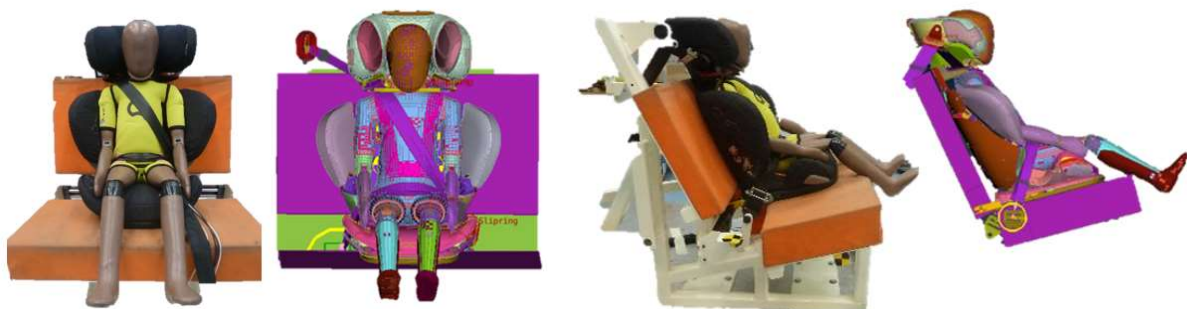


Figure 2-9. Front and side views of the validation test setup. ECER129 test bench, the booster seat and a Q6 ATD; physical and numerical.

2.2 Other Models developed within the Project

In addition to the VIRTUAL OS models, available at the VIRTUAL OpenVT platform, three concept seat models were developed to be used within the project, addressing novel seating and restraint principles.

2.2.1 Faurecia Concept Seat Models

The Faurecia concept seat models have been designed such that they can be adjusted into possible novel seating positions in future AD cars. Variant 1 (V1) is a standard seat design. Variant 2 (V2) is the same seat as Variant 1 but has a belt-guide on the top outboard corner of the seatback to guide the shoulder belt. Variant 3 (V3) is a novel seat design with a split seatback and an integrated seatbelt, designed using a shoulder belt belt-guide and a belt retractor integrated under the seat cushion. The three seat models are shown in Figure 2-10 and are described in detail in Appendix C.

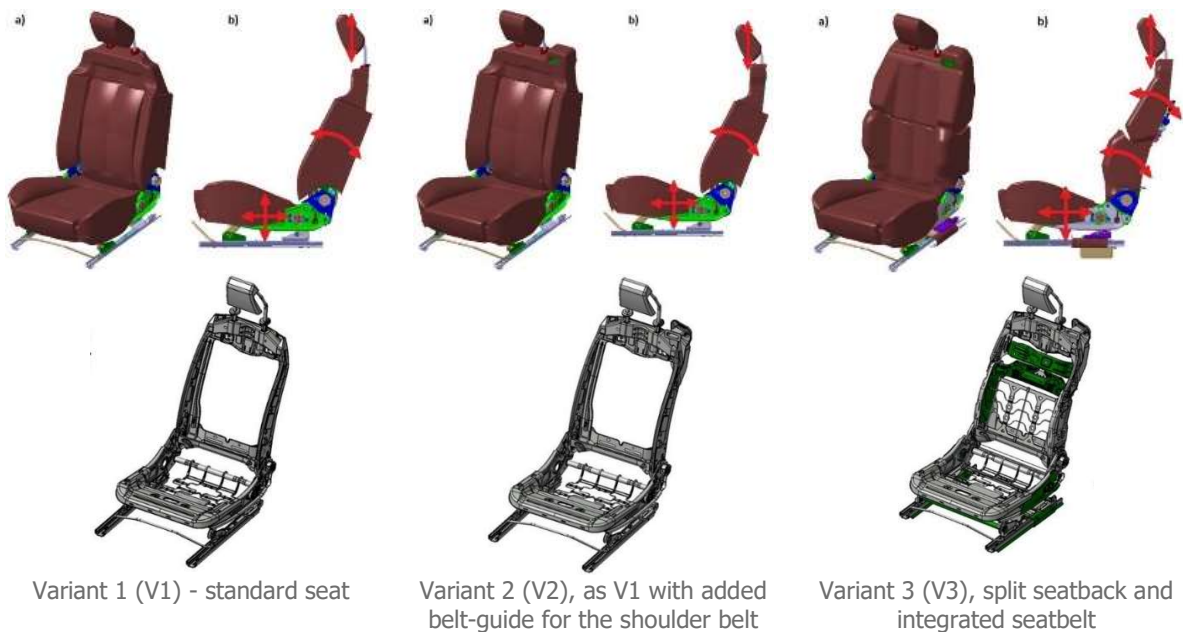


Figure 2-10. The three Faurecia concept seat models

All three concept seat models comply with the seatbelt anchorage strength tests of UN ECE R-14 Series 8. This loadcase is particularly difficult for seats with integrated seatbelts. Therefore, the V3 seat was reinforced to sustain the load. The concept seats include a passive head-restraint, which can be adjusted upward and downward, see Figure 2-11. This head-restraint contains interior Expanded Polypropylene (EPP) parts to provide sufficient support for the head of a 50th percentile female, as suggested by the ADSEAT EU project (Lemmen et al., 2013). The head-restraint form was oriented forward, as shown in Figure 2-11.



Figure 2-11. Head-restraint design with EPP insert (orange) and a forward oriented shape.

3 The Adult Occupant Protection case

This chapter serves the purpose of demonstrating relevant parts of the VT protocol applied to adult occupant protection in passenger cars, by investigating potential future seated positions and relevant impact scenarios.

Addressing one of the main goals of the VIRTUAL project, steps in the VT protocol are summarised to define and demonstrate the general workflow of such protocol. One of the sub-chapters focuses on demonstrating the VT protocol for rear-end impacts, using physical tests and virtual simulations. The other sub-chapter uses simulation studies to address the challenges of novel seating exposed to rear-end impacts, as well as a variety of frontal and side impacts.

In addition, addressing the development of the CBT, one of the sub-studies provides input for the adult car occupant application.

3.1 Demonstration of VT protocol for Rear-End Impact

The standardised rear-end impact test aims to evaluate the whiplash injury protection performance of the front seat (including head-restraint) of a given car model (EuroNCAP, 2019). The VT protocol targets enabling a more robust assessment, considering the real-world variability.

The first step of the workflow consists of a physical rear-end impact test. The setup is a sled test, where the car seat is mounted on the crash test sled, and a physical loading device (Seat Evaluation Tool – SET v0.1) representing the human body is placed on the seat. The SET is similar to an ATD, but it is developed and instrumented to recreate the load condition that the human body exerts on the seat during the impact. The test setup, including the SET and the seat, are instrumented to acquire test data that can be used to validate the response of a numerical FE seat model under the corresponding loading conditions.

In the second step of the workflow, the FE seat model is validated in an FE virtual simulation setup consisting of the seat model and an FE model representing the human body. This FE model of the human body will ideally interact with the seat-model in exactly the same way as the SET interacts with the physical car seat.

The third and final step of the workflow consists of a matrix of virtual tests (numerical simulations), where the validated seat model is tested in a range of different collision conditions. The simulation matrix may involve a range of impact speeds (ΔV) and varying acceleration time histories (acceleration pulses). It may also involve different impact directions and varying occupant properties including sex, age, body mass, seat adjustment, seating positions and sitting postures.

In the VIRTUAL project, the separate steps of this workflow are demonstrated in several isolated sub-studies to show the feasibility of each step. The compilation of the sub-studies then demonstrates the feasibility of a future seamless chain that will make up the entire VT protocol workflow. The sub-studies include one validation study of the SET, a sled test series using the SET and two simulation studies using the VIVA+ models to demonstrate the principle of the second and third steps of the workflow.

One of the simulation studies also generates output data according to the assessment protocol that can be fed into the CBT.

3.1.1 Validation Tests using the Seat Evaluation Tools

With the purpose to demonstrate a validation setup, sled tests were performed with the Seat Evaluation Tool (SET) and compared to results from corresponding volunteer tests.

The overall design and the evaluation of the SET is presented in Karemyr et al. (2022). Two SETs are available, the average-sized female (SET 50F) and the average-sized male (SET 50M), Figure 3-1. The SETs have the geometry of the seated male and female VIVA+ HBMs. The SETs were developed in VIRTUAL WP2, with the purpose of providing a physical loading tool for evaluation tests. The SETs are similar to a crash test dummy but are specifically developed and instrumented to recreate the load condition that the human body exerts on the seat during a low severity rear-end impact.



Figure 3-1 The SET 50F (left) and the SET 50M (right) seated in the Chalmers lab seat.

3.1.1.1 Methods

The SET 50F and 50M of SET v0.1 were tested in rear-end impact sled tests at Δv 7km/h in the Chalmers lab seat, a seat that was developed and used in a series of tests with volunteer. The test set-up was designed to reproduce the test conditions to those used in the volunteer tests (Linder et al., 2013), and the results of the SETs were compared to those volunteer responses. Figure 3-1 shows the SET 50F and 50M seated in the sled test set-up.

The aim of the SETs was to create an interaction with a vehicle front seat representative of that of a human. The SET 50F and 50M have the geometries of an average female and male (based on the humanshape.org data) of 50 years of age, which is also that of the VIVA+ 50F and 50M models and includes the equivalent mass and mass distribution. The sled tests were carried out to evaluate how well the SETs interacted with the seat in a rear impact.

3.1.1.2 Results

The results show an overall good resemblance in terms of the rearward horizontal displacement, but lower maximum rearward angular motion of the SETs compared to the volunteers, see further details in Karemyr et al. (2022).

3.1.1.3 Discussions and Conclusions

The results demonstrate the output data provided by the SETs in a rear-end impact sled test set-up where a front passenger seat is mounted on a sled and exposed to an acceleration corresponding to a

rear-end impact. This output data could be used to validate FE-models of the seat. In addition, FE-model of the SETs could be created and used to finetune the properties of the detailed design of the SET 50F and 50M. The physical and virtual models of the SETs could be used as an interim step to bridge the gap between physical testing and virtual testing.

3.1.2 Sled Test Series with the Seat Evaluation Tools

With the purposes to demonstrate the whole tool chain of the VT protocol and to showcase the SET 50F and the SET 50M, a sled test series was run in crash pulses used for standardized whiplash assessment tests.

The specific objectives of the sled tests series were to:

- Compare trends for the SET 50F and 50M in the same seat, as a function of impact severity
- Investigate repeatability and sensitivity of the SET 50F and 50M for different types of seats

3.1.2.1 Methods

In total 19 sled tests were run at Volvo Cars Safety Centre in Gothenburg, Sweden. Three different seats were used; the Chalmers lab seat, a Toyota seat and a Volvo seat, see Figure 3-2. The Chalmers lab seat and the Toyota seat have corresponding VIRTUAL OS seat models (see Chapter 2.1).

Three rear-end impact crash pulses were used; referred to as the low, mid and high pulses, and shown in Appendix D. Mid and high pulses are part of the current EuroNCAP whiplash assessment protocol (EuroNCAP 2019), while the low pulse was part of a prior version of the protocol. See Appendix D for further details on the test setup, including instrumentation and positioning of the SETs and the test matrix. SETs v0.1 were used.



Figure 3-2 The three seats used in the study; Chalmers lab seat (left), Toyota seat (mid) and Volvo seat (right)

Seven different configurations were run with SET 50F, whereof five configurations also with SET 50M, see Table 3.1. The configurations with the Chalmers lab seat were excluded for SET 50M, due to risk for bottoming-out of the seat backrest. The tests in the mid pulse were repeated providing data for evaluation of repeatability.

Table 3.1. Configurations included in the sled test series

Configuration	Seat	Crash pulse	SET Model
C-L	Chalmers lab seat	Low	SET 50F
C-M	Chalmers lab seat	Mid	SET 50F
T-L	Toyota seat	Low	SET 50F and SET 50M
T-M	Toyota seat	Mid	SET 50F and SET 50M
T-H	Toyota seat	High	SET 50F and SET 50M
V-M	Volvo seat	Mid	SET 50F and SET 50M
V-H	Volvo seat	High	SET 50F and SET 50M

3.1.2.2 Results

The repeatability was overall good, providing support for the robustness of the SETs as well as a capable positioning procedure, see details in Appendix D. For SET 50F the head and pelvis acceleration correlated well for all three seats, while the T1 acceleration was influenced by fluctuations in the z-component when in the Chalmers lab seat and the Toyota seat. Differences in spine segment kinematics were seen, requiring more attention. For the SET 50M, only the tests with the Volvo seats could be used for evaluating repeatability. Similar repeatability as for SET 50F was seen.

Snapshots at 0ms, 40ms, 80ms, 120ms and 160ms for each configuration are shown in Figure 3-3, Figure 3-4 and Figure 3-5 for SET 50F. The similar Figures for the SET 50M, as well as kinematics Tables and Figures for both SETs (such as head to head-restraint contact times and X-Z displacements for head, T1 and pelvis) are presented in Appendix D. The linear x, z and resultant acceleration from the four sensors in SET (referred to as head, T1, L8 and pelvis) are plotted as complement to the kinematics and analysed with the purpose of trend comparison for the SET 50F and 50M in the same seat, as a function of crash pulse impact severity. Some results are provided here, while further results and discussions are provided in Appendix D.

The three seats exposed the SET 50F to different kinematics. The SETs were shown sensitive to the difference in seat model as well as crash severity. Although the head x-displacement relative to the sled was similar between the three seats (Figures D12-D14 in Appendix D), the kinematics and acceleration in the spine at head, T1, L1 and pelvis varied between the seats (Figures D17-D19 in Appendix D).

The shortest initial head to head-restraint distance as well as movement, in addition to the longest head to head-restraint contact time was seen in the Volvo seat, see Table D1 in Appendix D and Figure 3-3 for SET 50F. This seat provided the most balanced and supported interaction, which also resulted in the overall lowest acceleration, including similar level of resultant acceleration for the four sensors (Figures D19 and D21 in Appendix D, for the two SETs). The Chalmers lab seat provided the most unbalanced interaction with SET 50F (Figure 3-4), resulting in the highest and less synchronised acceleration (Figure D17 in Appendix D).

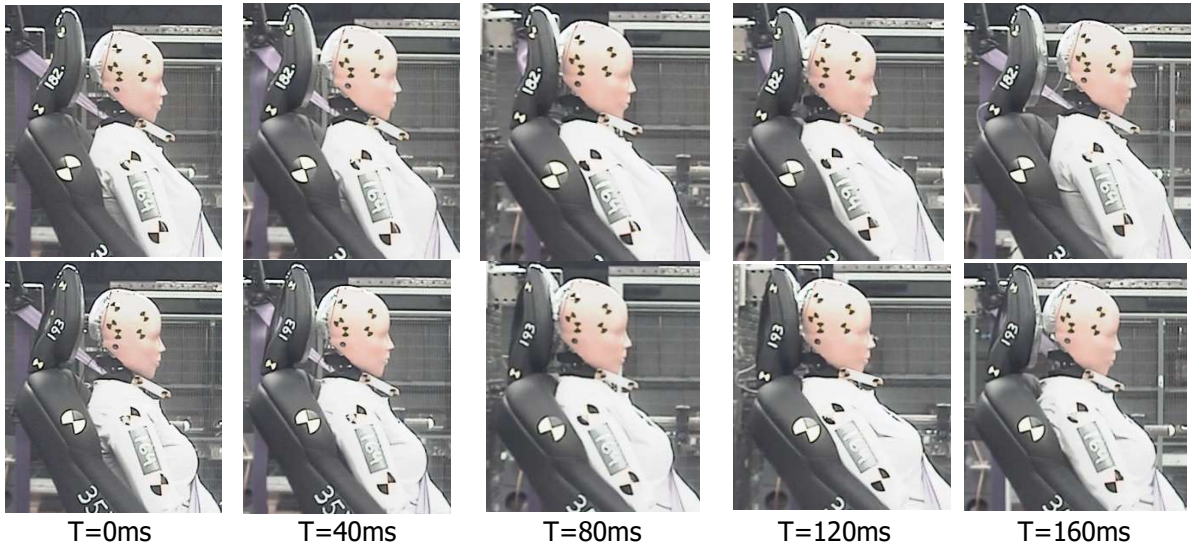


Figure 3-3 SET 50F in Volvo seat at mid (top) and high (bottom) crash pulses. Tests No. V3 and V4.

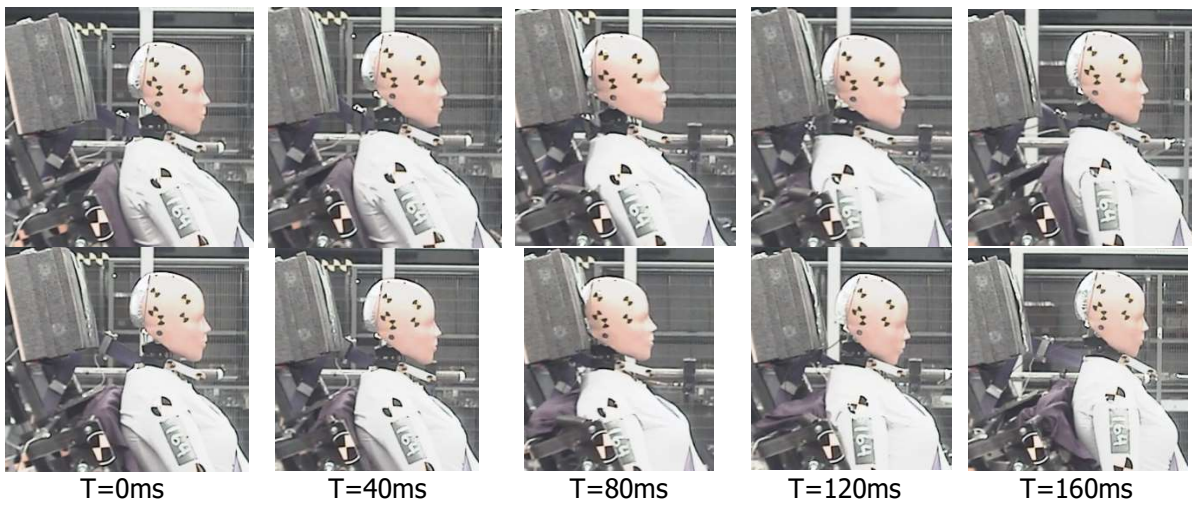


Figure 3-4 SET 50F in Chalmers lab seat at low (top) and mid (bottom) crash pulses. Tests No. C1 and C2.

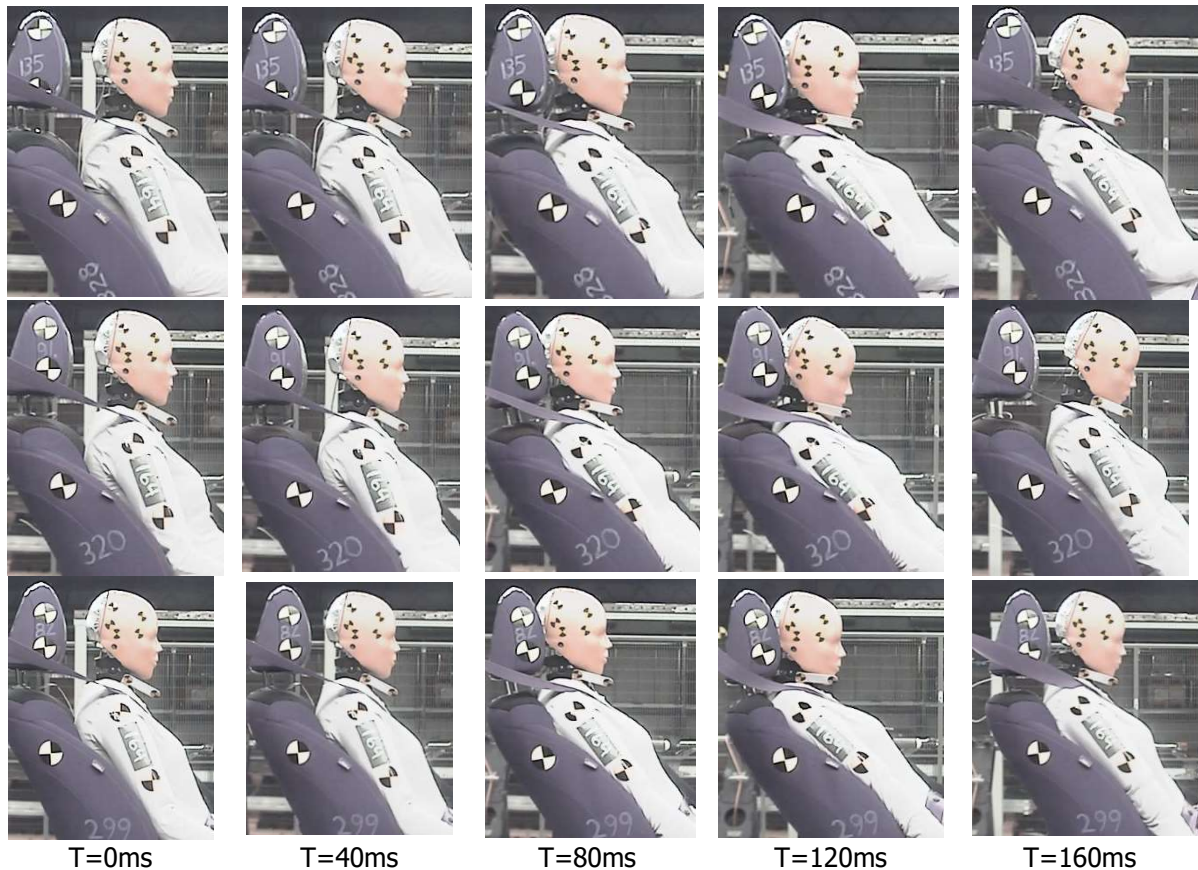


Figure 3-5 SET 50F in Toyota seat at low (top), mid (middle) and high (bottom) crash pulses. Tests No. T1, T2 and T4.

For the Volvo and Toyota seats, the x-displacements were longer with higher crash pulse. This was not seen to the same extent for the Chalmers lab seat (SET 50F only), for which the head and T1 x-displacements were of similar extent for the low and mid pulses (Figure D12 in Appendix D) which was not the case for the comparable tests with the Toyota seat (Figure D13 in Appendix D). This was likely due to the design of the Chalmers lab seat, with a fixed seatback frame and that the upper horizontal seat panel only can move to a certain extent, before stopped by a beam.

3.1.2.3 Discussions and Conclusions

A thorough discussion is provided in Appendix D. A short summary addressing the study objectives and the overall purpose is presented here.

The sled series comprising 19 tests was the first time the two SETs were exposed to the standardised rear-end impact crash pulses of ΔV 16 and 24 km/h. They were found durable and overall repeatable, and hence capable of being exposed to this level of crash severity. The main issues concerned the neck design, especially for the SET 50F. The SETs were sensitive to variations in seat design, and both showed comparable trends with respect to impact severity, within each seat model. A positioning procedure was successfully applied for all the tests. Further details are provided in Appendix D.

The overall purpose of the SETs within the VIRTUAL project is to serve as loading devices to help validate seat models as a part of the VT protocol, providing seat models to be used in virtual testing with an expanded set of configurations and occupant models. The current study did not aim to evaluate

the feasibility of the SETs for that purpose, mainly due to its early phase, lack of validation studies and limited measurement capabilities. Nevertheless, it provided some insights which could be of value for this purpose. Mainly, their robustness and repeatability are promising, so is their sensitivity of capturing differences in seat design and crash pulses. However, although not fully evaluated in the current study, the SETs' sensor data might not be enough to capture all seat parameters needed for seat model validation.

3.1.3 Simulation Series

Two simulation series were performed addressing the VT protocol in rear-end impacts using the VIRTUAL OS seats and the VIVA+ models. One of the studies also serves as input to the development of the CBT, including variations in head-restraint position as the countermeasure for occupant protection in rear-end impacts.

3.1.3.1 VIVA+ 50F in Chalmers Lab Seat Model

The objective of this sub-study was to carry out a first rear-end impact simulation series with the VIVA+ 50F and to demonstrate the simulation part of the rear-end impact VT protocol. The study is described in detail in Appendix E and a summary is provided in this chapter.

Methods

With the rationale to connect to the virtual tool chain, two simulations with the VIVA+ 50F were run using the Chalmers lab seat model in rear-end impacts at a deltaV of 5 km/h, representing the impact condition from published volunteer tests (Carlsson et al., 2011). Although representing the same seat as described in Chapter 2.1.4, the FE model used in this sub-study was an earlier version, similar to one used by Kleinbach (2019). The VIVA+ 50F was seated in a posture representative of female volunteers in the Chalmers lab seat, arms positioned as a passenger (see Figure 3-6). The parameter evaluated in the study was the head to head-restraint distance; 100mm and 150mm, respectively (Figure 3-7). The parameter was selected as a potential whiplash protection system with adaptive features that allow the protection to be adapted to the individual occupant.



Figure 3-6 Oblique view of the simulation setup with the Chalmers lab seat model and VIVA+ 50F. Only the right half of the VIVA+ 50F is visible.

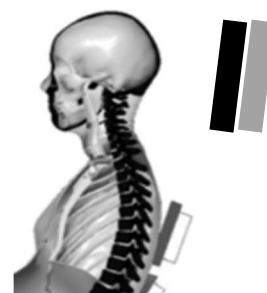


Figure 3-7 The two simulation setups, showing the two head to head-restraint distances of 100mm and 150mm.

A novel tissue-based injury criterion, called Aldman Pressure, was introduced for HBM application in this study. It addresses the same injury mechanism as does the neck injury criterion (NIC), namely nerve cell membrane dysfunction in the cervical dorsal root ganglia. The novel criterion and other parts of the methods are further described in Appendix E.

Results

Figure 3-8 shows the initial position and the position approximately at the maximal displacement (120ms) for the simulation with a head-restraint distance of 100mm.

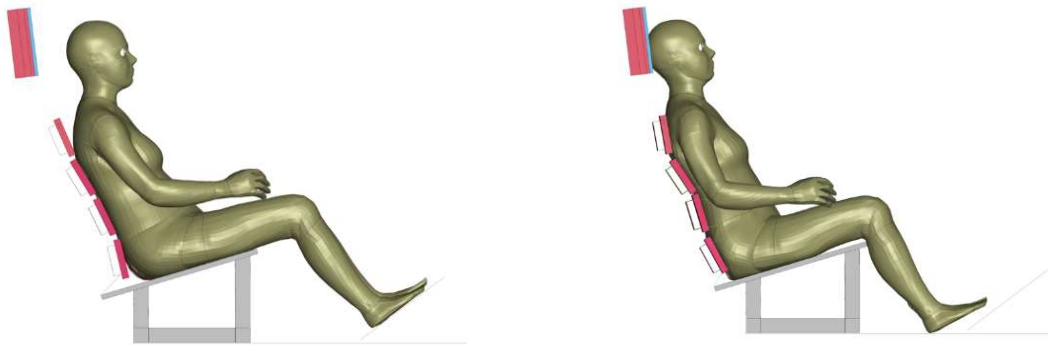


Figure 3-8 The simulation of the seat with head to head-restraint distance at 100mm, initially $t=0\text{ms}$ (left) and at $t=120\text{ms}$ (right)

When comparing the horizontal displacement of the head and T1 (see Appendix E), the maximum rearward T1 displacement is equal in the two simulations, however the rebound is faster at the shorter head to head-restraint distance. For the head, a longer horizontal displacement is seen for the larger head to head-restraint distance, leading to a later rebound. This is reflected by the head to T1 horizontal displacement in Figure 3-9 by the head horizontal velocity (Figure 3-10) and influences the NIC. The NIC_{max} resulted in 6.9 and 9.4, respectively, which correspond to an estimated risk of 0.139 and 0.144 when using the NIC risk calculation based on Ono et al. (2009). Details on the vertebral rotations and Aldman pressure calculation are summarised in Appendix E

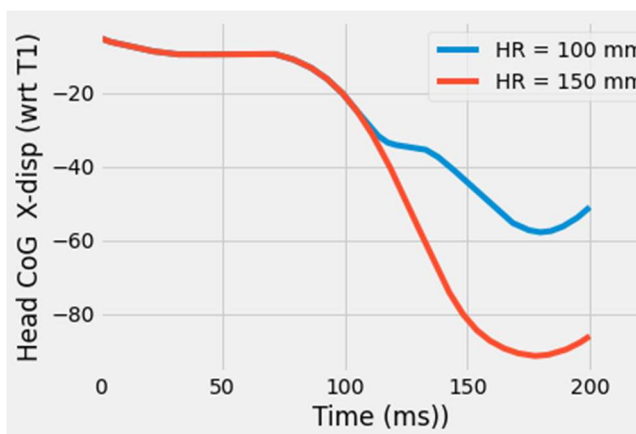


Figure 3-9 Head to T1 horizontal displacement

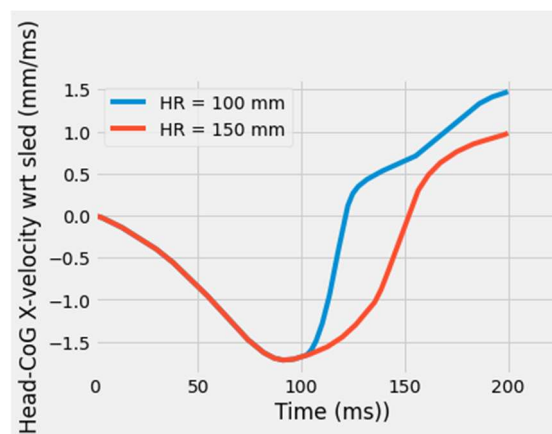


Figure 3-10 Head horizontal velocity

Discussion and Conclusion

This sub-study was carried out as a first rear-end impact simulation series to demonstrate the simulation part of the virtual rear-end impact test protocol within WP3. The study was limited to the VIVA+ 50F, only, since the VIVA+ 50M was not yet available at the time of this simulation series.

The seat model was a prior version of the current VIRTUAL OS Chalmers lab seat, which is made available as part of the project. The advantage of this well-defined seat design is that it has previously been used in published volunteer tests.

The results indicate that, for a front seat passenger exposed to a rear-end impact at $dV=5\text{km/h}$, a reduction in head to head-restraint distance from 150 mm to 100 mm lowered the estimated risk of Whiplash Associated Disorder (WAD) from 0.144 to 0.139. At the same time the peak vertebral angular displacement was lowered from 50° to 30° . This reduction in vertebral kinematics led to a reduction in the tissue-based injury criterion Aldman Pressure from a maximum magnitude of 1.5Pa to 0.7Pa. This is further discussed in Appendix E.

3.1.3.2 Input to CBT - Whiplash Accident Reconstruction Simulations

With the main purpose of providing input to the CBT, a set of simulations were conducted. Specifically, the objective of this sub-study was to evaluate the effects of different head to head-restraint distances on the WAD2+ injury risk, by conducting accident reconstruction simulations based on real-world accident data. See Appendix F for details on this sub-study.

Methods

The VIVA+ 50F and 50M were utilised to represent female and male occupants, used with the VIRTUAL OS Vehicle seat model. Real-world accident studies have shown that a shorter head to head-restraint distance is related to lower risk of sustaining whiplash injuries. Therefore, for the purpose of providing input for the CBT, two head to head-restraint distances were simulated, 120mm and 95mm (Figure 3-11). To reduce the head to head-restraint distance, the head-restraint of the seat was moved in the x-direction. In total, 24 simulations were run with six different crash pulses from real-world cases provided by the associated partner Folksam. The ΔV of the six pulses ranged between 9 and 16km/h, with resultant peak acceleration from 4.9g to 11.6g. See Appendix F for details on the crash pulses.

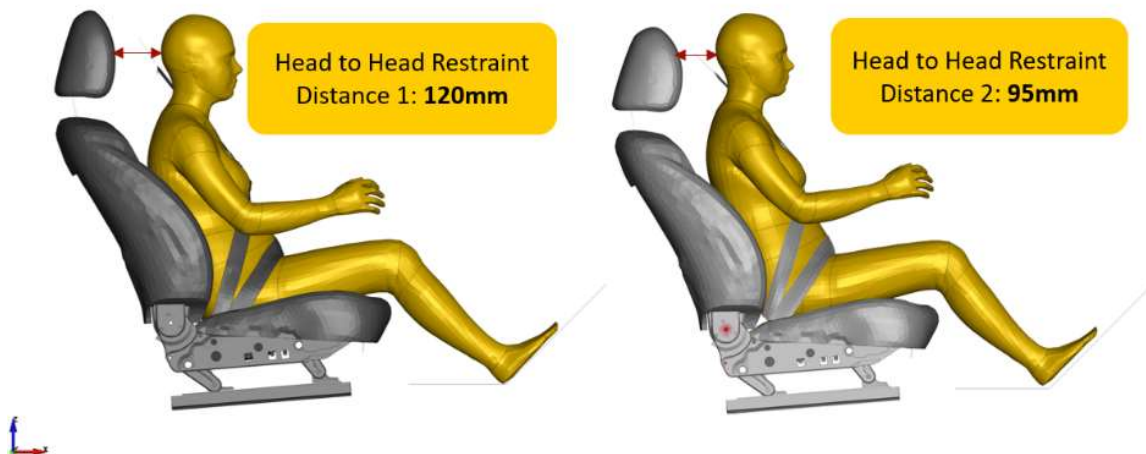


Figure 3-11 The two configurations showing the head to head-restraint distance of the VIVA+ 50F seated in the VIRTUAL OS Vehicle seat model with modification of the head-restraint.

Results

Lower NIC values were seen for both VIVA+ 50F and 50M, comparing the shorter head to head-restraint distance to the longer distance. Hence, NIC indicated a lower injury risk, in line with the real-world experiences of shorter head to head-restraint distance. Using the risk curve by Ono et al, (2009), the risk was reduced from 61% to 42% and from 60% to 39%, for 50F and 50M, respectively.



Discussion and Conclusion

This sub-study served dual purposes; to investigate the influence of the parameters head to head-restraint distance on WAD2+ injury risk in rear-end impacts as input to demonstrate the VT protocol and to provide input data to the CBT, reflecting improvements when potentially introducing a countermeasure.

The probability of sustaining WAD2+ injury was evaluated using the injury risk curve based on Ono et al. (2009). Due to the lack of a similar risk curve, the study by Ono et al. (2009) was chosen, although there are several uncertainties related to that particular risk curve, especially in the area of the upper and lower confidence interval shape. Consequently, the WAD2+ injury risk was higher in a simulation involving shorter head to head-restraint distance when the lower confidence interval curve was used to derive the injury risk, which is inconsistent to the average value of the risk calculation. This inconsistency highlights the importance of data availability and reliability of every step involved, especially when the simulation results will be used as input to the CBT.

3.2 Simulation Series investigating Novel Seating

Four sub-studies were executed with the purpose of investigating potential occupant protection challenges in novel seating. Novel seating includes new types of seat design and adjustments as well as novel seating positions. One study focused on rear-end impacts, while the other three included variations of frontal and side impact crash configurations. A variety of seat models and occupant models were used.

3.2.1 Rear-End Impacts

Using concept vehicle seat models serving the main purpose of investigating the challenges and possibilities with novel seating, the rear-end impact sub-study also provides insights valuable to the wider task on demonstrating the VT protocol (Chapter 3.1). Specifically, it demonstrates the possibilities of including a large variation of parameters when using simulations, and a comparison to an ATD model. However, since the seat models do not have physical counterparts at this stage, the whole VT protocol cannot be included.

3.2.1.1 Novel Seats and Seated Positions

The objective of this sub-study was to quantify the variation of injury criteria in low speed rear-end impacts for various novel seated positions which could occur in automated driving, which are not measurable with the BioRID, with the exception of the upright driving position. The novel seating included classic seats in new adjustment positions, such as reclined seatbacks or inboard rotated positions, as well as novel seats with integrated seatbelts in several reclined seatback positions. The three concept seat models were used together with the VIVA+ 50M and 50F, in addition to the BioRID model when deemed suitable for attaining a relevant position with the BioRID model.

Methods

This sub-study focused on novel seated positions in rear-end impacts, beyond what is included in standardised testing today. This includes the following configurations: simulations with the mid-sized female VIVA+ 50F, simulations in various reclined seat positions for VIVA+ 50F and 50M, occupant postures with the head leaning towards the head-restraint, in addition to inboard rotated seat positions. In the two configurations, simulations with the BioRID model were included enabling comparison with the VIVA+ 50M. In total, 38 simulations were included, see Appendix G.

The seating positions investigated in the study have been defined as follows (Figure 3-12):

- **Upright position** – a standard driving position, which is commonly used in contemporary cars, where the seatback is set to a reference position which corresponds to a torso angle of 25° from vertical.
- **Reclined position** – the seatback is reclined backwards.
- **Inclined position** – a position where the whole seat (seatback and cushion) is rotated backwards.
- **Inclined-reclined** – a seat position where the whole seat is rotated backwards, and additional reclining of the seatback is added. In this position the backward reclining of the seatback is exceeding the backward reclining of the seat cushion.
- **Rotated position** – a position where the whole seat is rotated inboard around a vertical axis with the seatback in an upright position.

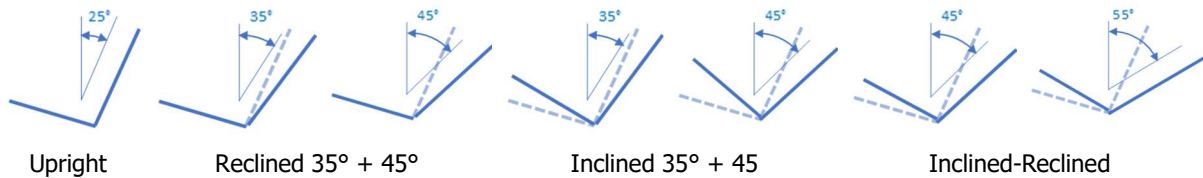


Figure 3-12 Illustration of the different seating positions

The three Faurecia concept seat models as presented in Chapter 2.2.1 and Appendix C. Variant 1 (V1) was used in upright and reclined positions, Variant 2 (V2) addressed rotated positions, while Variant 3 (V3) was used in various reclined and inclined positions. Two head postures were included: upright and leaning towards the head-restraint. The sitting postures were predicted using a study by University of Michigan Transport Research Institute (UMTRI) (Reed and Ebert, 2018). The UMTRI study presents different reclined occupant postures depending on the seatback recline angle and whether a head-restraint is present or not. 'Head posture upright' was based on the UMTRI predictions for reclined occupant postures without head-restraint, and 'head posture leaning' on reclined occupant postures with head-restraint. The UMTRI study also showed that occupants prefer to have the head-restraint closer to the head when reclining the seat (Figure 3-13). Instead of using a head-restraint which would be adjustable in the forward direction, the upper seatback forward rotation option of V3 was used to bring the head-restraint in the desired forward position.



Figure 3-13 Posture study by UMTRI (Reed and Ebert, 2018), showing occupant's head position preferences when reclining the seatback.

The VIVA+ 50M and 50F were positioned using a two-step positioning procedure for every simulation. The first step was setting an initial position based on the UMTRI study, while the second was a gravity settling of the HBM on the seat. The two-step procedure was chosen as the VIVA+ 50M or 50F only partially compressed the seatback foam. The predicted UMTRI positions and the HBM positions after the two-step positioning procedure are shown in Appendix G. All simulations were run with the International Insurance Whiplash Prevention Working Group (IIWPG)/European New Car Assessment Programme (EuroNCAP) mid rear-end impact crash pulse of ΔV at 15.9km/h and maximum acceleration of 10.1g (Appendix G).

Results

NIC was used as the main injury criterion and the corresponding WAD2+ injury risks were based on Ono et al. (2009), for calculations see Appendix G. In addition, Aldman pressures were determined based on the rotations of the vertebrae. For six simulation cases, the algorithm for Aldman pressure calculation showed errors; therefore, the results are not included in this report. One-pagers for each simulation case are included in Appendix G, summarising details on the simulation case as well the results.

Table 3.2 shows NIC_{max} and WAD2+ injury risk predictions for the three different seatback positions in the V1 seat, for VIVA+ 50M and 50F in the upright head position. While no influence on NIC_{max} was seen for the VIVA+ 50F, the VIVA+ 50M varies from 31 in upright to 12 in the most reclined position.

In the same comparison for the V3 seat, a different trend was seen for the two VIVA+ models, both with respect to the influence of the seatback angle and between the SETs (Table G5, Appendix G).

Table 3.2. NIC_{max} and WAD2+ injury risks at different seatback angles of the V1 seat, initial head upright position.







V1 seat		Seatback 25°	Seatback 35°	Seatback 45°
				
VIVA+ 50M	NIC_{max}	31.3	28	12
	WAD2+	96%	92.6%	30.2%
				
VIVA+ 50F	NIC_{max}	10.1	10.4	9,6
	WAD2+	22.8%	23.6%	20.9%

Table 3.3 shows NIC_{max} and WAD2+ injury risk predictions comparing reclined and inclined seat positions using the V1 and V3 seats, providing insight into the influence of the seat cushion design, in addition to differences of seat design. The head positions of the VIVA+ 50M and 50F were upright in V1, while leaning towards the head-restraint in V3. No consistent trend was seen.


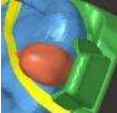
Table 3.3. NIC_{max} and WAD2+ injury risks for the reclined 35° and inclined 10° seat positions (V1 seat) and injury risks for the reclined 45° and inclined 20° position (V3 seat).

		V1 seat Seatback 35° Cushion not inclined	V1 seat Seatback 35° Cushion inclined by 10°	V3 seat Seatback 45° Cushion not inclined	V3 seat Seatback 45° Cushion inclined by 20°
VIVA+ 50M	NIC_{max}	28	26.2	26.3	30.6
	WAD2+	92.6%	89.6%	89.7%	95.6%
VIVA+ 50F	NIC_{max}	10.4	41.5	21.9	36.4
	WAD2+	23.6%	99.5%	77.8%	98.6%

With the head leaning towards the head-restraint, the effect of reclining the seatback, was investigated for the V3 seat. This seat allows an upper seatback adjustment, which was needed for seatback angles of 45° and 55° to accommodate the head to head-restraint position. In the situation with the cushion in nominal position, a trend of higher NIC_{max} was seen with the seatback more reclined for VIVA+ 50M, but not for VIVA+ 50F (Table G6 in Appendix G). When the cushion was inclined backwards, none of the VIVA+ models showed a consistent trend in NIC_{max} related to the change of the seatback angle (Table G7 in Appendix G).

The effect of seat positions in different rotated initial positions are shown in Table 3.4, comparing NIC_{max} . Only the head and T1 movements and acceleration in the sagittal plane were taken into account. These simulations were realised with the V2 seat, which unlike the V1 seat includes a belt-guide at the top of the frame and lateral wings added to the head-restraint. The seat deviator seems to contribute positively, but a more detailed analysis is needed to evaluate the real effect in detail.

Table 3.4. NIC_{max} for rotated initial positions at two different angles, compared to unrotated. V2 seat and VIVA+ 50M and 50F in the upright head position.

V2 seat		Rotation 0°	Inboard rotation 10°	Inboard rotation 20°
				
VIVA+ 50M	NIC_{max}	10.8	13.7	10.7
	WAD2+	25,5%	38.3%	25,1%
VIVA+ 50F	NIC_{max}	5,5	6.4	10.3
	WAD2+	9,9%	11,9%	23.5%

A significant discrepancy was observed when comparing NIC_{max} and WAD2+ injury risk predictions for the BioRID and the VIVA+ 50M in the two corresponding configurations. The BioRID's NIC_{max} were 14 and 10, respectively, while VIVA+ 50M reached 31 and 14 in the V1 and V3 seat, respectively. Movements of the head and the neck differed considerably (Figures G3 to G7), and injury risk prediction were in line with these differences (Table G4 in Appendix G). Based on these few configurations, it is questionable to what degree the NIC_{max} and the injury risk curve by Ono et al. (2009) can be transferred and compared between the BioRID and the VIVA+ models.

Discussion and Conclusion

The study setup enabled comparison of similar effects observed between a classical vehicle seat (V1) and a seat with an integrated seatbelt (V3). Different trends in NIC_{max} and the corresponding injury risk prediction were seen for the V3 seat and the V1 seat in reclined versus upright seat position. No specific relationship for whiplash risks comparing females or males were identified. Configurations with relatively higher risk for females as well as configurations with relatively lower risks were seen.

The seats studied were fitted with a head-restraint which is quite protrusive in the upright position (Figure 2-11). Instead of being an advantage for more reclined positions, this seemed to be a disadvantage for large recline angles. In such positions, the head-restraint became an obstacle compressing the neck during the low-speed rear-end impacts. It would therefore be interesting to study other types of head-restraint designs for reclined seating positions.

The head and neck behaviour differed considerably between the BioRID and the VIVA+ 50M in the two configurations assessed. The rearward head rotation of the BioRID was not seen in the VIVA+ 50M instead, rather a tendency for forward rotation was observed. Hence, configurations are needed to fully understand the differences between the BioRID and VIVA+ 50M.

The use of an HBM instead of an ATD gives new insights into the kinematics of the neck in low-speed rear-end impacts for different seat positions. However, NIC_{max} when used with the VIVA+ did not seem to capture neck movements potentially related to whiplash risks. Several seats with the same NIC_{max} showed very different neck movements. An example of this was the VIVA+ 50F in V1 for which the reclined seatback increased the neck movements due to a larger backset, but without any influence on the NIC_{max} .

The NIC alone is likely not sufficient to predict the whiplash injury risk in low speed rear-end impacts in novel seats. It is expected that additional criteria and other measures to reflect kinematics of the spine and compression of the neck of the VIVA+ will be required. The use of the Aldman pressure injury criterion was investigated in this study which, however, still needs technical improvements for easy use.

3.2.2 Frontal and Side Impacts

Three simulation sub-studies were performed as part of the project with regard to the frontal and side impact cases for adult occupants. In one of the studies, the VIVA+ 50F seated in a rearward-facing vehicle seat was exposed to frontal impacts of two different severities and with the seat adjusted to two different seatback angles. The other two sub-studies address a variety of different forward-facing seat positions, in a front passenger seat vehicle interior model, when exposed to four different crash configurations of frontal and side impact crashes. One including the VIVA+50M and 50F models, in addition to a comparison to the SAFER HBM models of similar sizes. The other study included a range of anthropometries of the SAFER HBM when seated in a variety of seating positions.

3.2.2.1 Rearward-Facing VIVA+ 50F in a Vehicle Interior Environment

This sub-study included frontal impacts for one type of novel seated positions, as part of WP3 to demonstrate a VT protocol for seated passenger car occupants. The VIVA+ 50F was positioned in a rearward-facing vehicle front passenger seat and exposed to frontal impacts (Figure 3-14). The aim was to investigate its sensitivity to changes in seatback angle and crash pulse variation. An additional aim was to integrate the VIVA+ 50F in a vehicle environment.

Methods

In total, four simulations were performed, varying the crash pulses and the sitting posture by adjusting the seatback angle. The two sitting postures were nominal, with a seatback angle of 25°, and semi-reclined, with an angle of 30° (Figure 3-14 and Figure 3-15), facing rearward and exposed to frontal impacts. The two seat configurations resulted in head to head-restraint distances of 51 mm and 61 mm, respectively. Two different crash pulses were used, 'deltaV 24km/h' and 'deltaV 16km/h'. More details can be found in Appendix H.

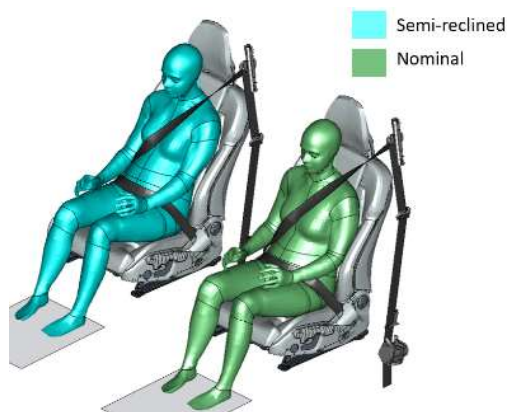


Figure 3-14 VIVA+ 50F HBM is seated on a production vehicle seat environment in nominal (25° seatback angle) and semi-reclined (30° seatback angle) configurations. The seat is placed rearward-facing in the vehicle, while exposed to frontal impacts.

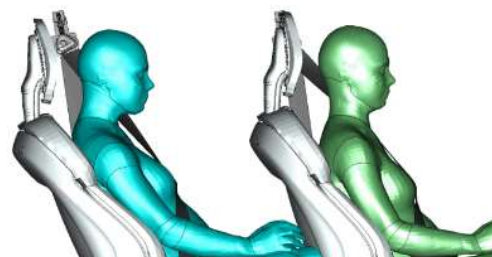


Figure 3-15 Side view of the VIVA+ 50F in nominal and semi-reclined configurations.

With the purpose of evaluating the sensitivity of the model to discriminate the two posture configurations for each of the crash pulses, the analysis focused mainly on kinematics. This was done by visual comparison and by analysing the head to head-restraint contact. As occupant response, Head and T1 relative velocity and acceleration in the x-direction were in focus. Based on these responses, NIC_{max} was calculated using the procedure described in the EuroNCAP protocol (EuroNCAP, 2019) and compared between the four simulations. Although not developed for a mid-sized female HBM, the injury



risk function for NIC_{max} by Ono et al (2009) was used to provide some further insights into the sensitivity when using a potential injury criterion.

Results

The occupant kinematics in the nominal and semi-reclined configurations are shown in Appendix H, together with the NIC, head and T1 relative velocity and acceleration. The time of head to head-restraint contact followed the trends in backset, with increased time for increased backset. This correlation trend was seen in both crash pulses. The head to T1 relative responses showed a consistent trend for the influence of the seatback angle, independent of the frontal impact crash pulse. Higher peak head and T1 relative acceleration and velocities were seen for the semi-reclined configuration. The same applies to NIC_{max} as well. Applying the injury risk function for NIC_{max} , the relative estimated risk differences were approximately 20%; ranging from approximately 16% in the 'deltaV 24km/h' to 23% in the 'deltaV 16km/h' configurations. The NIC_{max} responses only slightly deviated between the two crash pulses with somewhat higher values in the 'deltaV 16km/h' pulse. This was driven by the relatively higher contribution of the acceleration-based component in that pulse configuration.

Discussion and Conclusion

This sub-study was the first step in investigating novel seated positions in frontal impacts, using the VIVA+ models. The VIVA+ 50F was successfully integrated in the vehicle interior model and positioned into the target postures using common positioning techniques. The model was sensitive to change in posture between the nominal and the semi-reclined seat positions, as well as to the different crash pulses applied.

While the VIVA+ 50F was found sensitive to changes in the two posture configurations in the study, the degree of sensitivity and to what degree the differences in kinematics and amplitude of the response replicate the situation for a mid-sized female occupant in corresponding real-world situations, cannot be established based on this study. The trend of increased occupant responses with increased backset, caused by the semi-reclined seat position, replicated what would be expected based on earlier tests or simulation experiences in rear-end impacts for forward-facing occupants. Increased backset has been shown to be related to increased injury risk in real-world follow-up crash data studies (Jakobsson et al., 2008). However, the influence of the seatback angle, as such, creating the backset is not known as a separate variable from real-world follow-up studies of rear-end impacts. For frontal impacts with rearward-facing seats, the influence of backset, as well as the relative importance of whiplash injury risks are still to be understood. In frontal impacts, an increased likelihood of higher severity pulses is expected, which likely will pose additional challenges regarding the vehicle seat integrity when facing rearward. In addition, the space available behind a front row rearward-facing seat is likely less than a forward-facing seat. Hence, there are several seat design parameters that could influence the seatback movements, as well as options for seatback adjustments, when positioned rearward-facing in a vehicle.

Which injuries and injury mechanisms to focus on for a rearward-facing occupant in frontal impacts is not evident, especially at higher impact severities. As presented by Kang et al. (2020), a large variety of injury types were seen. It also became clear that the design of the seatback including the seatbelt attachments, in addition to the seatback strength and support, influenced the injury outcome. In the present study, focussing on kinematics, and including certain results in line with the injury responses proposed in VIRTUAL for forward-facing occupants in rear-end impact situations, was selected. However, due to all the uncertainties with respect to the novel HBM used, in addition to the novel seated position and the limitations in the setup as such, the calculated injury predictions should be treated with great caution. The injury predictions can be used for relative comparison with respect to whiplash injury assessment, but will likely neither reflect true injury risk, nor provide an overall injury assessment relevant for a rearward-facing occupant exposed to a frontal impact.

3.2.2.2 Forward-Facing VIVA+ 50M and 50F Simulations in a Variety of Seated Positions

The objectives of this sub-study were to investigate the sensitivity of the VIVA+ 50F and 50M to altered seat and seated positions while exposed to frontal and side impacts, as well as to examine their numerical stability in a vehicle environment. Additionally, the simulations were compared to corresponding simulations with similar size SAFER HBMs from the study in Chapter 3.2.2.3. Details of the current sub-study can be found in Appendix I.

Methods

The VIVA+ 50F and 50M, in addition to the SAFER HBMs in similar sizes, were positioned in a front passenger seat (Figure 3-16) and exposed to two frontal impact configurations and two side impacts (near-side and far-side). The seat was adjusted in six different configurations, including variation of the fore-aft positions and seatback angles. Three fore-aft positions, ranging from full-forward to full-backward positions, and two seatback angles were used: a nominal upright (25°) and semi-reclined (30°) seatback angle. State-of-the art restraints, including seatbelts and airbags, were used and activated when appropriate for the situation.



Figure 3-16 VIVA+ 50F (left) and 50M (right) seated in a front passenger seat in a vehicle interior model with nominal seat adjustment (25° seatback angle and 40% of the fore-aft travel).

Results

The VIVA+ 50F and 50M were successfully integrated into the vehicle interior model and positioned into the target postures using automated positioning methods. Twelve positioning simulations and 48 crash simulations were performed in total. All simulations reached the specified termination time.

Overall, similar kinematics trends were observed between the female (50F) and male (50M) VIVA+ models. They were sensitive to changes in the fore-aft position of the seat, while the seatback angle had only a minor influence on the occupant kinematics. In the near-side impact, the full-forward seat position resulted in a slightly larger head rotation. While in the far-side impact, a trend of the torso moving further inboard and the head further downward was seen for the full-forward seat position, as compared to when in a more rearward seat position. In the frontal impacts, the knee to instrument panel contact, which varied with fore-aft position, influenced the kinematics of the lower extremities, the torso and the head. No submarining occurred in any of the seat positions.

Overall, similar trends were observed between the VIVA+ and the similar sized SAFER HBM. The comparison showed overall similar kinematics patterns, with differences observed mainly on the shoulder and cervical spine of the models.

Discussion and Conclusion

The VIVA+ 50F and 50M could be integrated in the vehicle interior model and positioned into the target postures using common techniques for positioning HBMs and ATD models. The models were run successfully for the variety of seat and seating positions and the non-standardised crash configurations with the vehicle interior, including all the restraints under consideration.

The qualitative kinematics analysis performed in this study provided insights into the utilisation of the VIVA+ 50F and 50M as part of the virtual assessment tool chain. Despite the limited validation of the VIVA+ models, as well as the morphed SAFER HBMs, the similar kinematic trends between the models underline their applicability to evaluation of kinematics. Evaluating diverse anthropometries in multiple seat adjustments has the potential to enhance the robustness of the safety assessment.

3.2.2.3 The Influence of Occupant Size and Shape in a Variety of Seated Positions

This sub-study aimed to investigate the influence of car occupants' size and shape on kinematics and kinetic responses in multiple seat adjustments during frontal- and side- impacts (Leledakis et al., 2022). The rationale for this study was to enhance insight into the real-world occupant safety challenges due to variations in anthropometry and seat and seating position.

Methods

A simulation study was performed, in which occupant size and shape were varied, and multiple combinations of seat adjustments were used. The SAFER HBM v9.0 was morphed into 22 unique occupants of both sexes, with stature ranging from 1.47 to 1.90m and Body Mass Index (BMI) from 18 to 38kg/m² (Figure 3-17) The HBM was positioned in the front passenger seat of a passenger car, equipped with the current state-of-the-art restraint systems. The seat was adjusted in six steps in the fore-aft position (0–100%) and two seatback angles (nominal at 25° and semi-reclined at 30°). Four crash configurations were evaluated, including two frontal impacts (of varied overlap and severity) and two side impacts (one on the near-side and one on the far-side front corner).

A full-factorial design matrix was used for sampling, resulting in 944 simulations. A global sensitivity analysis method was developed and applied to identify the parameters with the largest influence on occupant kinematic and kinetic (load) responses.

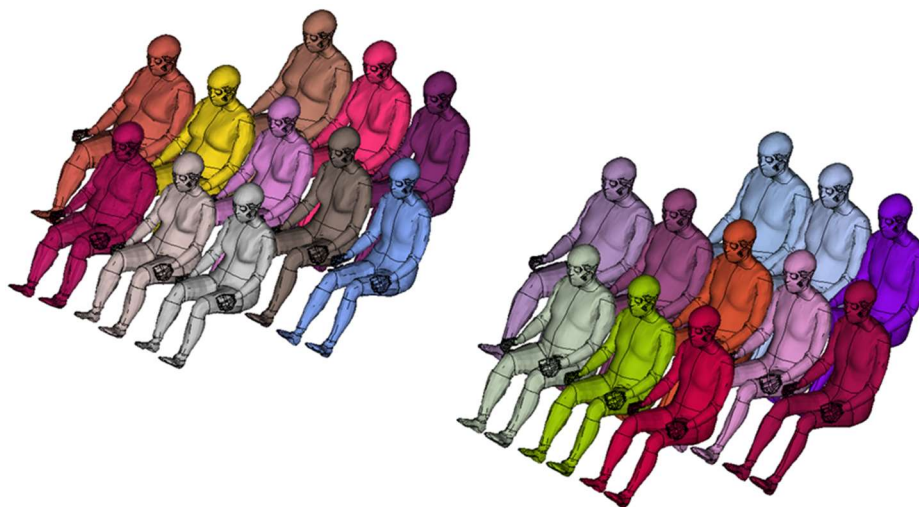


Figure 3-17 The SAFER HBM models used; females (left) with statures of 1.47-1.76m and BMIs of 18-38, and males (right) with statures of 1.62-1.90m and BMIs 18-38



Results

In all the crash configurations, taller occupants were associated with relatively higher upper and lower extremity loads, as compared to shorter occupants. In the frontal impacts, pelvis kinematics and kinetics were found to be influenced by BMI, sex, and the fore-aft seat position. Female occupant models predicted higher pelvic angle compared to male models, which also led to relatively higher lumbar resultant force. In the oncoming frontal impact, the fore-aft position altered the kinematics of the head, mainly by changing the coupling with the passenger airbag. The head reached 18% higher resultant relative velocity when the seat was adjusted to the full rear position compared to the nominal seat position. The semi-reclined seatback position had the least influence on lumbar loads compared to all other investigated parameters. In the far-side side impact, the peak head rotation was correlated with BMI, with occupants of lower BMI showing larger rotations.

Discussion and Conclusion

Performing simulations of a diverse family of occupants can identify occupant protection challenges and enhance the robustness of the crashworthiness evaluation of a vehicle. The selected design matrix and analysis method isolated the interaction effects of the studied parameters and uncovered the main mechanisms behind the influencing parameters. The fore-aft position of the seat influenced the occupants' interaction with the vehicle interior and the restraint systems, leading to altered occupant responses in frontal impacts. Additionally, BMI was found to be a significant factor for occupant kinetics. Further details are found in Leledakis et al. (2022).

This sub-study offers a systematic comparison of the effect of diverse occupant anthropometries and seat position adjustments. Together with a global sensitivity analysis method enabling a large-scale multi-input multi-output analysis, it was possible to identify trends which should be studied in more detail in the future. The study provides contributions to an enhanced understanding of occupant heterogeneity and insights into novel seating aspects, serving as an example of the benefits of virtual testing, in line with the overall goals of the VIRTUAL project.

4 The Child Occupant Protection Case

When riding in cars, children need child restraint systems (CRSs) appropriate for their size and age. For the smallest children, a rearward-facing child seat provides optimal protection, preferably up to at least 4 years of age (Jakobsson, 2017). When the child has reached 4 years and is facing the direction of travel, there are still differences in biomechanics compared to adults, requiring the use of a CRS. The iliac spines of the pelvis, which are important for good lap belt positioning and for reducing the risk of the belt interacting with the abdomen, are not well developed until about 10 years of age (Burdi et al., 1968). The development of the iliac spines, together with the fact that the upper part of the pelvis of a seated child is lower than of an adult, are facts that must be taken into consideration in order to provide a child with equivalent protection as an adult.

The first belt-positioning booster cushion was introduced 1978 by Volvo (Norin et al., 1979). The booster elevates the child and positions the lap part of the vehicle seatbelt over the thighs, which helps keep the lap belt away from the abdomen. The booster also encourages the child to sit comfortably with their legs, helping to avoid slouching and increasing the likelihood of good seatbelt routing (DeSantis Klinich et al., 1994, Jones et al., 2020). By elevating the child, the booster will also help position the shoulder part of the seatbelt more comfortably and safe over the shoulder. Children also benefit from seatbelt technologies such as pretensioner and load limiters (Bohman et al., 2009, Forman et al., 2009, Jakobsson et al., 2017).

An increasing number of boosters are so-called booster seats, i.e., boosters including a seatback. The seatback was initially intended to provide head support in cars without head-restraints, and to help route the shoulder belt over the child's shoulder and chest. In the last decade, the designs of the seatbacks have evolved towards large side supports both at the level of the torso and the head. The child restraint manufacturers emphasise two reasons for this; to provide improved side impact protection and to provide comfort for children by keeping them upright when relaxed or asleep (Bendjellal et al., 2011). However, studies have shown that protruding side supports increase the time children spend in forward leaning postures outside the potential protective area of these supports (Andersson et al., 2010, Jakobsson et al., 2017).

Boosters are effective tools to protect children from injuries in frontal impacts as well as other crash directions (DeSantis Klinich et al., 1994, Jakobsson et al., 2005, Arbogast et al., 2005 and 2009). Arbogast et al. (2009) showed that seatbelt syndrome related injuries to the abdomen and spine were nearly eliminated in crashes with children using boosters compared to those restrained by seatbelts only. Children aged 4 to 8 using boosters were 45% less likely to sustain injuries than similarly aged children who were using the vehicle seatbelt only. Children in side impacts derived the largest relative protection from boosters, with a reduction in risk of 68% and 82% for near-side and far-side crashes, respectively. No differences in booster seats versus booster cushions (without backrest) were seen.

When studying children during on normal car journeys it is obvious that children adopt a variety of postures. Only for a limited time during the ride, the children are in the ideal posture for which the crash test dummy is positioned in testing (Jakobsson et al., 2017). Children's sitting postures are influenced by comfort and activities as well as by vehicle dynamics, such as evasive manoeuvres, in addition to the booster design. From a real-world crashworthiness perspective, the vehicle and CRS work together to protect the child. Hence, the use, misuse and 'misfit' aspects are essential for real-world protection. This is as essential today as it likely will be in future novel seating configurations.

The objective of this chapter is to study the influence of variations in current and novel seating, exemplified by seat orientation, e.g., reverse seat position, and seat adjustments, e.g., reclined seat, using a child HBM or an ATD representing a 6-year-old, restrained using a booster (booster seat or booster cushion, Figure 4-1) and a seatbelt, when exposed to a frontal impact. In addition, some 'misfit' situations are included, where either the vehicle seat or the booster is adjusted incorrectly. An additional objective is to correlate the VIRTUAL OS Vehicle seat model and its interaction with the VIRTUAL OS Booster seat model using the HIII6y ATD, exposed to a frontal impact in a rearward-facing configuration. Three sub-studies were performed, using the PIPER HBM or the HIII6y ATD, exposed to frontal impacts.



Figure 4-1 The two booster models used; booster cushion model (left) and OS booster seat model (right).

4.1.1 HIII6y in a Rearward-Facing Vehicle Seat; Sled Tests and Simulations

A series of physical sled tests and corresponding FE simulations were carried out with three main purposes:

- To correlate the VIRTUAL OS Vehicle seat model to its physical counterpart.
- To study child occupant protection for 6-year-olds in booster seats in a rearward-facing vehicle seat, exposed to frontal impacts.
- To study the influence of 'misfit' by booster and vehicle seat adjustments.

4.1.1.1 Methods

The vehicle seat was placed facing rearward on the sled rig. The booster seat was placed in the vehicle seat and the HIII6y was seated on the booster seat, restrained by a seatbelt. The seatbelt was a three-point non-retractor belt with geometry similar to the vehicle from which the vehicle seats were taken. This setup was exposed to two different frontal impact crash pulses of 30km/h and 50km/h impact speed, respectively (see Appendix J). Booster seats corresponding to the VIRTUAL OS Booster seat model and vehicle seats corresponding to the VIRTUAL OS Vehicle seat model were used. A physical HIII6y and a commercially available HIII6y model were also used. The sled test setup and its virtual counterpart are shown in Figure 4-2. In addition, simulations were run with the PIPER HBM.

The booster seat was adjusted in three different positions: (i) according to the user guide for the size of the HIII6y (headrest in mid-position), (ii) with the headrest in the lowest possible position and (iii) in the highest possible position (Figure 4-3). Following the recommendations in the booster seat user-guide, the head-restraint of the vehicle seat was removed in the tests with the booster seat headrest positioned in the low- or mid-position. As opposed to that, the tests with the booster seat headrest in its highest position were performed with the vehicle seat head-restraint in place. In line with the 'misfit' definition used within VIRTUAL, the low- and high-positions are examples of 'misfit' situations of the booster seat, since they disagree with the setting as recommended by the user-guide of the booster

seat. Furthermore, the configuration with the booster seat headrest in mid-position, although in line with the recommendations in the booster seat user-guide, can be seen as an example of 'misfit', but then from the vehicle seat perspective due to the removal of the head-restraint. The rationale for that is that it may potentially not provide optimal support in the current test conditions.



Figure 4-2 Sled test setup (left) and the corresponding numerical setup (right), booster seat headrest mid-position configuration and removed vehicle seat head-restraint. The vehicle seat is positioned rearward-facing in relation to direction of travel.

Thirteen physical sled tests were performed using six vehicle seats, see Table J1 in Appendix J. The varied parameters included the two different crash pulses and the three configurations of booster seat headrest positions: mid-, low- and high-position. Additionally, a second booster seat, called booster seat Version 2, was tested in each of the two pulses, in the headrest mid-position configuration. There was no major difference in design of the two booster versions. Some configurations were tested twice.

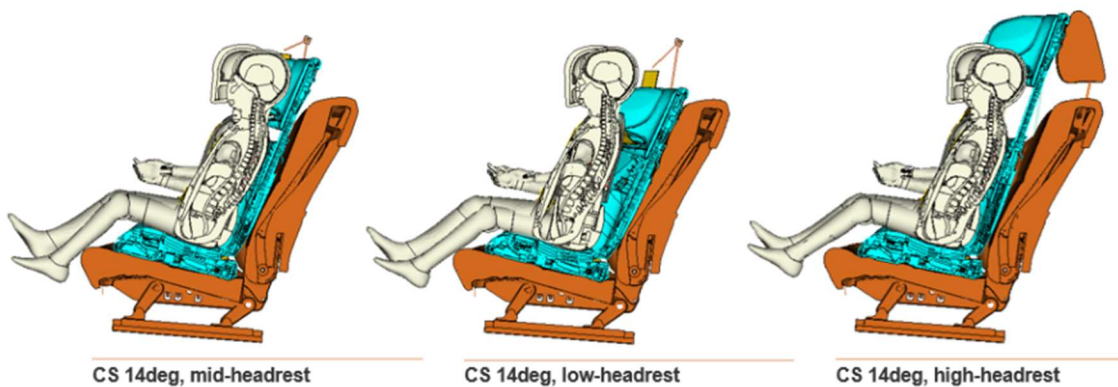


Figure 4-3 The three configurations of booster and vehicle seat positions, numerical setups with HIII6y and PIPER overlaid. The head-restraint of the vehicle seat was removed in the tests with the booster seat headrest in the mid- and low- positions (left and mid), while it was in place in the tests with the booster seat headrest in high-position (right).

Three simulation models were created, representing the three configurations of booster headrest positions: low, mid and high. These three models were run with the two different crash pulses (30km/h and 50km/h), resulting in six simulation configurations. The vehicle seatback angle was adapted to replicate the tested seats. Some adjustments of the vehicle seat model were made to adapt to the kinematics of the physical seat. All six simulation models are shown in Figure 4-4, overlaid with the

corresponding sled test scenario, at time of impact. See Appendix J for more details on the models, positioning and simulation matrix.

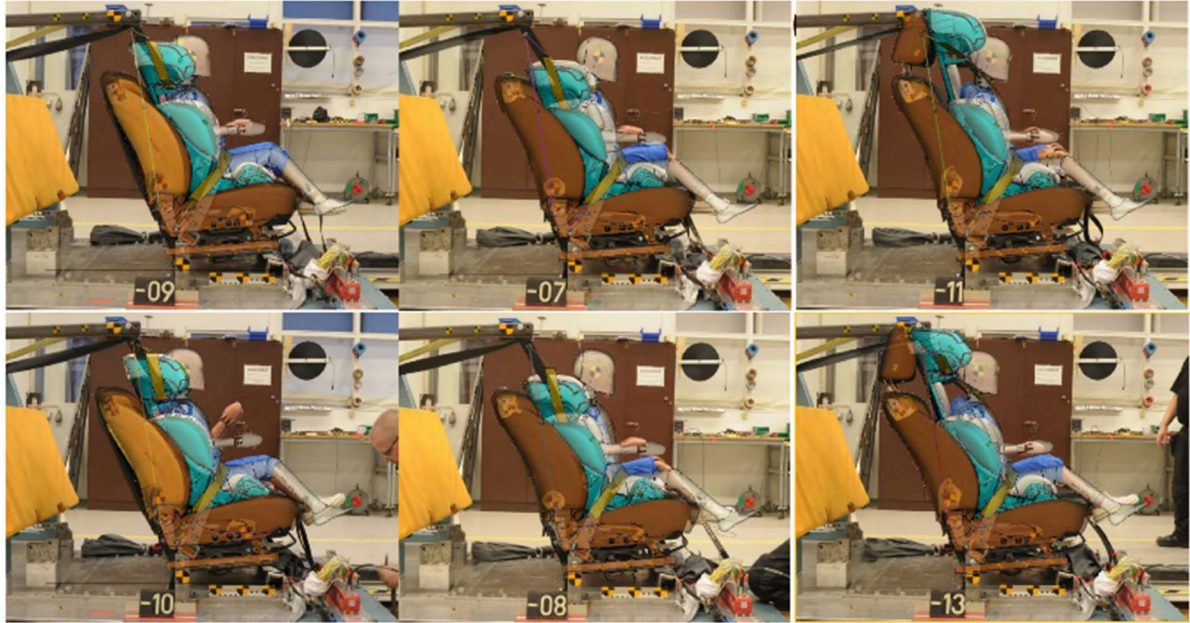


Figure 4-4 The six simulation models at time of impact (after pre-simulation) overlaid with corresponding sled test scenario. Booster seat headrest positions; mid (left), low (middle) and high (right), at 30km/h (upper row) and 50km/h pulse (lower row), respectively.

4.1.1.2 Results

Correlation with Numerical Models

To correlate the VIRTUAL OS Vehicle seat model and the VIRTUAL OS Booster seat models to the physical counterparts, the corresponding configurations (as listed in Table J3 in Appendix J) using the HIII6y model were analysed pairwise. Figure 4-5 shows the three configurations with the 50km/h pulse, overlaid with the simulations and sled tests, in side view. It is seen that the vehicle seatback rotations in the simulations match well with the corresponding physical tests. This is a result of the tuning of the vehicle seat during the setup phase of the simulations. The overall kinematics comparison provides generally good agreement between simulations and tests.

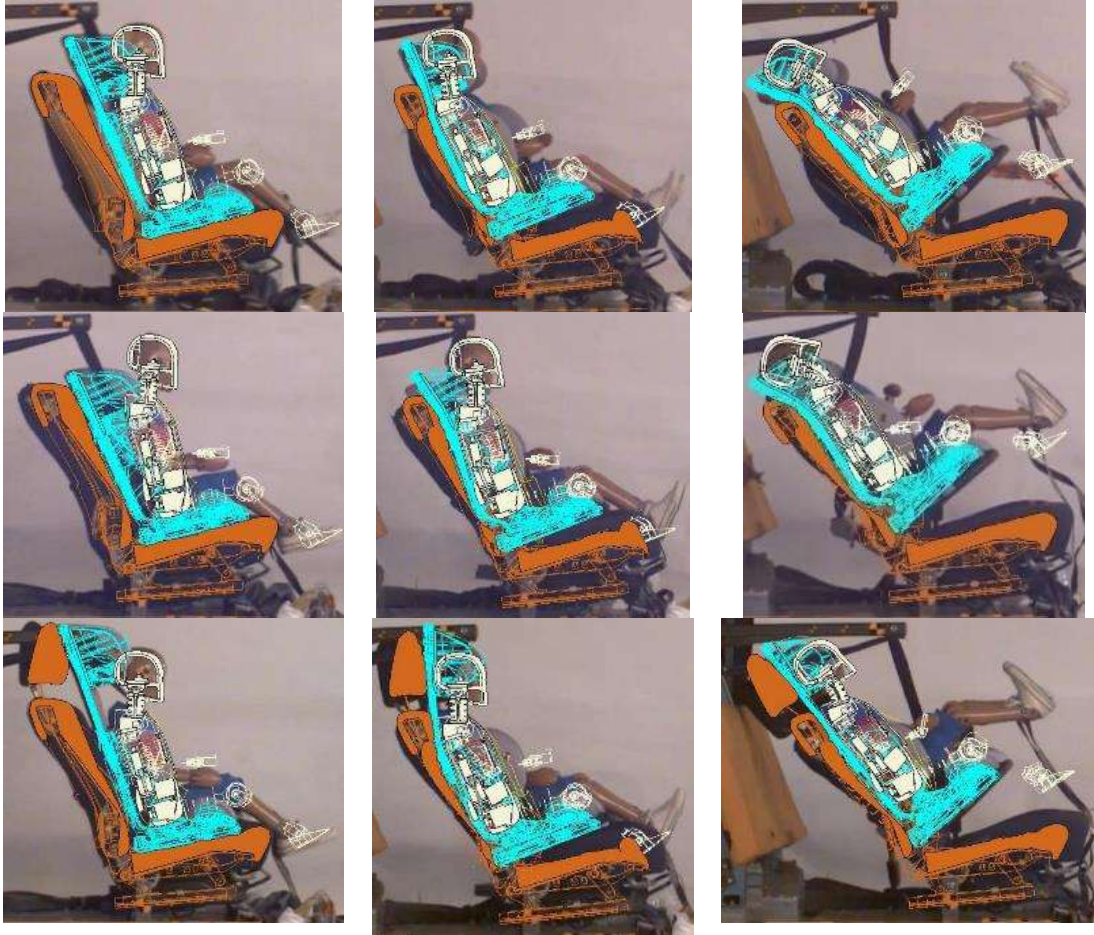


Figure 4-5 The simulation overlaid the corresponding sled test. Images at time 0, 50 and 100ms (left to right), for the 50km/h configuration. The booster seat headrest in mid-position (upper row), in low-position (middle row) and in high-position (lower row)

Sled Test Series

When exposed to a frontal impact, the HIII6y, seated in the booster seat in the rearward-facing vehicle seat, sank into the booster seat and moved together with the booster seat and vehicle seat towards the direction of impact. When reaching the maximum vehicle seatback deformation, the HIII6y rebounded back towards where it started in the seat. This is exemplified in Figure 4-6 providing snapshots from the test at 30km/h with the headrest of the booster seat in mid-position (T01).



Figure 4-6 The sled test sequence from test T01; HIII6y with headrest in mid-position, exposed to a 30km/h frontal impact pulse (from left). Sequence starting top left (start of impact) to top right (maximum seatback deflection), followed by bottom left to bottom right (the rebound phase).

Snapshots from the sled tests at time of the maximum vehicle seatback deformation are shown in Appendix J. For all three configurations, the higher crash pulse resulted in larger seatback deflection. The head trajectory was influenced by the seatback deformation as well as by the availability of the vehicle seat head-restraint. It was observed with regard to the configurations without a vehicle seat head-restraint (Figures J3 and J4 in Appendix J), especially for the 50 km/h pulse, that the head rotated over the top of the seat, even when the booster seat headrest initially was high enough to cover the whole head. In the tests with the vehicle head-restraint providing extra support to the booster seat headrest (Appendix J, Figure J5), the head was supported in line with the torso, keeping the neck straight.

Resultant acceleration (3ms) for the head, pelvis and chest, are presented in Appendix J, Table J4, for each test categorised by configuration and crash pulse. The average was not calculated due to large and unsystematic test variability. Plots of the acceleration components are also seen in Appendix J. Overall the responses are relatively low, which provides evidence of principally good protection of a 6-year-old on a booster seat in a rearward-facing vehicle seat, exposed to a relatively high severity frontal impact. The head and chest resultant acceleration (3ms) were below the Injury Assessment Reference Values for the HIII6y as proposed by Mertz et al (2003) of 189g and 93g, respectively. However, it should be emphasised that the HIII6y is not designed for use in this type of configuration, especially the impact to the back of the head. Nevertheless, the low acceleration together with the kinematics, including limited exposure of the neck, provide comforting results for satisfactory protection, even if some potential 'misfit' situations are included.

Higher pelvis and chest acceleration were seen for the 50km/h pulse as compared to the 30km/h pulse. This reflects the increased severity exposed to the torso and pelvis through the vehicle seat and booster seat. No major relative increase of the vertical (z) component of the chest and pelvis acceleration in the 50km/h pulse tests as compared to 30km/h pulse tests were seen. This reflects that the difference in seatback deformation seen between these two severity levels have limited influence on the vertical movement of the HIII6y. Seatbelt force sensors were not available to confirm any influence of the lap belt.



Although no major differences in chest and pelvis acceleration were seen between the three configurations, some differences were observed for the head acceleration. For the booster headrest in the mid-position or low-position in the 50km/h pulse, there was a clear difference with respect to the head acceleration components as compared to the other tests. In those tests, the head vertical (z) component was dominant, in contrary to the longitudinal (x) component for all the other tests. This is a clear indication of the head rotation over the vehicle seatback, as also seen in Appendix J, Figures J3 and J4. This motion will likely increase the loads to the neck, in comparison to when the loading to the head and torso is balanced, as exemplified in Appendix J, Figure J5. Unfortunately, no neck force transducer was included in the sled test series. Upper neck forces and moments would most likely be more relevant injury risk indicators than the head acceleration in this context.

No statistical test was used for repeatability evaluation. However, it can be seen that there was a substantial test variability between the repeated tests, deviating mostly in amplitude and less in the time sequences. No differences beyond overall test variations were seen between the two types of booster seats, see Appendix J.

Simulation Series

Figure 4-7 shows an example of corresponding simulation and test for the HIII6y in the two pulses, for the configuration of booster seat headrest in the mid-position, at the time of maximum vehicle seat deformation. It appears that the HIII6y model replicates the physical HIII6y overall satisfactory. In addition, during analysis it provided a better insight into the kinematics and load distribution of the HIII6y. The option of selecting the mid-section of the HIII6y model for analysis, provides more information on potential neck bending than can be seen by analysing the physical tests only.

Comparing acceleration in the head, chest and pelvis for the physical HIII6y and the HIII6y model, the responses of the model were generally higher than in the corresponding sled tests. Although head acceleration is somewhat similar, there are large discrepancies for the chest and pelvic area. Nevertheless, the trends between the different configurations were captured by the model, in line with the results from the sled tests. A summary of the resultant head acceleration (3ms) for the simulations is provided in Appendix J.

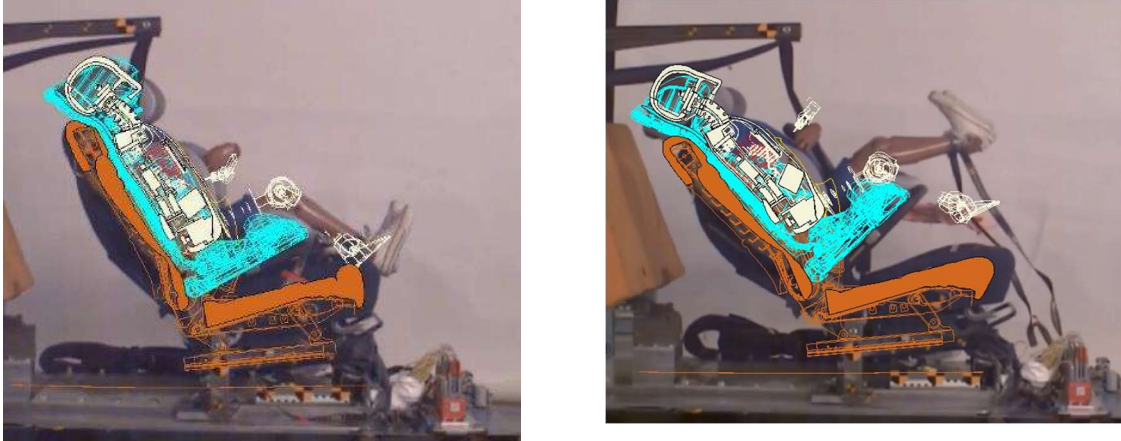


Figure 4-7 Simulation overlaid with sled test, side view, at time of maximum vehicle seat deformation. Configuration with booster seat headrest in the mid-position; 30km/h at 75ms (left) and 50km/h at 100ms (right).

Figure 4-8 shows a comparison of the HIII6y model and PIPER, in the configuration of the booster seat headrest in the mid-position at 50 km/h, at the time of maximum vehicle seat deformation (100ms). It was observed that PIPER slid further upwards and rearwards together with the booster seat, as compared with the HIII6y model. This effect may be due to the more reclined initial position of the PIPER (head leans more rearward, and the hip placed further forward), or its overall more flexible design. This flexible, and more human-like, design of PIPER enables more detailed analyses of interactions as well as the influence on spinal curvature, as also applies to the other child occupant sub-studies.

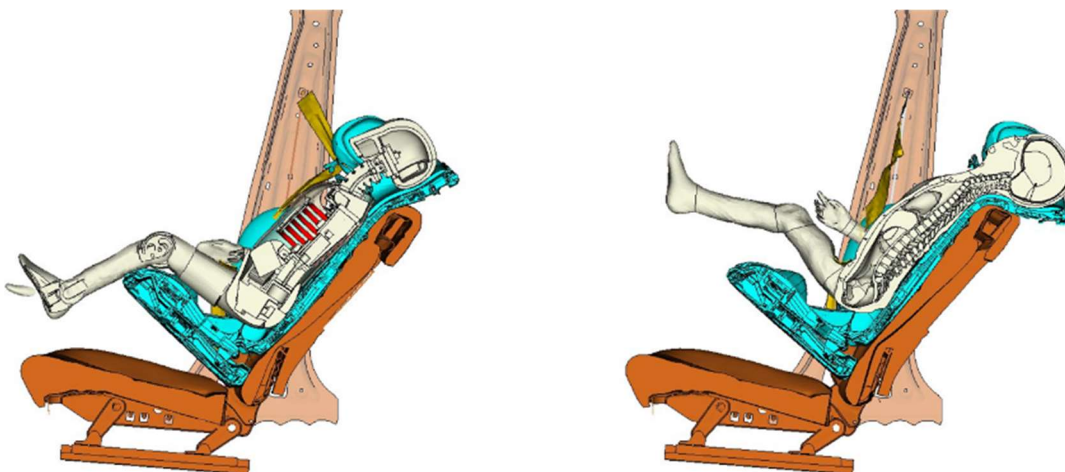


Figure 4-8 Simulations of the HIII6y model (left) and PIPER (right) at the time of maximum vehicle seatback deformation in the configuration of the booster seat headrest in the mid-position at 50 km/h.

Resultant head acceleration for each of the eight simulation configurations are listed in Appendix J, Table J4, comparing the HIII6y model and the PIPER HBM. It can be concluded that the PIPER HBM consistently measured lower head acceleration for the simulated configurations compared to the HIII6y model. This was a result of the different geometry and kinematics of the models. In fact, the model responses should not be compared in this way, due to significant modelling differences. An important

question is whether they lead to similar conclusions when investigating the influence of different parameters of the restraint system, by looking at the relative change in response for each model. For example, the headrest high-position gives lower head acceleration compared to the mid-position for both models. Similarly, the headrest low-position gives higher head acceleration compared to the mid-position for both models.

The PIPER head acceleration showed a slight trend towards higher acceleration for the headrest in the low position, while lowest for the headrest in the high position. This confirms the trends seen in the test results when using the physical HIII6y, although the latter is not specifically designed for this particular load case. The results from the PIPER simulations support the hypothesis that a rearward-facing position would be beneficial when exposed to a frontal impact, even for a 6-year-old on a booster seat. In addition, PIPER's head responses in this sub-study were generally lower than in the two other child occupant sub-studies in this report, in which the 6-year-old was travelling forward-facing. In the current sub-study, the maximum head acceleration ranged from 32-56g, including both crash pulses, while in the two other studies, the acceleration (3ms) values were within the range of 60-78g.

4.1.2 PIPER HBM in Forward-Facing Concept Vehicle Seat Models

With the objective of investigating the influence of child occupant protection in future vehicle seat designs in a variety of seated positions, the PIPER HBM using a booster seat or booster cushion was seated on three concept vehicle seat models and exposed to a frontal impact.

4.1.2.1 Methods

The concept vehicle seat models were designed to accommodate potential seated positions in future AD cars. Variant 1 (V1) is a standard seat design, Variant 2 (V2) is the same principal design as V1 but with a belt-guide on the seat to guide the shoulder belt, while Variant 3 (V3) is a novel seat design with a split-seatback together with a belt-guide, in addition to a belt retractor integrated under the seat cushion. The concept seat models were designed by Faurecia and are further described in Chapter 2.2.1 and Appendix C. The booster cushion and booster seat models shown in Figure 4-1 were used. No direct connection between the booster and the vehicle seat was made. PIPER HBM was restrained together with the booster using a three-point seatbelt with a pretensioner (activation at 10ms) and a 4kN load-limiter.

Four different seating positions were investigated. They are shown in Figure 4-9 and defined as follows:

- **Upright position** –a standard driving position, commonplace in contemporary cars, seatback angle is set at around 25° from vertical.
- **Reclined position** –the seatback is reclined backwards to an angle of 40°.
- **Articulated position**– this position can only be achieved with the V3 seat model, which seatback is in two parts. The position is achieved by reclining the whole flat seatback to an angle of 40°, after which the upper part is moved forward 10°. This position is designed to provide improved shoulder support when reclined.
- **Inclined position** –a position where the whole seat (seatback and cushion) is rotated backwards to achieve a seatback angle of 40°.

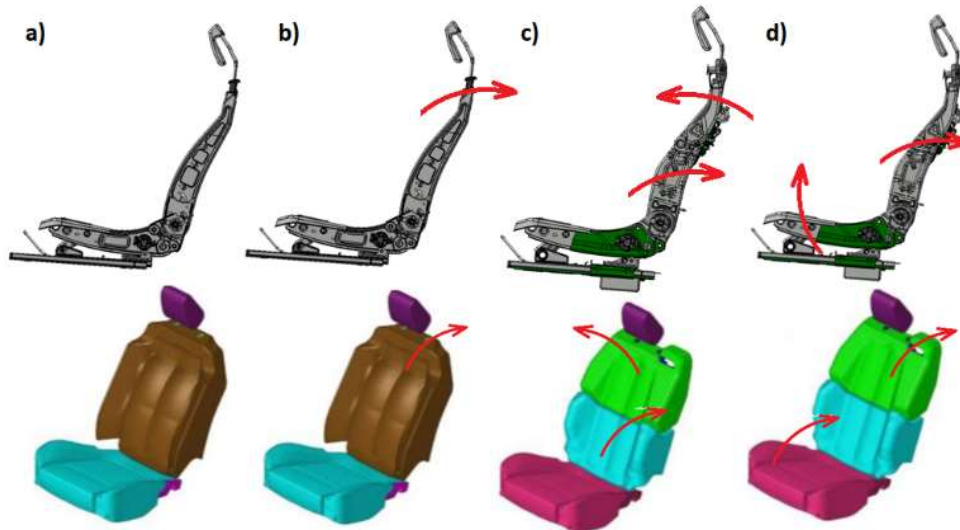


Figure 4-9 Illustration of the seating positions included a) Upright, b) Reclined, c) Articulated, d) Inclined.

Eight configurations were included in the simulation matrix. The upright and reclined configurations were run with all three seats, while articulated and inclined only with the V3 seat. The booster cushion was used in all simulations, except for the V3 in the inclined position where the booster seat was used. Figure 4-10, Figure 4-11 and Figure 4-12 show the setup for each simulation at start, also displaying the seatbelt routing. The simulation matrix and the crash pulse are shown in Appendix K.



Figure 4-10 Seatbelt routing in the upright position for a) V1 seat, b) V2 seat, c) V3 seat.



Figure 4-11 Seatbelt routing in the reclined position for a) V1 seat, b) V2 seat, c) V3 seat.

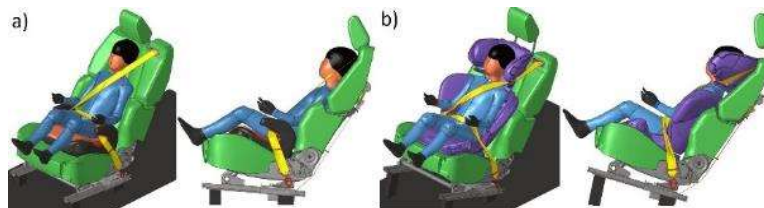


Figure 4-12 Seatbelt routing on V3 seat in the a) Articulated position, b) Inclined position

4.1.2.2 Results

Figure 4-13 shows the kinematics of the PIPER HBM in the upright position with the booster cushion, comparing the three seat variants, displaying overlaid pictures for four time frames: (0ms, 50ms, 100ms and 150ms). It can be seen that the HBM in V1 has the largest forward excursion, while the shortest is for V2. The seatbelt routing (B-pillar installation) for V1 likely influences the forward motion, so does the higher forward flexion of the V3 seat, as compared to the V2 seat. Head excursion (x displacement vs time), head and pelvis trajectory (x and z displacement) and head resultant acceleration are shown in Appendix K, comparing the three seat variants. The shortest head forward excursion, pelvis displacement and head acceleration occurred in the tests with the V2 seat. The shoulder belt routing through the belt-guide on top of the seatback helped to limit the forward movement, as compared to when in the V1 seat, for which the belt was routed from the B-pillar without a belt-guide. It was seen that the PIPER HBM to seatbelt interaction occurred later in V1. As can be seen in Figure 4-13, the shoulder belt was located closer to the shoulder at the start of the simulation, due to the belt-guide in the V2 seat.

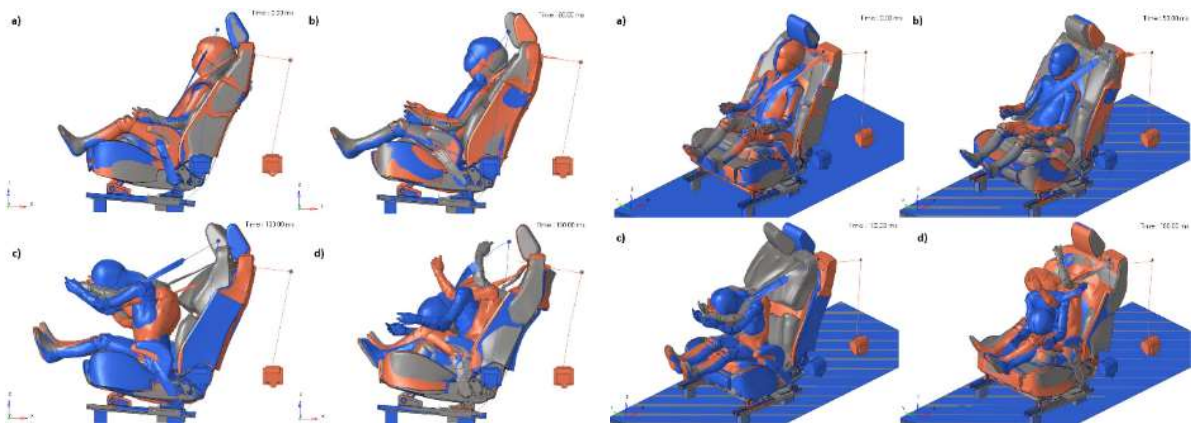


Figure 4-13. Side view (left) and isometric view (right) simulation kinematics for the **upright position** and **booster cushion** at a) 0ms, b) 50ms, c) 100ms, d) 150ms. V1 (standard seat) – Blue, V2 (standard seat with belt-guide) – Orange, V3 (seat with split seatback) – Grey.

A similar trend was seen for the upright position, with the largest forward excursion in the V1 seat and shortest in the V2, although not reflected in the head acceleration to the same extent (Appendix K).

Generally, the head forward excursion was longer for every seat variant comparing the reclined position and upright position, except for the V3 seat, which was reflected by the head acceleration. The higher head acceleration observed for the V1 seat was mainly caused by an initial gap between the occupant and the shoulder belt, since the shoulder belt slipping was positioned in front of the occupant's shoulder when in the reclined seated position. This led to delayed engagement of the shoulder belt and, as a result, to a higher head acceleration. For the V3 seat, the magnitude of the head acceleration was similar in the two seated positions. In that seat, the routing of the seatbelt was not influenced by the seated position, due to the belt-guide and the integration of a seatbelt retractor under the seat cushion. However, for the V2 seat, having the same principal seatbelt design as the V3 seat, the head acceleration was higher in the reclined position than when in the upright position. This was influenced by the position of the seatbelt inside the belt-guide when the seatback was reclined. A difference in relative position between the seatback and shoulder belt slipping caused disturbed movement of the seatbelt inside the belt-guide, due to higher friction inside the belt-guide leading to higher head acceleration (illustration in Appendix K, Figure K4).

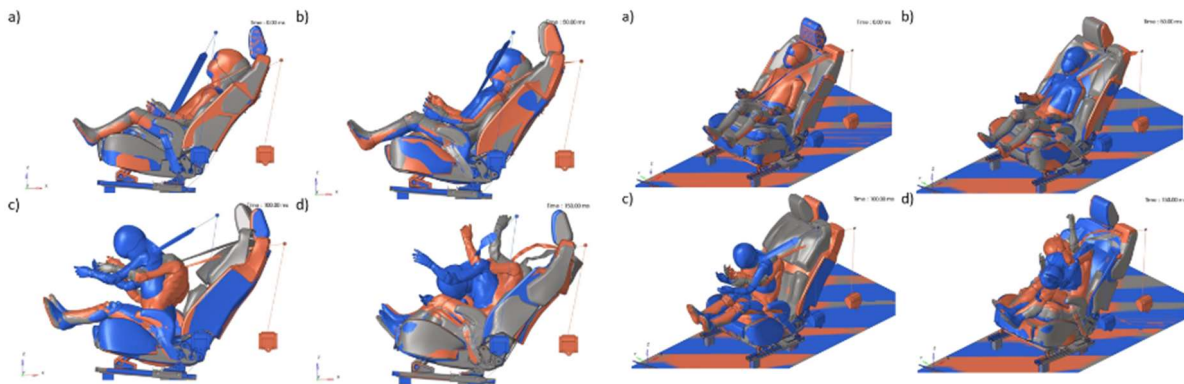


Figure 4-14 Side view (left) and isometric view (right) simulation kinematics for the **reclined position** and **booster cushion** at a) 0ms, b) 50ms, c) 100ms, d) 150ms. V1 (standard seat) – Blue, V2 (standard seat with belt-guide) – Orange, V3 (seat with split seatback) – Grey.

Figure 4-15 and Figure 4-16 show the kinematics of the PIPER HBM in the articulated position with the booster cushion and in the inclined position with the booster seat, respectively. The V3 seat was used for both positions. Although the vehicle seat cushion had different initial angles, it can be seen that the upper body kinematics were similar. The kinematics is also influenced by the backrest of the booster seat (in the inclined position) being flexible, moving together with the seatbelt and hence not interacting too much with the shoulder belt path during the impact. The similarities of upper body trajectories were also seen when comparing the head trajectories and the head forward excursions (Figures K7 and K8 in Appendix K), while the pelvis trajectories were different in the articulated and inclined positions. The plotted pelvis trajectories correspond to the H-point movement of the PIPER HBM. The coordinate system was set at the H-point at the beginning of the simulation and was therefore different in every case. Pelvis trajectories were influenced by the cushion inclination, which influenced the forward movement of the pelvis. In the inclined position, the lap belt routing was also different in comparison to the articulated position. Both of these differences had an effect. Resulting in shorter forward pelvis displacement (see Appendix K, Figures K7 and K8), and lower pelvis acceleration, (see Appendix K, Figure K13), in the inclined position.

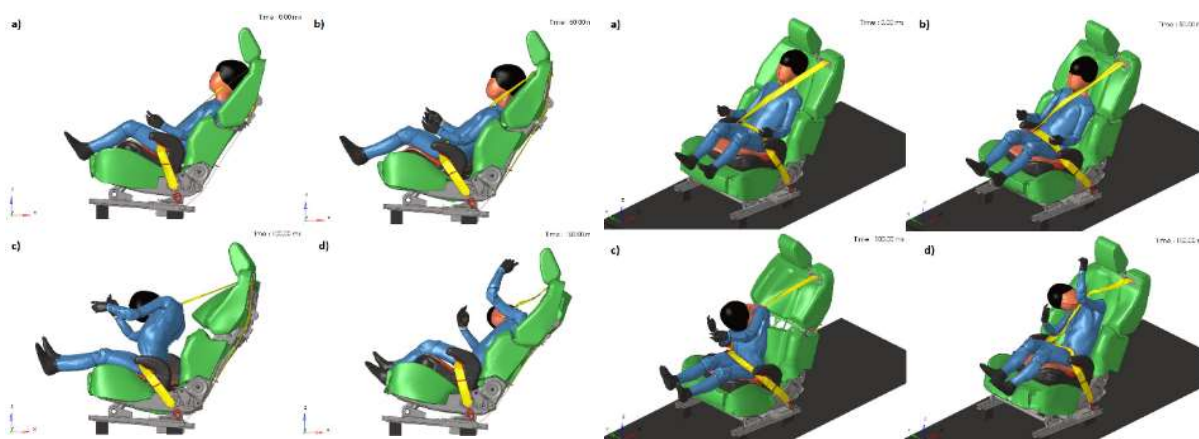


Figure 4-15 Side view (left) and isometric view (right) simulation kinematics for the **articulated position** and **booster cushion** in V3 seat, at a) 0ms, b) 50ms, c) 100ms, d) 150ms

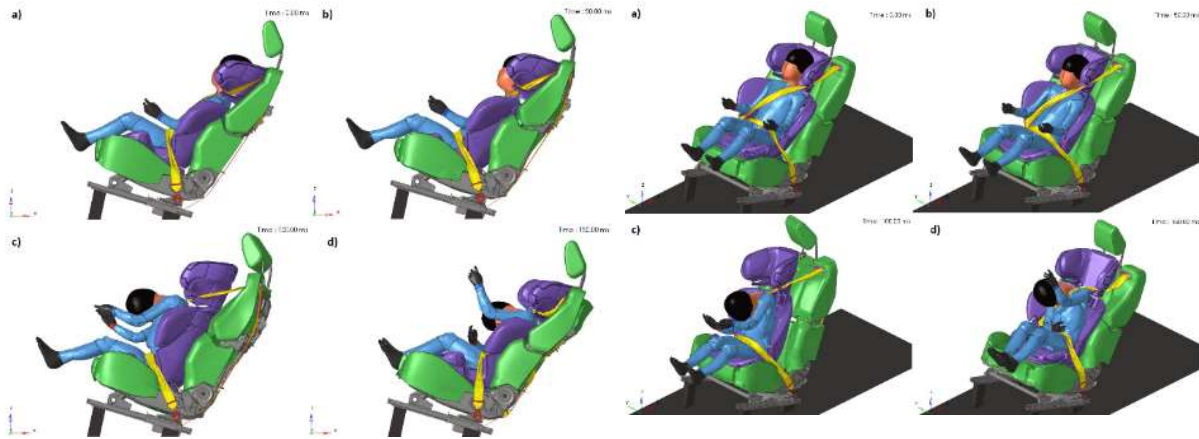


Figure 4-16 Side view (left) and isometric view (right) simulation kinematics for the **inclined position and booster seat** in V3 seat, at a) 0ms, b) 50ms, c) 100ms, d) 150ms.

Compared to an ATD, the PIPER HBM allows studying the spine kinematics in much more detail. Figure 4-17, Figure 4-18, Figure 4-19 and Figure 4-20 show side and rear views of the spine curvature at four times during the frontal impact for the upright, reclined, articulated and inclined positions, respectively. Based on a visual analysis, the most pronounced s-shape was observed in the reclined and articulated positions. For the inclined position, the booster seat likely had an influence. However, a more in-depth analysis is needed to understand the contribution of the backrest of the booster seat in comparison to a booster cushion, as well as the influence of the different vehicle seatback designs and seatbelt routings in different seated positions.

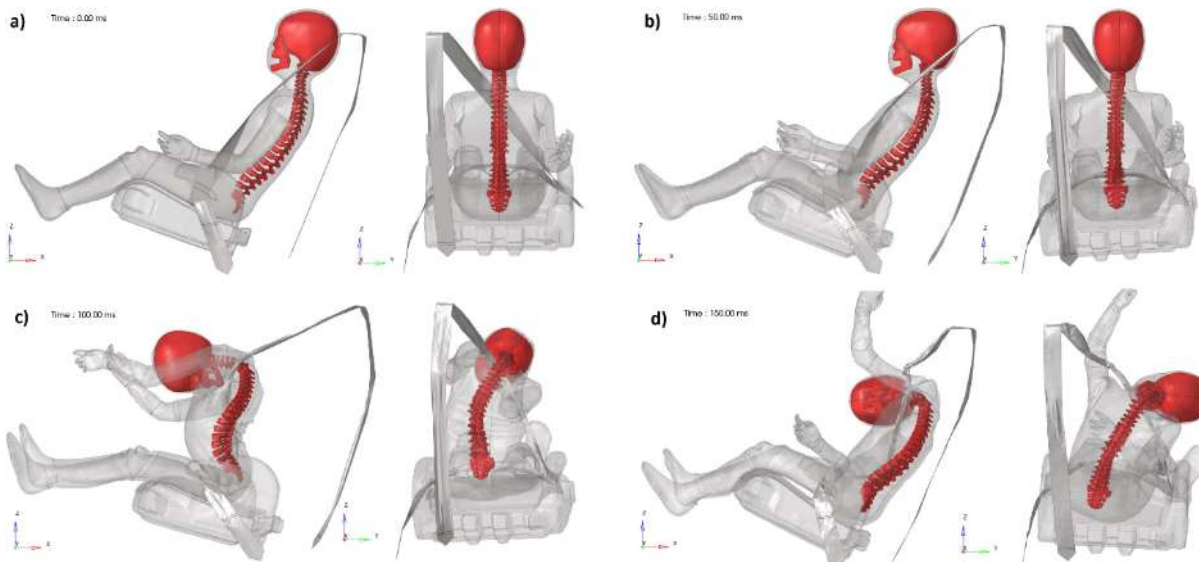


Figure 4-17 **Upright position** in V3 seat. Side and rear view of the PIPER spine at four times; a) 0ms, b) 50ms, c) 100ms, d) 150ms.

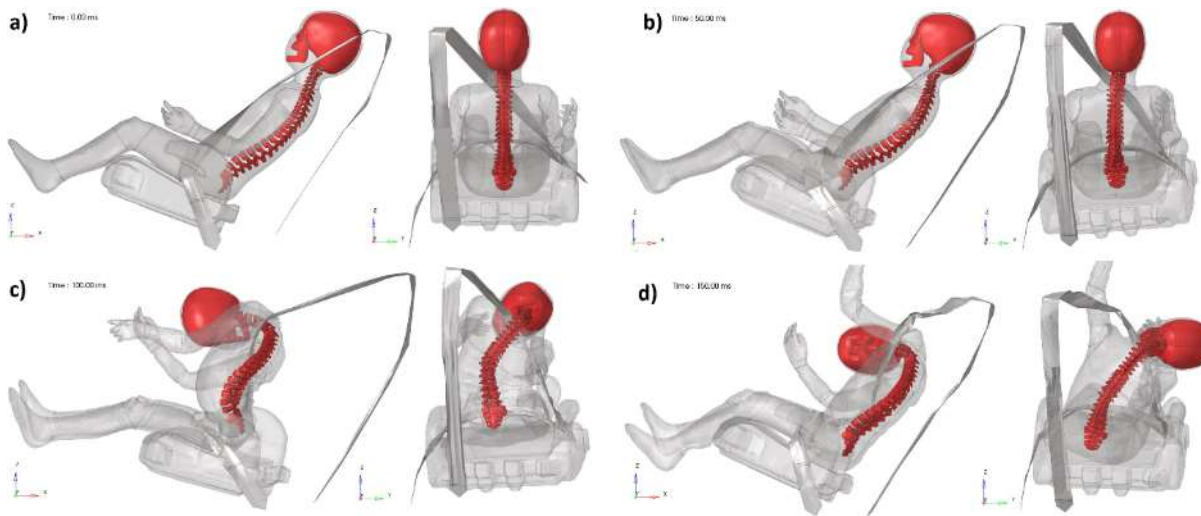


Figure 4-18 **Reclined position** in V3 seat. Side and rear view of the PIPER spine at four times; a) 0ms, b) 50ms, c) 100ms, d) 150ms.

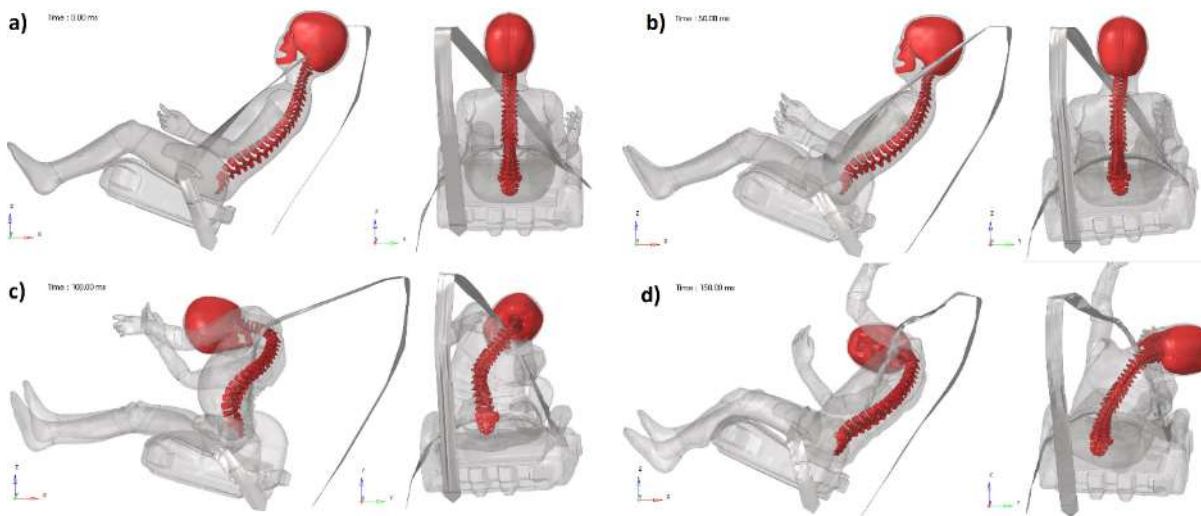


Figure 4-19 **Articulated position** in V3 seat. Side and rear view of the PIPER spine at four times; a) 0ms, b) 50ms, c) 100ms, d) 150ms.

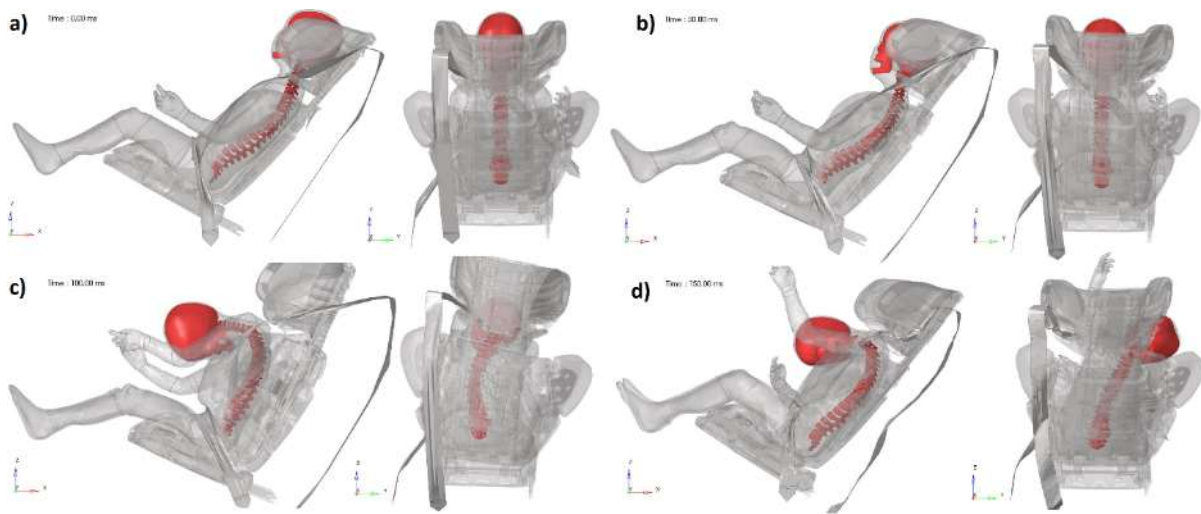


Figure 4-20 **Inclined position** in V 3 seat. Side and rear view of the PIPER spine at four times; a) 0ms, b) 50ms, c) 100ms, d) 150ms.

4.1.3 PIPER HBM in a Forward-Facing Production Vehicle Seat Model

The overall purpose of this study is to contribute to the understanding of which challenges prevail for child occupant protection when travelling in a reclined seated position, applying contemporary protection systems. The specific aims are to compare a reclined seated position to an upright seated position in a standardised front passenger vehicle environment, by investigating the influence of booster type and shoulder belt geometry in a simulation model, as well as studying the effect of seatbelt pretensioning and attachment to the ISOFIX anchorages, using one child size exposed to frontal impacts. This sub-study was presented and published at the annual International Protection of Children in Cars Conference in December 2021, entitled 'Reclined seating in frontal impacts – a simulation study using the PIPER 6y HBM (Bohman et al., 2021).

Methods

Five parameters were varied in the simulation study using the PIPER HBM. The parameters included two different boosters (booster cushion and booster seat), two vehicle seat positions ('upright position' and 'reclined position'), two shoulder belt geometries ('nominal D-ring position' and 'rearward D-ring position'), in addition to with or without pretensioner activation and with and without attachment to the ISOFIX anchorages. In total, 20 simulations were conducted using a full-frontal crash pulse of 56 km/h. Side views of the initial position for the different configurations are shown in Figure 4-21.

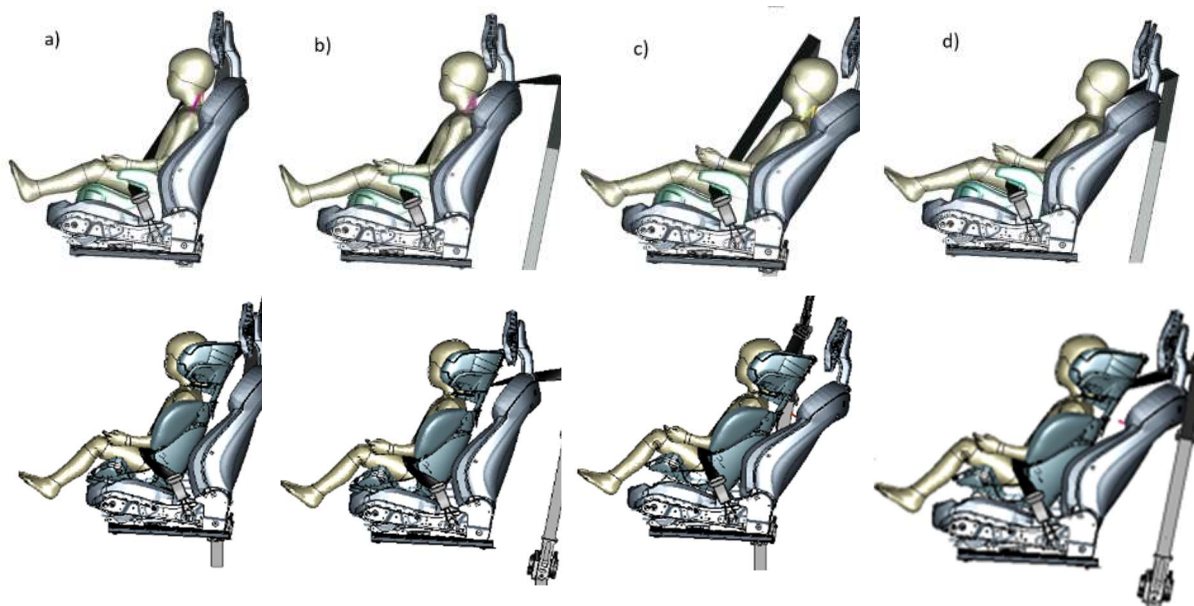


Figure 4-21 Side views of PIPER's initial posture when using a booster cushion (top row) and booster seat (bottom row). From left to right; a) 'upright position' and 'nominal D-ring position', b) 'upright position' and 'rearward D-ring position', c) 'reclined position' and 'nominal D-ring position'.

Results

Submarining occurred when seated on the booster cushion in the 'reclined position' without pretensioner. In all other simulations, the booster combined with the pretensioner helped keep the lap belt on the pelvis and avoided submarining. Hence, submarining can be addressed in reclined seating using current booster design in combination with a vehicle seatbelt pretensioner.

The shoulder belt remained on the shoulder in all configurations with pretensioners. The shoulder belt moved more inboard in the 'reclined position' during the crash as compared to when in the 'upright position', see Figure 4-22. This applied for both boosters. For several configurations without

pretensioner, a late belt slip-off (just before rebound) was seen. Configurations with pretensioner resulted in lower head and neck loadings, in addition to reduced head excursion, as compared to the configuration without pretensioners. Furthermore, the initial shoulder belt geometry was important for restraining the torso sufficiently. The more rearward position of the shoulder belt D-ring improved initial shoulder belt contact for both seated positions when using the booster cushion.

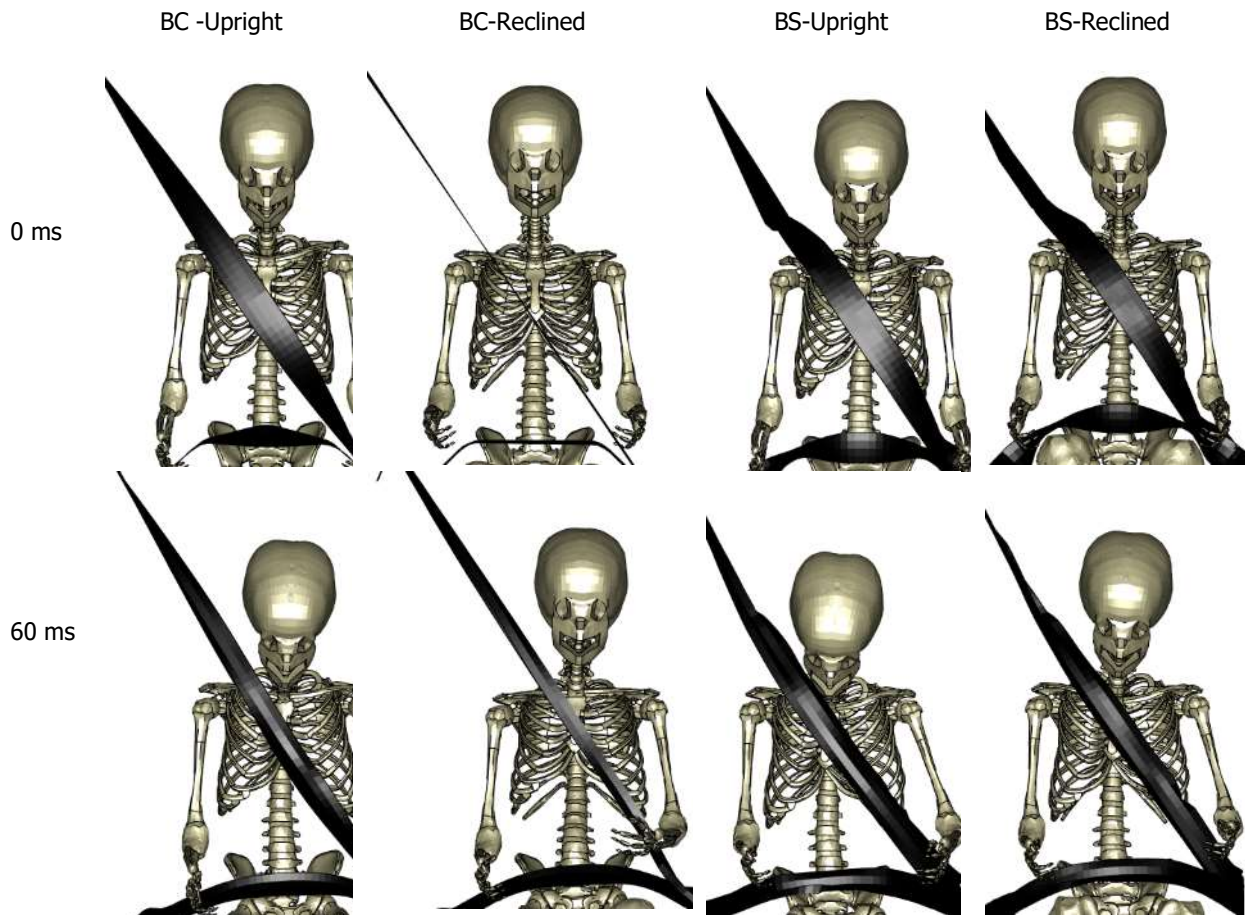


Figure 4-22 Initial seatbelt positions (top row) and shoulder belt positions at 60 ms (bottom row) for the following configurations (left to right): booster cushion 'upright position', booster cushion 'reclined position', booster seat 'upright position', booster seat 'reclined position'. 'Nominal D-ring position' for all configurations.

Neither of the two boosters included in the study are specifically designed to be used in reclined vehicle seats. Still, no submarining for either booster occurred when used together with a pretensioner. In studies with adult occupants in reclined seats, submarining has been shown to occur if no specific countermeasures are added to the restraint system. The present study indicates that the belt-guides of the booster help to maintain the lap belt on the pelvis during frontal impact even when the seatback is reclined. The two boosters differed, both with respect to being or not being equipped with a backrest and by different lap belt-guide designs. These two parameters cannot be separated clearly in this study, due to the 8° more upright posture of the PIPER model, because of the interaction of the booster seat backrest with the vehicle seatback when in the 'reclined position'.

This study provides evidence of the importance of including the whole context of child occupant protection when investigating novel seating. The interaction and compatibility of the booster, the vehicle seat and seatbelt are essential, as exemplified by the importance of the pretensioner and the static incompatibility of the booster seat backrest and the vehicle seatback.

4.1.4 Discussion and Conclusion

The sub-studies complement each other, addressing different aspects of the protection of 6-year-old children in current and novel seating in frontal impacts. All tests and simulations used a belt-positioning booster (with or without backrest), which is the appropriate CRS for this age group.

Two of the sub-studies provide insights into the child occupant protection case within the VT protocol, using the PIPER HBM in forward-facing configurations exposed to frontal impacts. The simulation series included novel seats and variations of seatbelt routing and seat adjustments. It was shown that the combination of the seat design and position, in addition to the seatbelt position, influenced the kinematics and responses of the child occupant. Using the PIPER HBM, detailed information on restraint interaction and spinal kinematics, for instance, provide insights beyond what standardised tests or simulations using an ATD would provide.

One of the sub-studies included physical sled tests with corresponding numerical simulations, using both the HIII6y and PIPER models, demonstrating some other important parts of the VT protocol. The sled tests facilitated eliciting accurate information with regard to the performance of the vehicle seat and the booster seat compatibility, such as the need for support by the vehicle head-restraint to stabilise the booster seat backrest. This was especially pronounced at the higher severity, providing a varied validation challenges to the model validation. The simulations facilitated insights which would not have been elucidated as easily from the physical tests. This was particularly noticeable for the detailed information on neck extension caused by the imbalance between the head and the torso, which was more easily detected using the numerical models, especially the PIPER model which spine is more realistic anatomically.

When comparing forward excursion and resultant acceleration of the PIPER's head in the study with the different types of vehicle seats and recline adjustments, the lowest head acceleration was seen in the upright position in the V2 seat, with added seatbelt belt-guide. For the standard vehicle seat (V1), with the seatbelt attached to the B-pillar, the head acceleration was higher in the reclined than in the upright position, which was not the case for the seat with the integrated seatbelt model used in the current study (V3 seat of Appendix C). This indicates that the seatbelt routing influenced the head acceleration and that an influence of reclined seating can likely be compensated by the seatbelt design and the interaction with the seat. The highest predicted concussion risk was seen for the reclined position of a standard seat model, while the articulated position with the integrated seatbelt showed the lowest risk. Since this tissue-based brain injury criterion is a new approach to assess injury risk during a crash and has not yet been validated for use with the PIPER HBM, the presented results should be considered as basis for future research.

Although spanning over a variety of frontal impact crash pulses and vehicle seat designs including two fundamentally different configurations regarding direction of travel, the study is limited in scope with respect to the type of CRS and the representation of the child occupant's size. However, the 6-year-old in a booster represents one of the most challenging cases, due to the interaction with the vehicle seat and the seatbelt. The smallest children should optimally travel rearward-facing and hence use a CRS that is separate from the vehicle restraint. The oldest children are more similar to adults and share the same challenges as small adults.

There are several benefits of using HBMs. Their human-like representation and their omni-directional capability, in contrast to the limitations of an ATD, enable insights into detailed restraint interactions. This was illustrated by the simulation series using the three different concept seats in four different seated positions, and the study of spinal kinematics as a result of the reclined versus upright position. Further developments on injury prediction means for the PIPER model are encouraged, preferably



including tissue-based criteria for the different body regions. The head tissue-based criterion as used in this study is a starting point for this.

For child occupant protection, the child restraint – in this case a booster – adds to the complexity by serving as occupant positioner as well as seatbelt router. In the current study, the headrest of the booster seat also served as a head-restraint in a high-load situation, which it was not primarily developed for. This is one of the examples of 'misfit' situations that were evaluated in this study. Other 'misfit' situations included deviation from the nominal vehicle seat position in relation to the seatbelt, which is likely to become more common in novel seated positions.

5 Discussion

This report addresses the VT protocol for the adult and child occupant protection cases within the VIRTUAL project. The general workflow of a VT protocol incorporates starting with a physical test, serving as a reference for validation of the virtual simulation environment. The virtual simulation setup is then compared to the physical test setup by replicating the physical test conditions. The virtual simulation test setup can then be employed to study a range of parameter variations, with the purpose of enabling a more robust assessment in line with real-world variability. In total eight test and simulation sub-studies are included in this report, addressing different parts of the workflow. Although the sub-studies were somewhat isolated, together they demonstrate the feasibility of each step.

For the adult occupant protection case, the physical tests as described in Chapters 3.1.1 and 3.1.2 provide insight into the first steps with the SET, connecting to the volunteer tests enabling the link to humans, as well as linking to the seat model validation in the VT protocol, when applied for seat assessment purposes. The two simulation sub-studies in Chapter 3.1.3 provide insights into applying the VIVA+ models in combination with the VIRTUAL OS seat models, in addition to investigating the influence of variations of the head to head-restraint distance. In one of them, VIVA+ was applied as FE model representation of human volunteers that were involved in earlier physical tests of the corresponding physical seat. This process demonstrated the principles of the second step of the workflow and also briefly demonstrated the third step of the workflow by investigating the influence of the head to head-restraint distance. This was also explored in the other sub-study, using another seat model and other crash pulses, which furthermore, generated output data, according to the assessment protocol, that was fed into the CBT. The context of this data is further described in Winjnen et al. (2022).

For the child occupant case, the sub-study in Chapter 4.1.1, included a physical test series with HIII6y, corresponding simulations with a HIII6y model, as well as with the PIPER HBM. The setup comprised a rearward-facing vehicle seat with a HIII6y on a booster seat exposed to frontal impacts. This sub-study served several purposes, such as input to seat model development, comparison on contribution from an HBM (PIPER) compared to an ATD model (HIII6y) and furthermore, contributing to demonstrating the VT protocol (see further discussion in Chapter 4.1.4). The child occupant case also included two of the sub-studies providing insights into the workflow with respect to varying parameters, enabling a more robust assessment in line with real-world variability and especially investigating the challenges of reclined seats. One of the sub-studies (Chapter 4.1.3) was presented as a 'first of its kind' study on children in reclined seating at the international Protection of Children in Cars Conference 2021 (Bohman et al., 2021). A particularly interesting result is that, although challenging with reclined seats, the booster did a good job in helping to protect the 6-year-old HBM in situations that are challenging for adult protection. The overall benefit of a booster was also seen in the other simulation sub-study, which also raised the importance of the shoulder belt position in frontal impact. It was shown that the combination of the seat design and position, in addition to the seatbelt position, influenced the kinematics and responses of the child occupant. Using the PIPER HBM, detailed information such as restraint interaction and spinal kinematics, provided insights beyond what standardised tests using an ATD would provide, which is in line with the overall purpose of the VT protocol as proposed by VIRTUAL.

For the occupant protection case within the VIRTUAL project, a complete workflow from the physical test, from validation of a FE seat model to a simulation study using that model for inclusion of a large variation of parameters, could not be done following the same vehicle seat through all steps. This would be a next step, once all the tools and models are in place. The different tools and models were developed



in parallel and, therefore, were depending on their respective progress to fit into the workflow. Mainly delays in development of the adult occupant tools, such as the SETs and the VIVA+models, influenced the type of studies possible.

A number of activities were conducted to develop the three VIRTUAL OS seat models (Vehicle seat model, Chalmers lab seat model and Booster seat model), comprising activities such as CAD and mesh developments in addition to physical tests and numerical simulations for validation purposes. The models are essential parts of enabling a VT protocol. They were important in the work on demonstrating the range of parameter variations, put in the context of OS models. As a complement, simulation sub-studies were also executed using production vehicle seat models by Volvo Cars, and three concept seat models that Faurecia developed and used for addressing novel seating challenges. These seat models were essential, especially in the area of novel seating. They mainly contributed by enabling investigations on influence of seat adjustments and seat and seatbelt design, in addition to expanding the occupant protection case beyond the seat only. Specifically for the topic of novel seating when exposed to frontal and side impact situations, occupant protection assessment involves more than the seat. Therefore, the sub-studies in Chapter 3.2.2 contribute to a widened scope and context with respect to robust assessment in line with real-world variability.

The validation of the VIRTUAL OS Vehicle seat model, as described in Chapter 2.1.3 and Appendix A, was mainly based on physical component tests with corresponding simulations replicating the impactor tests. While the results of these tests, at least after fixing a number of flaws in the initial version of the seat model, showed reasonable agreement of numerical and physical tests, they cannot serve as a validation of the VIRTUAL OS Vehicle seat model in rear-end impact conditions. The child occupant protection sub-study in Chapter 4.1.1 provided additional correlation work by using the VIRTUAL OS Vehicle seat model together with the VIRTUAL OS Booster seat model to replicate corresponding sled tests with the HIII6y. However, this loadcase with two seat models and the rearward facing configuration in a frontal impact was rather complex and required additional tuning of some parts of the seat model. Therefore, even though a generally good agreement was seen for overall kinematics and acceleration, these tests were not directly applicable for validation purposes. Hence, at this stage the full validation of the VIRTUAL OS Vehicle seat model for rear-end impact is still a pending task. Awaiting the validation of the SET, it is proposed to use physical tests with the BioRID and simulations using the most updated BioRID model.

6 Conclusion

For the VT adult occupant protection case, the specific objectives include demonstration of the whole tool chain for rear-end impacts, demonstration of the VT protocol for novel seated positions and providing input data for the CBT. Eight sub-studies in this report address these objectives: two physical test series and six simulation series. Half of the simulation sub-studies investigated influence of variations in seat adjustments, novel seats and seated positions, when exposed to rear-end impacts. Using vehicle interior models of a front passenger seat environment, the other half explored the influence of seat position and occupant anthropometry when exposed to some different frontal and side impact configurations. One of the sub-studies also served the purpose as input to the CBT by providing injury risk reduction calculations for a potential countermeasure for whiplash injuries in rear-end impacts.

For the VT child occupant protection case, three sub-studies were performed with models representing 6-year-olds exposed to frontal impacts. Two of the sub-studies showed that the PIPER human body model's kinematics and responses were influenced by several parameters, such as vehicle seat adjustments, e.g., reclined seats and novel seatback designs, booster design and seatbelt routing, when forward-facing. This emphasises that seat design, as well as seatbelt position and routing are essential design parameters for child occupant protection in current and novel seated positions. In a rearward facing seated position, the importance of interaction of the booster seat and vehicle seat was highlighted. In that study, the headrest of the booster seat also served as a head-restraint in the crash, which it was not primarily developed for. This is one of the examples of 'misfit' situations that were evaluated as part of the study. Other 'misfit' situations included deviation from the nominal vehicle seat position in relation to the seatbelt, which are likely to become more common in novel seating.

The VT protocol includes enabling that virtual simulation test setups can be employed to study a range of parameter variations. Hence, several models were developed within the project and are available as part of the VIRTUAL project. This report includes the development of several seat models, two of which are vehicle seats, (the VIRTUAL OS Vehicle seat model and the VIRTUAL OS Chalmers lab seat model), and one booster seat model (the VIRTUAL OS Booster seat model). They are openly available and can be downloaded from the VIRTUAL OpenVT platform. In addition, three Concept seat models were developed and used in two of the simulation sub-studies.

References

- Andersson M, Bohman K, Osvalder A-L (2010). Effect of booster seat design on children's choice of seating positions during naturalistic riding. The 54th AAAM Annual Conference, *Annals of Advances in Automotive Medicine (AAAM)*, Vol 54:171-80
- Arbogast KB, Ghali Y, Menon RA, Tylko S, Tamborra N, Morgan R (2005). Field investigation of child restraints in side impact crashes. *Traffic Inj Prev*. Vol 6:4, pp351–360
- Arbogast K, Jermakian JS, Kallan M, Durbin DR (2009). Effectiveness of belt positioning booster seats: an updated assessment. *Pediatrics* 124, pp1281 –1286
- Beillas P, Giordano C, Alvarez V, Li X, Ying X, Chevalier MC, Kirscht S, Kleiven S (2016). Development and performance of the PIPER scalable child human body models. *14th Int. Conf. Protection of Children in Cars*, Munich, Germany, Dec 2016
- Bendjellal F, Scicluna G, Frank R, Grohspietsch M, Whiteway A, Flood W, Marsilia R (2011). Applying side impact cushion technology to child restraint systems, *Proc of 22nd Int. ESV Conf.*, Paper no. 11-0138, Washington DC, USA, June 2011
- Bohman K, Rosén E, Sunnevang C, Boström O. (2009) Rear seat occupant thorax protection in near side impacts. The 53rd AAAM Annual Conference, *Annals of Advances in Automotive Medicine* 53, October 2009: 3-12.
- Bohman K, El-Mobader S, Jakobsson L (2021). Reclined seating in frontal impacts – a simulation study using PIPER 6y. *19th Int. Conf. Protection of Children in Cars*, Dec 2021
- Burdi AR, Huelke DF, Snyder RG, Lowrey GH (1968). Infants and children in the adult world of automobile safety design: Pediatric and anatomical considerations for design of child restraints. *J. Biomechanics*, Vol. 2, pp267-280
- Carlsson A, Linder A, Davidsson J, Hell W, Schick S, Svensson M (2011). Dynamic kinematic responses of female volunteers in rear impacts and comparison to previous male volunteer tests. *Traffic Inj Prev* 12(4), 347-357.
- Davidsson J, Deutscher C, Hell W, Linder A, Lövsund P, Svensson MY (1998). Human volunteer kinematics in rear-end sled collisions. *IRCOBI Conf. Gothenburg, Sweden*
- DeSantis Klinich K, Pritz HB, Beebe MB, Welty KE (1994). Survey of older children in automotive restraints. *Proc. 38th Stapp Car Crash Conf. SAE-942222*, pp245- 264
- Euro NCAP (2019). The dynamic assessment of car seats for neck injury protection testing protocol. Version 4.1 November 2019 <https://cdn.euroncap.com/media/57828/euro-ncap-whiplash-test-protocol-v41.pdf>
- Forman J, Lopez-Valdes F, Lessley D, Kindig M, Kent R, Ridella S, Bostrom O (2009). Rear seat occupant safety: an investigation of a progressive force-limiting, pretensioning 3-point belt system using adult PMHS in frontal sled tests. *Stapp Car Crash J*, Vol 53, pp49- 74
- Genzel J, Carlsson A, Linder A, Pipkorn B, Svensson M. (2022) An Open-source Finite Element model of a generic car seat: Development and validation for low-severity rearimpact evaluations. *IRCOBI Conf.*, Porto, Portugal
- Giordano C, Li X, Kleiven S (2017). Performances of the PIPER Scalable Child Human Body Model in Accident Reconstruction. *PLoS One*:12(11): e0187916.
- Jakobsson L, Isaksson-Hellman I, Lundell B (2005). Safety for the growing child – Experiences from Swedish accident data. *Proc of 19th Int. ESV Conf.*, Paper No. 05-0330, Washington DC, USA
- Jakobsson L, Isaksson-Hellman I, Lindman M (2008). WHIPS (Volvo Cars' Whiplash Protection System) – The Development and Real-World Performance. *Traffic Inj Prev* 9:6, 600-605

- Jakobsson L, Bohman K, Svensson M, Wimmerstedt M (2017). Rear seat safety for children aged 4-12: Identifying the real-world needs towards development of countermeasures, *Proc of 25th Int. ESV Conf.*, Paper no. 17-0088, Detroit, USA, June 2017
- Jakobsson L (2017). Rearward-facing child seats – past, present and future, *15th Int. Conf. Protection of Children in Cars*, Munchen, Germany, Dec 2017
- John J, Klug C, Erlinger N, Svensson M, Thomson R, Svenning E, Krasna S, Kranjec M, Trajkovski A, Levallois I, Recko P, et al. (2021). Validated seated OS-HBM models published on the OpenVT platform and described in scientific paper, *Deliverable D2.2 of the H2020 project VIRTUAL*.
- Jones MLH, Ebert S, Manary MA, Reed MP, Klinich KD (2020). Child posture and belt fit in a range of booster configurations, *Int. J. Environ. Res. Public Health*, 17,810, doi:10.3390/ijerph17030810
- Karemyr M, Pettersson T, Svensson, M, Linder A (2022). Seat Evaluation Tools (SETs) Development of prototype concepts of the SETs of an average female and male for low severity rear impact crash testing. *VTI report 1147A*.
- Kang YS, Stammen J, Ramachandra R, Agnew AM, Hagedorn A, Thomas C, Kwon HJ, Moorhouse K, BolteIV JH (2020). Biomechanical responses and injury assessment of post mortem human subjects in various rear-facing seating configurations. *Stapp Car Crash Journal*, pp155-212
- Kleinbach (2019). Simulation of Occupant Kinematics using Active Human Body Models. *Doctoral thesis, Institut für Technische und Numerische Mechanik der Universität Stuttgart*, Germany
- Leledakis A, Östh J, Iraeus J, Davidsson J, Jakobsson L (2022). The influence of occupant's size and shape in frontal and side impacts for varying seat positions, *IRCOBI Conf.*, Porto, Portugal
- Lemmen P, Gupta A, Lakshminarayana A, Carlsson A, Svensson M, Schmitt K-U, Levallois I, Linder A, Tomasch E (2013). Seat optimisation considering reduction of neck injuries for female and male occupants – Applications of the EvarID model and a loading device representing a 50th percentile female. *23rd Int. ESV Conf.* Paper no. 13-0220, Seoul, Korea, May 2013
- Linder A, Svedberg W (2019). Review of average sized male and female occupant models in European regulatory safety assessment tests and European laws: Gaps and bridging suggestions, *Accident Analysis & Prevention*, Volume 127, pp 156-162, <https://doi.org/10.1016/j.aap.2019.02.030>.
- Linder A, Schick S, Hell W, Svensson M, Carlsson A, Lemmen P, Schmitt K-U, Gutsche A, Tomasch E (2013). ADSEAT – Adaptive seat to reduce neck injuries for female and male occupants. *Accident Analysis & Prevention*, Volume 60, pp 334-343. <https://doi.org/10.1016/j.aap.2013.02.043>
- Mertz HJ, Irwin AL, Prasad P (2003). Biomechanical and scaling bases for frontal and side impact injury assessment reference values, *Stapp Car Crash Journal*, Vol. 47 (October 2003), pp 155-188
- Norin H, Saretok E, Jonasson K, Andersson Å, Kjellberg B, Samuelsson S. (1979) Child Restraints in Cars – An Approach to Safe Family Transportation. *SAE Congress and Exposition*, SAE-790320, SAE International, Warrendale, PA, USA
- Ono K, Ejima S, Yamazaki K, Sato F, Pramudita JA, Kaneoka K, Ujihashi S (2009). Evaluation criteria for the reduction of minor neck injuries during rear-end impacts based on human volunteer experiments and accident reconstruction using human FE model simulations. *IRCOBI Conf.*, UK
- Reed MP, Ebert SM (2018). Effects of recline on passenger posture and belt fit. UMTRI-2018-2. *Univ of Michigan Transportation Research Institute (UMTRI)*, Ann Arbor, USA, Sept 2018
- Winjnen W, Bützer D, Elvik R, Pokorny P, Putra IPA (2022). Calculating the socio-economic costs and benefits of vehicle safety systems. Submitted to TRA Conference
- Wågström L, Bohman K, Lindman M, Laudon O, Tomasch E, Klug C, Schachner M, Levallois I, Recko P, Renaudin F, Salters E, Linder A, Gross J, Keller A, Schmitt K-U (2020). Impact scenarios and pre-crash seated positions for Automated Driving, *Deliverable D3.1 of the H2020 project VIRTUAL*.

Appendix A VIRTUAL OS Vehicle Seat Model

This Appendix is a compilation of the following VIRTUAL internal reports:

- *Seat models available to the project*, Milestone Report 3.3. of the H2020 project VIRTUAL (2020), by Linus Wågström and Edvin Eriksson Johansson (Volvo Cars) and Ines Levallois and Patryk Rećko (Faurecia)
- *Component tests of Toyota seats*, H2020 project VIRTUAL (2020), by Jonny Genzel (VTI)
- *Validation tests of the VIRTUAL open access car seat model*, the H2020 project VIRTUAL (2020), by Linus Trummler and Arne Keller (AGU)

The text was compiled by Lotta Jakobsson (Volvo Cars), supported by Arne Keller and Linus Trummler (AGU), and Linus Wågström and Jonas Östh (Volvo Cars)

1. Introduction

As a vital component of modern occupant restraint systems, car seats have a significant influence on the injury risk of seated vehicle occupants, particularly (but not only) in rear-end collisions. Moreover, modern car seats can be adjusted very precisely to each occupant's body shape. Therefore, for research on passenger injury risk using Finite Element (FE) models, high-quality models of vehicle seats are crucially important.

Although there are several numerical vehicle seat models, they are either proprietary or of too poor quality for the purpose of occupant injury risk assessment. Hence, the VIRTUAL project required a seat model that is available open access under the terms of the GNU Lesser General Public License (L-GPL) and can be adjusted to an ATD or an HBM. By releasing an open access seat model, the VIRTUAL project aims to reach a wider audience that can contribute to the success of virtual crash testing. Therefore, as part of WP3, an open access FE model of a vehicle seat was developed. The development and validation of the model was done as a collaborative task by the VIRTUAL beneficiaries Faurecia (scanning of physical seat), Volvo Cars (meshing), VTI (physical component tests for validation) and AGU (virtual tests for validation).

2. The Seat

A Toyota Auris seat was selected (Figure A1). The specifications of the seat include:

- Driver seat from Toyota Auris I phase 2 (2010-2012).
- Seat with manual height adjustment.
- Seat with manual longitudinal adjustment.
- Seat equipped with N03 seatback, 72020 cushion and fabric trim.
- Discontinuous recliner.

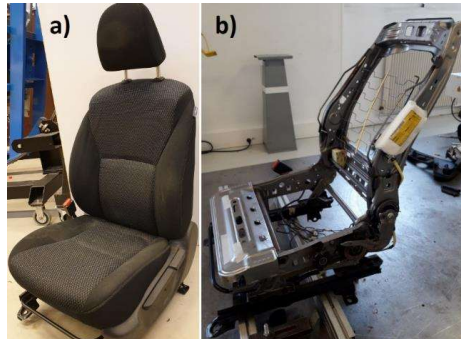


Figure A1. Toyota Auris seat a) complete seat, b) seat frame.

3. CAD Model

The first step of making the CAD model incorporated scanning a physical seat. The seat was scanned at the Faurecia facility in Brières, France. The seat was secured to the jig and digitised to a point cloud using a 3D Faro arm laser scanner. Surfaces (.step file) of the foams (Figure A2) and the seat frame (Figure A3) were generated. To further simplify the process of creating a CAD model, the scanned data was split into the following parts:

- Seatback, cushion and head-restraint foam
- Seatback side members
- Seatback upper cross member
- Seatback lower cross member
- Cushion side members
- Cushion seat pan
- Cushion reinforcing tubes
- Fixed and mobile gusset

All required measurements and pictures were also taken during the scanning session. Based on the data, a simplified CAD model of the seat was created using the Catia V5 software. To simplify the meshing process, the seat frame was modelled using surface geometry and the seat foam using solid geometry.

Although simplified in comparison to the real seat, the main construction geometry of the seat remains. Only details deemed to not have an impact on the overall performance of the seat were omitted, such as the seat tracks assembly, brackets between track and height adjuster system, recliners, head-restraint sleeves and interior parts, airbag and electric wires.

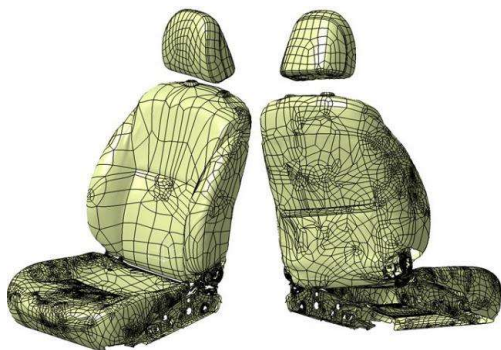


Figure A2. Complete seat scanned data.



Figure A3. Seat frame scanned data.

4. Meshing

Figures A4 and A5 show the complete seat CAD model and Table A1 shows the corresponding specifications. This, together with documentation on the design of the height adjuster system and suspension mats in addition to rivets, welds, screws and similar, provided the basis for meshing, targeting a numerically stable and efficient FE model in LS-DYNA format.



Figure A4. Complete seat CAD model.



Figure A5. Seat frame CAD model.

Table A1. Toyota Auris seat part thicknesses, corresponding to Figure A4 and A5.

Part name	Colour	Thickness
Upper cross member	Cyan	1,1 mm
Seatback side member	Blue	1,2 mm
Lower cross member	Violet	1,1 mm
Mobile gusset	Green	3 mm
Fixed gusset	Light brown	3 mm
Cushion side member	Yellow	2 mm
Cushion seat pan	Orange	1 mm
Cushion front tube	Red	2,2 mm
Cushion rear tube	Pink	2 mm
Height adjuster links	Dark blue	4 mm
Height adjuster bracket	Brown	2 mm
Height adjuster gear	Grey	Solid
Suspension mats metal parts	Dark grey	Solid
Suspension mats plastic parts	Dark green	0,5 - 1 mm

Aiming at a high-quality mesh, quality criteria such as element size, skewness, aspect, warp ratios and taper were measured and followed. A lower limit on the critical time step of 2E-4ms was fulfilled, in addition to the limit on added mass of maximum 10%.

The rail systems were imported from a public domain model of a Toyota car available at <https://www.ccsa.gmu.edu/models/>. The rail system was reshaped to fit the measurements on the actual seat regarding length and width. An overview of the FE model is shown in Figure A6.

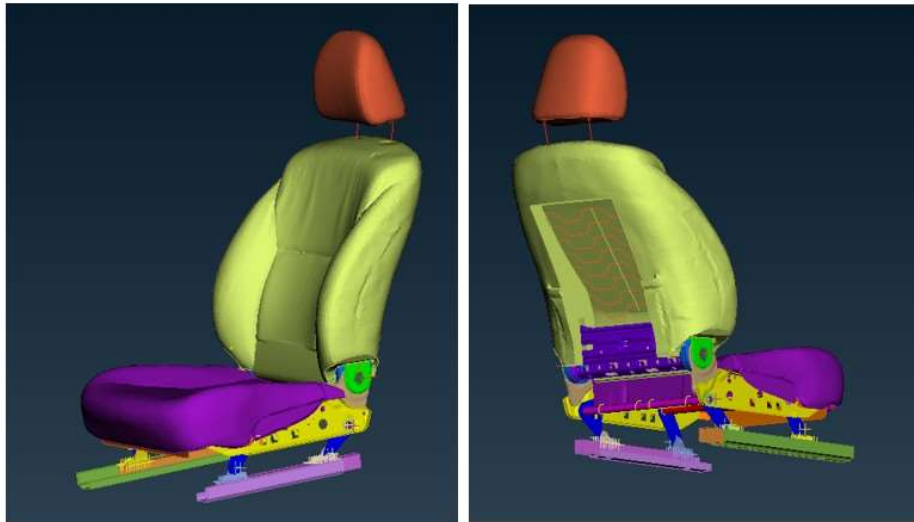


Figure A6. Overview of the FE model.

The head-restraint beam shape was created based on assumptions and shares nodes with surrounding solid foam elements in the head-restraint, see Figure A7.

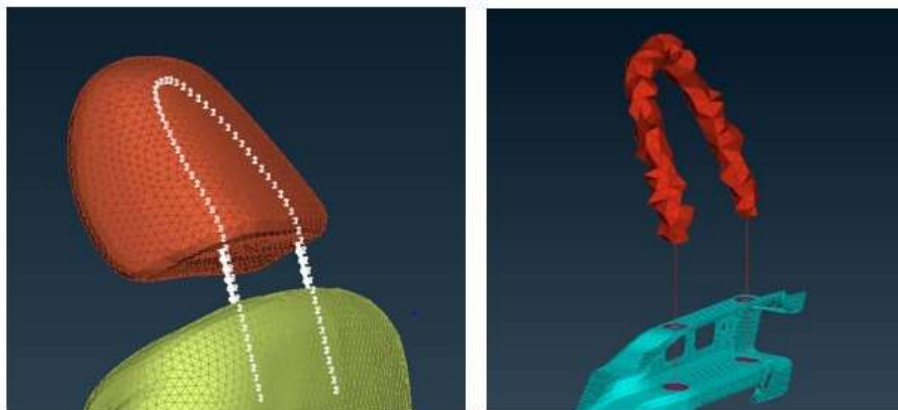


Figure A7. Head-restraint shape and neighbouring solid foam elements sharing nodes.

The cushion foam and seatback foam were morphed to stay tight around the metal members and spring mats for good contact between the parts (Figures A8 and A9).

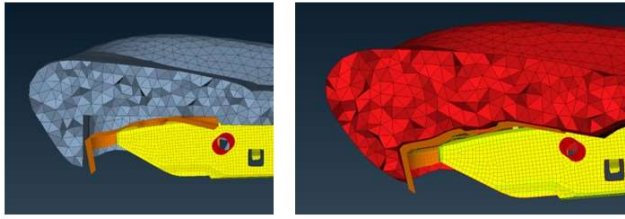


Figure A8. Example of tightening of foam around the seat pan and side members.

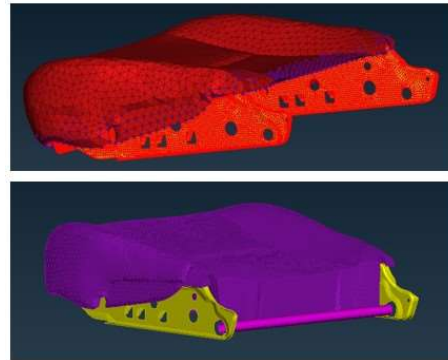


Figure A9. Example of cushion morphed thicker for better contact with the spring mat at and fastened in rear.

5. Properties and Mechanics

The metal and plastic parts were modelled as shell elements with material parameters set conforming to the OS Toyota model (Marzougui, Brown, Park, Kan, & Opiela, 2014). Tetrahedral solid elements were used for the seat foam, using material parameters suggested by Markert (2005).

Most metal parts are connected with spot welds or nodal rigid bodies, because the connection has been assumed to be very stiff. In order to connect the seat foam to the metal and plastic members, node-to-surface contacts were used. Revolution joints were used for the front and rear tubes together with rigid bodies. Rivets, spot welds and welds on gussets were all modelled as spot welds (Figure A10). Gussets were connected using rigid bodies around tilt mechanism and connected through a beam element with stiffnesses in all 6 degrees of freedom (DOF) (Figure A11). This enabled control of a response that is not fully rigid. Bolt connections and L brackets mounting onto rails that were assumed to be very stiff were modelled using nodal rigid bodies or extra nodes added to a part with rigid material.

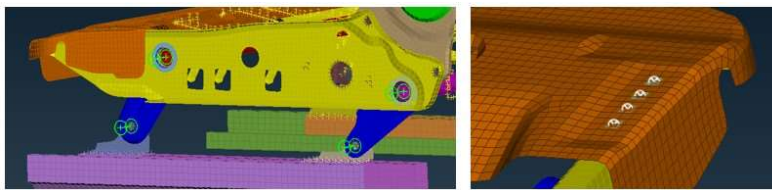


Figure A10. Used revolution joints and example of spot weld connections

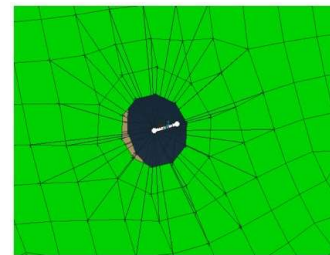


Figure A11. Seatback tilt connection. Beam element in white.

Node-to-surface contacts were added between the spring mats and the cushion and seatback foam. Skin nodes on the foam were modelled as tied offset contact to metal members, with a limited search distance, making the nodes of the solid elements that are close to the shell surface, attached onto the shell seat frame structure. The upper and lower rails were modelled with a similar contact allowing sliding, and the nodes that will be attached in a new position were updated.

Adjustments of seat height, seatback tilt, head-restraint position and longitudinal seat travel position were added in the model with kinetic joints in ANSA. A maximum and minimum limit on the seat height and longitudinal seat travel positions were set based on measurements. Head-restraint, seat height and

longitudinal seat travel positions were placed in the middle positions, on which the H-point measurements were set, and a marker was added to the model.

6. First Test Run of the Seat Model

To verify the numerical stability of the FE model, a simulation of the seat impacting into a rigid wall was used. The simulation verified that the included parts could handle high forces and behaved in accordance to the expected behaviour of a seat in such situation, see Figure A12.

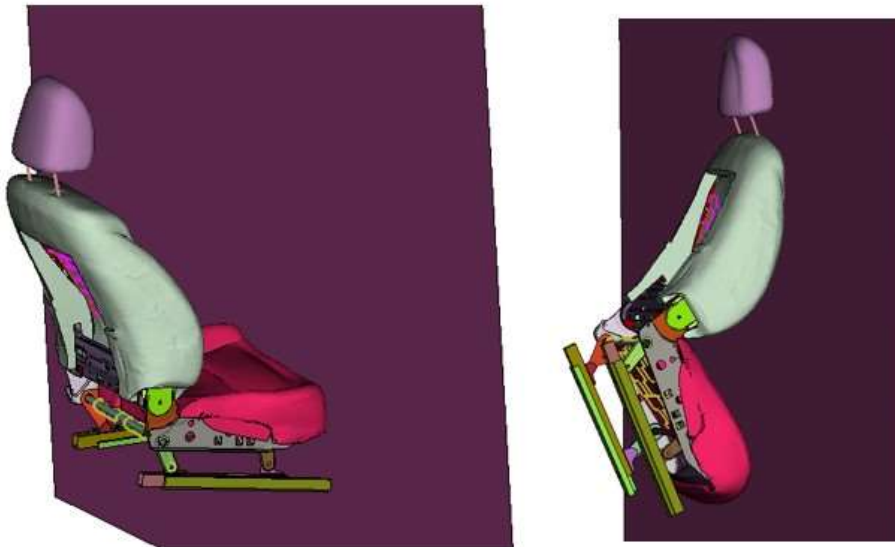


Figure A12. Test run simulation of the seat model impacting into a rigid wall; early time step (left) and later time step (right).

7. Validation of the FE Seat Model using Impactor Tests

As a validation of the dynamic behaviour of the numerical seat model and its components, a set of impact tests with different impactors, impact speeds and impact locations were performed.

Physical Tests

A test series of physical impactor tests were performed by VTI in Linköping, Sweden, to serve as platform for validation of the seat model. The seat was fixated to a steel plate that could be inclined to different angles (called 'mousetrap'), enabling a position perpendicular to the direction of travel of the impactor, allowing the correct location to be impacted. In order to resemble the driving position in a Toyota car, the seat was arranged and positioned on the 'mousetrap' accordingly. All impactors were instrumented with an accelerometer recording the resultant acceleration at 250 Hz. In addition, the test was monitored with high speed video in order to observe the deformation of the seat and the rebound trajectory of the impactor, see Figure A13 for one of the tests.

A combination of five different impact positions (Figure A14) using four different impactors at varied speed based on impactor drop height (Figure A15) were included, see test configurations in Table A2. The 17 test configurations were repeated three times and at three different heights, resulting in a total of 153 tests.

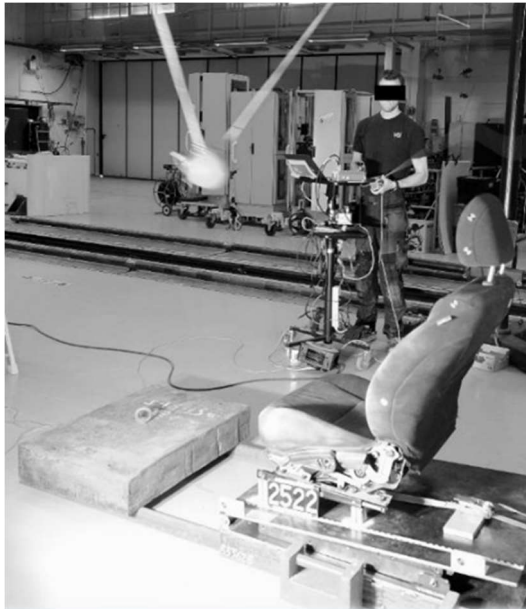


Figure A13. Pendulum test setup for test with Impactor 3. The seat is attached to the 'mousetrap'.



Figure A14. Impact positions at the physical test.

**Drop Test
Impactor 1**
Weight: 2.8 kg
Height: 0.25-0.50 m



**Pendulum
Impactor 2**
Weight: 4.6 kg
Height: 0.50-1.50 m



**Pendulum
Impactor 3**
Weight: 6.8 kg
Height: 0.50-1.50 m



**Pendulum
Impactor 5**
Weight: 22.8 kg
Height: 0.50-1.50 m



Figure A15. The impactors used in the physical tests. Impactor 1 was used in a drop test while Impactors 2, 3 and 5 were used in a pendulum setup.

Table A2. Test configurations

Test no.	Test type	Seat no.	Impactor no.	Impactor mass (kg)	Drop height (m)	Impact position
1	Drop test to seat cushion	1	1	2.8	0.25, 0.4 and 0.5	B
2	Drop test to seat cushion	2	1	2.8	0.25, 0.4 and 0.5	B
3	Drop test to seatback	1	1	2.8	0.25, 0.4 and 0.5	D
4	Drop test to seatback	2	1	2.8	0.25, 0.4 and 0.5	D
5	Pendulum to seat cushion	1	2	4.6	0.5, 1.0 and 1.5	A
6	Pendulum to seat cushion	2	2	4.6	0.5, 1.0 and 1.5	A
7	Pendulum to seatback	1	2	4.6	0.5, 1.0 and 1.5	C
8	Pendulum to seatback	2	2	4.6	0.5, 1.0 and 1.5	C
9	Pendulum to seat cushion	1	3	6.8	0.5, 1.0 and 1.5	A
10	Pendulum to seat cushion	2	3	6.8	0.5, 1.0 and 1.5	A
11	Pendulum to seatback	1	3	6.8	0.5, 1.0 and 1.5	C
12	Pendulum to seatback	2	3	6.8	0.5, 1.0 and 1.5	C
13	Pendulum to head-restraint	1	3	6.8	0.5, 1.0 and 1.5	E
14	Pendulum to head-restraint	2	3	6.8	0.5, 1.0 and 1.5	E
15	Pendulum to seat cushion	4	5	22.8	0.5, 1.0 and 1.5	A
16	Pendulum to seatback	3	5	22.8	0.5, 1.0 and 1.5	C
17	Pendulum to seatback	4	5	22.8	0.5, 1.0 and 1.5	E

The Numerical Environment

LS-PrePost 4.7.0 (Livermore Software Technology Corporation) was used for any changes to the seat model. The simulation itself was calculated using a double precision massively parallel processing (MPP) version of the LS-DYNA 10.1 solver (suse102_pgi165_sse2_platformmpi).

Changes to the seat model

At the start of the simulation study for this work, it became evident that the version of the seat model available at that time still had a number of numerical instabilities which required to be corrected before running the simulations. Furthermore, some parts of the seatback and seat cushion (foam and wire spring mats) were diverging substantially from the geometry of the physical seat. These had to be re-scanned in order to replicate the physical seat realistically.

It is generally considered good practice not to make further changes to a numerical model during the validation. However, due to the limited resources of the project, it was not possible to follow a strict development-verification-validation workflow. Therefore, we decided to relax this rule to some extent in order to obtain a useful model within the project duration. It shall be stressed, nevertheless, that no parameters were calibrated in order to match the validation tests; all modifications of the seat model were based on measurements and observations on the physical seat.

Numerical Tests

An overview of the test series, including test type, impactors and impact locations, used for the simulations are shown in Figure A3. The main information used from the physical tests were the resultant acceleration filter with cfc300 and the high-speed video footage. After examination of the high-speed recordings, some unintended movements of the setup could be observed. This mainly concerned Test Series 3001-3009, 3101-3109, and 3110-3119, where the whole setup including the seat, 'mousetrap' and the fixation, moved for a short moment during the impact. In the physical tests with the more lightweight impactors (1, 2 and 3), the unintended motions were limited to small movements at the hinges (Test Series 1701-1709 and 1801-1809); the support pillars (Test Series 1819-1827 and 1901-1909) and oscillation of the 'mousetrap'. As opposed to that, the tests of series 1601-1609 and 1910-1918 were, within the limits of what can be detected in the high-speed videos, free of additional movements of the support structure.

Table A3. Test series for numerical comparison.

Test Series	Test type	Seat no.	Impactor mass (kg) + (no.)	Impact position
1601-1609	Impactor 1 to seat cushion	1	2.8 (1)	B
1910-1918	Impactor 1 to seatback	1	2.8 (1)	D
1901-1909	Impactor 2 to seat cushion	1	4.6 (2)	A
1701-1709	Impactor 2 to seatback	1	4.6 (2)	C
1819-1827	Impactor 3 to seat cushion	1	6.8 (3)	A
1801-1809	Impactor 3 to seatback	1	6.8 (3)	C
1810-1818	Impactor 3 to head-restraint	1	6.8 (3)	E
3101-3109	Impactor 5 to seat cushion	1	22.8 (5)	A
3001-3009	Impactor 5 to seatback	1	22.8 (5)	C
3110-3118	Impactor 5 to seatback	1	22.8 (5)	D

The five impact positions (A, B, C, D and E) for the simulations are shown in Figure A16. The numerical impactor models are shown in Figure A17. All impactors were modelled as rigid bodies and matched the physical impactors in size, weight, and inertial properties, with masses ranging from 2.8 kg to 22.78 kg.



Figure A16. The five impact locations.

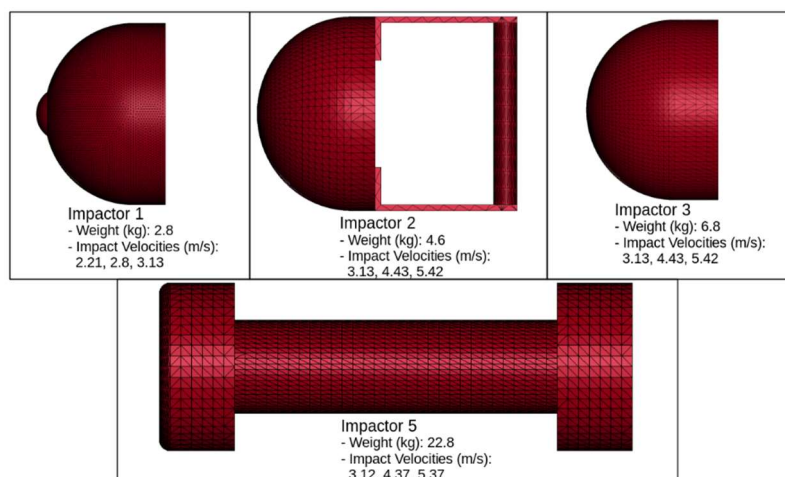


Figure A17. The meshed impactor devices.



A numerical version of the 'mousetrap' was built. It consisted of a 10 mm thick plate of dimensions 1,015 mm x 700 mm. Material MAT_024_PIECEWISE_LINEAR_PLASTICITY with the properties of steel¹ was used. Additionally, two hinges were modelled as front support. The welded parts of the physical mousetrap were simulated with virtually fixed single point constraint nodes. The seat model was fixated on the mousetrap with several spotweld elements. As in the physical tests, the fore-aft locking position, height adjustment, seatback and seat cushion tilt were adjusted according to the EuroNCAP protocol (EuroNCAP, 2021).

With the help of orientation markers on the physical seats and impactors, the coordinates of the impact locations were calculated. The impactors were translated to the corresponding positions and lifted by an additional 5mm from the seat surface to prevent any initial penetration.

The impact velocity was applied with the *INITIAL_VELOCITY_RIGID_BODY command. The impactors were constrained to move only along an axis perpendicular to the seat cushion at the impact location. In order to hit the seat cushion perpendicularly, the mousetrap was rotated to different angles according to the impact location. For the contact between the seat skin and the impactor, an *AUTOMATIC_SURFACE_TO_SURFACE contact was used.

In the numerical model, the longitudinal acceleration of the impactor during the impact on the seat was recorded with the *DATABASE_HISTORY_NODE keyword applied to a node at the centre of mass of the impactor. The data were extracted and plotted using the Dynasaur and Matplotlib Python packages.

Each experimental test was compared to the corresponding numerical test. In order to assess the agreement of the acceleration curves, an objective rating metric according to ISO18571 was calculated. ISO18571 defines the following grades for the overall rating (OR) results as:

- OR > 0.94 → Excellent
- 0.80 < OR ≤ 0.94 → Good
- 0.58 < OR ≤ 0.80 → Fair
- OR ≤ 0.58 → Poor

¹ Mass Density: 7.89e⁶ kg/mm³, E-Module: 210 GPa, Poisson-Ratio: 0.3



Results

Tables A4 and A5 provide summaries on grades and mean OR, for overall, with/without Impactor 5 and for each impact location, respectively. Mean OR of each test series are presented in Table A6. Each test series was replicated by one numerical test and the mean was computed over the three tests of the series. Figures A18-A27 provide plots on comparison of the numerical and the physical tests. In these plots, the blue lines represent the unfiltered longitudinal acceleration extracted from the numerical model, while the orange, black and grey lines illustrate the cfc300 filtered results of the physical tests. The OR for each test is included in the plots.

Table A4. Grades of the overall rating of all tests combined

Grades	Occurrence Overall	Occurrence (Impactor 5 excluded)	Occurrence (only Impactor 5)
Excellent	0	0	0
Good	27	23	4
Fair	55	35	20
Poor	7	4	3
Mean Overall Rating	0.734	0.756	0.685

Table A5. Grades of the overall rating and mean overall rating according to different impact locations (Impactor 5 excluded).

Grades/Rating	Impact location A	Impact location B	Impact location C	Impact location D	Impact location E
Excellent	0	0	0	0	0
Good	0	9	10	1	3
Fair	14	0	8	7	6
Poor	3	0	0	1	0
Mean Overall Rating	0.687	0.893	0.763	0.703	0.784



Table A6: Mean overall ratings of all test series. Each test series is replicated by one numerical test and the mean is computed over the three tests of the series.

Test Series	Mean overall rating	Grade
1601-1603	0.88	Good
1604-1606	0.89	Good
1607-1609	0.90	Good
1910-1912	0.63	Fair
1913-1915	0.74	Fair
1916-1918	0.74	Fair
1901-1903	0.52	Poor
1904-1906	0.69	Fair
1907-1909	0.72	Fair
1701-1703	0.80	Good
1704-1706	0.81	Good
1707-1709	0.82	Good
1819-1821	0.72	Fair
1822-1824	0.75	Fair
1825-1827	0.74	Fair
1801-1803	0.87	Good
1804-1806	0.67	Fair
1807-1809	0.61	Fair
1810-1812	0.74	Fair
1813-1815	0.84	Good
1816-1818	0.77	Fair
3101-3103	0.77	Fair
3104-3106	0.75	Fair
3107-3109	0.71	Fair
3001-3003	0.74	Fair
3004-3006	0.78	Fair
3007-3009	0.79	Fair
3110-3112	0.38	Poor
3113-3115	0.61	Fair
3116-3118	0.63	Fair

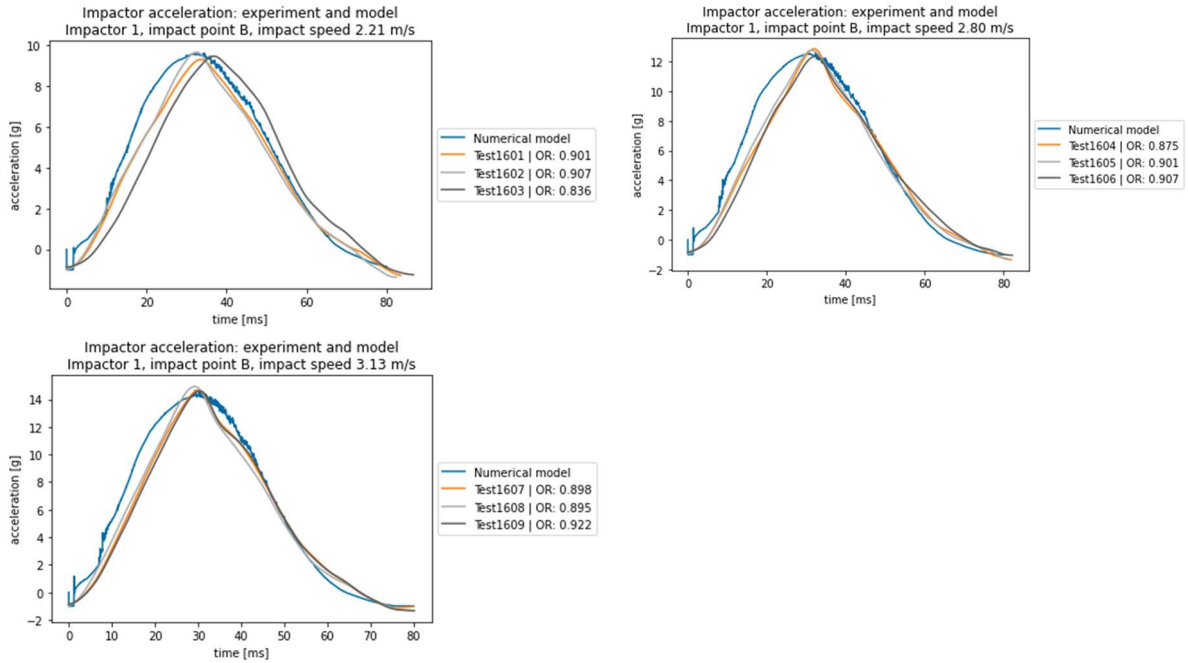


Figure A18. Comparison of the numerical model with the corresponding physical tests for Impactor 1 to seat cushion.

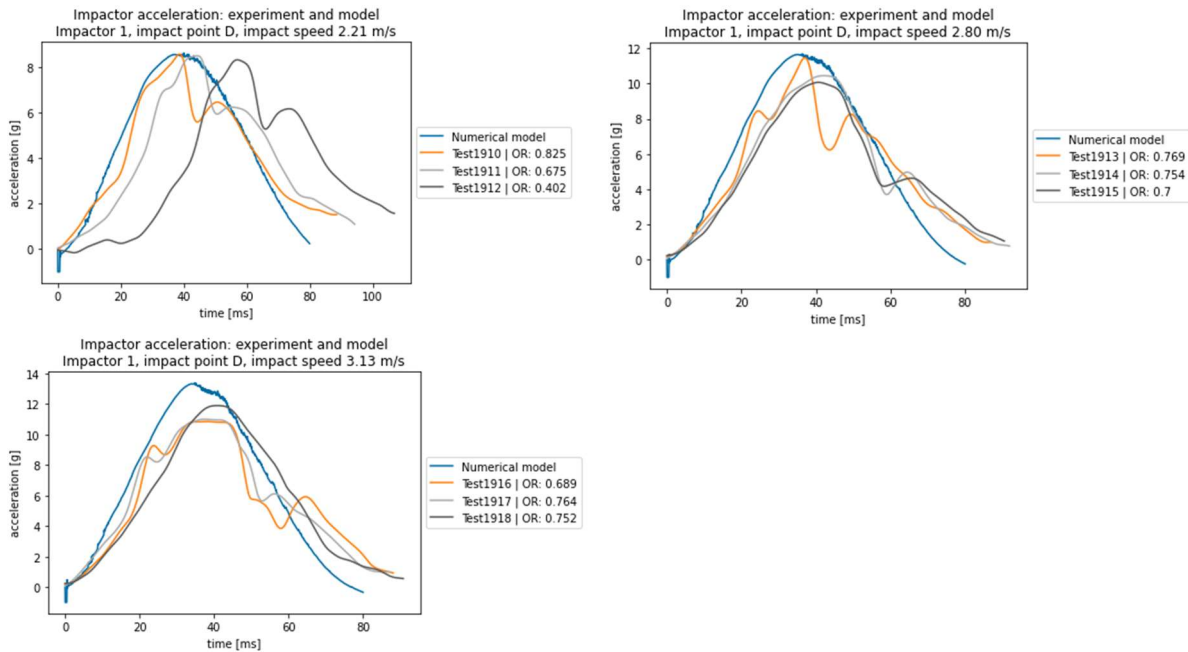


Figure A19. Comparison of the numerical model with the corresponding physical tests for Impactor 1 to seatback.

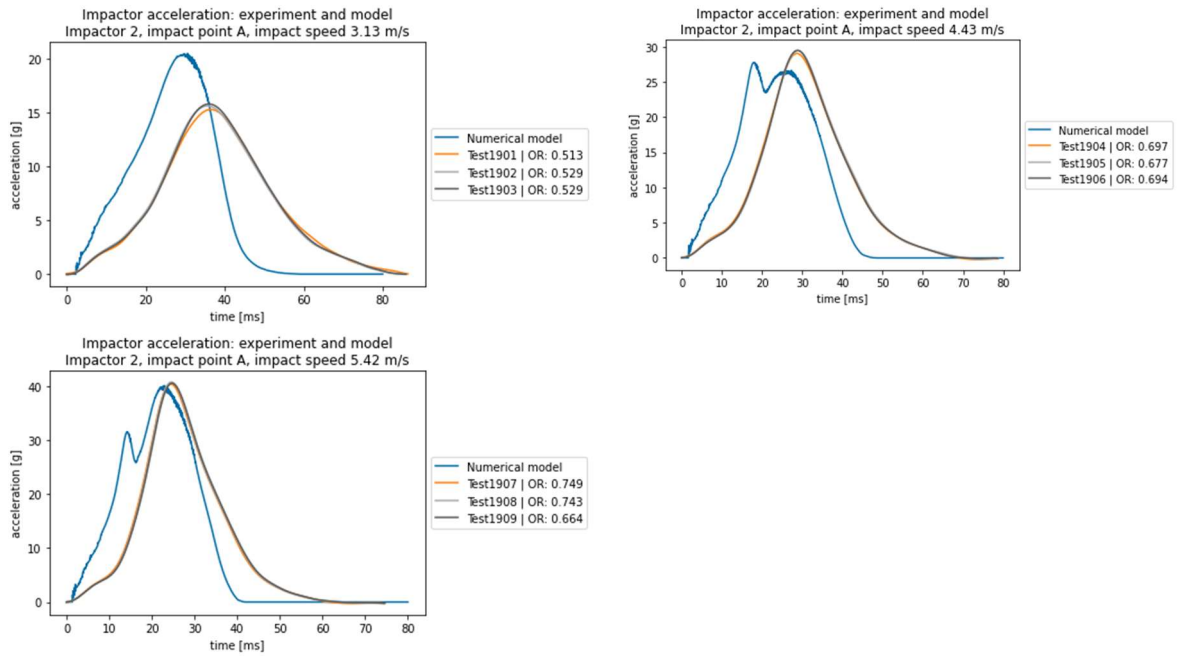


Figure A20. Comparison of the numerical model with the corresponding physical tests for Impactor 2 to seat cushion

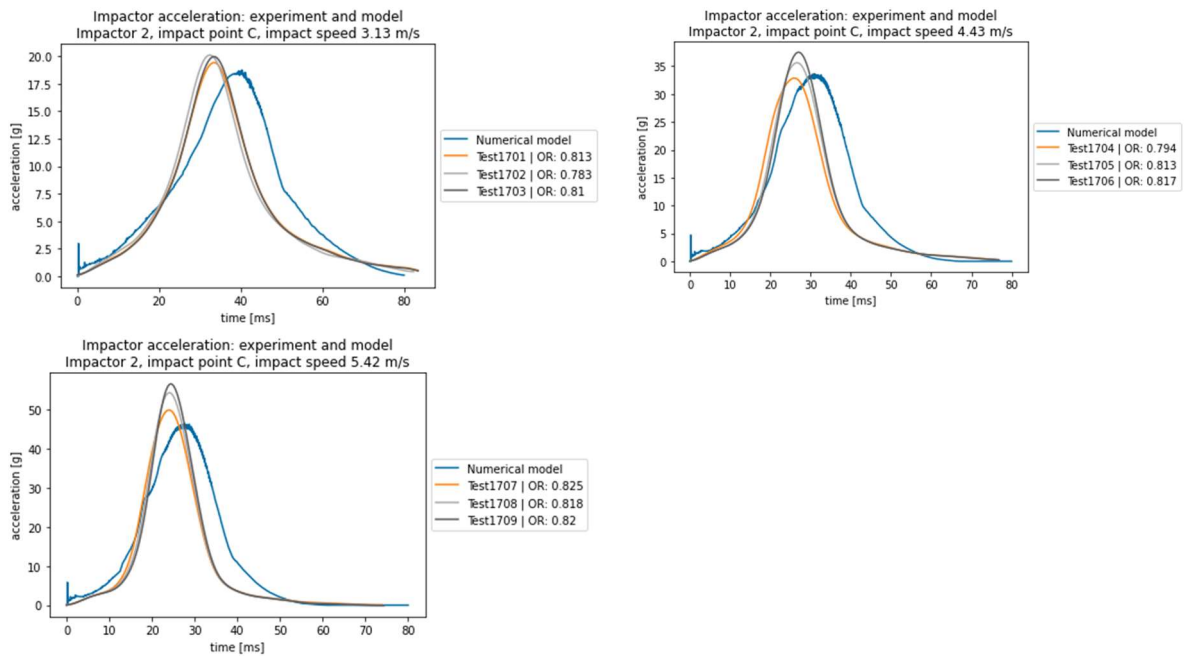


Figure A21. Comparison of the numerical model with the corresponding physical tests for Impactor 2 to seatback

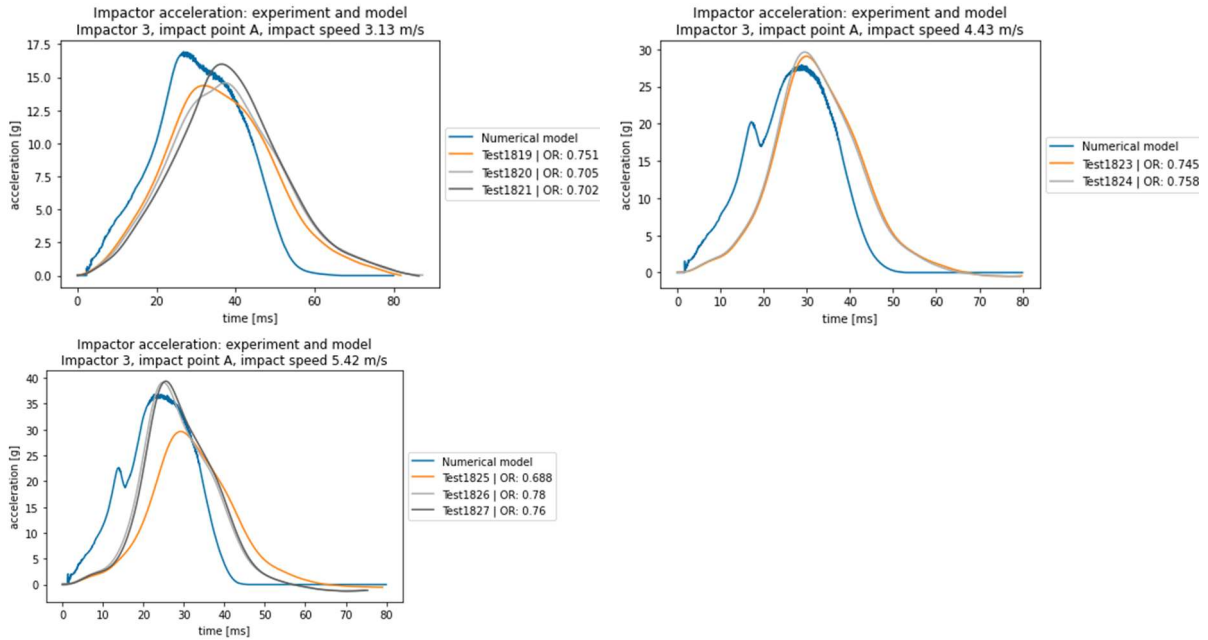


Figure A22. Comparison of the numerical model with the corresponding physical tests for Impactor 3 to seat cushion

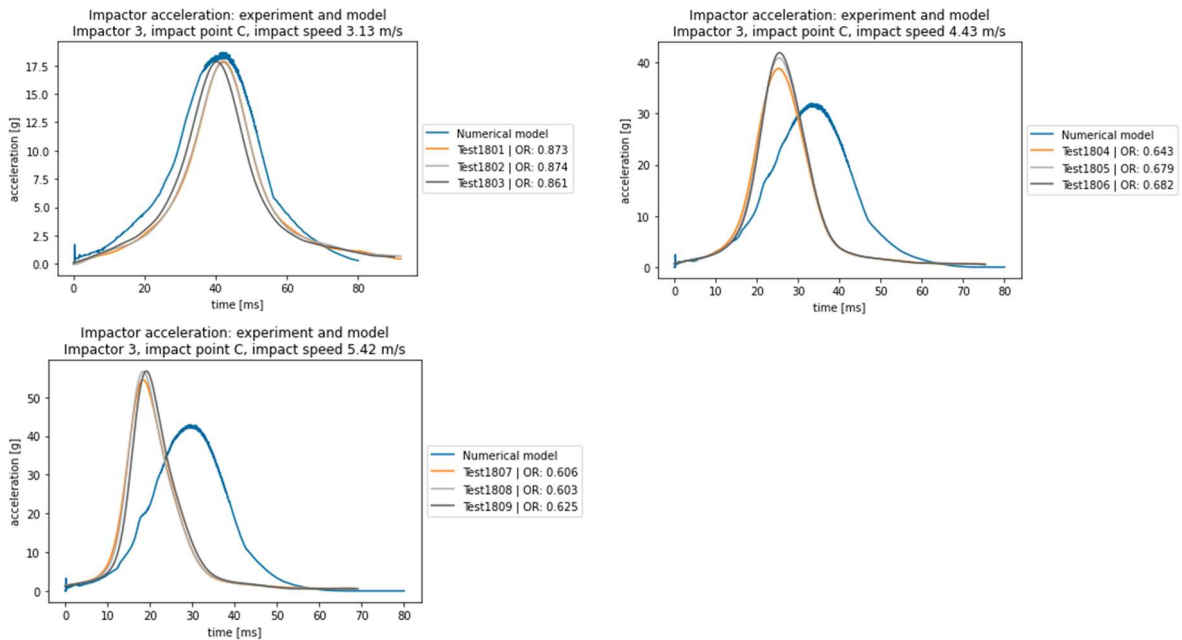


Figure A23. Comparison of the numerical model with the corresponding physical tests for Impactor 3 to seatback

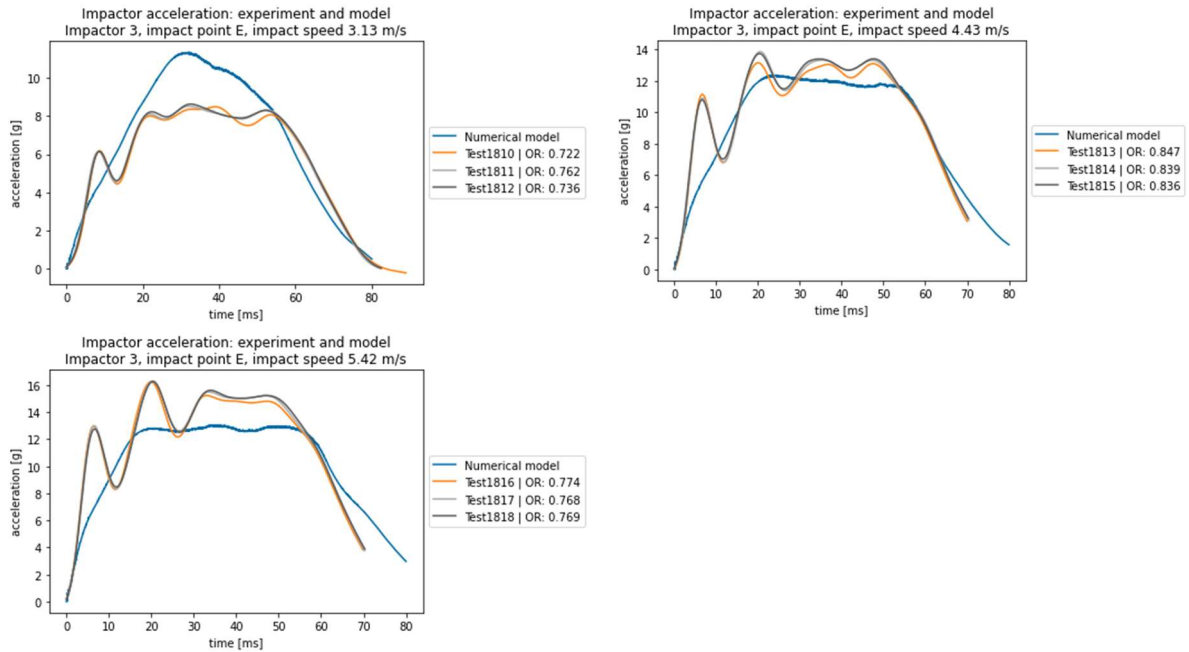


Figure A24. Comparison of the numerical model with the corresponding physical tests for Impactor 3 to head-restraint

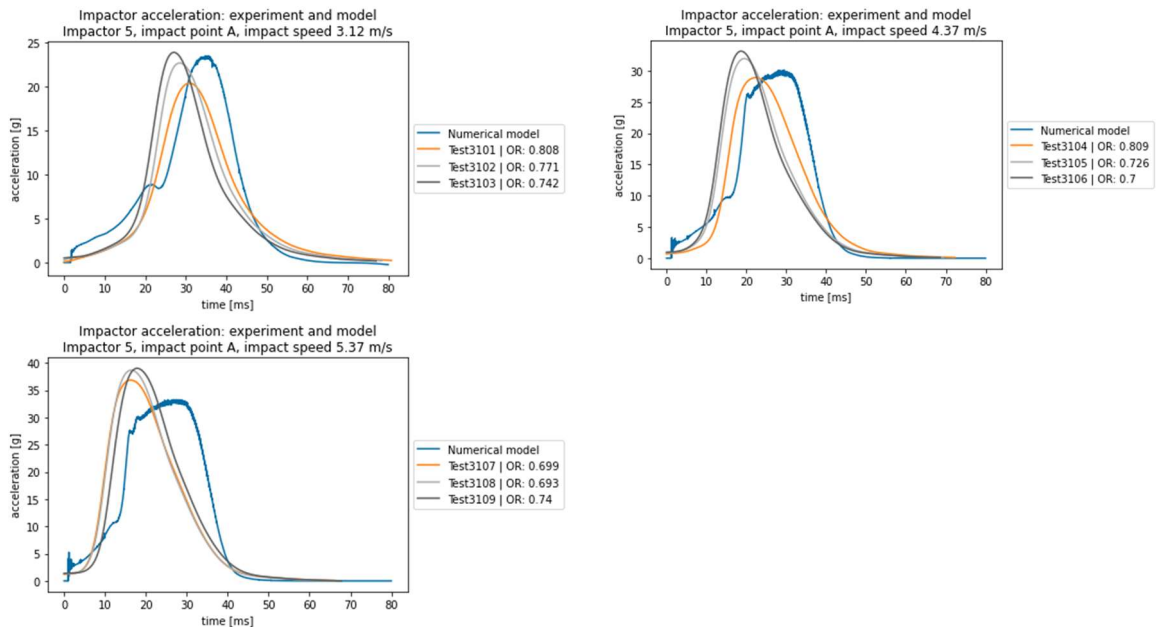


Figure A25. Comparison of the numerical model with the corresponding physical tests Impactor 5 to seat cushion

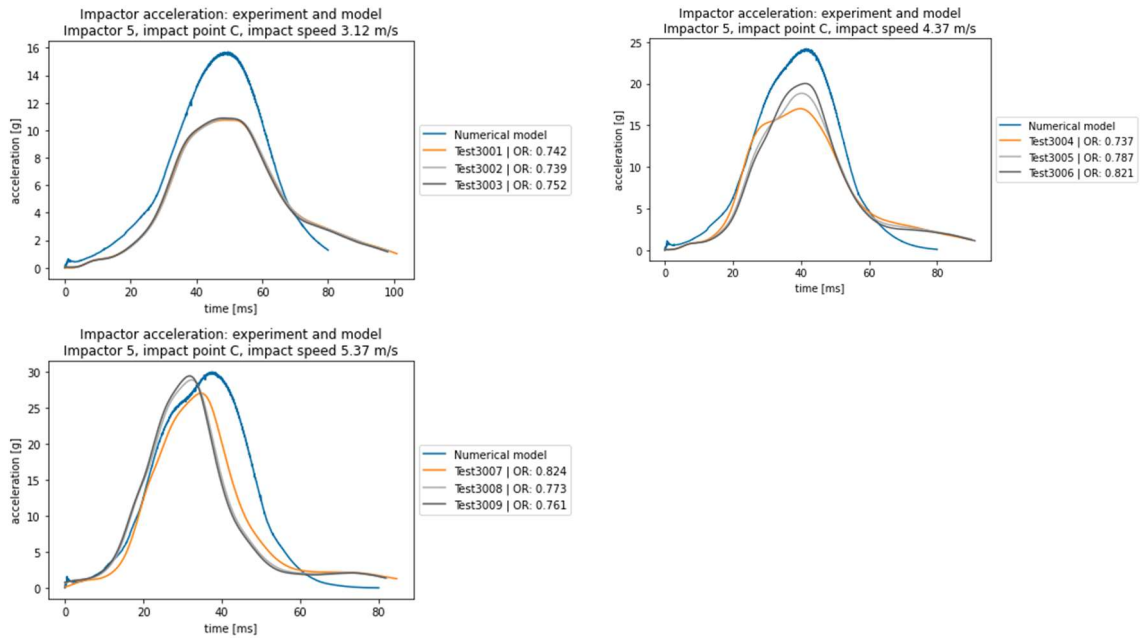


Figure A26. Comparison of the numerical model with the corresponding physical tests for Impactor 5 to seatback

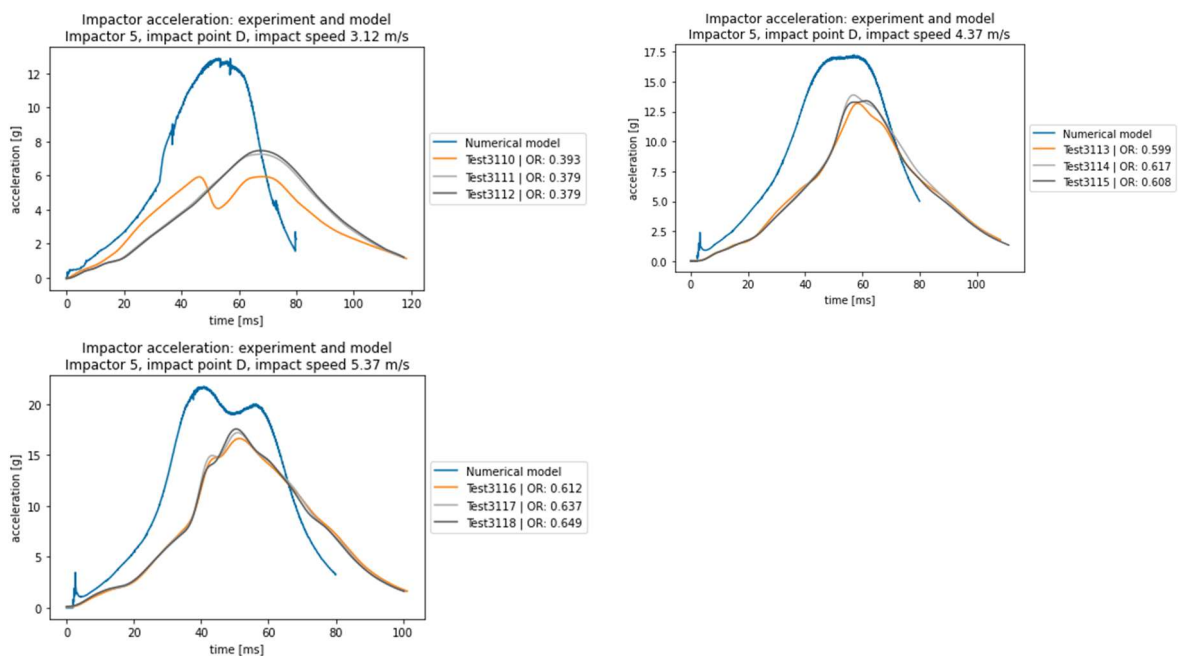


Figure A27. Comparison of the numerical model with the corresponding physical tests for Impactor 5 to seatback

Visual inspection of the seat model after impact revealed considerable permanent deformation of some parts of the seat. At Impact Location A, the cushion seat pan (brown) was deformed during the impacts at the highest speed (Figure A28). Additionally, under the same impactor and velocity conditions, the

lower cross member (light red) at Impact Location C was deformed (Figure A29). Similar permanent deformation was detected in the seat after exposure to the physical tests (Figures A28 and A29).

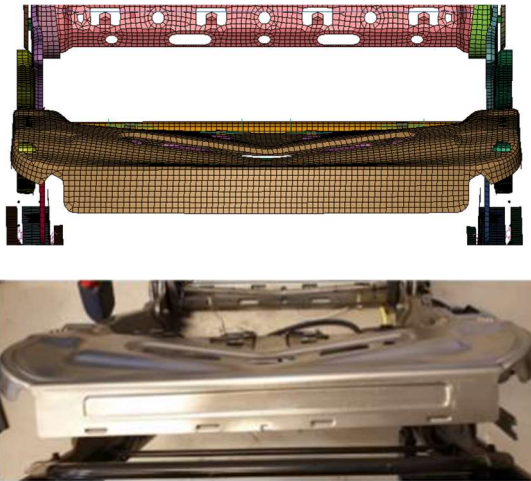


Figure A28. Front view. Top: after simulation of tests 1825-1827 (Location A, Impactor 3, 5.42 m/s). The brown part represents the deformed seat cushion pan. Bottom: Rear view photo of Seat No. 1 after finalisd tests.

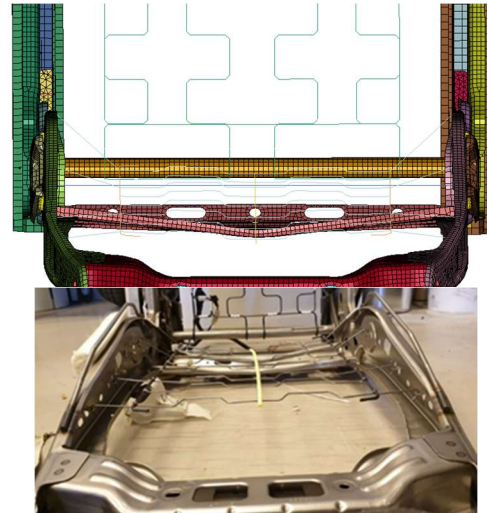


Figure A29. Top view, after simulation of tests 1807-1809 (Location C, Impactor 3, 5.42m/s). The light red part represents the deformed lower cross member. The photo is of Seat No. 1 after finalised tests.

8. Discussion

Throughout all physical tests, more or less prominent motion and oscillation of the 'mousetrap' were visible in the high-speed videos, the effects of which in the measured acceleration signals are superposed on the reaction of the seat structure. For the tests with the more lightweight impactors 1,2 and 3, these motions were less prominent and could be reproduced in the numerical tests with a detailed numerical model of the 'mousetrap', hence a comparison of the numerical and physical results was meaningful. In the tests with the heaviest impactor (Tests 3001-3009, 3101-3109 and 3110-3119), the 'mousetrap' sometimes actually lifted for a short moment. This effect would be very tricky to reproduce reliably in a numerical model. The mean OR also reflects this problem, where the results of the tests with Impactor 5 show lower ratings than those with the lighter impactors. Hence, the tests with Impactor 5 have been assumed unfit for validation purposes and the results are only shown for the sake of completeness. In future validation experiments, this problem should be avoided in order to provide a more reliable database.

In the remaining tests, with a mean rating of 0.756 and all but four out of 62 tests being rated either "fair" or "good", a reasonable agreement between the numerical model results and the physical tests were observed. However, in comparison to the physical tests, the numerical model tended to overestimate the acceleration for lower impact speeds, while underestimating the acceleration for higher speeds. This behaviour is apparent, i.e., in Test Series 3001-3009 and 1801-1809. This effect might be caused by the foam model (or at least its parameters) not replicating the foam behaviour on short time scales in a completely satisfactory way. In order to rectify that problem, the foam behaviour should be considered in isolated rate dependent deformation experiments, a task which was beyond the scope of the present validation study.

The agreement of physical and numerical tests also varies for the different impact locations. Particularly Locations A and D received lower overall ratings than the other locations, which may be due to higher torques transmitted to the recliner joint in these loading conditions. This hypothesis is corroborated by



the fact that in an earlier version of the model with an unrealistically soft recliner joint, the effect was even more prominent. On the other hand, it is unclear why Location E, which is the furthest away from the recliner joint, seems not to be affected by this problem. This issue, in addition to the behaviour of the recliner joint in general, should be investigated further in future research and applications. Nevertheless, with most ratings being in the “Fair” or “Good” categories even for impact Locations A and D, this problem is far from a severe shortcoming of the seat model.

In high-speed impacts, the numerical seat model shows considerable permanent deformation of some parts of the seat. Similar deformation was also observed in the physical tests. However, it is unknown at which point in time the deformation occurred in the physical tests. Hence, it is possible, that some physical tests were carried out with an already partly damaged seat. Given that the agreement of the physical and numerical tests is good overall even for the tests later in the series, the effect of permanent deformation on the test results seems to be rather insignificant. However, should a more precise validation of the model be required in the future, we recommend checking the seat for damage after each test run.

9. Conclusion

This work describes the validation of the VIRTUAL OS Vehicle seat model, a numerical model of a Toyota Auris driver seat (model year 2010-2012). Multiple impactor tests were performed on the physical seat, which were subsequently replicated in a virtual environment. The results of the numerical and physical tests were compared in terms of the acceleration experienced by the impactors and permanent deformation observed in the seat frame. Due to limitations in the experimental setup, only parts of the experimental tests could be taken into account, as some tests with the heaviest impactors induced strong unintended motions of the laboratory setup which contaminated the accelerometer data. For the reliable parts of the data set, the seat model was capable of reasonably reproducing the measured acceleration curves both in terms of shape and magnitude, as shown by a mean ISO overall rating in the “fair” category. Also, the observed permanent deformation closely matched any observed deformation in the experiment. Some minor deficiencies remain to be rectified, namely in the foam model and in the implementation of the recliner joint.

Overall, it can be concluded that the VIRTUAL OS Vehicle seat model in its current state already provides a fairly realistic replication of its physical counterpart in loading conditions similar to the validation experiments, readily applicable in research on occupant safety. As the first high-resolution seat model available open access, it closes an important gap in VIRTUAL’s open access tool chain for virtual testing in vehicle safety. In the future, seated occupant load cases (particularly rear-end impacts) can be solved from pre- to post-processing completely with open access tools, which opens new possibilities of understanding injury mechanisms and creating safer vehicles.

10. References

- EuroNCAP (2021). The dynamic assessment of car seats for neck injury protection: Testing protocol. Version 4.1.1. <https://cdn.euroncap.com/media/67263/euro-ncap-whiplash-test-protocol-v411.pdf>
- Markert B (2005). Porous media viscoelasticity with application to polymeric foams. PhD dissertation, Universität Stuttgart, Germany. https://elib.uni-stuttgart.de/bitstream/11682/232/1/diss_markert600.pdf
- Marzougui D, Brown D, Park HK, Kann CD, Opiela KS (2014). Development & Validation of a Finite Element Model for a Mid-Sized Passenger Sedan. *Proceedings of the 13th International LS-DYNA Users Conference, Dearborn, MI, USA*. 2014:8–10

Appendix B VIRTUAL OS Booster Seat Model

This Appendix is a compilation of the following VIRTUAL internal reports:

- *Open source child seat models (2019)*, Milestone Report 3.4. of the H2020 project, VIRTUAL, by Damien Submit and Francois Renaudin (Dorel)
- *Scientific publication on child model applications in VIRTUAL (2021)*, Deliverable D2.3 of the H2020 project VIRTUAL, by Mats Svensson, Johan Iraeus and Lauren Meredith (Chalmers) and Linus Wågström (Volvo Cars), including a publication with co-authors Pooja Umeshkumar and Dag Thuvesen (CEVT).

The text was compiled by Lotta Jakobsson (Volvo Cars)

1. Introduction

The expectation that virtual testing will aid safety researchers and engineers designing restraint systems is high. To fully exploit virtual testing, models representing both female, male and child human bodies and different crash environments are required. While human body models are available (under various licenses), generic crash environments, e.g., vehicle geometry, laws for materials and energy absorption and acceleration profiles, are scarce, if available at all. For child safety, the child FE model PIPER (Beillas et al., 2016) opens new opportunities of carrying out computational analyses to understand child injury biomechanics. Unfortunately, child restraint models compatible to be used with the PIPER model has not been made available by the PIPER project.

Therefore, as part of WP3, development of an OS model of a child restraint system compatible with the PIPER HBM, to be made available on the VIRTUAL OpenVT platform, was undertaken. Specifically, the aim was to develop a FE model of a representative booster seat.

2. The Booster Seat

The selected product was the RodiFix Air Protect, sold by the brands Béb  confort and Maxi Cosi. 'Air Protect' refers to the foam embedded in the vented bags placed inside the head rest for side impact protection. The seat is compliant with the R44/04 regulation, group 2/3 (children 15-36kg, 4-12 years old).

The RodiFix Air Protect is shown in Figure B1. The seat has several specific features, also shown in Figure B2:

- Two recline positions: the seatback tilts backward while the seat-pan moves up when the seat is reclined.
- Can be used with and without attachments connected to the ISOFIX anchorages in the vehicle.
- 'Airprotect pads', foam blocks embedded in vented bags located inside the headrest on both sides.
- Headrest height adjustable.
- Side structures located in the area of the torso opens as the headrest moves upwards, in order to provide more space for the arms and shoulders of taller children.



Figure B1. RodiFix Air Protect



Figure B2. RodiFix Air Protect features

3. Specifications of the FE model

The FE mesh was created from CAD files following the symmetry of the booster seat structure (symmetry about the mid-plane in the longitudinal direction), see Figure B3. The mesh was broken down into parts that coincide with the physical assembly. 3D tetrahedric elements were used and screws were included as BOLT elements. The two main components of the booster seat are the plastic shell and the foam blocks.

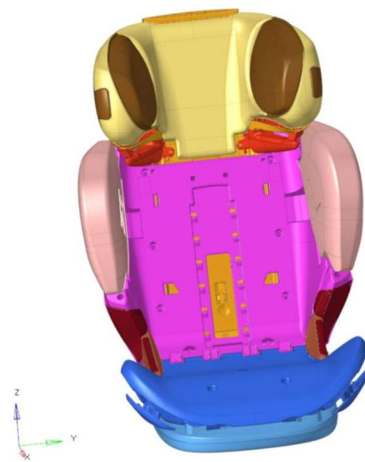


Figure B3. Overview of the seat geometry

The plastic shell has been composed of four parts meshed with shell elements of varying thickness, including the reinforcement ribs (Figure B4). The foam in the booster seat is meshed with tetrahedric elements, with a constant element size throughout each part. The element sizes are shown in Figure B5.

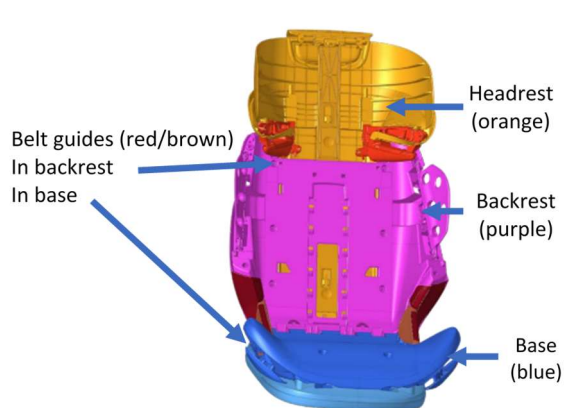


Figure B4. Main components of the plastic shell.

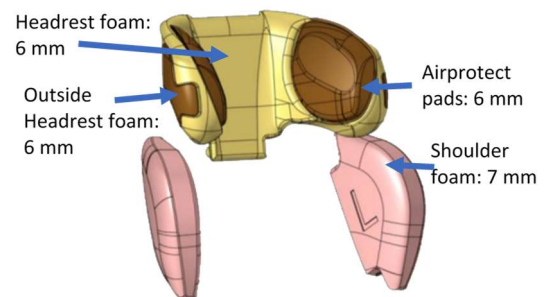


Figure B5. Main foam components.

4. Validation

Validation of the model was done using the UN ECE R129 frontal impact test specification with an LS-Dyna Q6 child ATD. For this purpose, an LS-Dyna model of the R129 test setup was developed, including the seat geometry and seat cushion stiffness properties. The VIRTUAL OS Booster seat model will be made available on the VIRTUAL OpenVT platform. Information of the validation study, including calibration of the UN ECE R129 seat cushion, is available in the VIRTUAL WP3 D2.3 report (Svensson et al., 2021) and is in the process for journal publication (Iraeus et al., 202x). A summary is provided below.

The validation includes comparison of the numerical and physical tests using the Q6 in the booster seat exposed to the R129 frontal impact test configuration. The booster seat was attached to the ISOFIX anchorages in the rig and the Q6 was restrained, together with the booster, using the seatbelt (Figure B6)

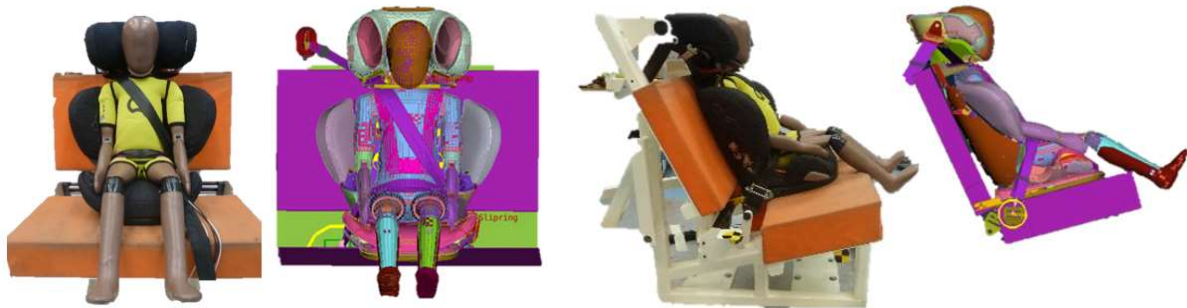


Figure B6. Front and side views of the validation test setup. UN ECE R129 test bench, the booster seat and a Q6 ATD; physical and numerical.

The FE models of the R129 sled and the booster seat closely matched the physical test (Iraeus et al, 202x). A comparison between the simulation and the physical test of Q6 responses and booster seat motions, are shown in Figure B7 and Figure B8, respectively.

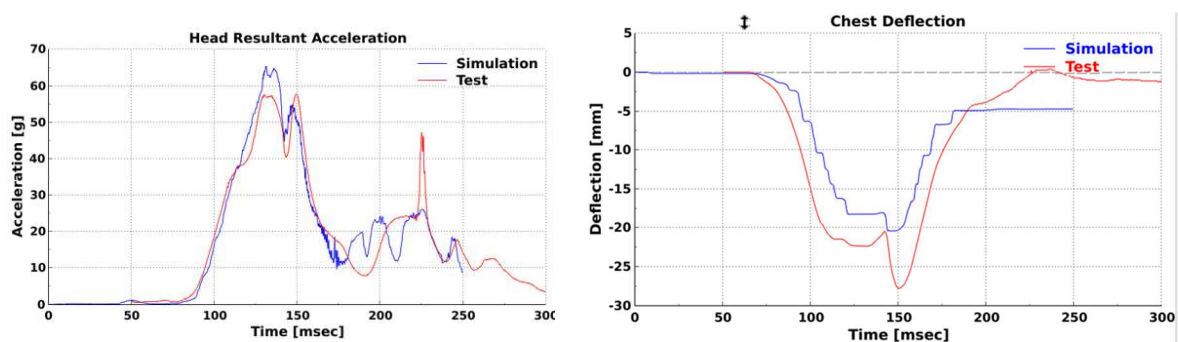


Figure B7. Q6 resultant head acceleration (left) and chest deflection (right), comparing physical test (red) and FE simulation (blue).

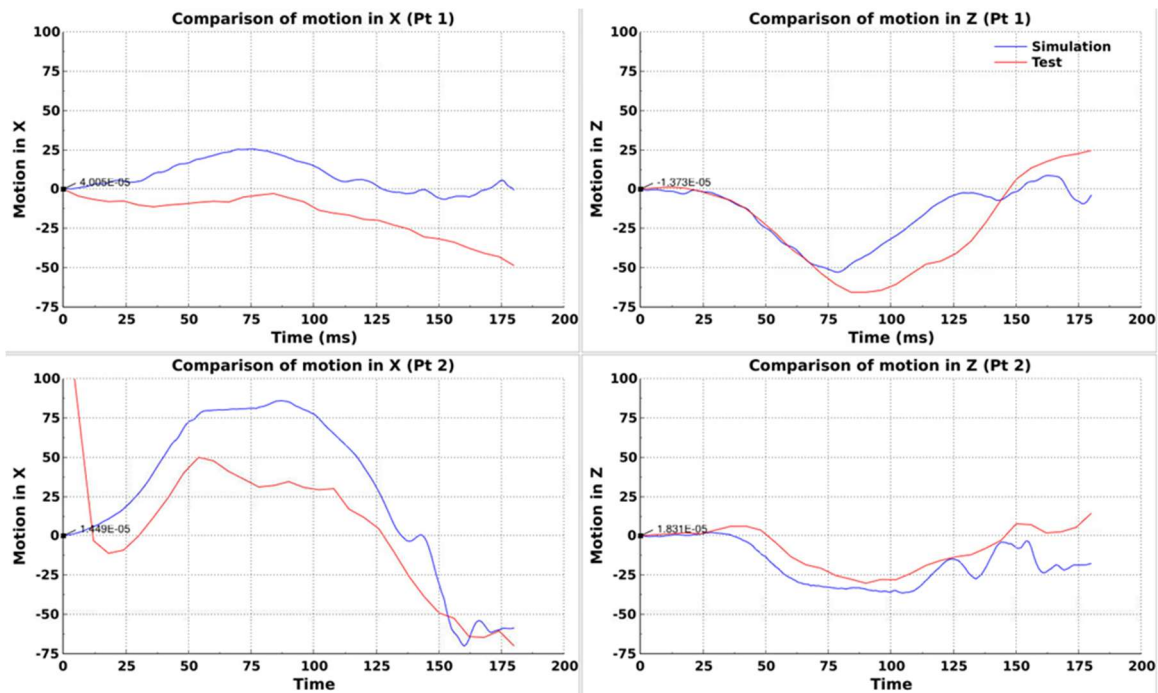


Figure B8. Booster seat motion in the longitudinal (x) and vertical (z) plane comparing physical test (red) and FE simulation (blue). Point (Pt) 1 is located on the front part of the cushion and Pt 2 on the headrest.

5. References

- Beillas P, Giordano C, Alvarez V, Li X, Ying X, Chevalier MC, Kirscht S, Kleiven S. (2016) Development and performance of the PIPER scalable child human body models. *14th Int. Conf. Protection of Children in Cars, Munich, Germany, Dec 2016*
- Iraeus J, Umeshkumar P, Thuvesen D, Meredith L, Svensson M. (202x) A method to adapt Q-series child ATD injury risk curves to the PIPER human body model – to be submitted
- Svensson M, Iraeus J, Meredith L, Wågström L. (2021) Scientific publication on child model applications in VIRTUAL, *Deliverable D2.3 of the H2020 project VIRTUAL*.

Appendix C Faurecia Concept Seat Models

Authors: Ines LEVALLOIS*, Patryk Recko**, Michal Kowalik**, Agnieszka Call**
 Faurecia Automotive Seating, *France, **Poland

1. Introduction

With the purpose of addressing novel seating in future AD cars, concept seat models relevant for such studies were developed within WP3. Specifically, the objective was to develop three variants, suitable for parameter studies, complying with standardised strength and frontal and rear-end impact tests. Some seats are equipped with several manual and electric adjustment options. Seats may also have additional features such as monitors, armrests, tables on the back, heating, ventilation, etc. How such features will evolve in the future when AD vehicles are available is difficult to predict. In addition to seatbelt design, this study has mainly been focused on seat adjustments.

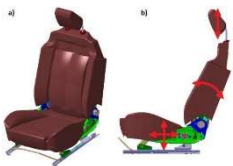
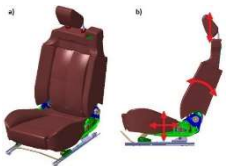
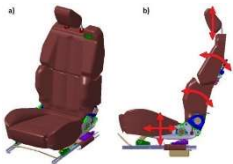
2. Concept Seat Model Variants

Three types of concept seat model variants were developed (see Chapter 2.2.1, Figure 2-10):

- Variant 1 (V1): a standard seat adjustable to relax position.
- Variant 2 (V2): as V1, also including a belt-guide for the shoulder belt, rotatable into a 20° swivel position.
- Variant 3 (V3): a novel seat design, with a split seatback and integrated seatbelt, designed using a shoulder belt belt-guide and a belt retractor integrated under the seat cushion. The seat can provide a more comfortable relaxed position, as well as rearward-facing positions.

Table C1 summarises the functionalities.

Table C1. The adjustment options of the three concept seat models

	Base adjustment	Additional adjustment
V1	 <ul style="list-style-type: none"> • Seat length/height adjustment. • Seatback angle adjustment. • Head-restraint height adjustment. 	A more reclined position is realised by using podiums instead of mechanisms.
V2	 <ul style="list-style-type: none"> • Seat length/height adjustment. • Seatback angle adjustment. • Head-restraint height adjustment. 	A swivel position up to 20° is realised by using rotated podiums instead of mechanisms.
V3	 <ul style="list-style-type: none"> • Seat length/height adjustment. • Seatback angle adjustment. • Head-restraint height adjustment. • Shoulder adjustment (10° forward movement of upper seatback part). 	A more reclined position is realised by using podiums instead of mechanisms.

The relaxed position has been defined as a 115° opening angle between the seat cushion and the seatback, see Figure C1. This angle was applied for V1 and V3. Additionally, for V3, the upper shoulder adjustment can rotate forward 10° (shown in Figure C1). This opening angle results in about 20° of cushion angle and 45° of seatback angle. The swivel position, used for V2, is a 20° inboard rotation, shown in Figure C2.

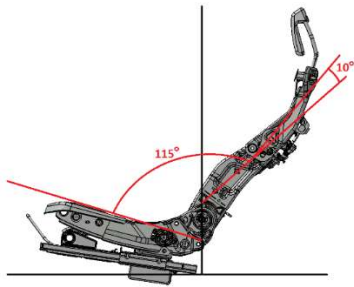


Figure C1. Relaxed seating, angles.

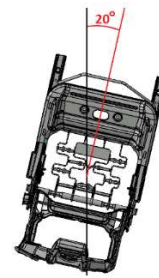


Figure C2. Swivel position, angle.

3. FE Analysis of the Concept Seat Models

With the objective of confirming numerical stability of the models and ensure that the frames are resistant to sustaining the test forces, the seat models were exposed to ECE14 (UNECE Regulation No. 14) static force test, and frontal and rear-end impacts. An average male sized HIII ATD model was used in the numerical verification analyses, targeting 120% of the regulatory force level in the ECE14 tests. In addition, as a virtual quality check for the seats, regulation conformity (ECE14) as well as seat frame integrity in rear-end impacts were carried out. Figures C3-C5 show the load curve and crash pulses used in the simulations.

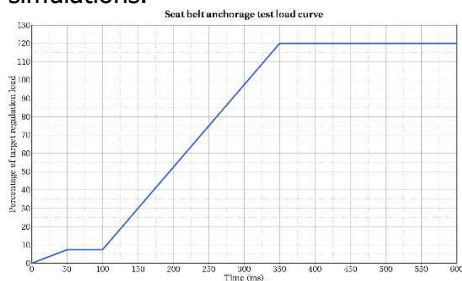


Figure C3. ECE 14 load curve.

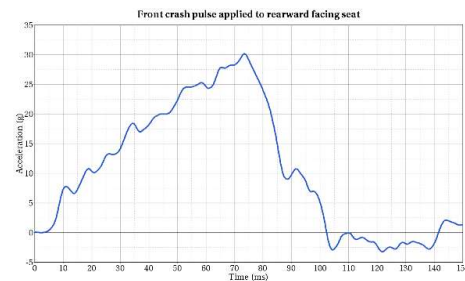


Figure C4. Frontal impact crash pulse.

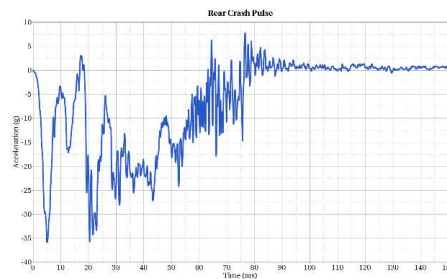


Figure C5. Rear-end impact crash pulse.

Tables C2-C4 summarise the simulation matrix for each variant. During the development process nine simulations were run for V1, 9 for V2 and 23 for V3, to find a structure compatible with all loadcases. The simulation results of the ECE14 and the rear-end impact loadcases are presented, together with the model development challenges, per seat model variant below. The results include frame deformation, normalised strains of the seat frame and dummy behaviour in different seated positions.

Table C2. Simulation matrix for the V1 seat model.

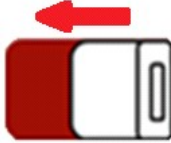

Test	Position	Position on tracks	Illustration	FEA status
ECE14	Standard forward-facing	Rearmost Downmost		OK
Rear-end impact	Relaxed forward-facing	Middle position Downmost		OK

Table C3. Simulation matrix for the V2 seat model.


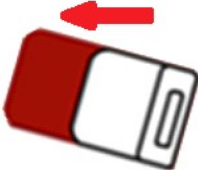
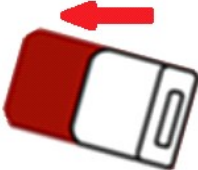


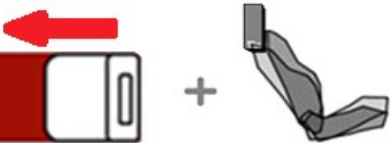
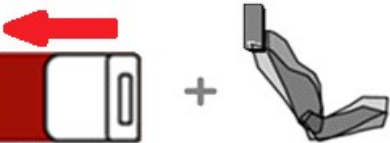

Test	Position	Position on tracks	Illustration	FEA status
ECE14	Standard forward-facing	Rearmost Downmost		OK
ECE14	Swivel forward-facing	Rearmost Downmost		OK
Rear-end impact	Swivel forward-facing	Middle position Downmost		OK

Table C4. Simulation matrix for the V3 seat model.

Test	Position	Position on tracks	Illustration	FEA status
ECE14	Standard forward-facing	Rearmost Downmost		OK
Rear-end impact	Standard forward-facing	Middle position Downmost		OK
Frontal impact	Relaxed forward-facing	Middle position Downmost		OK
Rear-end impact	Relaxed forward-facing	Middle position Downmost		OK
Frontal impact	Standard rearward-facing	Middle position Downmost		OK

Variant 1 Seat Model

The modelling activities started with the V1 structure, being a standard model, with a simple front seat frame without any special functionalities. The main difficulties was the unforeseen damage of the cushion-track links and brackets, because of track peeling effect in the 120% ECE14 loadcase. To resolve this issue, several changes were made to the model. The main steps taken in order to reinforce the frame involved extending the lower track profile, increasing the stiffness of the cushion side members and the stiffness of the cushion-track links and brackets (Figure C6), resulting in the final seat frame version (Figure C7). After the reinforcement of the frame to sustain the ECE14 force (Figure C8), no issues were noticed during the rear-end impact simulations in the relaxed position (Figures C9-11).

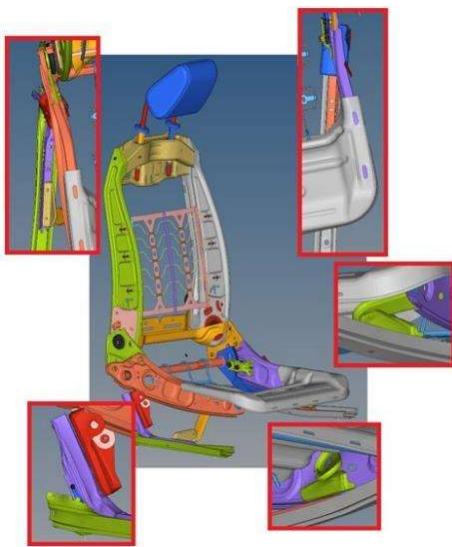


Figure C6. The main development difficulties for the V1.



Figure C7. V1 seat frame after improvements.

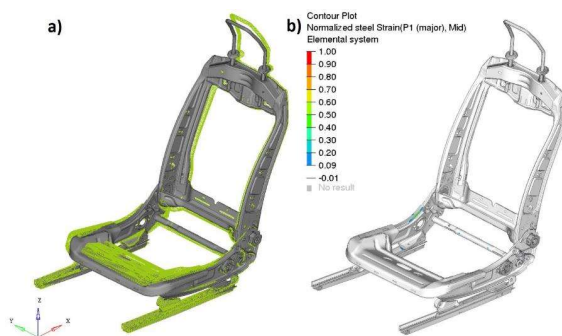


Figure C8. ECE14 test results of V1, standard forward-facing position (rearmost and downmost). a) Deformed shape, b) Normalised strain.

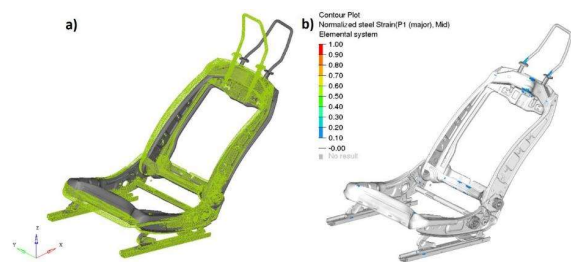


Figure C9. Rear-impact test results of V1, relaxed forward-facing position (mid and downmost). a) Deformed shape, b) Normalised strain.

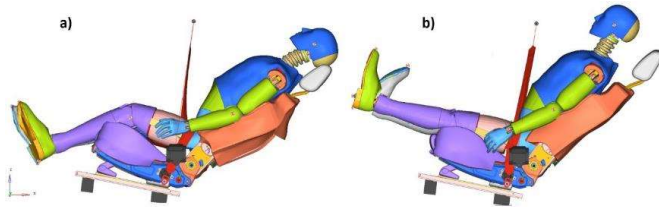


Figure C10. Dummy position in V1, relaxed forward-facing position (mid and downmost) during rear-end impact at: a) 100 ms and b) 150 ms.

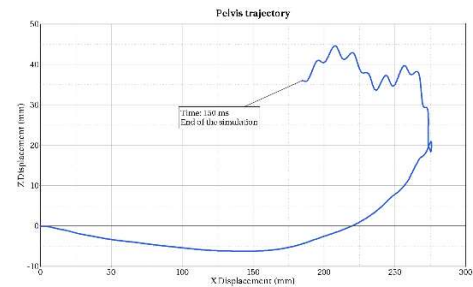


Figure C11. Pelvis trajectory (H-point displacement) in V1, relaxed forward-facing position (mid and downmost) during rear-end impact.

Variant 2 seat

During the development of V2 the main difficulties occurred during ECE14 simulation of the swivel position. Parts which stiffness was too low were the cushion-track right front bracket, cushion-track left rear bracket and both cushion side members. To solve these issues, the structure was changed by increasing the stiffness of the cushion side members and increasing the stiffness of the cushion-track links and brackets (Figure C12), resulting in the final seat frame version (Figure C13).

Figure C14 shows the results from the ECE14 test. Figures C15-C17 provide the results from the rear-end impact test results in the swivel forward-facing position.

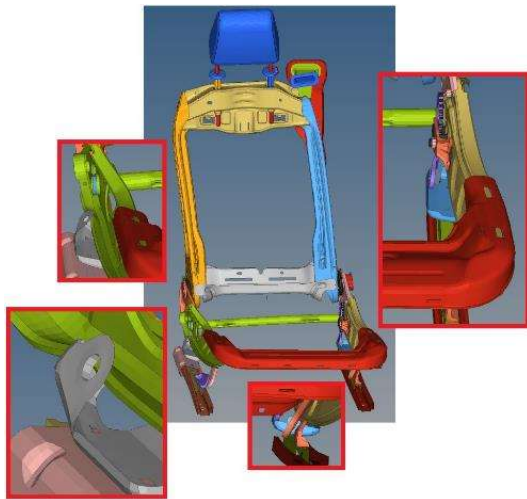


Figure C12. The main development difficulties for V1.

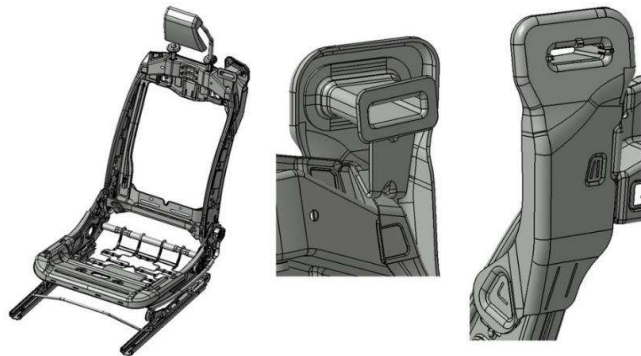


Figure C13. V2 seat frame after improvements.

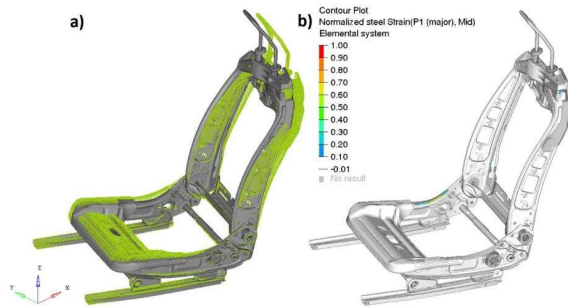


Figure C14. ECE14 test results of V2, swivel forward-facing position, (rearmost and downmost). a) Deformed shape, b) Normalised strain.

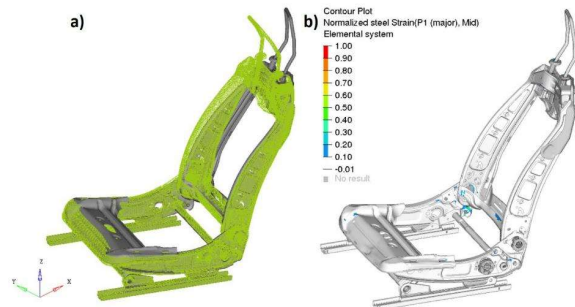


Figure C15. Rear-end impact test results of V2, swivel forward-facing position (mid and downmost). a) Deformed shape, b) Normalised strain.

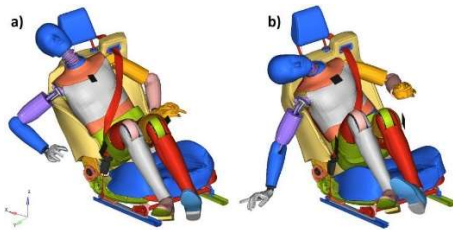


Figure C16. Dummy position in V2, swivel forward-facing position (mid and downmost) during rear-end impact at: a) 100 ms and b) 150 ms.

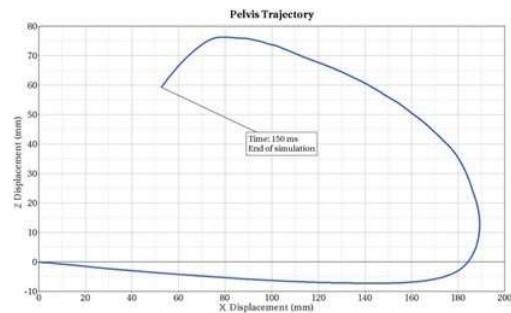


Figure C17. Pelvis trajectory (H-point displacement) in V2, swivel forward-facing position (mid and downmost) during rear-end impact.

Variant 3 seat

V3 was the most difficult to design because the seatbelt retractor was integrated under the seat cushion. This resulted in application of a 16.2 kN force (120% of the ECE14 test) directly to the seatback and the cushion parts. Several challenges with the overall structure strength were observed after the first simulation, such as (Figure 18):

- Left and right track peeling effect
- Integrated seatbelt retractor mounting
- Upper shoulder adjustment pivot points
- Left and right cushion side members
- All four cushion-track links and brackets
- Seatback side members
- The seatbelt belt-guide

Hence, designing additional cross member parts and reinforcing almost every structural part of the V3 frame was required, resulting in the final seat frame version (Figure C19).

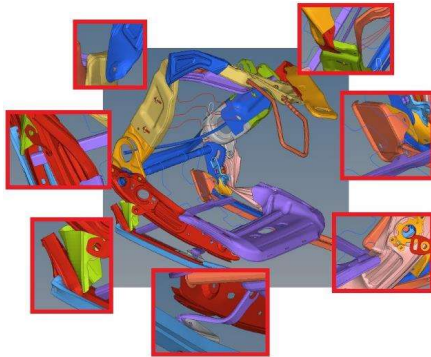


Figure C18. V3 seat main development difficulties.



Figure C19. V3 seat frame after improvements.

The ECE14 strength results are shown in Figures C20 and C21, for the standard forward-facing position.

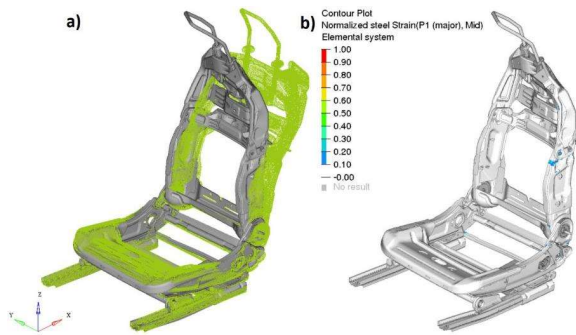


Figure C20. ECE14 test results of V3, standard forward-facing position, (rearmost and downmost). a) Deformed shape, b) Normalised strain.

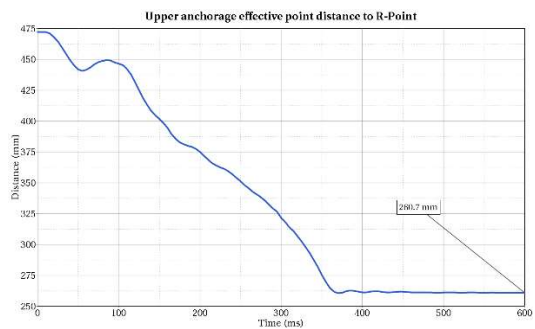


Figure C21. Upper effective anchorage point distance to R-point horizontal plane.

Figures C22-C24 show the rear-end impact results for V3 in the relaxed forward-facing position.

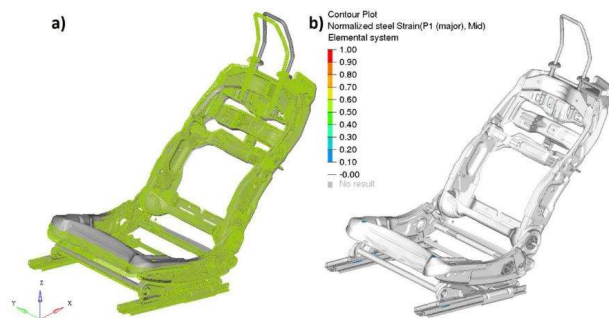


Figure C22. Rear-end impact test results of V3, relaxed forward-facing position (mid and downmost). a) Deformed shape, b) Normalised strain.

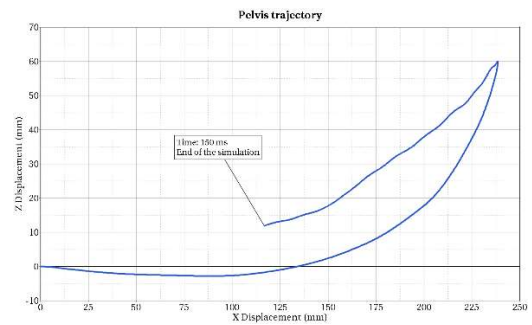


Figure C23. Pelvis trajectory (H-point displacement) in V3, relaxed forward-facing position (mid and downmost) during rear-end impact.

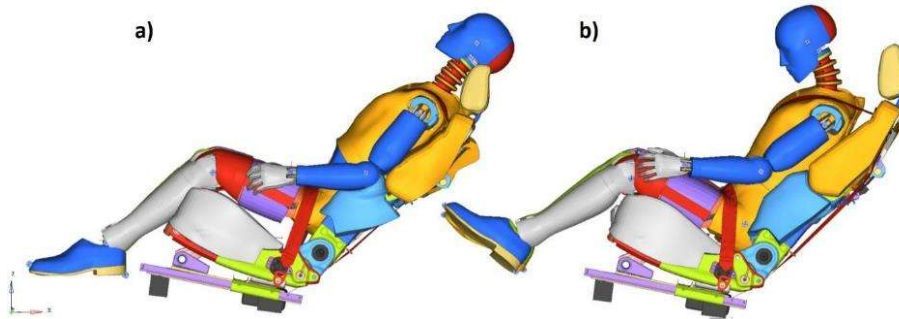


Figure C24. Dummy position in V3, relaxed forward-facing position (mid and downmost) during rear-end impact at: a) 100 ms and b) 150 ms.

Figures C25-C27 show the rear-end impact results for V3 in the standard forward-facing position.

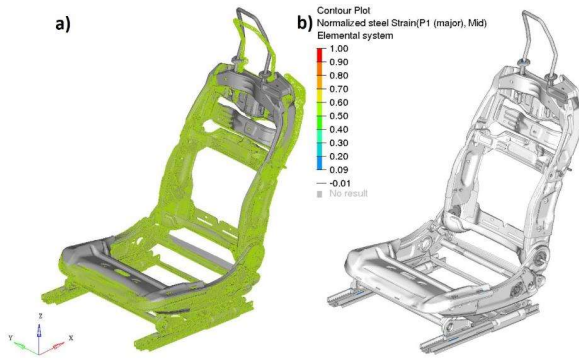


Figure C25. Rear-end impact test results of V3, standard forward-facing position (mid and downmost). a) Deformed shape, b) Normalised strain.

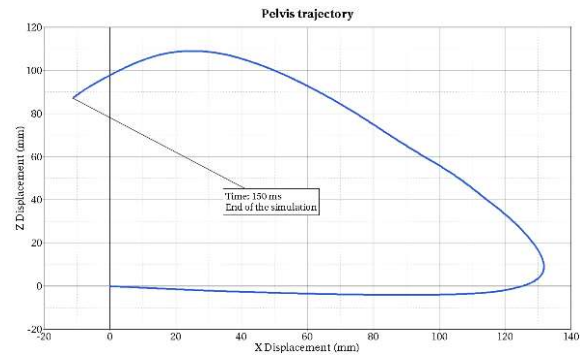


Figure C26. Pelvis trajectory (H-point displacement) in V3, standard forward-facing position (mid and downmost) during rear-end impact.

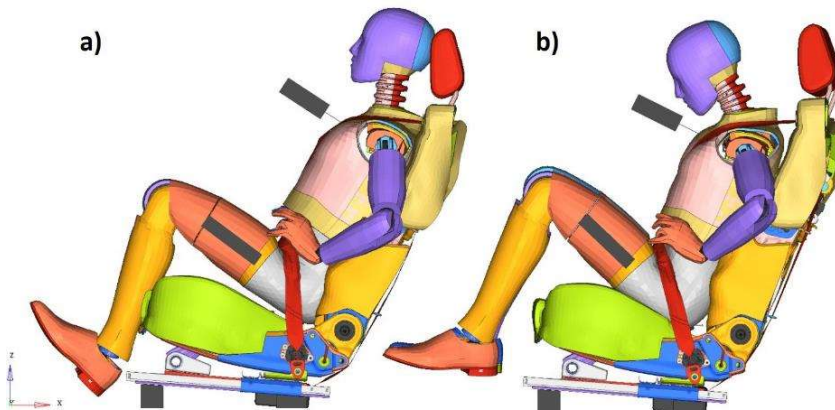


Figure C27. Dummy position in V3, standard forward-facing position (mid and downmost) during rear-end impact at: a) 100 ms and b) 150 ms.

Figures C28-C30 show the frontal impact results for V3 in standard rearward-facing position.

Middle Downmost:

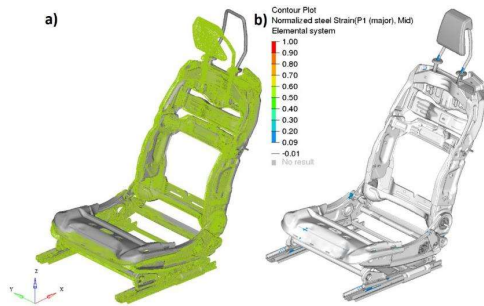


Figure C28. Frontal impact test results of V3, standard rearward-facing position (mid and downmost). a) Deformed shape, b) Normalised strain.

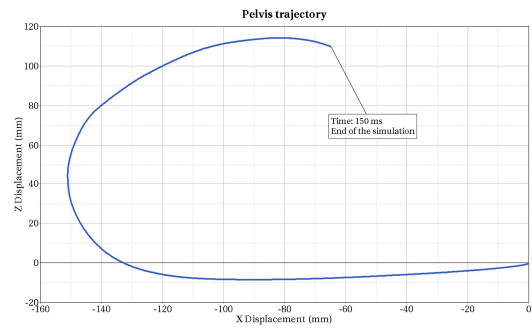


Figure C29. Pelvis trajectory (H-point displacement) in V3, standard rearward-facing position (mid and downmost) during frontal impact.

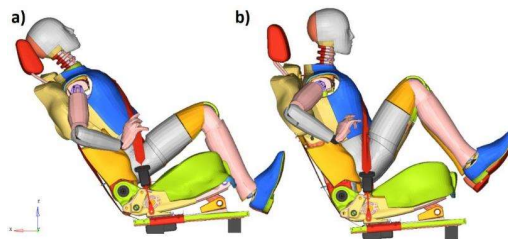


Figure C30. Dummy position in V3, standard rearward-facing position (mid and downmost) during frontal impact at: a) 100 ms and b) 150 ms.

Appendix D Sled Test Series with the Seat Evaluation Tools

Authors:

Lotta Jakobsson, Magnus Björklund, Thomas Forsberg, Lars Edlund, Volvo Cars Safety Centre
Tommy Pettersson, Magnus Karemyr, VTI

VTI developed the SETs and the positioning procedure, in addition to providing the Toyota seats. Chalmers contributed with the Chalmers lab seat. Volvo Cars supported with Volvo seats and was responsible for defining the objective, planning and execution of the sled test series, in addition to the analysis and the report.

This Appendix provides supplementary information to:
Chapter 3.1.2. Sled Test Series with the Seat Evaluation Tools.

Methods

In total 19 sled tests were run with the SET 50F and 50M (SET v0.1) using an acceleration sled at Volvo Cars Safety Centre, Gothenburg, Sweden (Seattle Safety Servo Sled), including three seat models and three crash pulses. Except for the Chalmers seat, each test was run with a new seat, not priorly tested. The Volvo seats were factory new, while the Toyota seats were from used cars.

Figure D1 shows the crash pulses used. The low pulse has a deltaV of 16 km/h and mean acceleration of 42 m/s², the mid pulse a deltaV of 16km/h and mean acceleration of 48 m/s² and the high pulse a deltaV of 24km/h and mean acceleration of 63 m/s². Mid and high pulses are part of the current EuroNCAP whiplash assessment protocol (EuroNCAP 2019), while the low pulse was part of a prior version of the protocol.

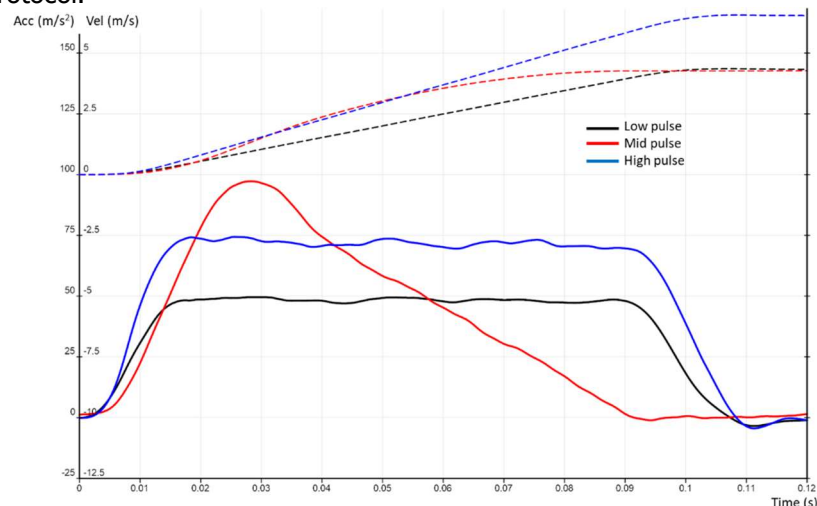


Figure D1. The crash pulses used in the sled test series, called low (black), mid (red) and high (blue) pulses. Acceleration (solid lines) and velocity (dotted lines) over time.

The sled was equipped with accelerometers. High-speed cameras recorded movements of the SET and the seat. The SET was equipped with four six-DOF triaxial rate and acceleration sensors (TE Connectivity Sensors, Model 633 6-DOF sensor). The acceleration signals were filtered according to SAE J211. The four sensors were positioned along the spine in four positions referred to as head (top of spine), T1, L1 and pelvis (bottom of spine). Figure D2 shows the sensor positions and orientation for SET 50F and SET 50M. The orientation of the sensors differs along the spine and between the two SETs, except for the pelvis sensor which is aligned with the pelvis plate.

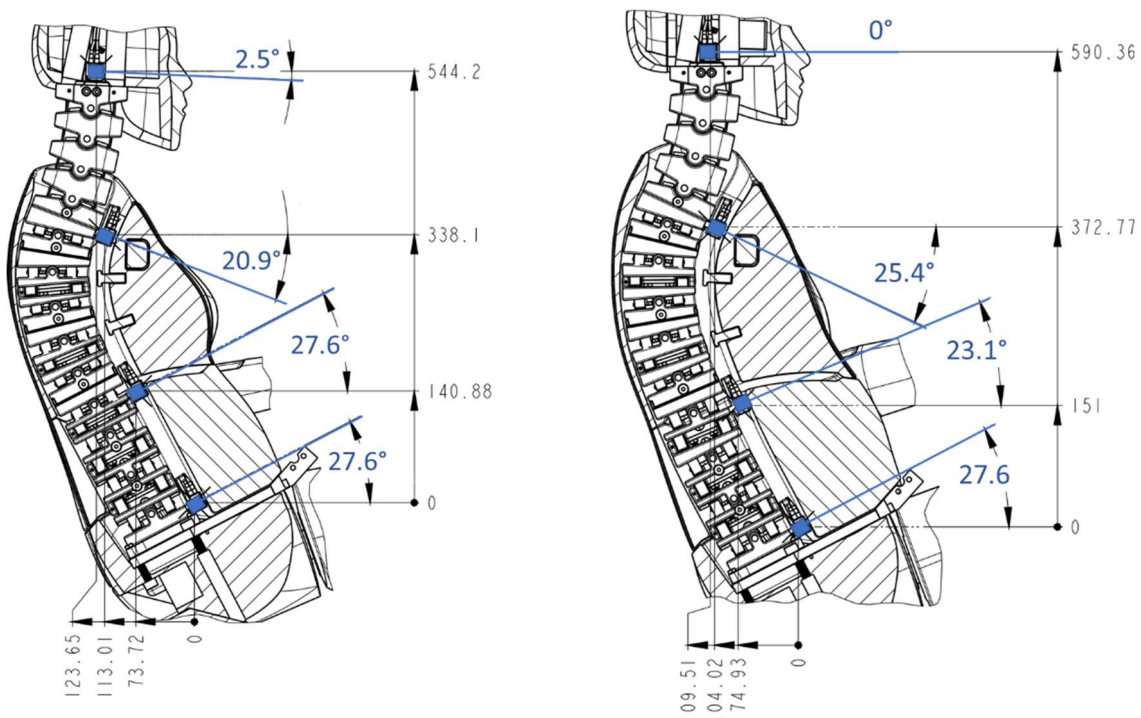
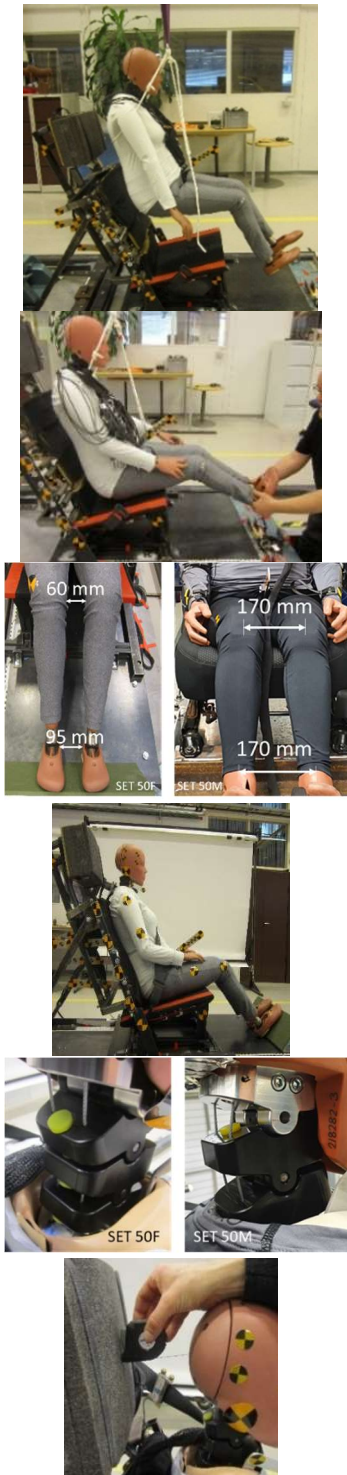


Figure D2. The spine of SET 50F (left) and the SET 50M (right), with sensor position and orientation indicated

Positioning

The Chalmers lab seat is fixed in height and the fixed-in-position seatback was in a seatback angle of 24°, corresponding to the published volunteer tests (Carlsson et al. 2011). The seatback angles of the Toyota and Volvo seats were positioned based on the H-point measurement using the EuroNCAP specification (2019), targeting a 25° torso angle. Further seat position details are listed in Table D1.

The SET is to be lifted by a specially designed single-point lifting system. The main lifting point is in the pelvis indicator. The part of the lifting system routed under the armpits and around the back, is mainly acting as a balance point. The SET must be handled with care and may not be lifted, moved or positioned by pulling the arms. Such action could cause damage to the arm attachments. A positioning procedure was developed and includes the steps shown in Figure D3.



A **Positioning on the seat**
Use the single-point lifting system and centre the SET over the seat, with the back of SET very close to the seatback, almost touching the seatback (A).

B
Lower SET very gently until the seat cushion is touched. While lowering, hold the legs and press gently into the seat, until the SET contacts the seatback. Release the single-point system by detaching the two shackles, when slack occurs. During the lowering, hold the ankles and lift to ensure that the thighs will be parallel to the seat cushion (B).

C **Positioning the lower extremities**
The heels are placed on the floor plate and the feet shall rest on the foot support and target knee and ankle distance as shown in C.

D **Positioning the upper extremities**
The humerus part of the arms is positioned parallel to line of the back/torso (D) and the elbow as close to the torso as possible.

The hands are placed flat on the thighs. Target a distance of 75mm between the thumbs for SET 50F and 120mm for SET 50M.

E **Neck configuration**
Configure the segments of the cervical spine as shown in E.

F **Head position**
The measurement of the head to head-restraint distance is shown in F.

When using the Chalmers lab seat with the 130mm padding on the head-restraint, target a distance of 100mm.

Figure D3. Positioning procedure for the SET

The positioning procedure in Figure D3 was followed with some exemptions. In the tests with the Toyota and Volvo seat, the hands were placed along the side of the thighs to provide a better visibility of the pelvis indicator marker. In all SET 50M tests, the three neck segments were positioned as shown in Figure D3E with the lowest segment in max extension and the mid and top segments in max flexion. However, for the SET 50F, there were some variations in neck segment configurations, see example in Figure D7. The seatbelt was used in all tests except one, as indicated in Table D1.

For each seat model and SET, 3D measurements using a faro arm were taken of approximately 30 points on the SET and the seat. For each test, two of these points (on the T1 and pelvis indicators, respectively) were measured and documented in relation to the seat to ensure repeatable positioning. Table D1 summarizes the angles of the pelvis and T1 indicators, in addition to height and for-aft horizontal seat position, seatback angle and head to head-restraint distance (backset). The Chalmers lab seat was used with a 130mm padding on the head-restraint. The Toyota seat's head-restraint was set in the same mid-position height for both SET 50F and 50M. The Volvo head-restraint is not adjustable.

Table D1. The test matrix, including measurements on the seat position and the SET indicator angles. For configuration specification see Table 3.1. The seatback angle of the Volvo seat is measured on the hardback on the back, while the seatback angle of the Toyota seat is measured on the head-restraint attachments. Seatback angle is missing for two of the tests due to different design of the head-restraint attachments. *Test with no seatbelt use.

Test No.	SET	Con-figuration	Height position	For-aft position	Seatback angle (°)	Backset (mm)	Pelvis indicator angle (°)	T1 indicator angle (°)
C1	50F	C-L	fixed	fixed	24.2	100	34.9	22.7
C2	50F	C-M	fixed	fixed	24.1	100	34.9	22.6
C3	50F	C-M	fixed	fixed	24.1	100	34.7	22.8
T1	50F	T-L	fixed	mid	3.9	52	29.3	27.3
T2	50F	T-M	fixed	mid	3.7	57	29.3	27.0
T3	50F	T-M	fixed	mid	3.9	58	29.3	27.6
T4	50F	T-H	fixed	mid	3.5	54	29.3	27.9
V1	50F	V-M	mid	mid	21.5	17	31.8	27.5
V2	50F	V-M	mid	mid	21.4	17	31.6	28.1
V3	50F	V-M	mid	mid	21.6	17	31.6	27.8
V4	50F	V-H	mid	mid	21.5	17	31.7	27.4
T5	50M	T-L	mid	mid	12.0	43	25.6	29.4
T6	50M	T-M	mid	mid	12.4	43	26.1	29.1
T7	50M	T-M	mid	mid	-	44	27.1	29.0
T8*	50M	T-H	mid	mid	-	44	24.3	30.8
V5	50M	V-M	mid	mid	22.2	22	29.9	29.4
V6	50M	V-M	mid	mid	22.2	26	28.4	31.2
V7	50M	V-M	mid	mid	22.2	28	29.2	29.6
V8	50M	V-H	mid	mid	22.2	25	29.1	20.2

Results

Repeatability and sensitivity

The mid pulse configuration was repeated for all combinations of seat and SETs. Figures D4-D6 show a comparison of the head, T1 and pelvis accelerations for SET 50F when exposed to the mid pulse in the three seats. Corresponding Figures for SET 50M in the Toyota and Volvo seats are shown in Figures D8 and D9.

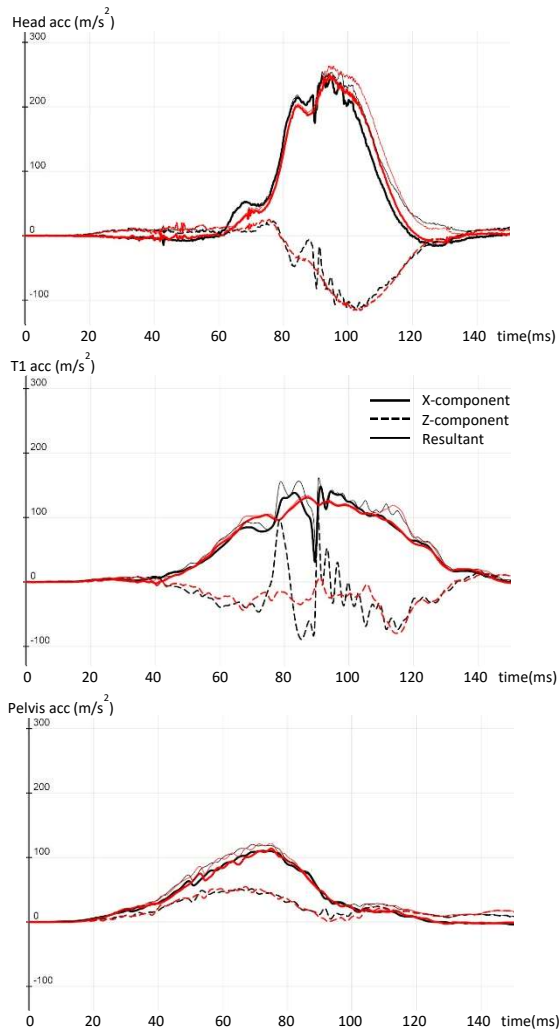


Figure D4. **SET 50F** accelerations (x, z and resultant) for head, T1 and pelvis for the **Toyota seat** in mid pulse (T-M). Tests No. T2 (black) and T3 (red).

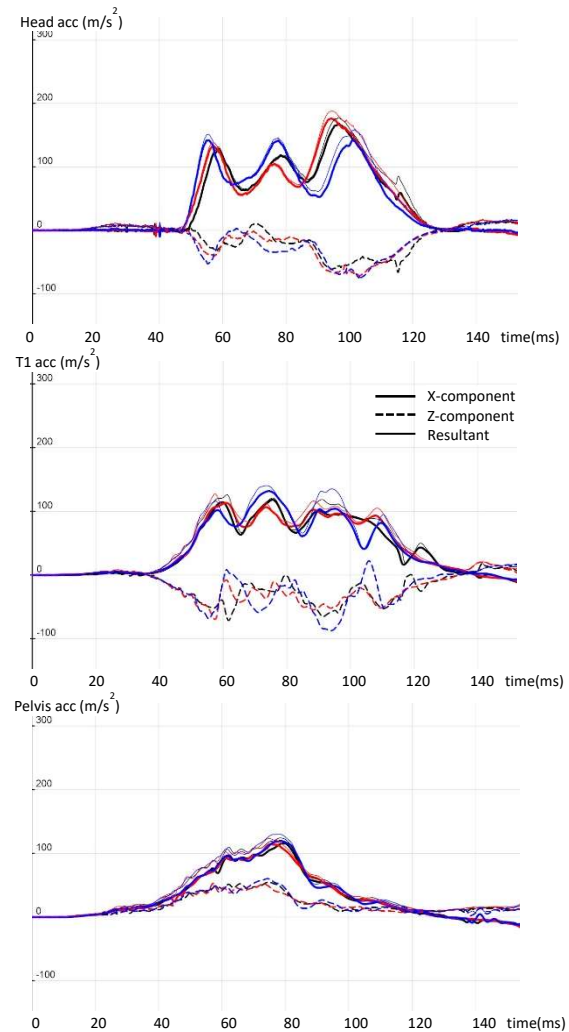


Figure D5. **SET 50F** accelerations (x, z and resultant) for head, T1 and pelvis for the **Volvo seat** in mid pulse (V-M). Tests No. V1 (black), V2 (red) and V3 (blue).

Figure D6. **SET 50F** accelerations (x, z and resultant) for head, T1 and pelvis for the **Chalmers lab seat** in mid pulse (C-M). Tests No. C2 (black) and C3 (red). The peaks of the T1 accelerations are cut in Figure.

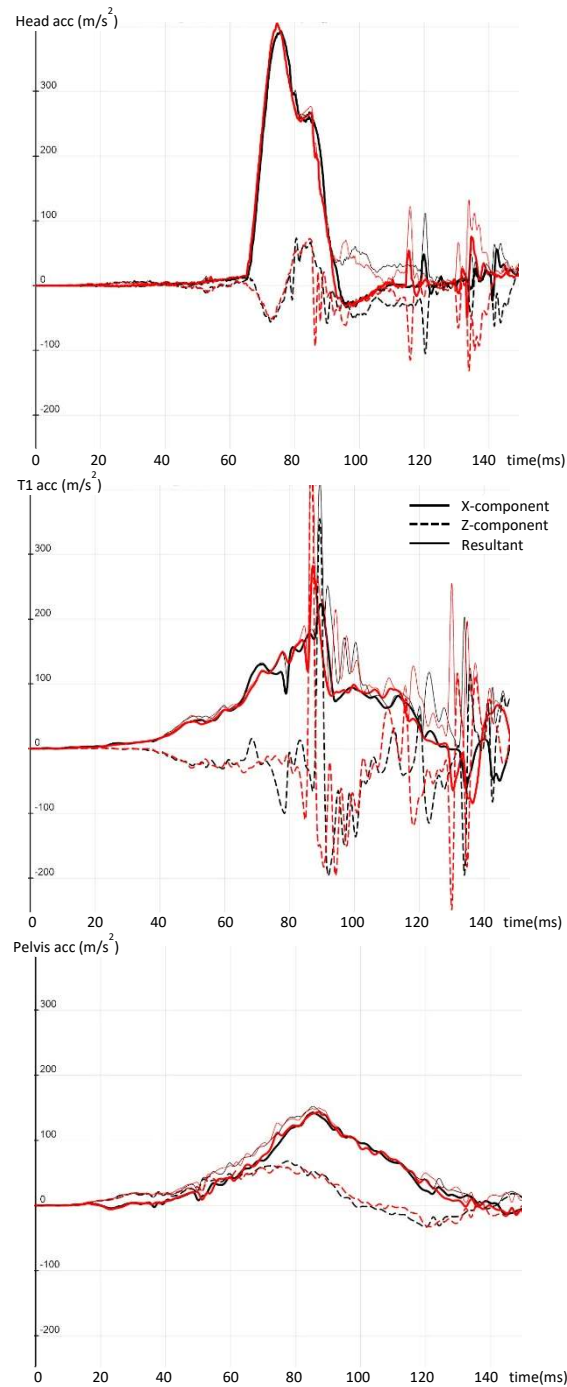


Figure D6. **SET 50F** accelerations (x, z and resultant) for head, T1 and pelvis for the **Chalmers lab seat** in mid pulse (C-M). Tests No. C2 (black) and C3 (red). The peaks of the T1 accelerations are cut in Figure.

Figures D4-D6 show that the correlation of head and pelvis accelerations for SET 50F was generally good for all the three seats, providing overall evidence of acceptable repeatability. For the Volvo seat, this applies to T1 accelerations as well, while for the two other seats, fluctuations were seen in T1 accelerations.

The initial configuration of the upper neck segment for SET 50F for the two tests with the Toyota seat in mid pulse differed, as shown in Figure D7. In Test No. T2, which showed a fluctuation in T1 z-acceleration (Figure D4), the neck of the SET 50F was configured the same way as the low and mid pulse tests. The same type of fluctuation was seen in the low pulse test (Test No. T1), while not in the high pulse test (Test No. T4). The initial fluctuation occurs prior to head to head-restraint contact, and there are no visible differences in neck kinematics at that time, nor does it change the overall kinematics. The substantial fluctuations in T1 accelerations for the Chalmers lab seat were consistent for the two compared tests. It occurred at time for maximum rearward movement with maximum seatback back-plate deflections, which also corresponded to the time of a contact by the upper neck segment to the head-restraint. At maximum seatback back-plate deflection, there is a likely contact between the upper back-plate and a cross beam behind, close to a bottoming-out of the lab seat structure. Whether the fluctuations are due to the seat or the neck segment to head-restraint contact is difficult to establish since they occur at the same time. These fluctuations are, however, not transferred to any of the other three sensors along the spine.

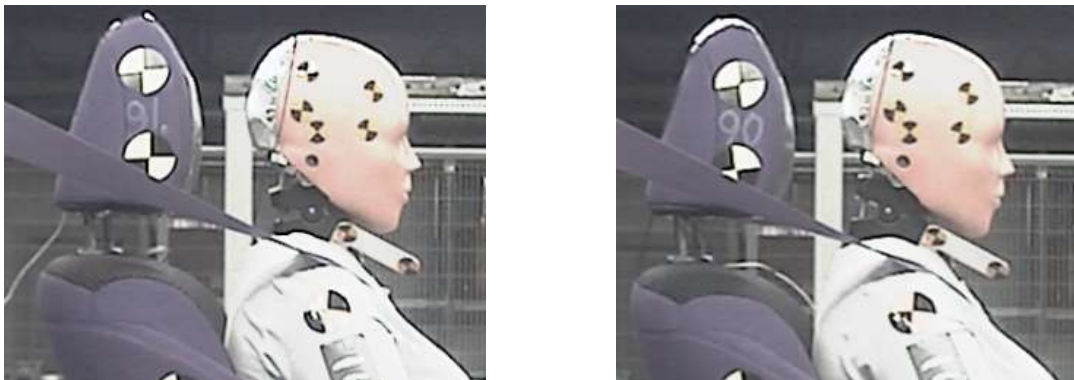


Figure D7. The initial neck configuration of the SET 50F in the comparative tests (T-M), at start of test Test No. T2 (left) and T3(right).

For the repeated tests with SET 50M larger variations than the corresponding configuration with SET 50F are seen, Figures D8 and D9. Unfortunately, the two Toyota seats used in the mid pulse tests were of somewhat different design, although of the same model. Hence, these tests (Figure D8) cannot be used for SET 50M repeatability evaluation, since they are affected by the seat variability as well.

The three repeated tests with the SET 50M in the Volvo seat (Figure D9), show a similar repeatability pattern as for the SET 50F (Figure D5).

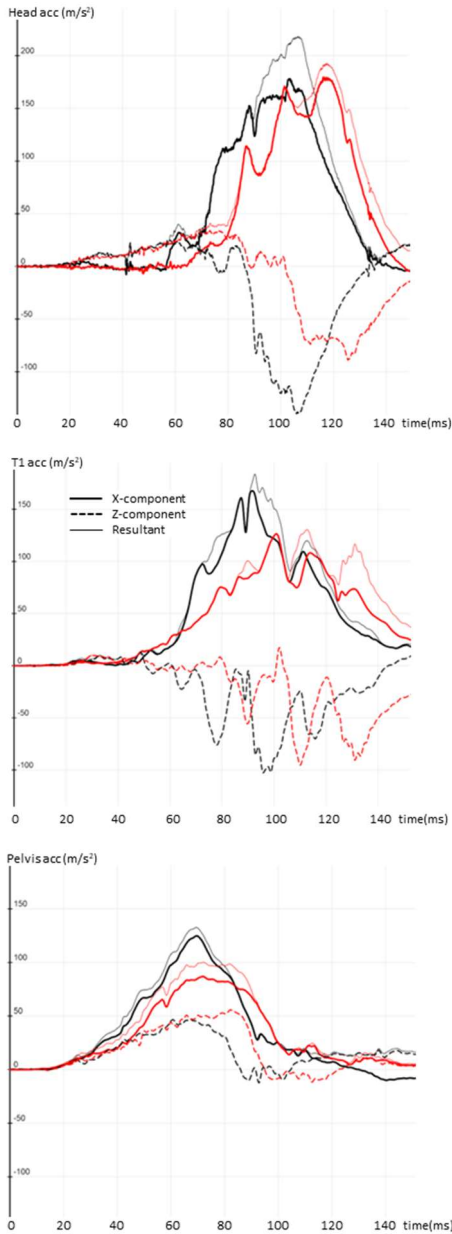


Figure D8. **SET 50M** accelerations (x, z and resultant) for head, T1 and pelvis for the **Toyota seat** in mid pulse (T-M). Tests No. T6 (black) and T7 (red). The Toyota seats used were not of exact same design.

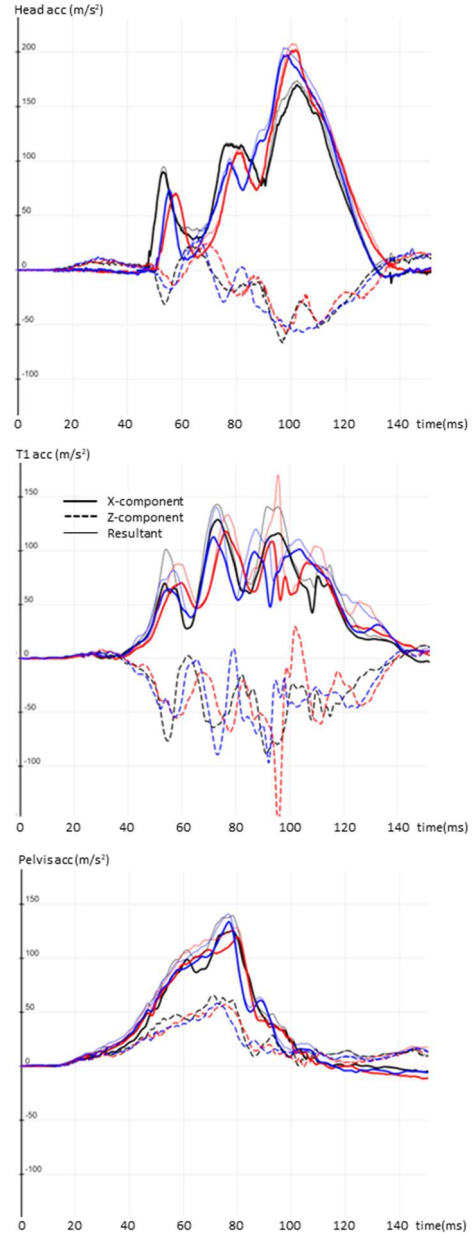


Figure D9. **SET 50M** accelerations (x, z and resultant) for head, T1 and pelvis for the **Volvo seat** in mid pulse (V-M). Tests No. V5 (black), V6 (red) and V7 (blue).

Kinematics

Snapshots at 0ms, 40ms, 80ms, 120ms and 160ms for each configuration using the SET 50M are shown in Figures D10 and D11. Corresponding information for the SET 50F is shown in Figures 3-3, 3-4 and 3-5 in Chapter 3.1.2.

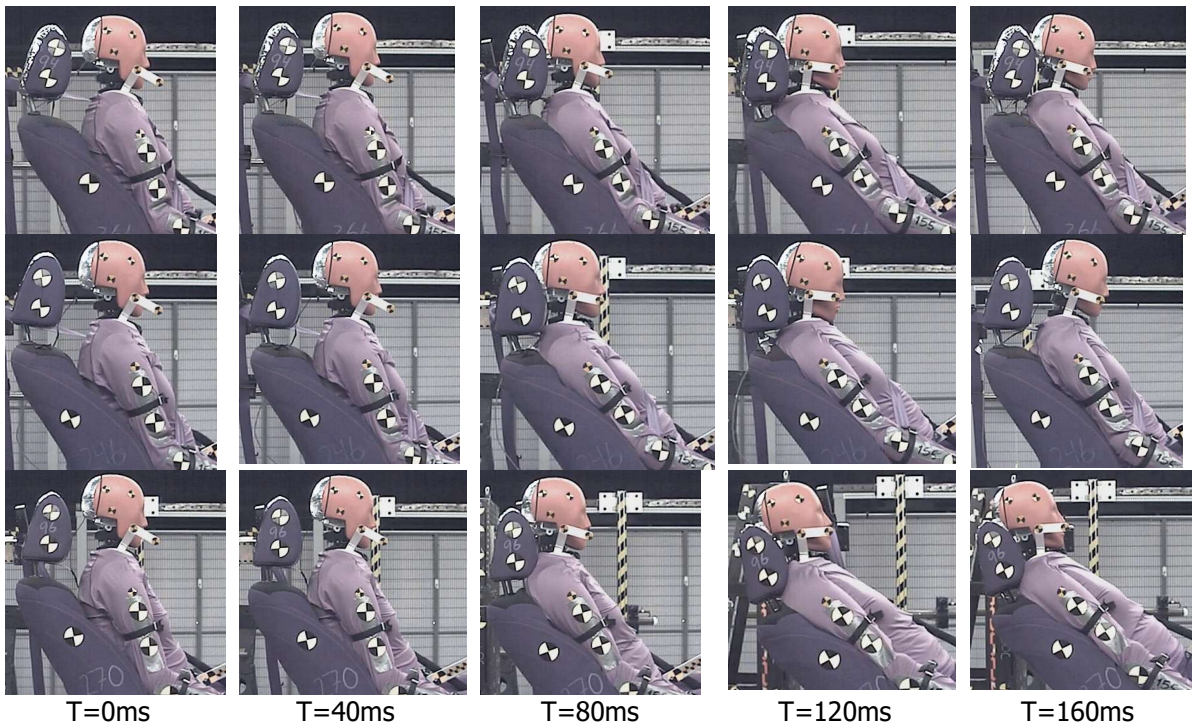


Figure D10. **SET 50M** in **Toyota seat** at low (top), mid (middle) and high (bottom) pulses. Tests No. T5, T6 and T8

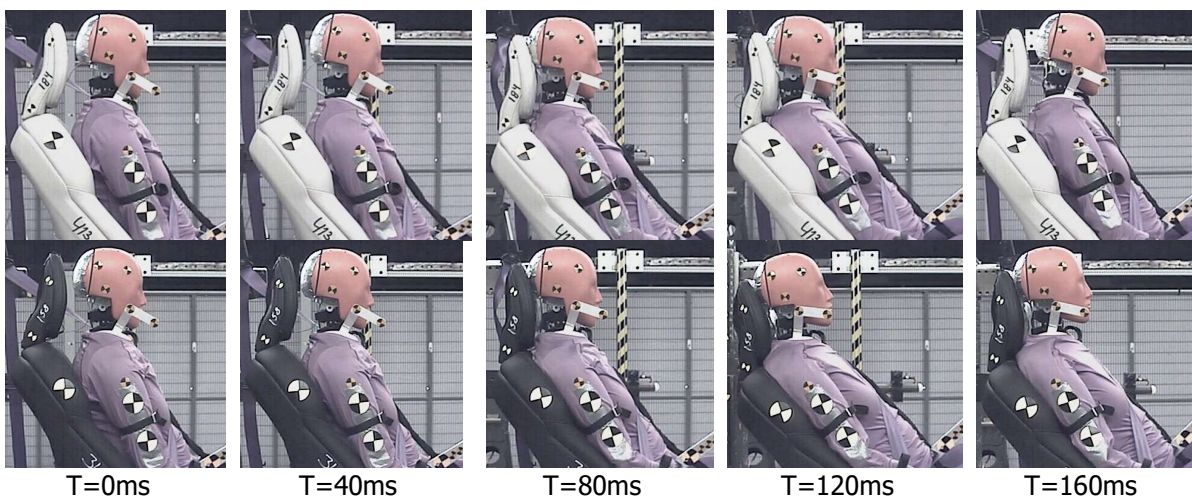


Figure D11. **SET 50M** in **Volvo seat** at mid (top) and high (bottom) pulses. Tests No. V7 and V8



Head to head-restraint contact times are summarized in Table D2 for each test. For SET 50F, start of contact varied from 44-49ms in the Volvo seat to 56-69ms in the Toyota seat and 63-73ms in the Chalmers lab seat. The differences between the Volvo and Toyota seats are in line with the differences in initial backset (Table D1). While for the Chalmers lab seat, the start of contact was just slightly later than the Toyota seat, while almost double backset distance. This is due to the design of the Chalmers lab seat, not allowing seatback deflection, whereby the head-restraint stays in position. The duration of the head to head-restraint contact was longest for the Volvo seat, followed by the Toyota seat. As for SET 50F, the SET 50M had earlier start of contact in the Volvo seat (45-51ms) as compared to the Toyota seat (59-67ms), also in line with the differences in initial backset. However, the duration of head to head-restraint contact was more similar between the two seats, 92-120ms and 88-117ms, respectively.

Table D2. Head to head-restraint contact start and end for each test. Configuration, see Table 3.1.

Test No.	SET	Configuration	Contact starts (ms)	Contact ends (ms)	Duration (ms)
C1	50F	C-L	73	109	36
C2	50F	C-M	63	96	33
C3	50F	C-M	63	96	33
T1	50F	T-L	68	145	77
T2	50F	T-M	59	127	68
T3	50F	T-M	59	127	68
T4	50F	T-H	56	145	89
V1	50F	V-M	49	135	86
V2	50F	V-M	47	139	92
V3	50F	V-M	47	136	89
V4	50F	V-H	44	142	98
T5	50M	T-L	64	162	98
T6	50M	T-M	59	147	88
T7	50M	T-M	66	155	89
T8	50M	T-H	67	184	117
V5	50M	V-M	47	142	92
V6	50M	V-M	51	145	94
V7	50M	V-M	50	139	89
V8	50M	V-H	45	165	120

Figures D12-D14 for SET 50F and Figures D15-D16 for SET 50M show the X-Z displacement trajectories per seat, for each configuration. The X-Z displacement trajectories trace one point on the head, one on the T1 indicator and one far out on the pelvis indicator.

Comparing the mid pulse configurations using SET 50F, the head x-displacement relative to the sled was similar between the seats, although for different reasons. While the head displacement in the Chalmers lab seat mainly reflected the distance between the head and the head-restraint, the head displacements when in the Volvo or Toyota seats were combinations of the initial backsets and the seatback deflections. For the Volvo and Toyota seats, the x-displacements were higher with higher crash pulse (Figures D13 and D14). This was not seen to the same extent for the Chalmers lab seat (Figure D12), for which the head and T1 x-displacements were of similar extent for the low and mid pulses.

This was likely due to the design of the seat, with a fixed seatback frame and that the upper horizontal seat panel only can move to a certain extent, before stopped by a beam.

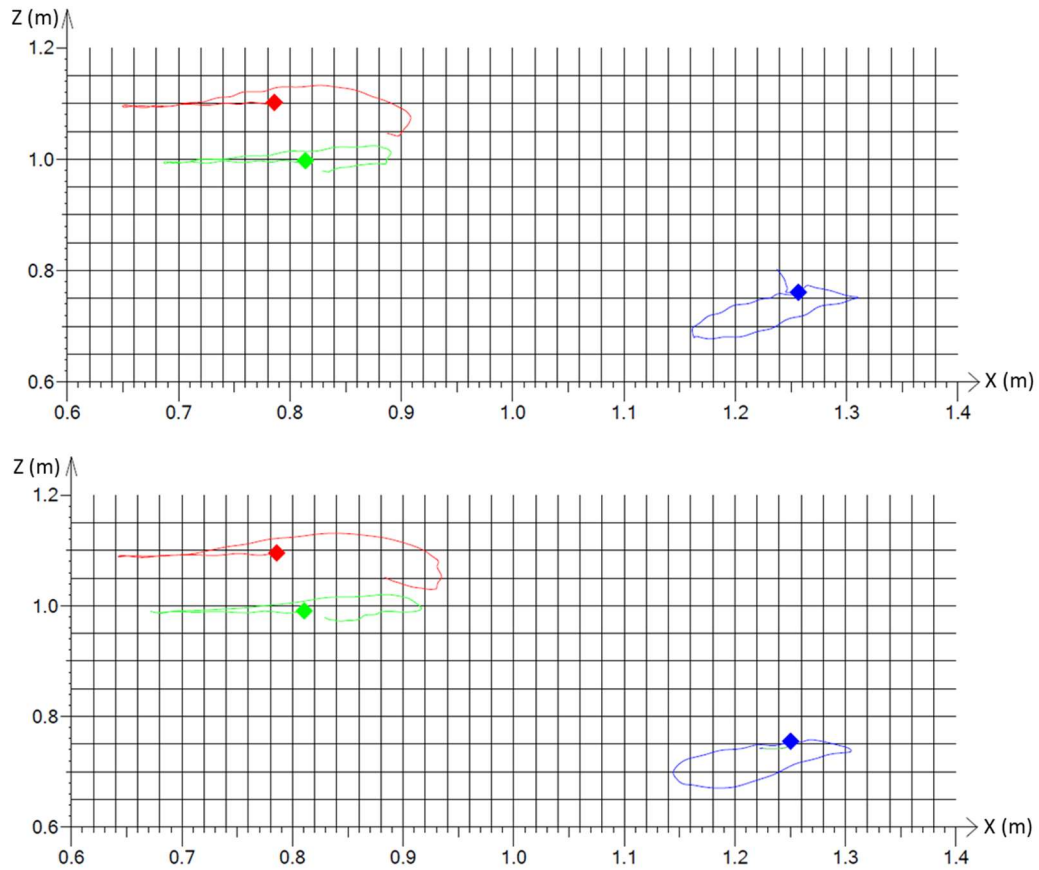


Figure D12. **SET 50F** X-Z trajectories relative the sled, in the **Chalmers lab seat** at low (top) and mid (bottom) pulses. Point on the head (red), point on the T1 indicator (green) and point on the pelvis indicator (blue). Tests No. C1 and C2.

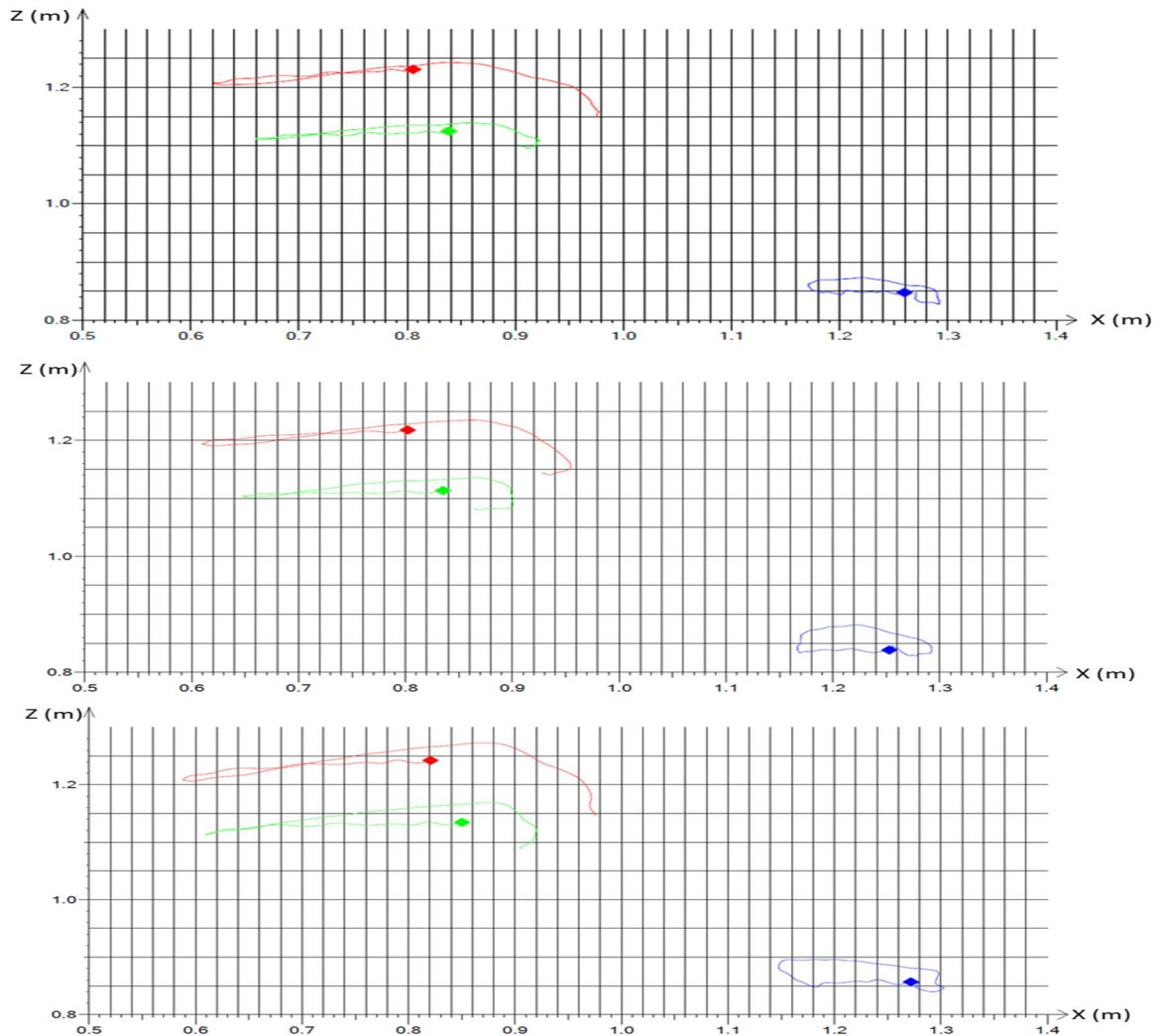


Figure D13. **SET 50F** X-Z trajectories relative the sled, in the **Toyota seat** at low (top), mid (middle) and high (bottom) pulses. Point on the head (red), point on the T1 indicator (green) and point on the pelvis indicator (blue). Tests No. T1, T2 and T4.

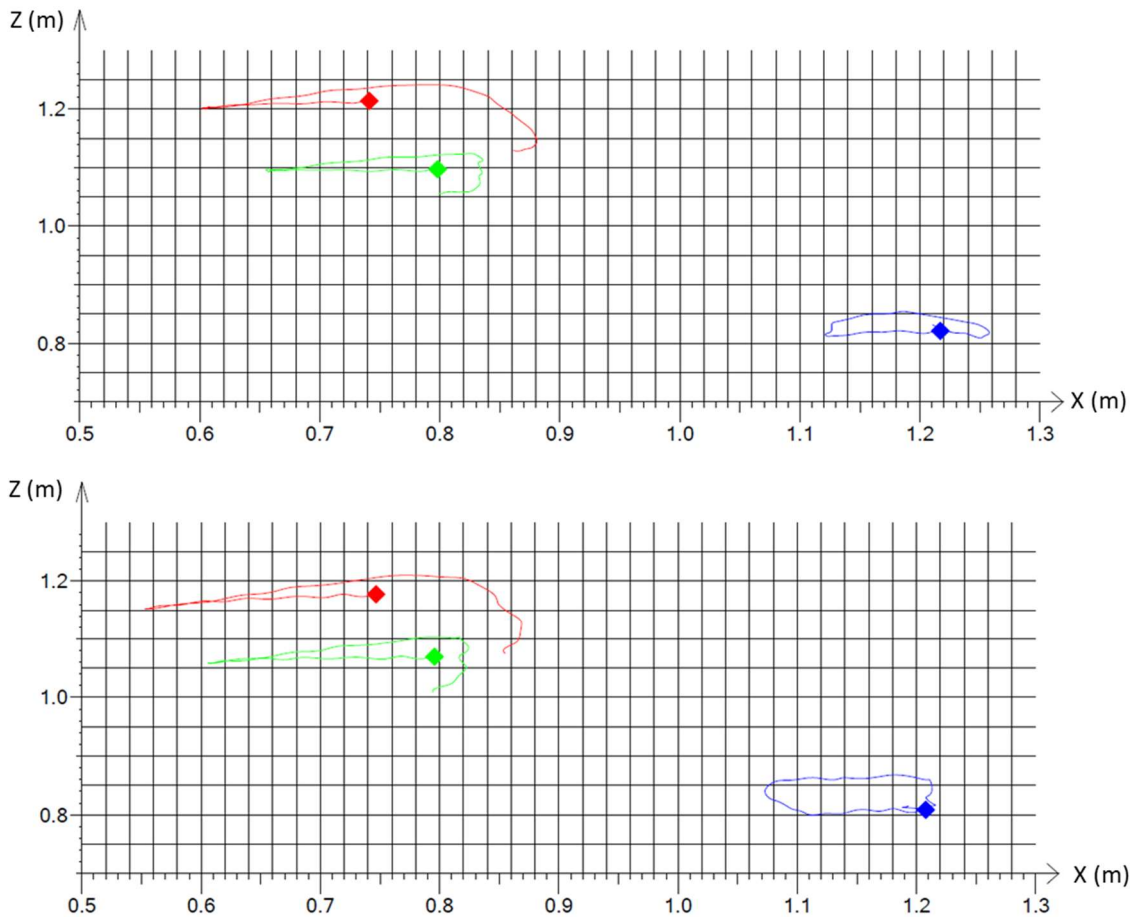


Figure D14. **SET 50F** X-Z trajectories relative the sled, in the **Volvo seat** at mid (top) and high (bottom) pulses. Point on the head (red), point on the T1 indicator (green) and point on the pelvis indicator (blue). Tests No. V3 and V4.

Comparing the mid pulse configurations using SET 50M (Figures D15 and D16), the pelvis x-displacement relative to the sled was similar between the Volvo and Toyota seats, while relatively longer for the Toyota seat in T1 and head x-displacements. For both seat types, the x-displacements were higher with higher crash pulse, as when using the SET 50F.

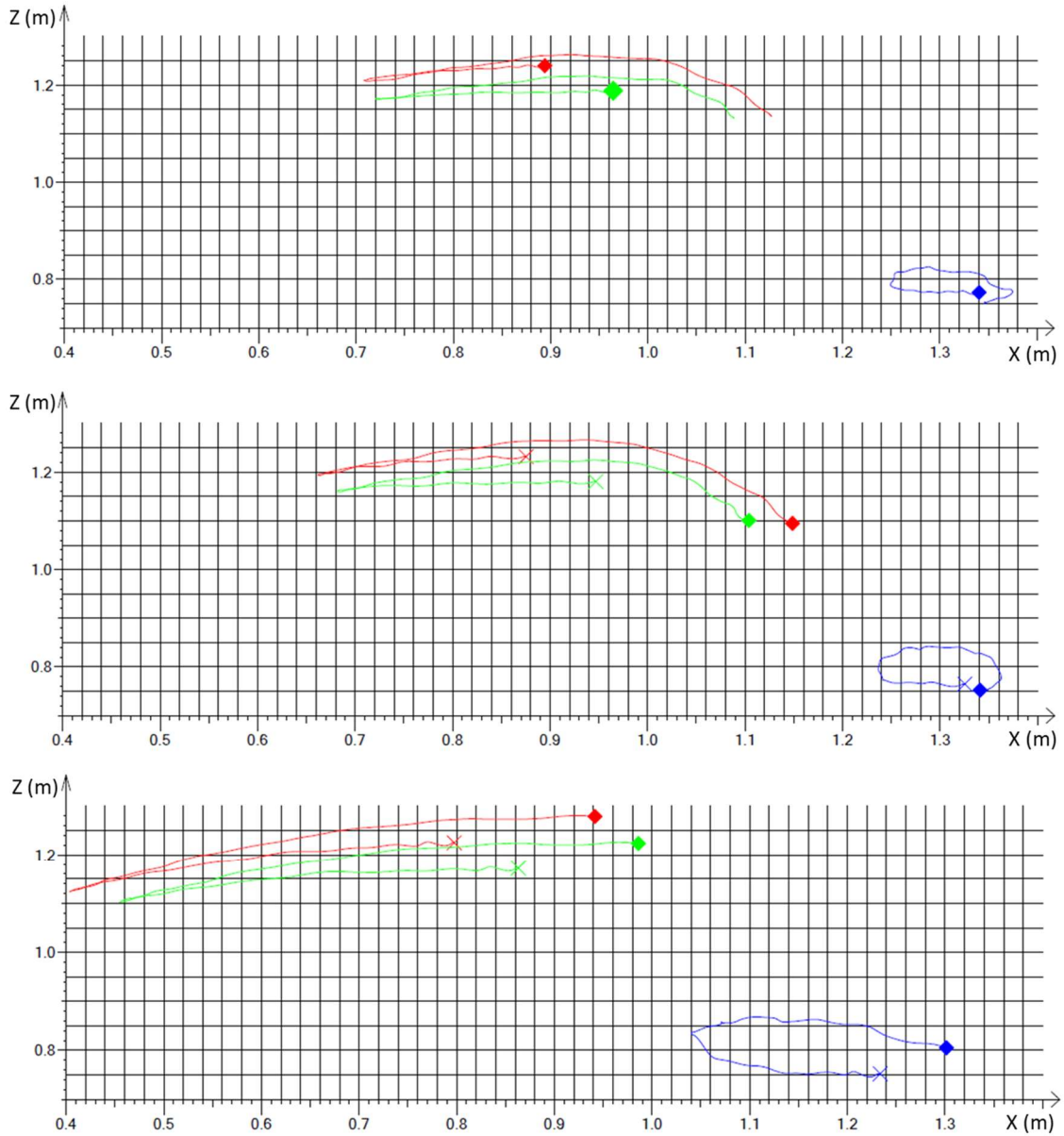


Figure D15. **SET 50M** X-Z trajectories relative the sled, in the **Toyota seat** at low (top), mid (middle) and high (bottom) pulses. Point on the head (red), point on the T1 indicator (green) and point on the pelvis indicator (blue). Test No. T5, T6 and T8. The x-axis is shifted for Tests No. T8, due to slightly different seat design.

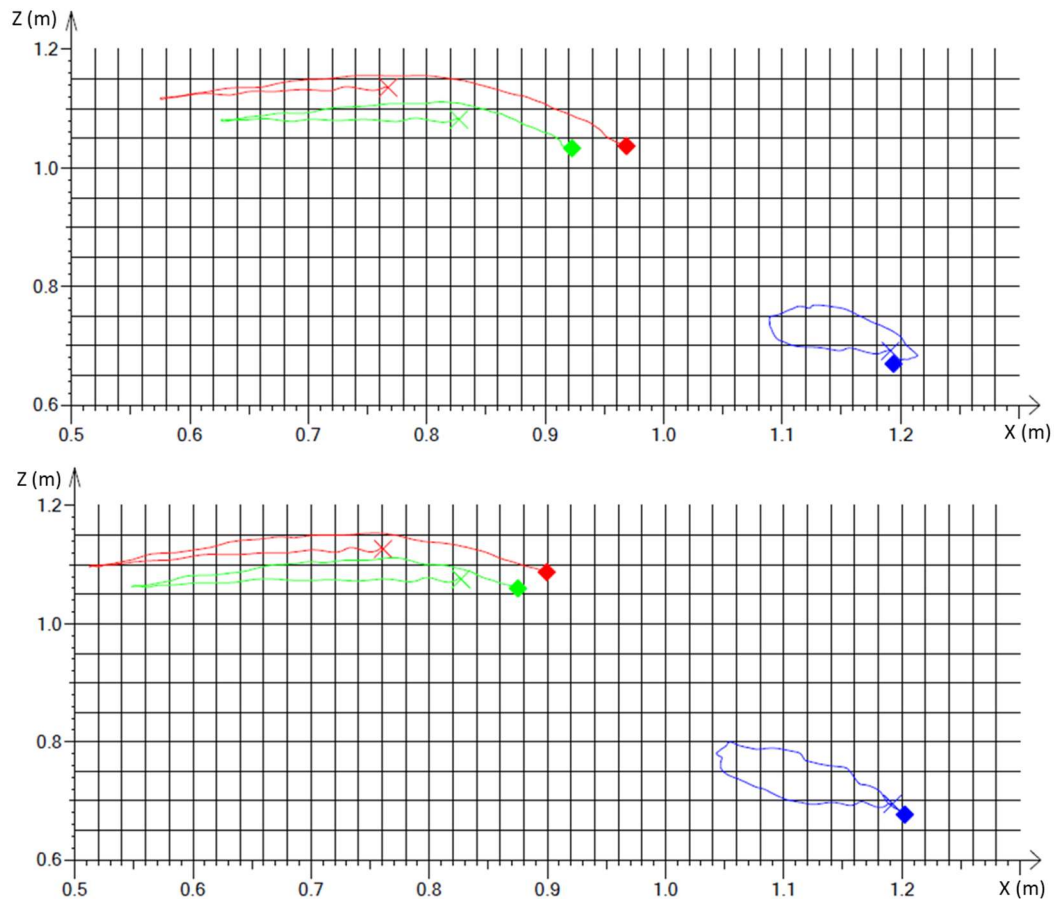


Figure D16. **SET 50M** X-Z trajectories relative the sled, in the **Volvo seat** at mid (top) and high (bottom) pulses. Point on the head (red), point on the T1 indicator (green) and point on the pelvis indicator (blue). Tests No. V7 and V8

Sensor data

For each configuration, the head, T1, L1 and pelvis acceleration x and z components and resultants, respectively, are plotted for the SET. The sensor positions are based on the spine shape and their axes are not aligned for SET 50F in comparison to SET 50M (Figure D2).

For SET 50F an overall trend of higher acceleration amplitudes for the higher pulse(s) as compared to the lower pulse is seen for each seat respectively (Figures D17-D19), although less pronounced for the Volvo seat. The Volvo seat is also the seat with lowest accelerations (Figure D19), and the acceleration is rather similar in shape and amplitude in the four positions over the spine. This is an indication of an even support throughout the torso and head by the seatback and head-restraint. This was seen for both crash pulses. The Chalmers Lab seat (Figure D17) exposed the SET 50F to the highest accelerations and with the largest difference in amplitudes between the four positions over the spine, with up to a three times higher head acceleration as compared to the pelvis acceleration.

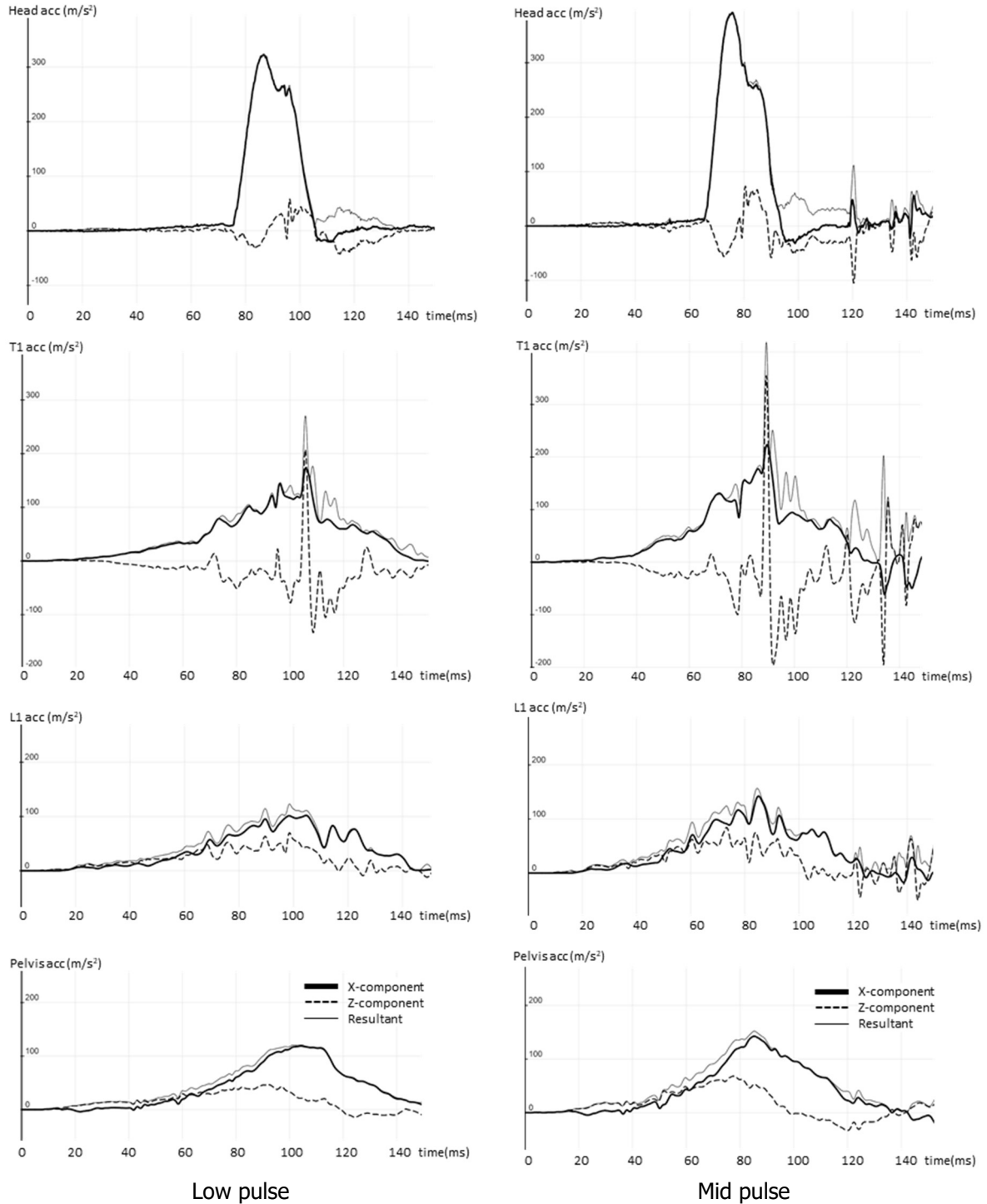


Fig D17. **SET 50F** in **Chalmers lab seat**. Head, T1, L1 and pelvis accelerations (x, z and resultant) for low pulse (left) and mid pulse (right). Tests No. C1 and C2.

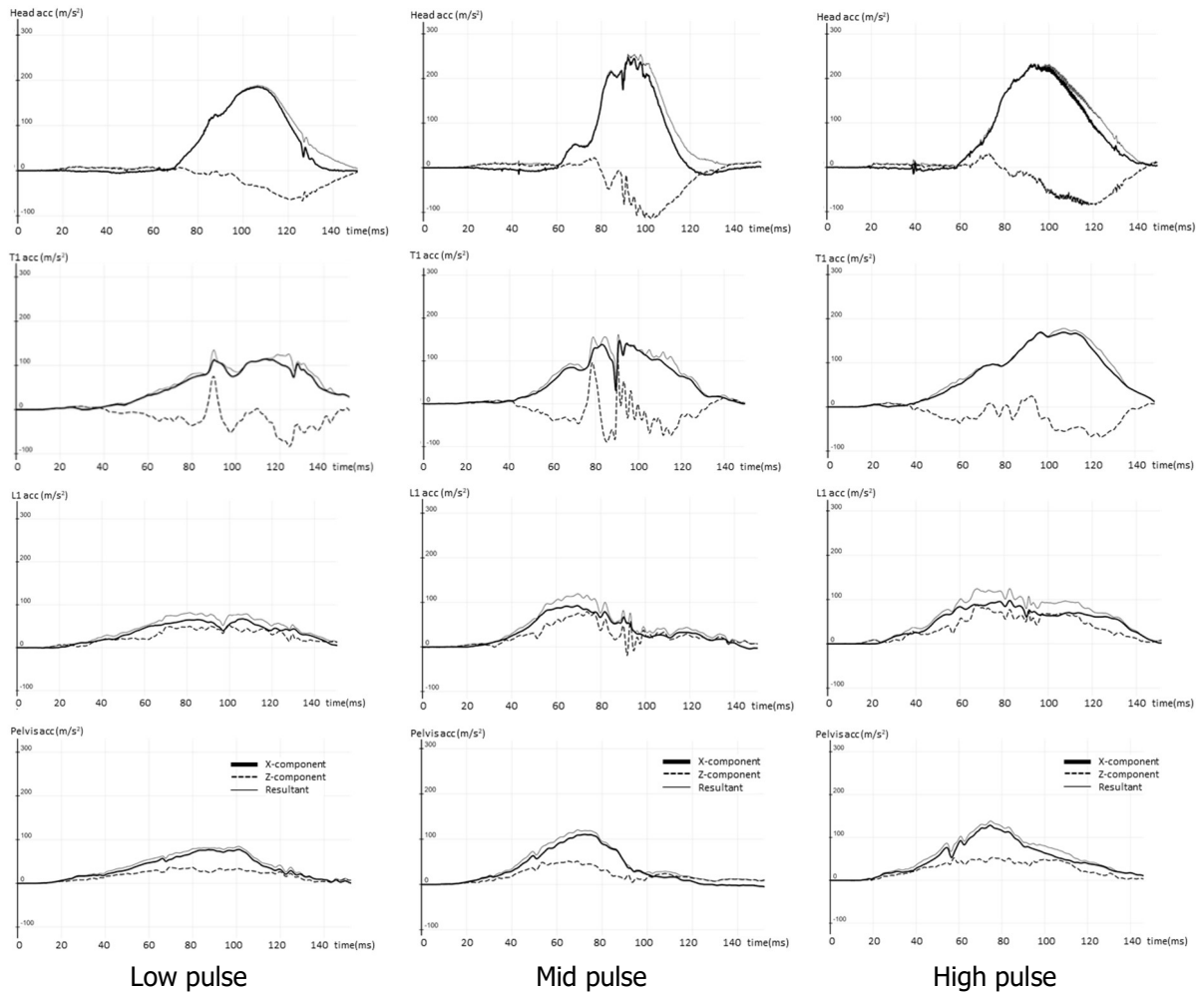


Fig D18. **SET 50F in Toyota seat.** Head, T1, L1 and pelvis accelerations (x, z and resultant) for low pulse (left), mid pulse (mid) and high pulse (right). Tests No. T1, T2 and T4.

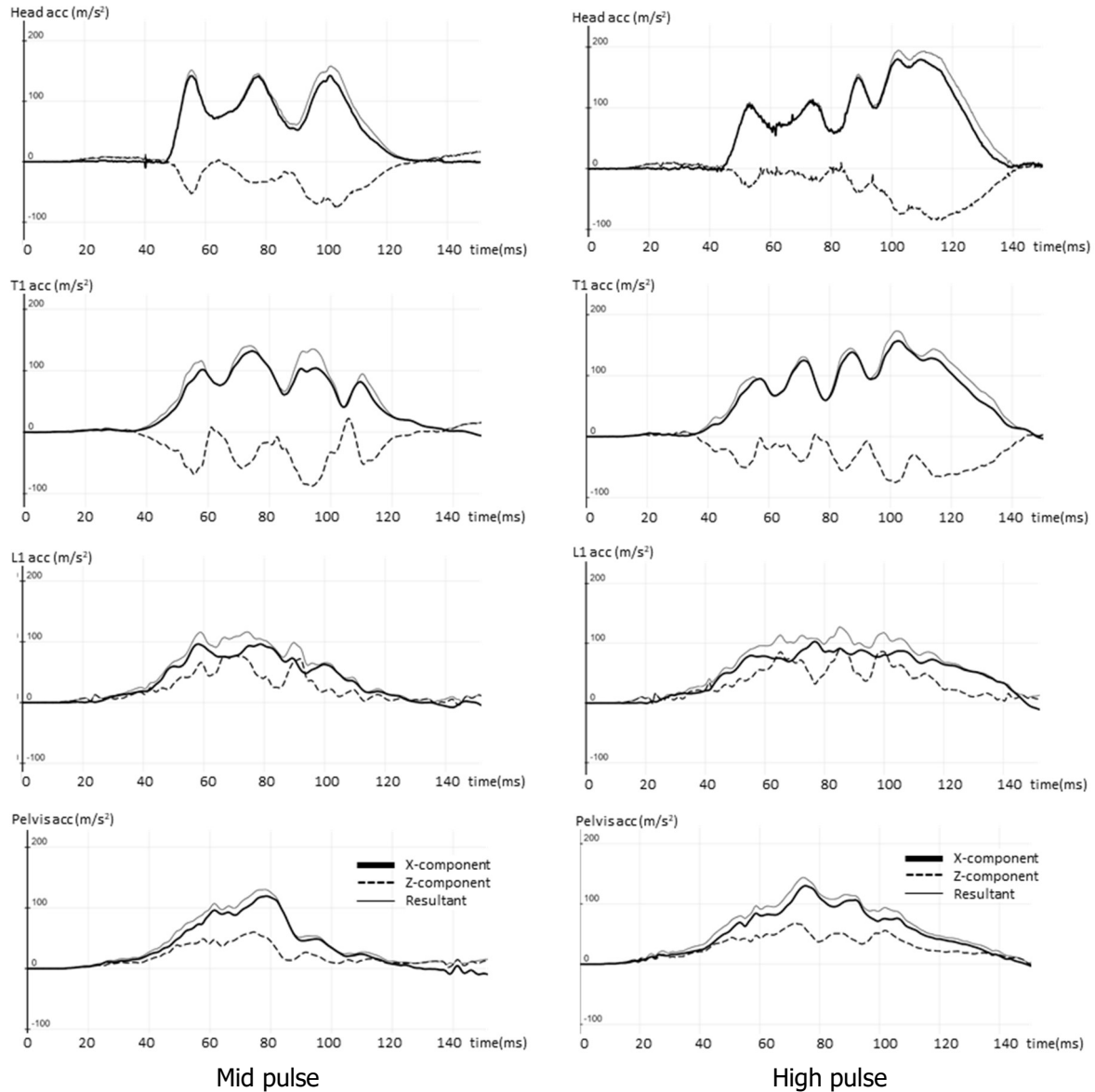


Fig D19. **SET 50F** in **Volvo seat**. Head, T1, L1 and pelvis accelerations (x, z and resultant) for mid pulse (left) and high pulse (right). Tests No. V3 and V4.

In Figures D20 and D21, the accelerations of the SET 50M in the tests with the Toyota and Volvo seats are plotted. As for the SET 50F, a trend of higher acceleration amplitudes with higher crash pulse is seen for the Toyota seat (Figure D20), especially between the low pulse and the other two pulses. This trend is not as pronounced for the Volvo seat, for which the acceleration amplitudes are rather similar between the two included crash pulses (mid and high pulses, see Figure D21).

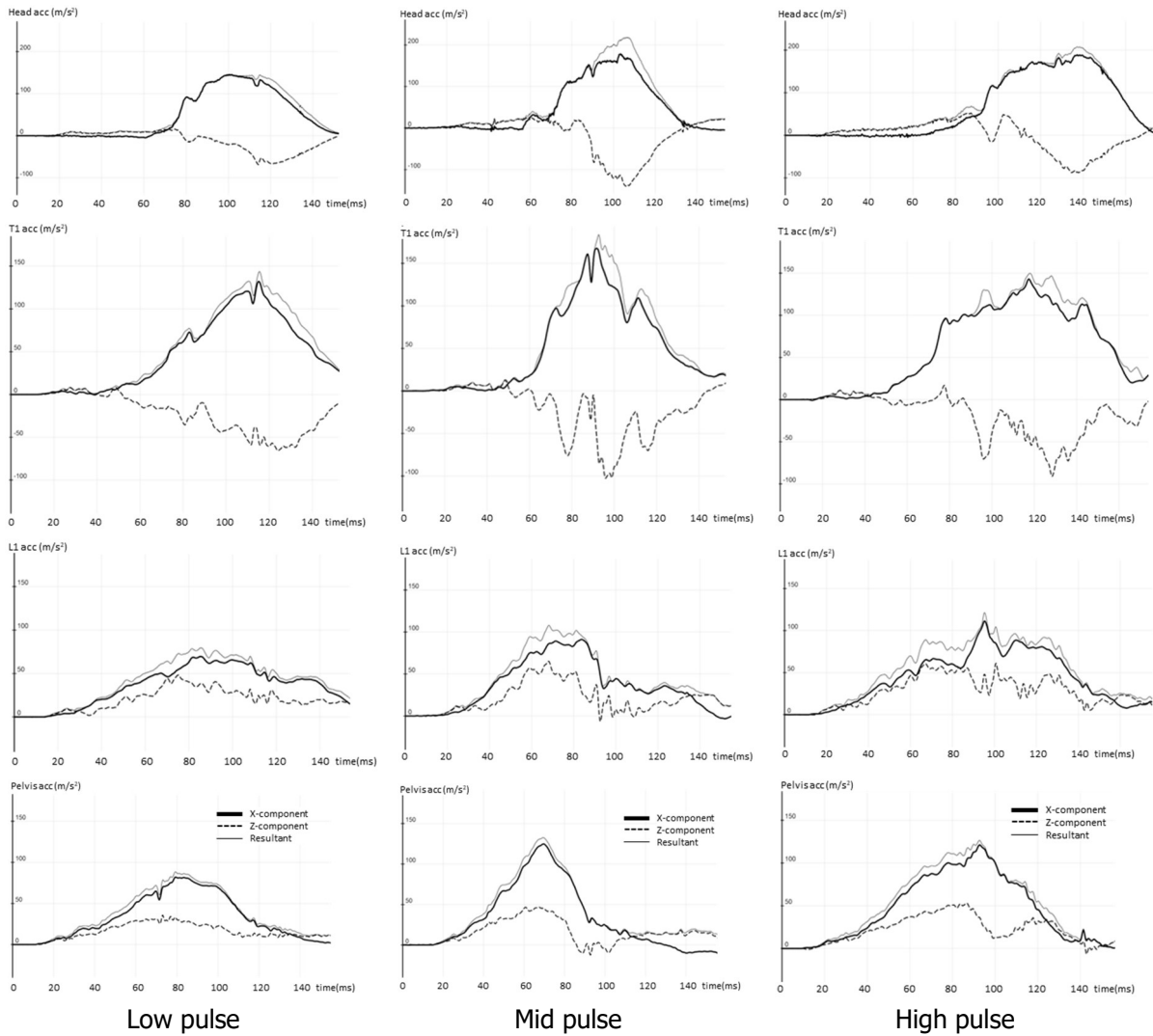


Fig D20. **SET 50M in Toyota seat.** Head, T1, L1 and pelvis accelerations (x, z and resultant) for low pulse (left), mid pulse (mid) and high pulse (right). Tests No. T5, T6 and T8

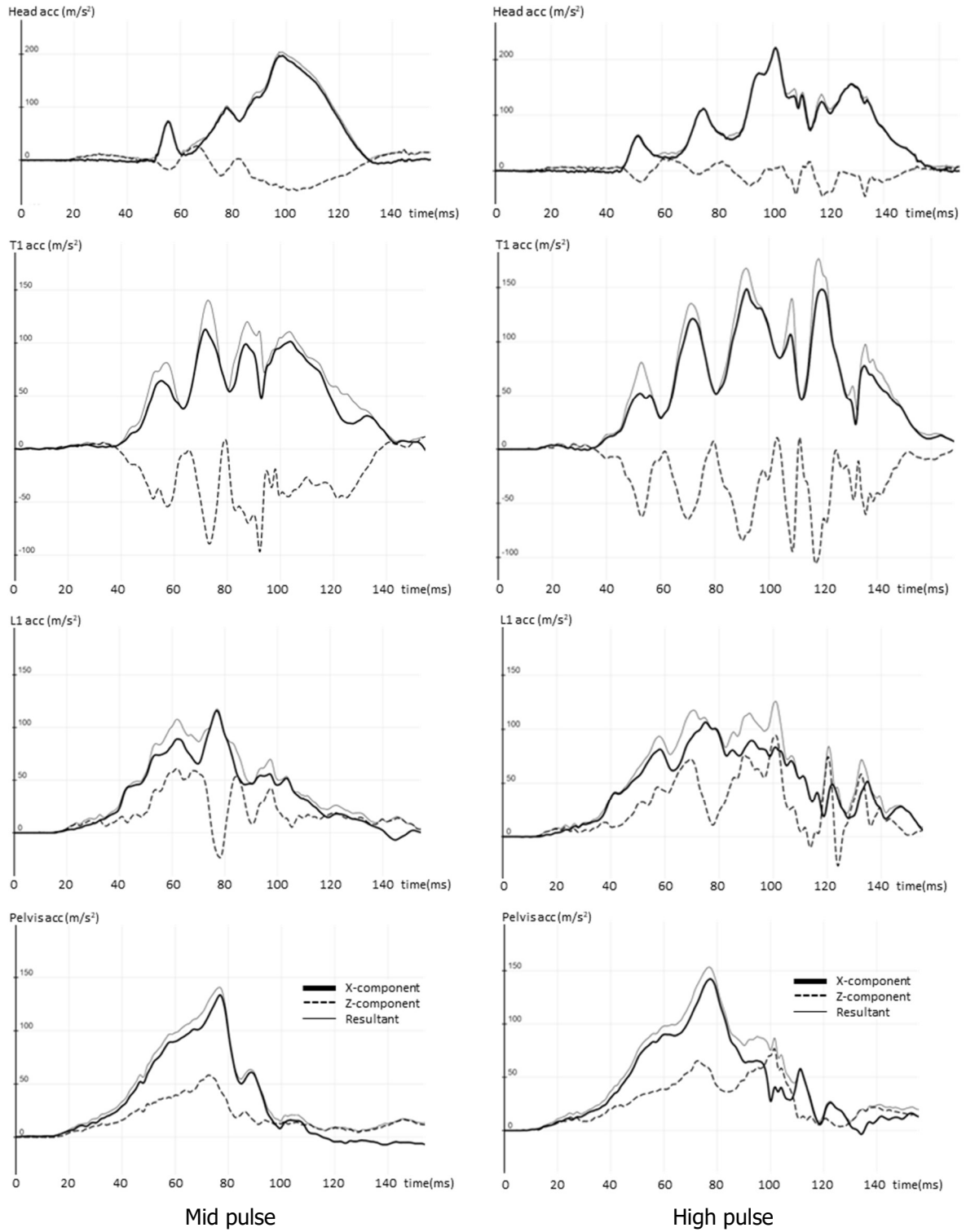


Fig D21. **SET 50M** in **Volvo seat**. Head, T1, L1 and pelvis accelerations (x, z and resultant) for mid pulse (left) and high pulse (right). Tests No. V7 and V8



Discussions

The SET 50F and 50M were durable and sustained no damage throughout the test series. The positioning procedure was easy to use and helped to position the SET in repeatable postures. The most challenging part was to ensure the neck segments in correct position. The neck segments were sensitive to whole-SET movements, especially for the SET 50F. This included direct contact to the head-restraint, which influenced the rotation of the upper segments with varied contact in front or back end with the surrounding neck segments (occurring during the rebound phase). The neck segments of the SET 50M were more stable. At time of the test series no validation of the SETs was available, hence the biofidelity of the SETs is not known. Similarly, no efforts were included to investigate potential injury measures. The study purely focused kinematics, also including the information provided by the linear acceleration output from the sensors in the spine.

The variation of seat designs included in the study enabled a diverse exposure for the SETs. The rigidly attached seatback frame and head-restraint of the Chalmers lab seat, forced the neck into a protracted shape when the torso moved into the seat and the head was restricted by the head-restraint, before the rebound. When seated in the Toyota seat, the initial long backset allowed for a longer part of head x-displacement without no support of the head-restraint, while the Volvo seat offered a balanced support over the head and torso throughout the event. The differences are reflected in the accelerations throughout the spine, which confirms that the SETs are sensitive for different types of seat interaction.

Repeated tests were made for each seat type and SET in the mid pulse. For the Volvo seat, three repeated tests were executed. The overall repeatability was good, see Figure D5 and D9, for SET 50F and SET 50M, respectively. When seated in the Volvo seat all accelerations were stable in all tests. This was due to the early and long head to head-restraint contact, whereafter the whole SET was evenly supported during the event. Fluctuations in the T1 z-accelerations were seen in some of the tests with the SET 50F in the Toyota seat, while not with the SET 50M. The first fluctuations (with the SET 50F) occurred prior to head-restraint contact. In all tests with SET 50F in the Toyota seat, the neck segment had direct contact with the head-restraint. When seated in the Chalmers lab seat, substantial fluctuations were seen for the T1 accelerations of SET 50F. The Chalmers lab seat also had issues with back-plate contact to seat structure in the SET 50F tests, whereby this seat was excluded for the heavier SET 50M.

No injury assessment measures are available for the SETs. Applying existing neck injury criteria, such as the NICmax would not be relevant. NICmax validated for BioRID, cannot be used with the SETs unless modifications are made with respect to the misalignment of the head and T1 sensor, adapting it to the differences in tools, following validation of the SETs' biofidelity. A software is being developed, combining the rotational sensor output with the linear sensor output, targeting to illustrate the spinal curvature during the event. The software will also take the differences in sensor alignment into account and adapt it to the differences between the two SETs. Given a humanlike kinematics of the tool, the spinal curvature during impact is a relevant measure for whiplash assessment. This was highlighted and investigated in a prior study as a means to evaluate the even support of a seat during the dynamic event (Jakobsson and Norin, 2002). This is of extra importance enabling a robust protection for a variety of occupant sizes. The inclusion of two tools of different sizes, such as the SET 50F and 50M has also added to these possibilities.

At time of the current study, the software for curvature estimation was not available, whereby the spine analysis was limited to linear accelerations in four positions along the spine. When analysing the acceleration patterns along the spine, differences were seen between the seats, providing insights into their influence on robust occupant protection. The low accelerations in the tests with the Volvo seat, which also were similar in shape and amplitude in the four sensors along the spine, reflected that the torso and head were evenly supported by the seatback and head-restraint. This is inline with the design



strategy of the Volvo WHIPS function targeting a balanced and even support of the spine, which is also essential to provide similar protection irrespective occupant size (Jakobsson et al., 2000 and 2015).

The overall purpose of the SETs within the VIRTUAL project is to serve as loading devices to help validate seat models as a part of the VT protocol, providing seat models to be used in virtual testing with an expanded set of configurations and occupant models. The current study did not aim to evaluate the feasibility of the SETs for that purpose, mainly due to its early phase, lack of validation studies and limited measurement capabilities. Nevertheless, it provided some insights which could be of value for this purpose. Mainly, their robustness and repeatability are promising, so is their sensitivity of capturing differences in seat design and crash pulses. However, although not fully evaluated in the current study, the SETs' sensor data also when combined into spinal curvature, is likely not enough to capture all seat parameters needed for seat model validation. This was exemplified by the SET 50F in the Chalmers lab seat analysis, which was enabled thanks to the visibility of the different parts of the seatback design. This was helpful for identifying the hard contact. Such analysis was not possible in the Toyota and Volvo seats, whereby more measurements than spinal accelerations and spinal curvature only, is likely required to address such purpose.

Conclusions

The sled series comprising 19 tests was the first tests exposing the SET 50F and 50M (SET v0.1) for the standardized crash pulses of deltaV 16 and 24 km/h. Both the tools were found durable, with an overall acceptable repeatability. The main issues concern the neck design, especially for the SET 50F. Both SETs were sensitive to variations in seat design, and both showed comparable trends with respect to crash severity, within each seat model.

References

- Carlsson A, Linder A, Davidsson J, Hell W, Schick S, Svensson M (2011). Dynamic kinematic responses of female volunteers in rear impacts and comparison to previous male volunteer tests. *Traffic Inj Prev* 12(4), 347-357.
- Euro NCAP (2019). The dynamic assessment of car seats for neck injury protection testing protocol. Version 4.1 November 2019 <https://cdn.euroncap.com/media/57828/euro-ncap-whiplash-test-protocol-v41.pdf>
- Jakobsson L, Lundell B, Norin H, Isaksson-Hellman I (2000). WHIPS-Volvo's Whiplash Protection Study. *Accident Analysis and Prevention* 32:307-319
- Jakobsson L, Norin H (2002). Suggestions for evaluation criteria of neck injury protection in rear end car impacts. *Traffic Injury Prevention*, 3(3):216-223
- Jakobsson L, Lindman M, Björklund M, Victor T (2015). Rear-end impact – Crash prevention and occupant protection. *IRCOBI Conference*, Lyon, France, 2015

Appendix E VIVA+ 50F in Chalmers Lab Seat, Rear-End Impacts

Authors of the original VIRTUAL Milestone report M3.6:

Mats Y. Svensson, Jobin John, Johan Iraeus, J., I.P.A. Putra; Chalmers University of Technology, Gothenburg, Sweden

Corina Klug, Schachner, M., Leo, C. TU-Graz, Austria

Adapted to the context of the VIRTUAL D3.2. report by Lotta Jakobsson (Volvo Cars)

This is the Appendix for Chapter 3.1.3.1

1. Introduction

Addressing one of the main goals of the VIRTUAL project, to define the general workflow of a virtual test procedure, this sub-study serves as the first study using the VIVA+ model in the context of demonstrating the adult occupant protection case. The adult occupant protection case aims to evaluate the whiplash injury protection of a seat and head-restraint for a given car model. The workflow of the VIRTUAL VT protocol starts with a physical test working as a reference for validation of the virtual simulation. The virtual simulation setup is then compared to the physical test setup by replicating the physical test conditions in order to verify the validity of the virtual simulation test setup. The virtual simulation test setup will then be employed to study a range of parameter variations, aimed at enhancing the robustness of assessments by accounting for real-world variability.

The aim of the work in this sub-study was to carry out a first virtual simulation series using the VIVA+ model, to demonstrate the simulation part of VIRTUAL's VT protocol on rear-end impact occupant protection assessment. Including variation of head-restraint position made for demonstrating an example of real-world variability as input to robust assessment, as well the role of the simulation series within the VT protocol for input to the CBT, possible.

2. Methods

Two simulations were executed using the the VIVA+50F seated in the Chalmers Lab seat model while exposed to a low-severity rear-end impact. Head-restraint position was varied between the two simulations.

Rear-end impact crash pulse

The most well-known and well established standardised rear-end impact test procedure is the one conducted by EuroNCAP (2019). The EuroNCAP test protocol initially included three crash pulses. The most used crash pulse corresponds to a velocity change of 15.65 km/h and a mean acceleration of 47.85 m/s². It is usually referred to as the mid-severity crash pulse.

However, the simulations in the current study were run with a crash pulse with a deltaV of 5 km/h, representative of volunteer tests previously run in the corresponding seat. The selection was driven by the validation of the seat model, as well as including the simulations into the context of the virtual tool chain relating to prior tests with the volunteers in that particular seat and crash pulse.

Seat model and VIVA+ 50F

Figure E1 shows the Chalmers lab seat model together with the VIVA+ 50F. The FE model used is based on a generic car seat developed by Chalmers during the 1990s which, although enhanced, has been used in several volunteer tests since (Davidsson et al., 1998, Carlsson et al., 2011). It is a simplified seat enabling tracking of volunteer kinematics for ATD developments. The seatback consists of four horizontal panels attached with coil springs to the side members of the seatback-frame.

The FE model used in the current study is similar to, but an earlier version of the VIRTUAL OS Chalmers lab seat, as described in Chapter 2.1.4. The seat model used is Version 2 and described in Kleinbach (2019). It is based on the seat model in Linder et al. (2018) representing the lab seat, V1, developed at Chalmers and used in volunteer tests by Carlsson et al. (2011). The simulations were carried out with the VIVA+ 50F seated in postures representative of female volunteers in the Chalmers lab seat.



Figure E1. Oblique view of the simulation setup with the Chalmers lab seat used in this sub-study, and the VIVA+ 50F. Only the right half of the VIVA+ 50F is visible.



Figure E2. The two simulation setups, showing the two head to head-restraint distances of 100mm and 150mm.

Parameter variations and protection improvements

The parameter evaluated in the study was the head to head-restraint distance; 100mm and 150mm, respectively (Figures E1 and E2). The parameter was selected as a potential whiplash protection system with adaptive features allowing the protection to be adapted to the individual on the seat. Such adaption may indeed be an automatic, almost momentary adaptation, at the time imminent to the crash. The adaptations could rely on sensor systems continuously monitoring obstacles approaching the rear side of the vehicle, monitoring the instantaneous posture of the occupant. An early example of such a system was presented by Muser et al. (1994).

Injury Detection Systems and Post Processing Tool

The injury detection system (IDS) employed with the VIVA+ model will initially be referred to as a Dummy-based IDS. It will correspond to selected output parameters from the EuroNCAP protocol, in addition to a so-called tissue-based IDS, the Aldman Pressure (ALP).

EuroNCAP uses the following performance criteria:

1. Head-restraint Contact Time (T- HRC(Start) T- HRC(End)).
2. T1 x-acceleration, T1.
3. Upper and Lower Neck Shear Force, Fx.
4. Upper Neck Tension, Fz.
5. Upper and Lower Neck Moment, My.
6. Head Rebound Velocity.
7. NIC.
8. Nkm.
9. Seatback Dynamic Deflection.

It was challenging to apply IDS that correspond to some of the EuroNCAP performance criteria (3, 4, 5 and 8) in the current study, since they use neck force transducer output from the BioRID. The neck forces in the BioRID go through a single load path in well-defined revolute joints. In contrast, these loads in the VIVA+ models are distributed over the entire horizontal cross section of the neck, at the OC and the C7-T1 levels. Hence, these force-based criteria are not included in the current study.

As part of the VIRTUAL project a post processing tool has been developed for use with the VIVA+ models. In the current sub-study, the tool was set to extract data to assess the following parameters:

- A. Head kinematics. Sagittal 3 DOF Head Centre of Gravity (CG) motion in global coordinates.
- B. T1 kinematics. Sagittal 3 DOF T1 motion in global coordinates.
- C. NIC calculation based on the Head and T1 acceleration.
- D. NIC_Max and NIC Risk (based on Ono et al, 2009) calculation.
- E. Aldman Pressure (ALP), calculated based on sagittal angular motion of each cervical vertebra.

The introduction of the ALP in an HBM is a unique new approach, currently obtained from a separate post processing tool. The ALP is a novel tissue-based injury criterion which addresses the same injury mechanism as the NIC, namely nerve cell membrane dysfunction in the cervical dorsal root ganglia. The ALD is, however, a direct fluid dynamics simulation of the fluid flows and resulting injurious transient pressure gradients along the cervical intervertebral canals (Yao et al.; 2016).

Injury risk assessment

Ideally the improvements in IDS responses can be transformed into risk reductions. The study of Ono et al. (2009) provides an example of WAD injury criteria, for an average size male HBM that correlate to injury risk and where risk functions were suggested for this criterion. The risk function of the NIC_Max is shown in Figure E3.

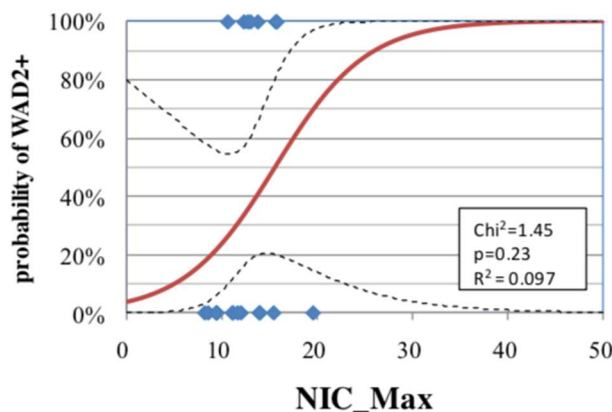


Figure E3. The probability of WAD2+ as a function of NIC_Max (Ono et al., 2009).

The ALP is hypothesized to correlate well with the NIC_Max. An attempt will be made to find a transfer function between NIC_Max and the negative ALP peak value. The same correlation and risk function of the ALP may then be used as a preliminary assumption also for female HBMs.

Postprocessing workflow using Dynasaur, Integration with VIVA+

The Dynasaur files required for object and calculation definition were generated for the VIVA+ 50F. The object definition files specify the entities of the model to be postprocessed. The calculation definition files are required to extract outputs of the model entities from the LS-Dyna output binaries. Landmarks required for output extraction were added to the VIVA+ 50F model.

3. Results

Figures E4 and E5 show the time of maximum rearward seatback deflection during the rear-end impact and initial position of the VIVA+50F, for the two simulations. Figure E4 provides a cut-through view of the VIVA+ 50F in the simulation with head to head-restraint distance of 150 mm. For that configuration, the maximum seatback deflection occurred at 160 ms. Figure E5 shows the VIVA+ 50F in the simulation with the shorter head to head-restraint distance of 100 mm, for which the maximum seatback deflection occurred at 120ms.

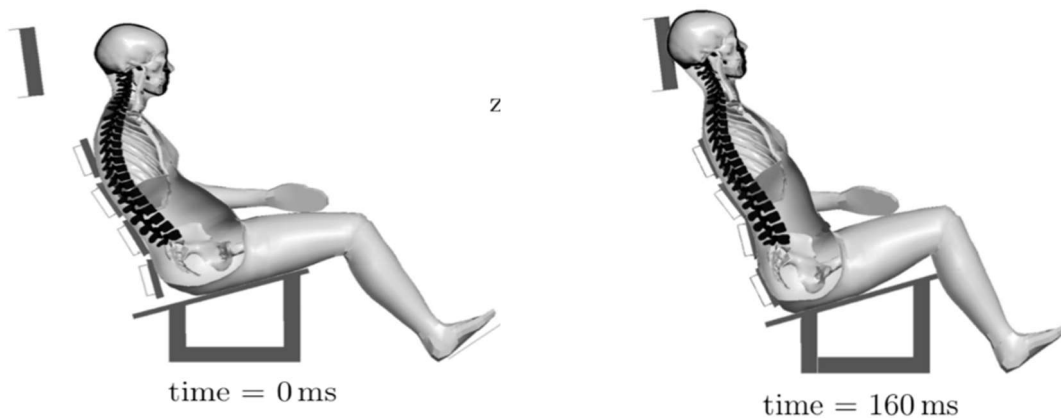


Figure E4. Simulation with a head to head-restraint distance of 150 mm. VIVA+ 50F position at start of rear-end impact sequence (t=0 ms) and at maximum rearward seatback deflection (t=160 ms)

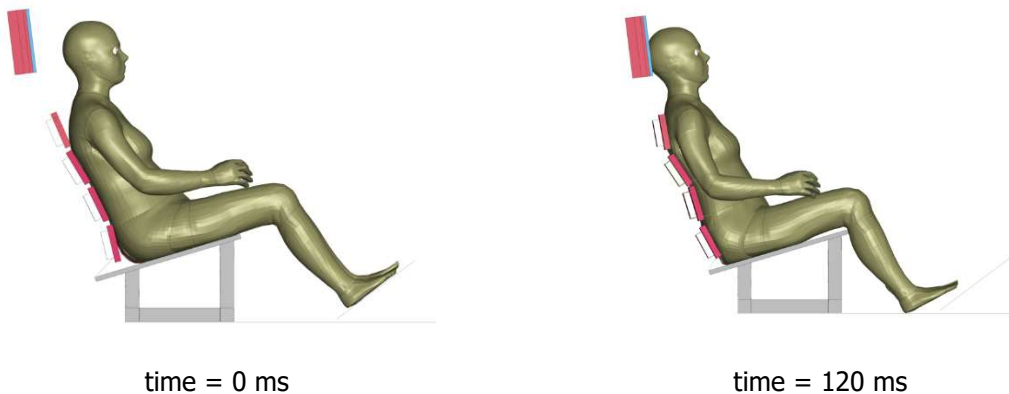


Figure E5. Simulation with a head to head-restraint distance of 100 mm. VIVA+ 50F position at start of rear-end impact sequence (t=0 ms) and at maximum rearward seatback deflection (t=120 ms)

Head and T1 Kinematics

The horizontal displacements of the Head CG and the T1 vertebra are shown in Figure E6, for the two head to head-restraint distances, HR=100mm and HR=150mm. The maximum rearward T1 displacements are equal but the rebound is faster after approximately 125ms in the HR=100mm compared to the HR=150mm. The head rearward displacement increased by about 35mm between HR=100 and HR=150. Figure E7 shows the head velocity relative to the sled and head relative T1 horizontal kinematics for the two head to head-restraint (HR) distances.

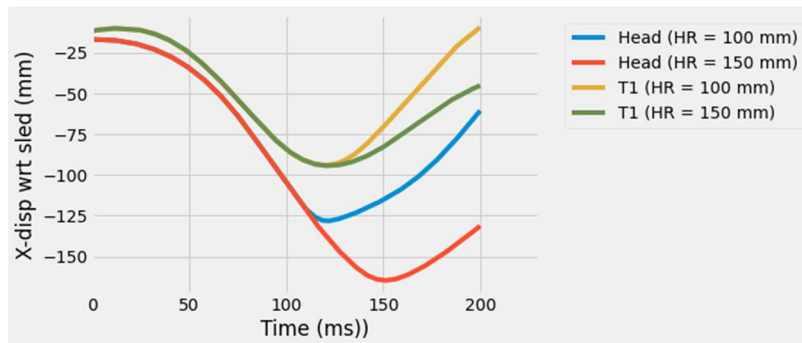


Figure E6. Head and T1 horizontal kinematics with respect to the sled for the two head to head-restraint distances (HR=100mm and HR=150mm).

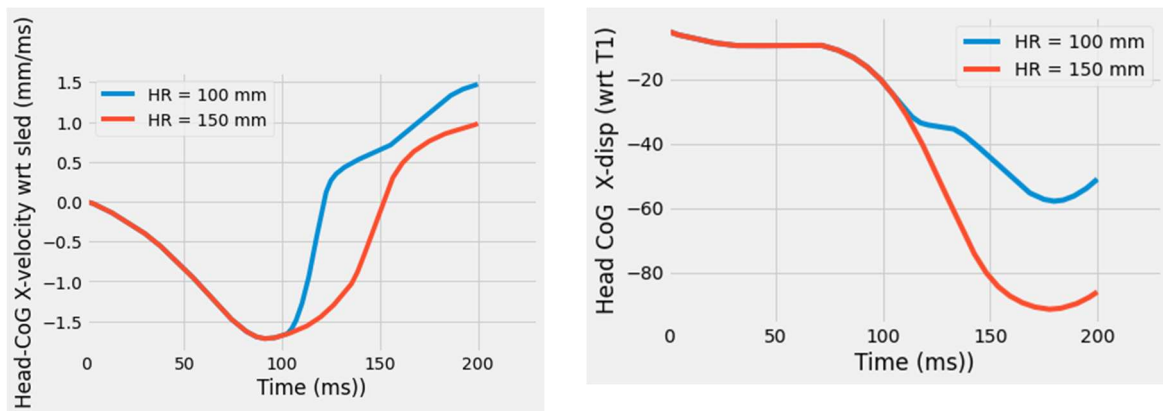


Figure E7. Head velocity relative to the sled and head relative T1 horizontal kinematics for the two head to head-restraint distances (HR=100mm and HR=150mm)

Neck Injury Criterion (NIC)

NIC time histories, NIC max and the risk corresponding to maximum NIC was calculated using Dynasaur functions. The NIC curves for HR=100mm and HR=150mm are shown in Figure E8.

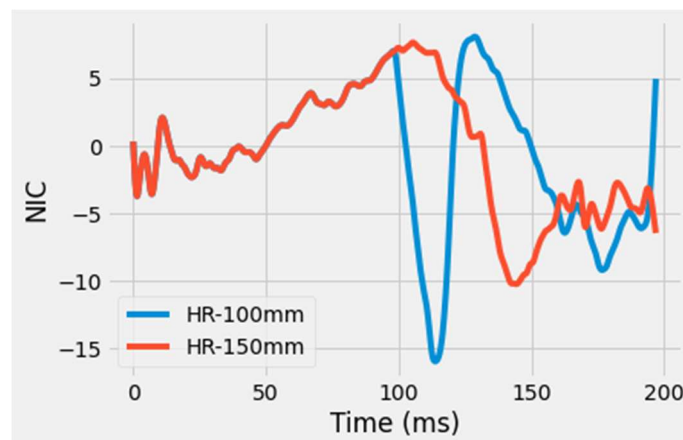


Figure E8. The NIC curves for HR=100mm and HR=150mm.

The NICmax, which is defined as the first peak before the NIC drops below zero are summarised in Table E1, together with the NIC risk calculated based on Ono et al. (2009).

Table E1. NICmax and NIC risk (based on risk curve from Ono et al., 2009)

Simulation	NIC Max	NIC risk
Head to head-restraint distance of 100 mm	6.90	0.139
Head to head-restraint distance of 150 mm	9.39	0.144

Vertebral Rotations and Aldman Pressure calculation

The individual sagittal angular displacement of each neck vertebra is shown in Figure E9. With the closer head-restraint position (HR=100mm), the maximum vertebral rearward angular displacement magnitude changed from approximately 50° to about 30°.

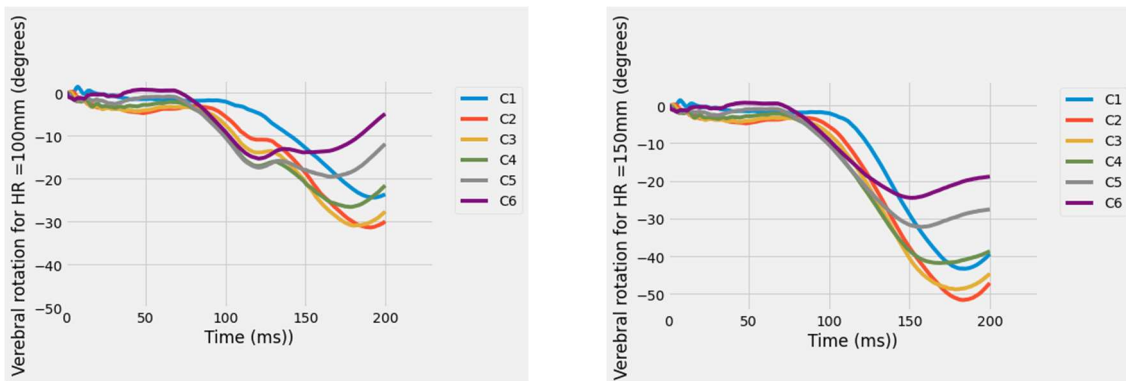


Figure E9. Cervical vertebrae rotation for HR = 100mm (left) and HR = 150mm (right).

The ALP shown in Figure E10 was simulated according to Yao et al (2016). With the closer head-restraint position (HR=100), the maximum ALP magnitude changed from 1,5Pa to 0,7Pa.

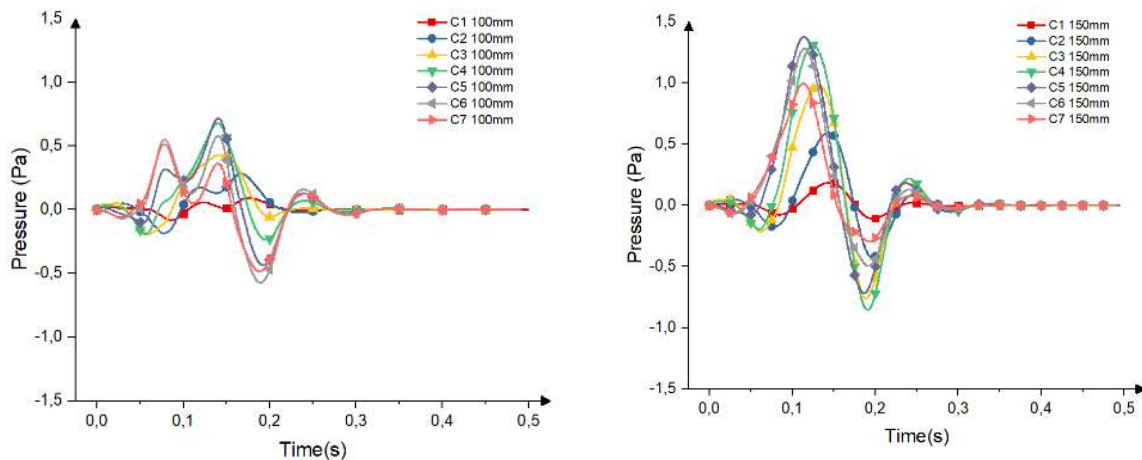


Figure E10. ALP at each vertebral level for HR=100mm (left) and HR=150mm (right).



The files used in this exemplary workflow (Binary outputs, Dynasaur definition files, Jupyter notebooks) are available on the VIRTUAL OpenVT platform at https://virtual.openvt.eu/wp-2/virtual-tool-chain-chalmers_seat

4. Discussion

The aim of this sub-study was to carry out a first rear-end impact test series to demonstrate the simulation part of the virtual rear-end impact test protocol. The final goal involved demonstrating the full virtual tool chain applied to whiplash protection assessment in rear-end impacts, in order to include both female and male vehicle occupants in the assessment. The scope of the present sub-study was, however, limited to average female occupants, using the most recent version of the VIVA+ 50F HBM. At the time of the execution of this sub-study, no male counterpart was available.

Although not having used the final version of the seat model in this sub-study, a VIRTUAL OS seat model of the Chalmers lab seat is made available as part of the VIRTUAL project, further described in Chapter 2.1.4). The seat model is a virtual version of the so-called Chalmers lab seat that has been used in volunteer testing. The advantage of this well-defined seat design is that it has already been tested with volunteers. The volunteer data can be used as a replacement for data from physical loading devices.

The simulations were run with the acceleration conditions previously used with the Chalmers Lab seat, at a ΔV of 5 km/h. The Chalmers lab seat model was validated in this acceleration condition. However, for future work, due to it being more representative of higher risk situations for the occupants, the EuroNCAP mid-severity rear-end impact test condition should be included as well.

The influence of head to head-restraint distance using the VIVA+ 50F was investigated. Future studies should include additional parameters in addition to the VIVA+ 50M, striving towards gender balance in the risk reduction.

The current study shows that, for front seat occupants in rear-end impacts with $\Delta V=5\text{km/h}$, a reduction in head to head-restraint distance from 150 mm to 100mm reduced the estimated risk of WAD from 0,144 to 0,139. This reduction was derived from the corresponding NIC_{max} reduction from 9.39 to 6.90. At the same time the peak vertebral angular displacement was lowered from 50° to 30° . This reduction in vertebral kinematics led to a reduction in the tissue-based injury criterion ALP, from a maximum magnitude of 1,5 Pa to 0,7 Pa. The stronger reduction in ALP indicates that ALP is a more sensitive criterion, intended to directly address a precise injury mechanism, The ALP mechanism is, however, only one of several potential mechanisms. Should we in future find that the ALP mechanism is a good predictor for WAD risk, it would become a much more sensitive and precise criterion.

The best available risk functions for WAD were found in a study by Ono et al. (2009). These risk functions are defined based on insurance data including both crash conditions and injury outcome. They were adapted to one type of HBM and one car model, and the risk functions have wide confidence intervals. The only applicable risk function was found to be NIC_{max} , which was selected to be used in the current study, although not designed for the exact context of the current study.

The ALP is hypothesised to correlate well with the NIC_{max} . A next step could include attempting to develop a transfer function between NIC_{max} and the negative ALP peak value. The same correlation and risk function of the ALP may then be used as a preliminary assumption also for female HBMs. It is recommended that a future evaluation of NIC ought to be carried out, using results of Ono et al. (2009) incorporating the ALP and including both of the VIVA+ 50F and 50M versions.

5. Conclusion

A first rear-end impact test series was carried out to demonstrate the simulation part of the virtual rear-end impact test protocol. The results show the change in injury detection parameters between a reference seat and a modified seat design with shorter head to head-restraint distance. An example of change in injury risk is given, based on the risk curves of Ono et al. (2009).

A whiplash injury risk curve for the average male HBM in Ono et al (2009) was used as the best available source to assess injury risk based on the NIC. Force based NIC have not been used in the VIVA+ in this study, since the translation from the ATD environment is not transferable at this stage. The tissue based ALP criterion has been implemented and evaluated for the load cases. It is recommended that new injury risk curves are adapted to the VIVA+ 50F and 50M for ALP, NIC and other appropriate criteria, using the same methodology.

6. References

- Carlsson A, Linder A, Davidsson J, Hell W, Schick S, Svensson M. (2011). Dynamic kinematic responses of female volunteers in rear impacts and comparison to previous male volunteer tests. *Traffic injury prevention*, 12(4), 347-357.
- Davidsson J, Deutscher C, Hell W, Limder A, Lövsund P, Svensson MY. (1998) Human volunteer kinematics in rear-end sled collisions. *IRCOBI Conf.* Gothenburg, Sweden
- Euro NCAP (2019). The dynamic assessment of car seats for neck injury protection testing protocol. Version 4.1 November 2019 <https://cdn.euroncap.com/media/57828/euro-ncap-whiplash-test-protocol-v41.pdf>
- Kleinbach (2019): Simulation of Occupant Kinematics using Active Human Body Models. *Doctoral thesis, Institut für Technische und Numerische Mechanik der Universität Stuttgart, Germany*
- Linder A, Holmqvist K, Svensson MY (2018). Average male and female virtual dummy model (BioRID and EvaRID) simulations with two seat concepts in the Euro NCAP low severity rear impact test configuration. *Accident Analysis & Prevention*, 114, 62-70.
- Muser MH, Dippel C, Walz F (1994). Neck injury prevention by automatically positioned head restraint. In: *Advances in Occupant Restraint Technologies. Proc of joint AAAM-IRCOBI special session*, September 22, 1994, Lyon France.
- Ono K, Ejima S, Yamazaki K, Sato F, Pramudita JA, Kaneoka K, Ujihashi S (2009). Evaluation criteria for the reduction of minor neck injuries during rear-end impacts based on human volunteer experiments and accident reconstruction using human FE model simulations. *IRCOBI Conf.* York, UK
- Yao HD, Svensson MY, Nilsson H (2016). Transient pressure changes in the vertebral canal during whiplash motion– A hydrodynamic modeling approach. *Journal of biomechanics*, 49(3), 416-422.

Appendix F Input to CBT - Whiplash Accident Reconstruction Simulations

Authors: I.P.A. Putra, Mats Y. Svensson
Chalmers University of Technology, Gothenburg, Sweden

This is the Appendix for Chapter 3.1.3.2.

1. Introduction

Generally considered as soft tissue neck injuries, Whiplash Injuries or Whiplash Associated Disorders (WADs) are a worldwide concern. Annually, around 300 000 European Union (EU) citizens suffer from whiplash injuries (Kullgren et al., 2007). Meanwhile, in the United States, the incidence of whiplash injuries was estimated to approximately 328 per 100.000 people (Quinlan et al., 2004). A 10 year based study in Australia concluded that one-third of the 150.794 traffic accident compensation claims were for whiplash injury (34%) (Berecki-Gisolf et al., 2013). In Japan, an online survey with 4,164 participants involved in traffic accidents revealed that 183 people had neck pain for more than six months, while another 333 subjects had minor neck pain requiring treatment within three months (Oka et al., 2017). Although WADs are not life-threatening, they can lead to long term consequences as well as permanent disabilities (Kullgren et al., 2007, Nygren, 1983, Krafft, 1998).

Many methods have been proposed to reduce the risk of whiplash injury such as improved seat design geometry and head-restraint dynamic properties, or an active system that would move the seat during a crash. The main idea of whiplash protection systems is to reduce the relative motion between the occupant's head and the torso, that occurs during a rear-end impact, and to control and absorb the impact energy. The reduction in head and torso relative motion will subsequently reduce the relative motion between the adjacent vertebrae in the neck. Based on a study by Kullgren et al. (2013), such systems could reduce the risk of sustaining WAD symptoms more than one month compared to standard seats (approximately 38% risk reduction using Volvo WHIPS and approximately 23% reduction for the Toyota WIL).

The present study was proposed to understand how a reduction in head to head-restraint distance would reduce the risk of whiplash injury with the main purpose of providing input to the CBT. Previous studies have shown that reducing head to head-restraint distance could lead to a lower risk of sustaining whiplash injuries (Olsson et al., 1990, Jakobsson et al., 2008). Finite Element (FE) Human Body Models (HBMs), especially the VIVA+ HBMs, which have been developed within the VIRTUAL project, would be suitable for gaining a better understanding of occupant kinematics during a crash. Accident reconstruction simulations were conducted using an open-source Toyota Yaris FE seat model and real-world accident data from Folksam. The specific objective of this study was to evaluate the influence of different head to head-restraint distances on the Whiplash Associated Disorders 2+ (WAD2+) injury risk, by conducting accident reconstruction simulations based on real-world accident data.

2. Methods

2.1 VIVA+ Human Body Models

VIVA+ FE HBMs representing the 50th percentile female (50F) and male (50M) occupants were used in the present study (Figure F1). The 50th percentile female occupant model was initially developed and used as a baseline to create other models by conducting rescaling and morphing. The derivative models include the 50th percentile male occupant model. The elements in the morphed models are identical to the baseline model; however, the nodal coordinates were adjusted accordingly. The original geometry of the baseline model (including outer body shape, ribcage, femur, tibia and pelvis) was based on several statistical shape models. Besides changes in geometry to develop an average male from an average female, several properties were also updated. These properties include head mass and inertial properties, the densities of soft tissues, knee ligaments and quadriceps muscles. The VIVA+ HBMs are described further in VIRTUAL Deliverable D2.2.

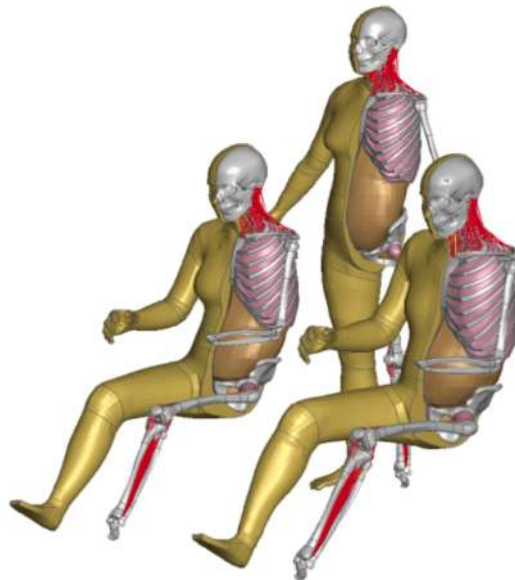


Figure F1. VIVA+ Human Body Models.

2.2 VIRTUAL OS Vehicle Seat Model

The open-source seat FE model (Figure F2) used in the current study was developed based on a Toyota Auris driver seat (model year 2010-2012). The model was developed within the VIRTUAL project and validated against an experimental test conducted by Genzel (2020), see Chapter 2.1.3. Shell elements with material parameters as in the open-source Toyota car model (Marzougui et al., 2014) were used to model the metal and plastic parts of the seat. Solid elements with material properties based on Markert (2005) were adopted for the seat foam. The validation results showed reasonable agreement between the numerical model and the physical test. More information on the development and properties of the seat model is presented in Appendix A. The open-access version of the seat model, the VIRTUAL OS Vehicle seat model, can be found on the VIRTUAL OpenVT platform at <https://virtual.openvt.eu/fem/open-access-adult-seat-model>.



Figure F2. The VIRTUAL OS Vehicle seat model representing a Toyota Auris seat.

2.3 Crash Pulses

Six crash pulses were selected based on the Folksam database. In total, there were 38 rear-end impact cases found with a similar seat model as the Toyota Auris FE Model (Auris 07-13). From those 38 cases, 24 cases were selected (10 females and 14 males) matching the defined criteria. The criteria included that the occupant should be an adult (>18 years old) driver or front seat passenger, with known gender. Additional criteria were applied to the 24 selected cases for selecting the 'injured cases' from the general cases. 'Injured cases' were defined as cases involving occupants who had experienced WAD Level 1-3 (Table F1), with symptom duration of more than one month, while the remaining cases were considered 'uninjured cases'. Three cases, all female, were found to match the definition of 'injured cases'. Table F2 and Figure F3 provide details on crash severity. The resultant delta velocities were 10.6 km/h, 10.7 km/h and 15.9 km/h, with a resultant peak acceleration of 11.6g, 4.9g and 8.6g, respectively. The mean acceleration were 4.8g, 3.1g and 4.8g. The crash pulses from the three cases were selected for use in the present study.

Table F1. Whiplash Associated (WAD) Level

Whiplash Associated Disorder (WAD) Explanation	
Grade 0:	No complaints of the neck. No physical sign(s).
Grade I:	Neck complaints including pain, stiffness, or tenderness only. No physical sign(s).
Grade II:	Neck complaint AND musculoskeletal sign(s). Musculoskeletal signs include decreased range of motion and point tenderness.
Grade III:	Neck complaint AND neurological sign(s). Neurological signs include decreased range of motion and point tenderness.
Grade IV:	Neck complaint AND fracture or dislocation.

Table F2. Impact severity measures for the crash pulses of ‘injured cases’

Delta Vel. Res. (km/h)	Mean Acc. Res. (g)	Peak Acc. Res. (g)	Pulse Name
15.9	4.8	11.6	Pulse 1 Injured
10.7	3.1	4.9	Pulse 2 Injured
10.6	4.8	8.6	Pulse 3 Injured

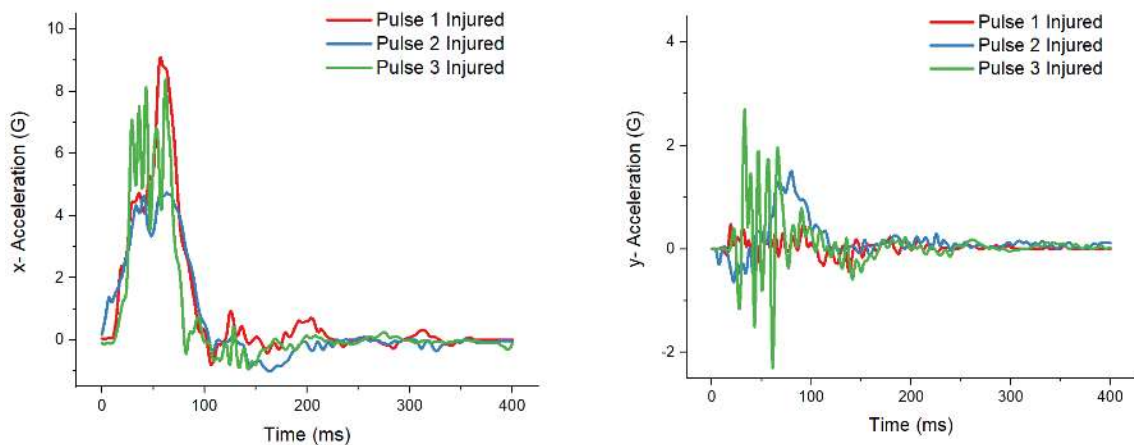


Figure F3. X and y acceleration for the for the crash pulses of ‘injured cases’.

Three other cases (Table F3) were selected to represent ‘uninjured cases’. These three cases were selected from the other female cases. Table F3 and Figure F4 provide details on the crash severity of these three cases. The resultant delta velocities were 11.5km/h, 9 km/h and 10.6km/h, with peak resultant acceleration of 11g, 4.9g, and 8.6g, respectively. The mean acceleration were 4.8g, 2g and 4.8g. It is worth mentioning that one injured and uninjured case had the same impact severity and came from the same car. In that car, the female driver was injured according to the definition, while the female front seat passenger was not.

Table F3. Impact severity measures for the crash pulses of ‘uninjured cases’

Delta Vel. Res. (km/h)	Mean Acc. Res. (g)	Peak Acc. Res. (g)	Pulse Name
11.5	4.8	11	Pulse 1 Uninjured
9	2	4.9	Pulse 2 Uninjured
10.6	4.8	8.6	Pulse 3 Uninjured

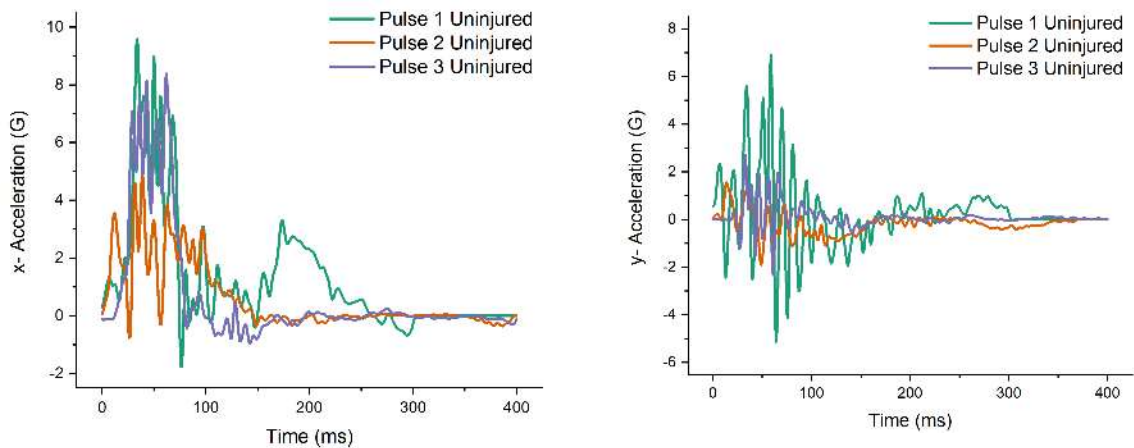


Figure F4. X and y acceleration for the for the crash pulses of 'uninjured cases'

2.4 Head to Head-restraint Distance

Two head to head-restraint distances (Figure F5) were simulated (120mm and 95mm) in order to investigate the effect of differences in head to head-restraint distance on the overall head-T1 kinematics and the risk of WAD2+ injury. At first, the model was positioned following the positioning protocol from EuroNCAP. The method resulted in a 120mm distance between the head and the head-restraint. The head-restraint of the seat was then scaled up in the horizontal x-direction to reduce the distance while maintaining the original surface curvature of the head-restraint. The scaled head-restraint resulted in a 95mm distance between the head and the head-restraint.

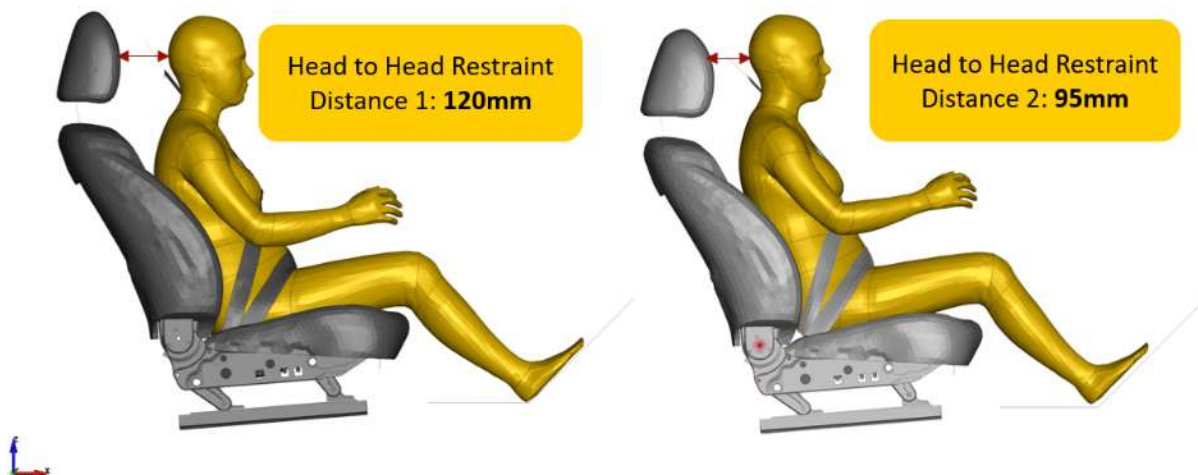


Figure F5. The two configurations showing the head to head-restraint distance.

2.5 Simulation Setup and Computational Environment

The duration of each simulation was 800ms, including 350ms of gravity settling. Each model was run with the same crash pulse in two different head to head-restraint distances. Therefore, four simulations (two for the female and two for the male models) were needed (Tables F4 and F5). In total, 24 simulations were performed. All simulations were run using LS-Dyna ver9.2 double precision. LS-Prepost 4.8 (64-bit), ANSA v18.1.0 (64-bit), Matlab R2019B and OriginPro 2019(64-bit) were used as pre-and post-processing software.

Table F4. Simulation matrix for VIVA+50F

Female Cases	Head to Head-Restraint Distance A (120mm)	Head to Head-Restraint Distance B (95mm)
Pulse 1 Injured (5762)	Sim1A-Injured	Sim1B-Injured
Pulse 2 Injured (6463)	Sim2A-Injured	Sim2B-Injured
Pulse 3 Injured (6605)	Sim3A-Injured	Sim3B-Injured
Pulse 1 Uninjured (6306)	Sim1A-Uninjured	Sim1B-Uninjured
Pulse 2 Uninjured (6309)	Sim2A-Uninjured	Sim2B-Uninjured
Pulse 3 Uninjured (6605)	Sim3A-Uninjured	Sim2B-Uninjured

Table F5. Simulation matrix for VIVA+ 50M

Male Cases	Head Head-Restraint Distance A (120mm)	Head to Head-Restraint Distance B (95mm)
Pulse 1 Injured (5762)	Sim1A-Injured	Sim1B-Injured
Pulse 2 Injured (6463)	Sim2A-Injured	Sim2B-Injured
Pulse 3 Injured (6605)	Sim3A-Injured	Sim3B-Injured
Pulse 1 Uninjured (6306)	Sim1A-Uninjured	Sim1B-Uninjured
Pulse 2 Uninjured (6309)	Sim2A-Uninjured	Sim2B-Uninjured
Pulse 3 Uninjured (6605)	Sim3A-Uninjured	Sim2B-Uninjured

2.6 Probability of WAD2+ based on Ono et al., 2009

The risk function that defines the probability of WAD2+ injury (Figure F6) was adopted from Ono et al. (2009) and was used to evaluate the WAD2+ injury risk. The risk function was derived from a combination of human volunteer tests and 20 cases of accident reconstruction simulations.

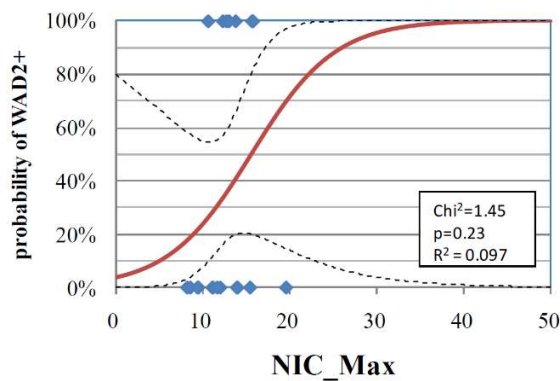


Figure F6. Risk function for the probability of WAD2+ injury in correlation with NICmax, based on Ono et al. (2009)

3. Results

3.1 Head CoG Displacement Relative to T1 Displacement

Comparison of head CoG displacements relative to T1 displacements are presented in Figures F7-F10. The displacements were analysed and compared between the two configurations (different head to head-restraint distance). The male model generally had a higher peak head CoG relative to T1 displacement, compared to the female model in any crash pulse. For both models, the shorter head to head-restraint distance and lower first peak displacements were seen for all crash pulses. The relative difference to the larger head to head-restraint distance was more pronounced in the horizontal head relative to T1 displacement (x-linear displacement) than in other directions.

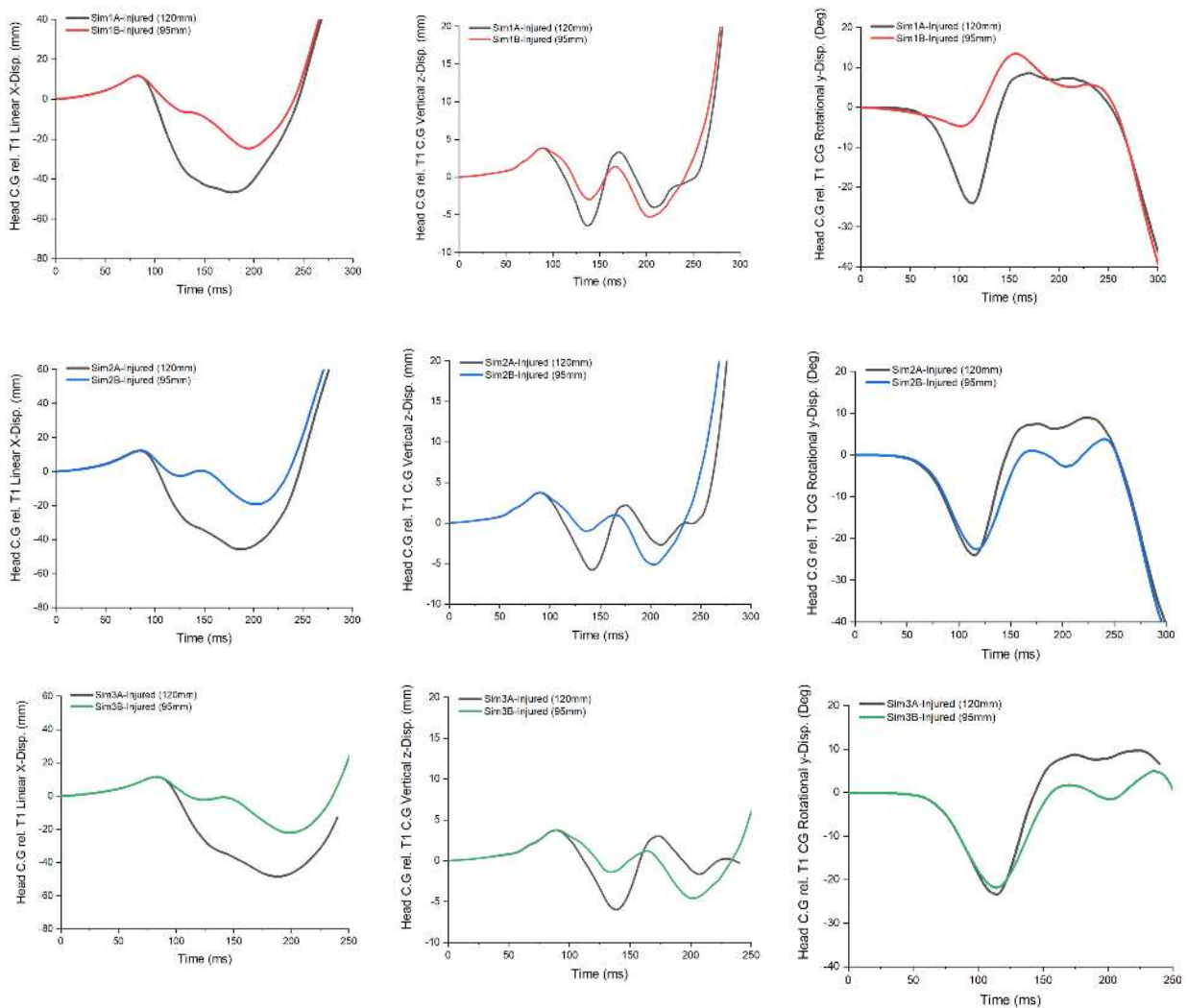


Figure F7. Head CoG displacement relative to T1 displacement of female 'injured cases'

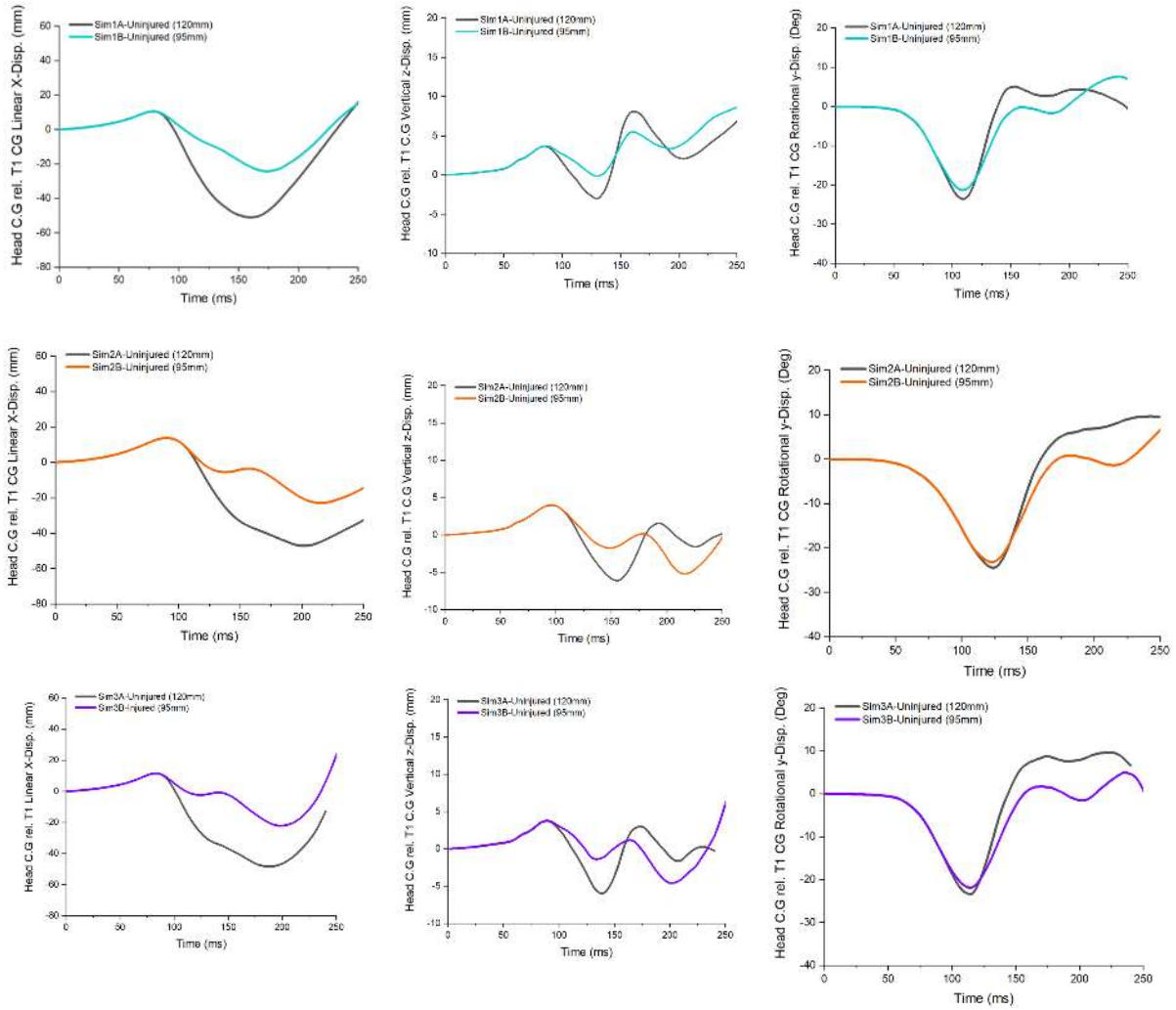


Figure F8. Head CoG displacement relative to T1 displacement of female 'uninjured cases'.

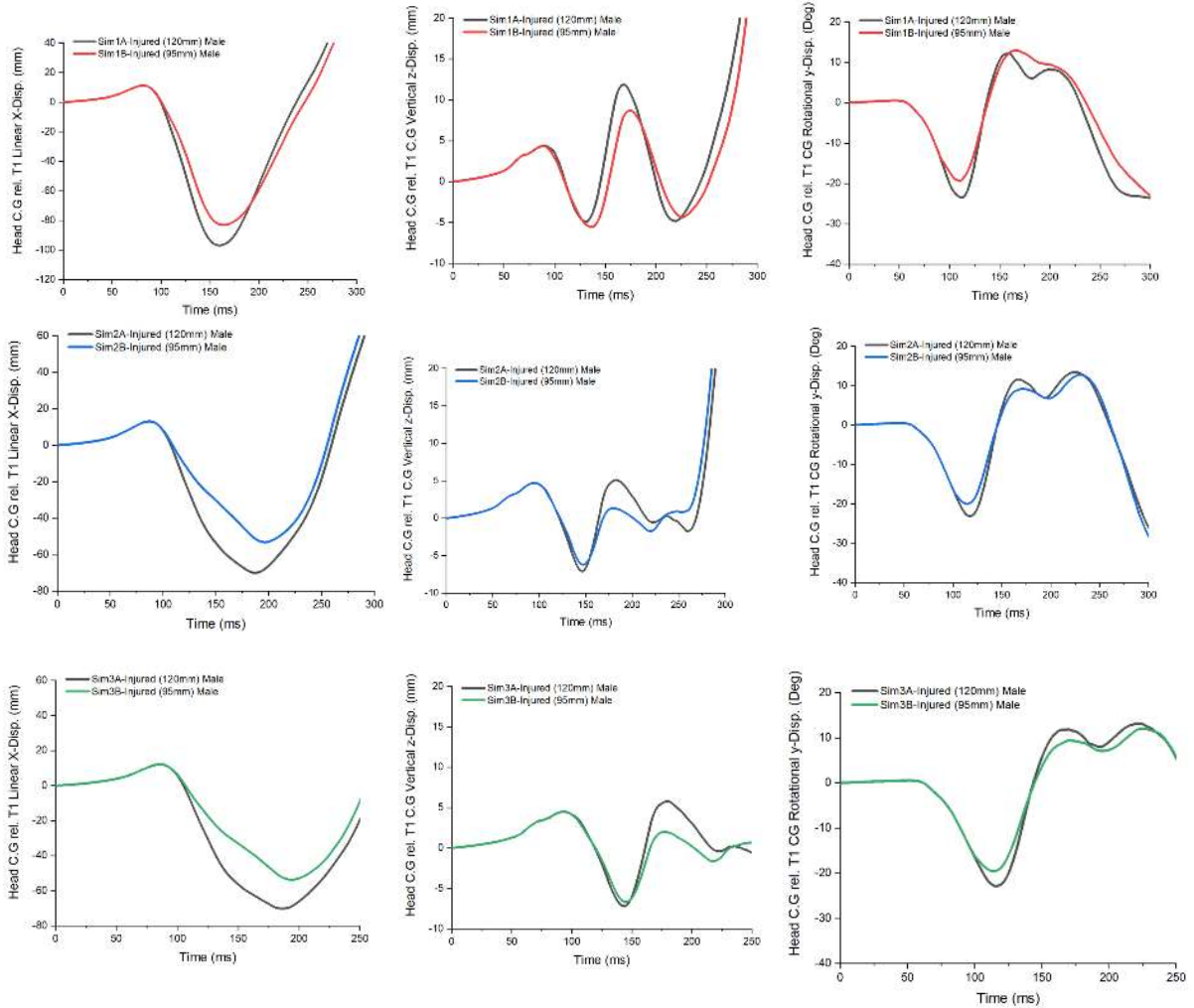


Figure F9. Head CoG displacement relative to T1 displacement of male 'injured cases'.

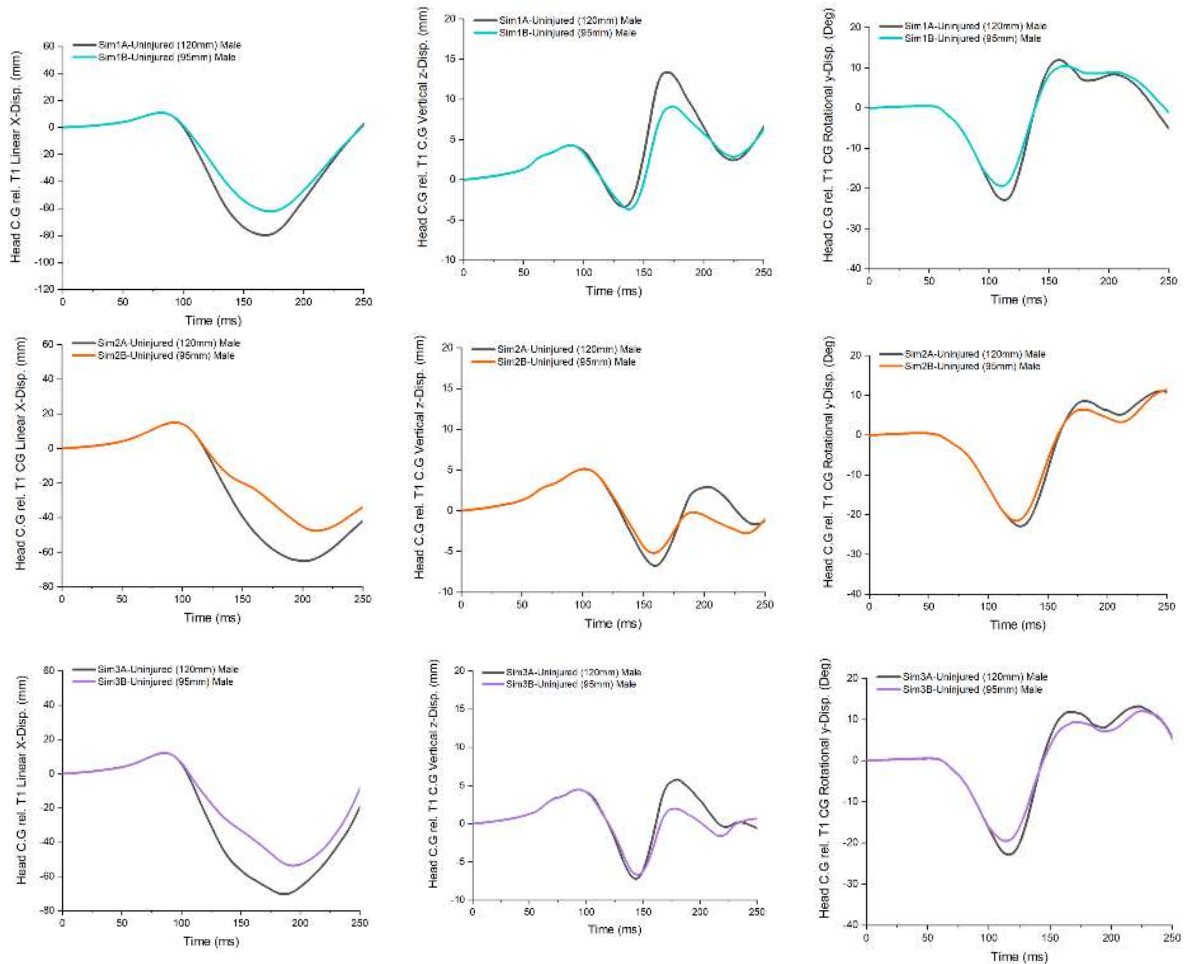


Figure F10. Head CoG displacement relative to T1 displacement of male 'uninjured cases'.

3.2 Neck Injury Criteria

For each case, the Neck Injury Criterion (NIC, in m^2/s^2) was calculated based on the protocol from the EuroNCAP Technical Bulletin – Data Format and Injury Criteria Calculation (June 2020). The NIC curves are plotted in Figure F11 for the female model simulations and Figure F12 for the male model simulations. The value of NIC_{max} , defined as the first peak value of NIC before or immediately after contact with the head-restraint, are presented in Tables F6 and F7. For both the female and male model, a lower NIC_{max} was observed in all crash pulses, for the shorter head-restraint distance as compared to the larger distance. For the female model, the difference in NIC_{max} values ranged from 1.36 to 8.99 (Table F6). Meanwhile, for the male model, the corresponding NIC_{max} differences ranged from 0.7 to 6.87 (Table F7).

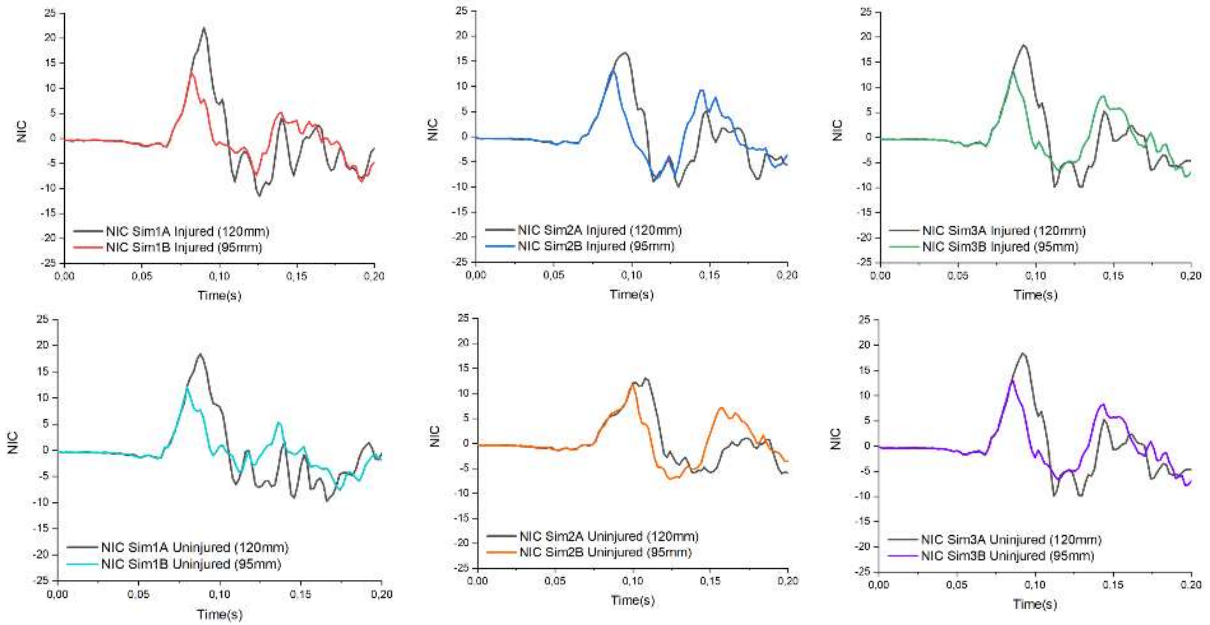


Figure F11. Comparison of NIC of VIVA+ Female Model Simulations.

Table F6. NIC_{max} of VIVA+ female model simulations

Simulation	NIC _{max}	
	Head to Head- Restraint 120mm	Head to Head- Restraint 95mm
Sim 1 Female Injured	22.10	13.11
Sim 2 Female Injured	16.74	15.05
Sim 3 Female Injured	18.43	16.20
Sim 1 Female Uninjured	18.45	11.92
Sim 2 Female Uninjured	13.09	11.73
Sim 3 Female Uninjured	18.43	16.20

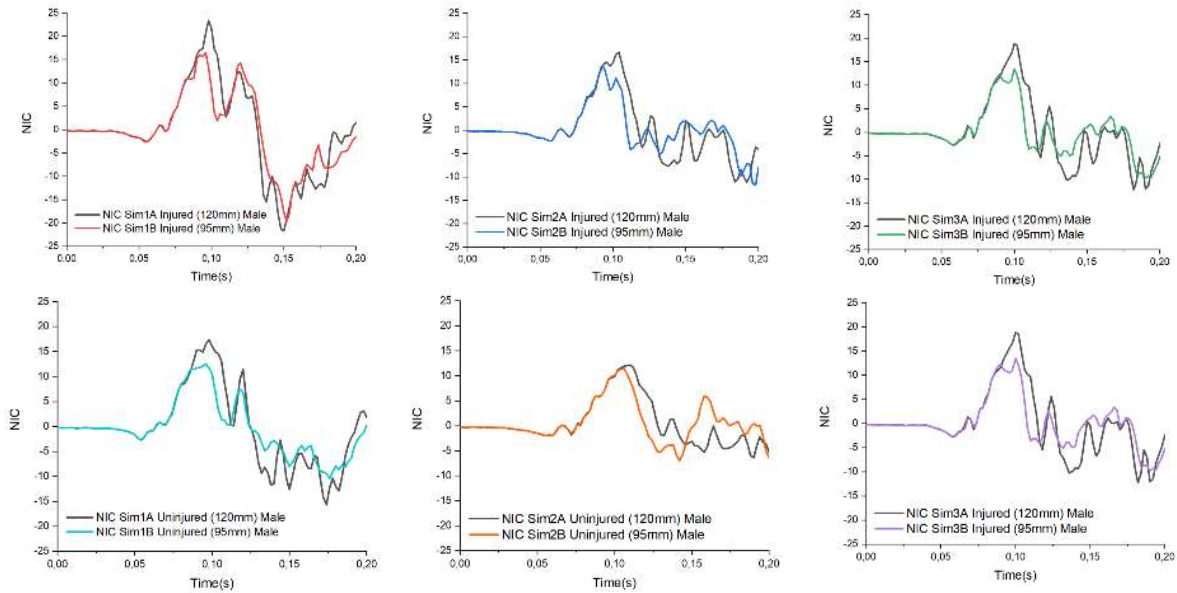


Figure F12. Comparison of NIC of VIVA+ male model simulations.

Table F7. NIC_{max} of VIVA+ male model simulations

Simulation	NIC _{max}	
	Head to Head-Restraint	Head to Head-Restraint
	120mm	95mm
Sim 1 Male Injured	23.37	16.50
Sim 2 Male Injured	16.66	13.62
Sim 3 Male Injured	18.83	13.47
Sim 1 Male Uninjured	17.31	12.56
Sim 2 Male Uninjured	12.16	11.46
Sim 3 Male Uninjured	18.83	13.47

3.3 Probability of WAD2+ injury using risk function based on Ono et al. (2009)

After the NIC_{max} value of each simulation was calculated, the probability of WAD2+ injury was analysed by plotting the NIC value of each case to the risk function proposed by Ono et al. (2009) (Figure F5). The risk function contains the probability of WAD2+ injury, based on the value of NIC_{max}. Using the average curve, it was found that the likelihood of WAD2+ injury was significantly lower in shorter head to head-restraint distances in both female and male cases (Tables F8 and F9). The average injury probability value went down from 61% to 42% after the intervention was introduced using the female model. A similar difference was also observed when the upper confidence interval from the risk curve was used to derive the injury probability. However, when the injury probability was derived using the lower confidence interval curve, the injury probability went up 1.45%, for the same simulations.

Table F8. Probability of WAD2+ injury based on Ono et al. (2009), female model simulations

Injury Group	Simulation	Injury Probability before Intervention			Injury Probability after Intervention		
		lower	best estimate	upper	lower	best estimate	upper
WAD2+ Injury risk, based on Ono et al. 2009	Sim 1 Female Injured	10.80%	79.22%	99.95%	18.40%	37.17%	60.91%
	Sim 2 Female Injured	19.14%	55.66%	87.68%	19.89%	47.00%	76.19%
	Sim 3 Female Injured	16.21%	63.84%	94.51%	19.64%	53%	84.57%
	Sim 1 Female Uninjured	16.18%	63.95%	94.61%	14.41%	31.42%	56.28%
	Sim 2 Female Uninjured	18.34%	37.05%	60.81%	13.62%	30.61%	55.81%
	Sim 3 Female Uninjured	16.21%	63.84%	94.51%	19.64%	53%	84.57%
	Average	16.15%	60.59%	88.68%	17.60%	42.03%	69.72%

The male model simulations showed a similar trend of injury probability for WAD2+ injury (Table 9). Using the average risk curve and upper confidence interval, the risk curve decreased when the intervention was introduced (21% and 22%, respectively). However, when the injury probability was based on a lower confidence interval, the WAD2+ injury probability increased from 16% to 18% instead.

Table F9. Probability of WAD2+ injury based on Ono et al. (2009), male model simulations

Injury Group	Simulation	Injury Probability before Intervention			Injury Probability after Intervention		
		lower	best estimate	upper	lower	best estimate	upper
WAD2+ Injury risk, based on Ono et al., 2009	Sim 1 Male Injured	9.84%	82.45%	100%	19.43%	54.52%	86.62%
	Sim 2 Male Injured	19.25%	55.33%	87.34%	19.34%	39.63%	64.90%
	Sim 3 Male Injured	15.61%	65.98%	95.64%	19.11%	38.90%	63.81%
	Sim 1 Male Uninjured	18.08%	58.52%	90.18%	17.15%	34.46%	58.31%
	Sim 2 Male Uninjured	15.57%	32.52%	56.92%	12.64%	29.45%	55.39%
	Sim 3 Male Uninjured	15.61%	65.98%	95.64%	19.11%	38.90%	63.81%
	Average	15.66%	60.13%	87.62%	17.80%	39.31%	65.47%

4. Discussion

The main objective of the current study was to evaluate the effect of a shorter head to head-restraint distance on the whiplash injury risk (WAD2+). Twenty-four simulations using the VIVA+ 50F and 50M were conducted. Six different crash pulses based on real-world accident data were simulated. Twelve simulations were conducted with 120mm head to head-restraint distance and another 12 simulations with 95mm head to head-restraint distance. Reducing the head to head-restraint distance is an example of a strategy used to minimise the whiplash injury risk. The main idea is to reduce the relative motion between the head and the torso (which reduces the relative displacement between cervical spine vertebrae). Several hypotheses of whiplash injury are postulating that the rapid relative motion in the cervical spine is unphysiological and more likely to cause whiplash injury.

As shown in Figures F7 to F10, reducing head to head-restraint distance is an effective measure to reduce the peak head CoG to T1 displacements and rotation. However, the peak reduction was more pronounced in the female model than in the male model. Potentially, the reason may be due to the

male head being heavier. With a heavier head, the male model was able to compress the head-restraint further than the female model, and thus, the effects of a shorter head-restraint would not be as pronounced as for the females. Another reason may be the interaction between the torso and the seat. Still, reducing head to head-restraint distance was shown to be a simple and effective measure.

Using NIC_{max}, the probability of suffering WAD2+ injury was evaluated using an injury risk curve based on Ono et al. (2009). Due to the lack of a similar risk curve, the study by Ono et al. (2009) was chosen, despite several uncertainties related to that risk curve such as the shape of its upper and lower confidence interval curves. Consequently, the WAD2+ injury risk was higher in a simulation involving shorter head to head-restraint distance when the lower confidence interval curve was used to derive the injury risk. The resulting injury risk highlights the importance of data availability and reliability of every step involved in such a study, especially when the simulation results will be used as input to the CBT.

5. References

- Berecki-Gisolf, J., Collie, A., McClure, R. (2013). Work disability after road traffic injury in a mixed population with and without hospitalisation. *Accid. Anal. Prev.* 51, 129–134. doi:10.1016/j.aap.2012.11.010
- Jakobsson, L., Isaksson-Hellman, I., Lindman, M. (2008) WHIPS (Volvo Cars' Whiplash Protection System) – The development and real-world performance. *Traffic Inj. Prev.*, 9(6):600–605.
- Kullgren, A., Stigson, H., Krafft, M. (2013). Development of Whiplash Associated Disorders for Male and Female Car Occupants in Cars Launched Since the 80s in Different Impact Directions. *Traffic Inj. Prev.* 46(0):51–62.
- Kullgren, A., Krafft, M., Lie, A., Tingvall, C. (2007). The effect of whiplash protection systems in real-life crashes and their correlation to consumer crash test programmes. *Proc. 20th ESV Conf.* (07-0468), Lyon, France.
- Markert, Bernd. (2005) Porous media viscoelasticity with application to polymeric foams. *Ph.D. dissertation*, Universität Stuttgart, Germany.
- Marzougui, D., D. Brown, H. K. Park, C. D. Kan, und K. S. Opiela. Development & Validation of a Finite Element Model for a Mid-Sized Passenger Sedan. *Proceedings of the 13th International LS-DYNA Users Conference*, Dearborn, MI, USA. 2014. 8–10.
- Nygren, Å. (1983). Injuries to Car Occupants-Some Aspects of the Interior Safety of Cars A study of a five-year material from an insurance company. *Acta Otolaryngol.* 95 sup395:1–135.
- Krafft, M. (1998). A Comparison of Short- And Long-Term Consequences of AIS1 Neck Injuries, In Rear-end impacts. *IRCOBI Conf.* September 1998, Gothenburg, Sweden, pp.235–248.
- Oka, H., Matsudaira, K., Fujii, T., Tanaka, S., Kitagawa, T. (2017). Epidemiology and psychological factors of whiplash associated disorders in Japanese population. *J. Phys. Ther. Sci.* 29 9, 1510–1513. doi:10.1589/jpts.29.1510
- Olsson, I., Bunketorp, O., Carlsson, G., Gustafsson, C., Planath, I., Norin, H., Ysander, L. (1990). An in-depth study of neck injuries in rear-end collisions. *IRCOBI Conf.* Bron, France, pp.269–280.
- Ono, K., Ejima, S., Yamazaki, K., Sato, F., Pramudita, J.A., Kaneoka, K., Ujihashi, S. (2009). Evaluation criteria for the reduction of minor neck injuries during rear-end impacts based on human volunteer experiments and accident reconstruction using human FE model simulations. *IRCOBI Conf.*, September 2009, York, UK, pp.381–398.
- Quinlan, K.P., Annest, J.L., Myers, B., Ryan, G., Hill, H. (2004). Neck strains and sprains among motor vehicle occupants - United States, 2000. *Accid. Anal. Prev.* 36(1):21–27. doi:10.1016/S0001-4575(02)00110-0

Appendix G Novel Seats and Seated Positions in Rear-End Impact

Authors: Ines LEVALLOIS*, Patryk Recko**, Michal Kowalik**, Agnieszka Call**
 Faurecia Automotive Seating, *France, **Poland

This is the supporting Appendix for the sub-study on 'Novel seats and seated position, rear-end impacts', presented in Chapter 3.2.1.1.

Figure G1 shows the rear-end impact crash pulse used in the sub-study. It corresponds to the IIWPG/EuroNACP medium severity pulse with delta V of 16km/h and maximum acceleration of 10g.



Figure G1 Rear-end impact crash pulse used in this sub-study.

Table G1 shows an overview of simulated low speed rear-end impact cases for all reclined positions.

The positions of the VIVA+ models after the 2-step positioning procedure are shown together with the corresponding predicted UMTRI positions in Table G2 for each VIVA+ simulation case. Figure G2 illustrates the specific landmarks used and Table G3 provides details on the VIVA+ landmark coordinates for each case. Thereafter follows the results summary in Tables G4-G7 and one-pagers with details on each of the 36 simulations.

Table G1. Overview of seat adjustment variations and seat variations of reclined simulated positions.

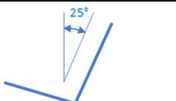
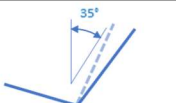
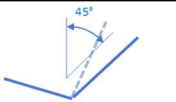
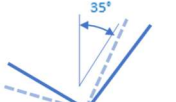
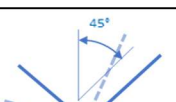
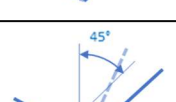
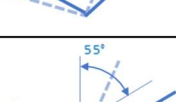
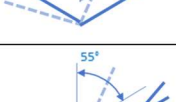
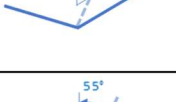
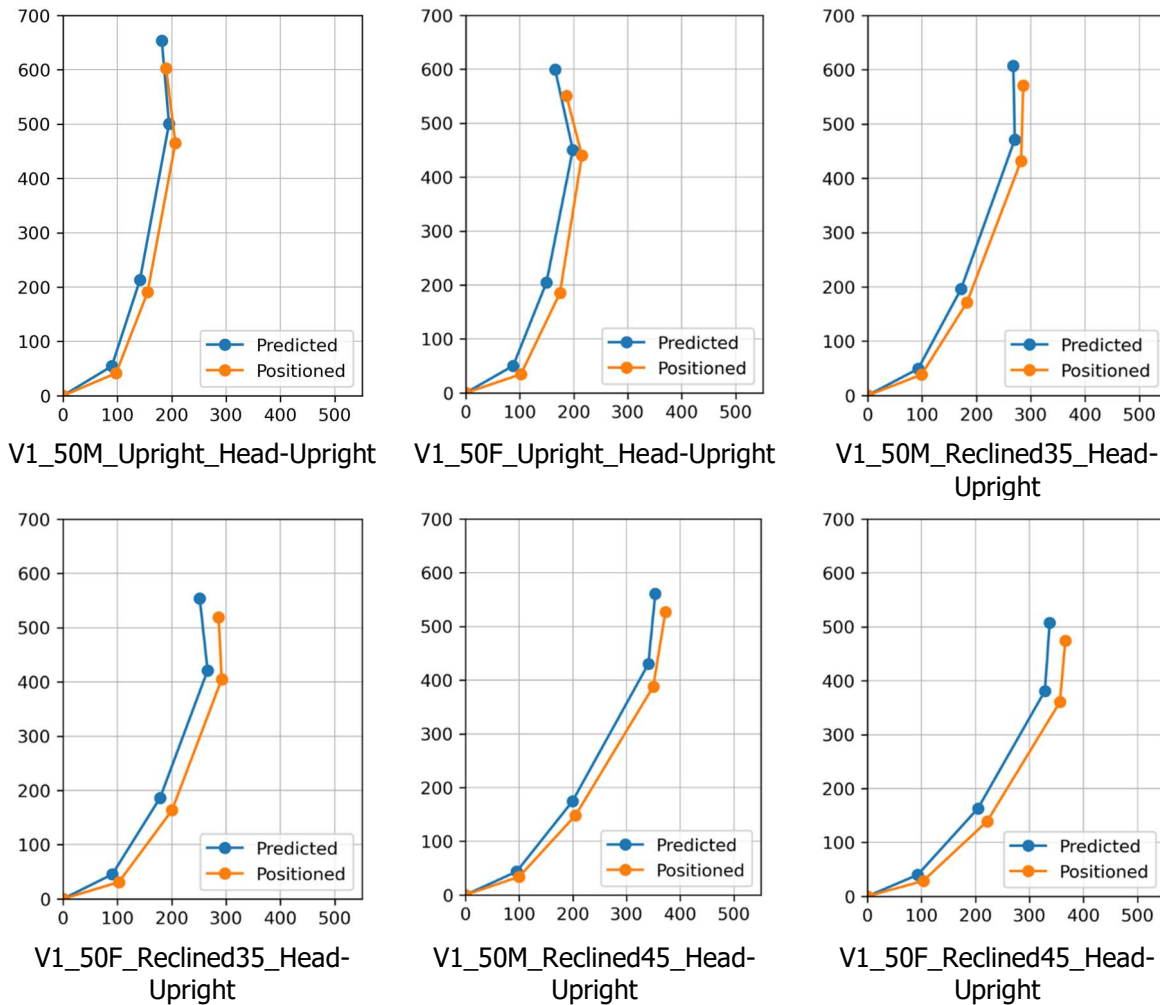
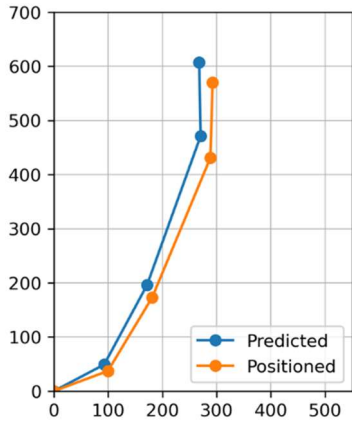
		Biorid	50M head upright	50F head upright	50M head leaning on head restraint	50F head leaning on head restraint
	upright	V1 - V3	V1 V2 V3	V1 V2 V3	- - V3	- - V3
	35° reclined (10°)		V1 V3	V1 V3	- V3	- V3
	45° reclined (20°)		V1 V3	V1 V3	- V3	- V3
	35° inclined (10°)		V1	V1	- V3	- V3
	45° inclined (20°)				V3	V3
	45° inclined (10°) + reclined (10°)				V3	V3
	55° inclined (10°) + reclined (20°)				V3	V3
	55° reclined (30°) + shoulder adjustment 10° forward				V3	V3
	55° inclined (20°) + reclined (10°)				-	-



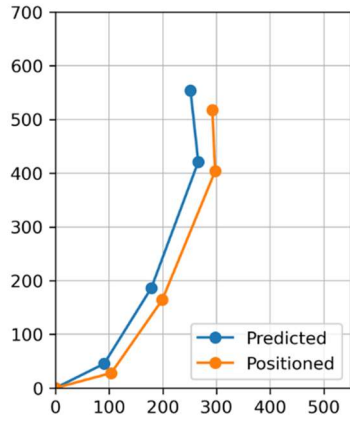
Figure G2. Indication of specific landmarks of VIVA+ HBM.

Table G2. VIVA+ 50M and 50F predicted and final posture after positioning.

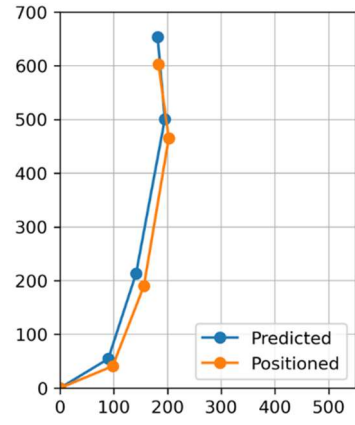




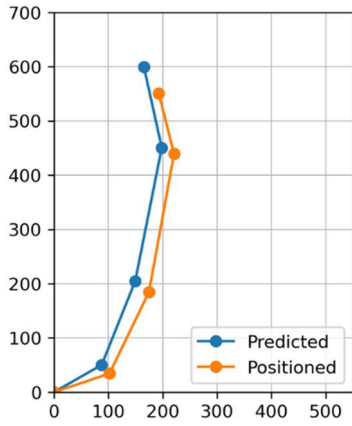
V1_50M_Inclined10_Head-Upright



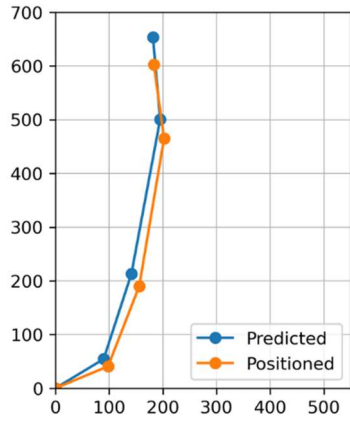
V1_50F_Inclined10_Head-Upright



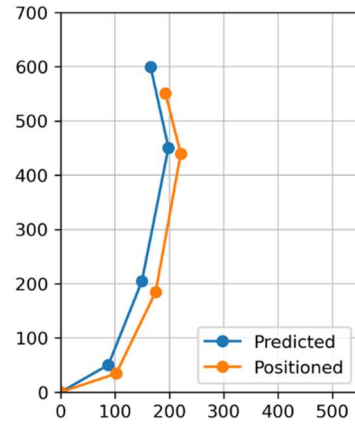
V2_50M_Sweveled10_Head-Upright



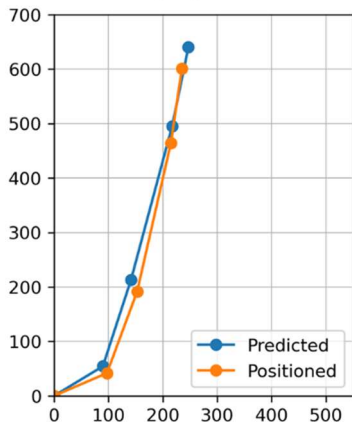
V2_50F_Sweveled10_Head-Upright



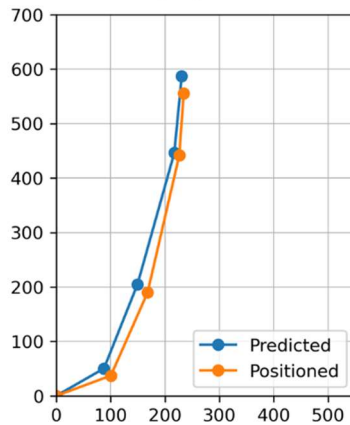
V2_50M_Sweveled20_Head-Upright



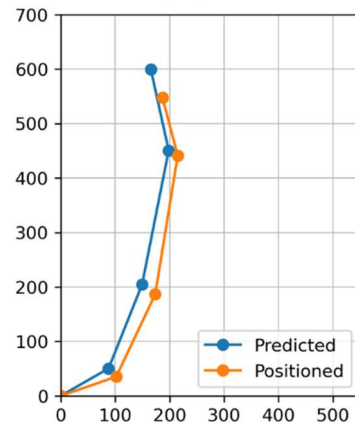
V2_50F_Sweveled20_Head-Upright



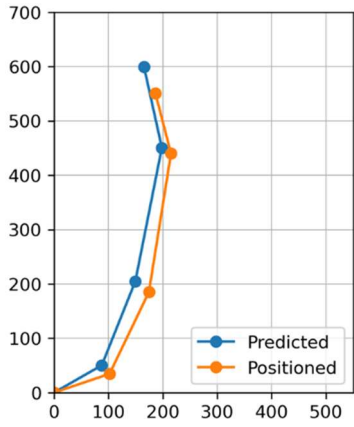
V3_50M_Upright_Head-Leaning



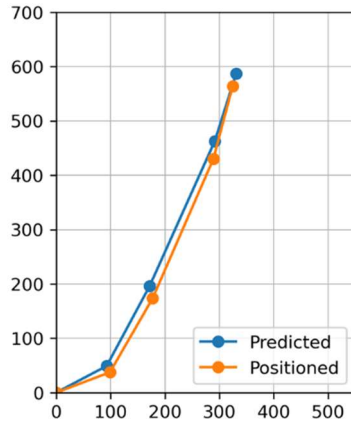
V3_50F_Upright_Head-Leaning



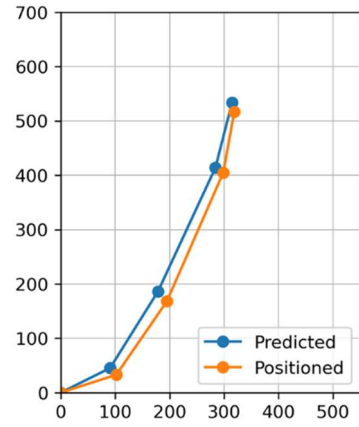
V3_50M_Upright_Head-Upright



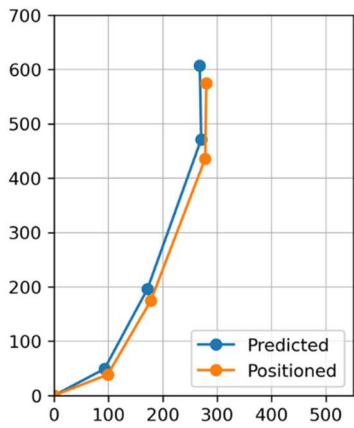
V3_50F_Upright_Head-Upright



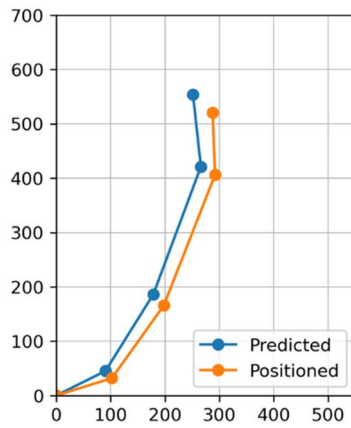
V3_50M_Reclined35_Head-Leaning



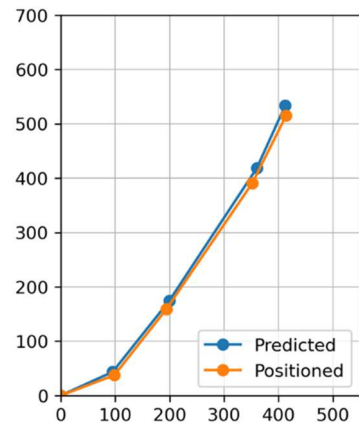
V3_50F_Reclined35_Head-Leaning



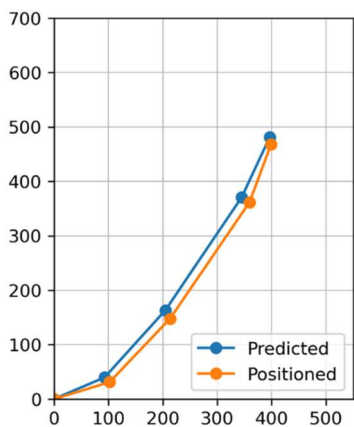
V3_50M_Reclined35_Head-Upright



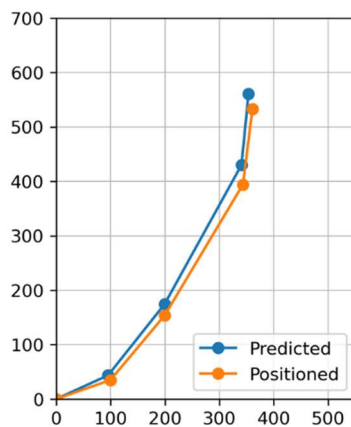
V3_50F_Reclined35_Head-Upright



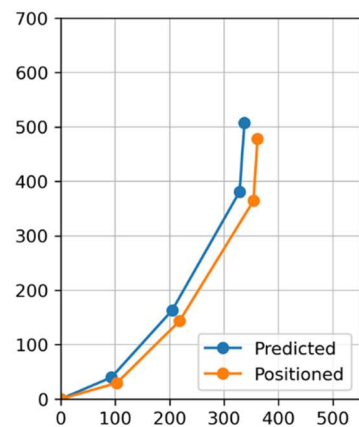
V3_50M_Reclined45_Head-Leaning



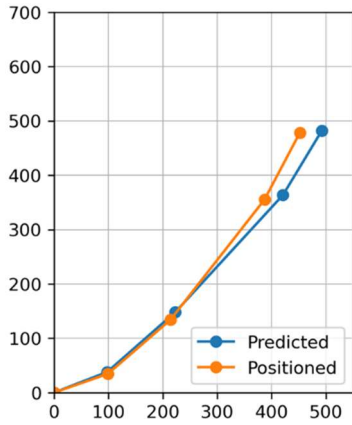
V3_50F_Reclined45_Head-Leaning



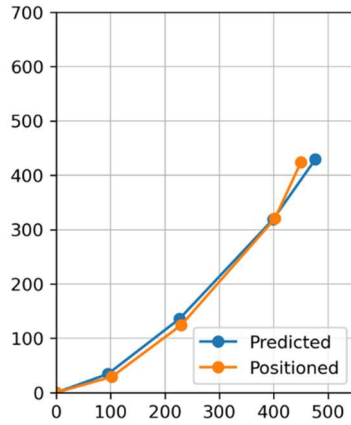
V3_50M_Reclined45_Head-Upright



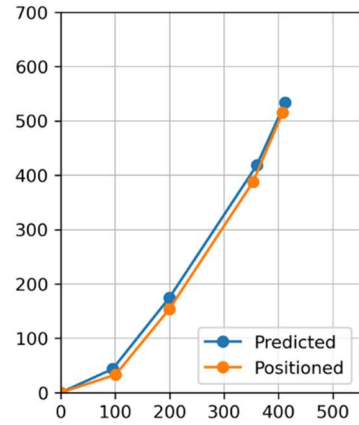
V3_50F_Reclined45_Head-Upright



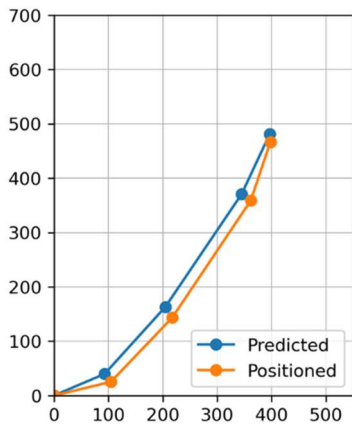
V3_50M_Reclined55_Head-Leaning



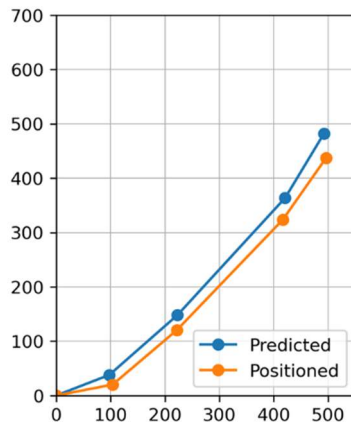
V3_50F_Reclined55_Head-Leaning



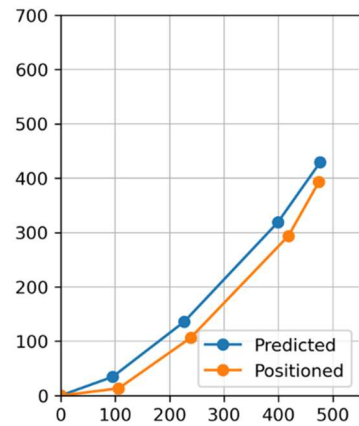
V3_50M_Inclined-Reclined45_Head-Leaning



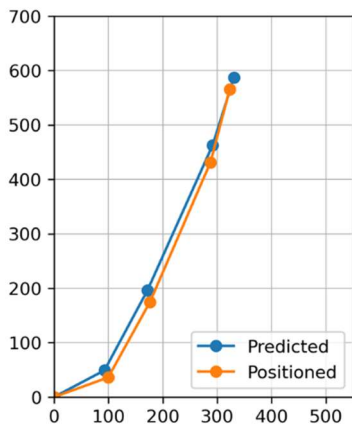
V3_50F_Inclined-Reclined45_Head-Leaning



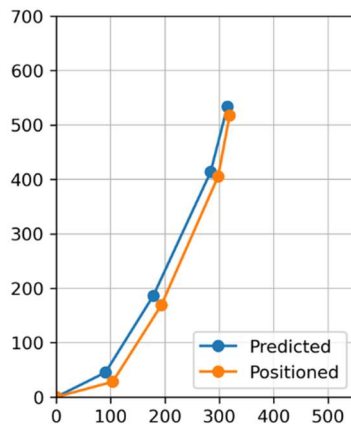
V3_50M_Inclined-Reclined55_Head-Leaning



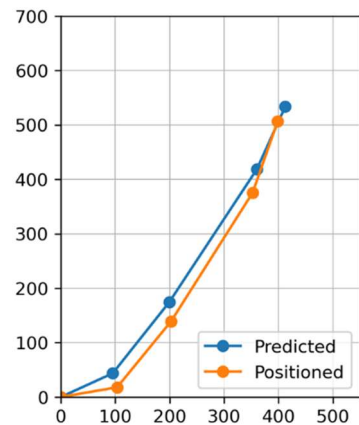
V3_50F_Inclined-Reclined55_Head-Leaning



V3_50M_Inclined10_Head-Leaning



V3_50F_Inclined10_Head-Leaning



V3_50M_Inclined20_Head-Leaning

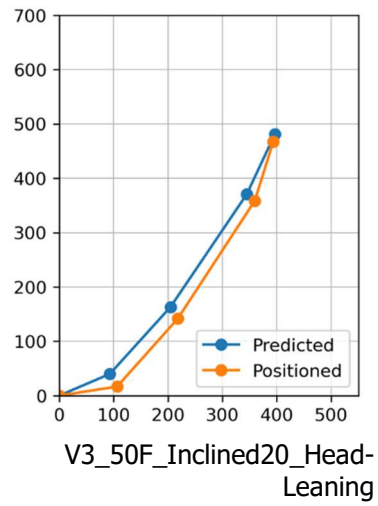




Table G3. Coordinates of VIVA+ landmarks after positioning.

Case		L5/S1	T12/L1	C7/T1	Tragion
V1_50M_Upright_Head-Upright	X	98	156	207	190
	Z	41	190	465	603
V1_50M_Reclined35_Head-Upright	X	99	183	282	286
	Z	38	171	432	571
V1_50M_Reclined45_Head-Upright	X	100	205	350	372
	Z	34	148	388	527
V1_50M_Inclined10_Head-Upright	X	100	181	288	293
	Z	37	173	431	570
V2_50M_Swiveled10/20_Head-Upright	X	98	156	202	183
	Z	41	190	465	603
V3_50M_Upright_Head-Upright	X	98	155	202	185
	Z	41	191	466	604
V3_50M_Reclined35_Head-Upright	X	99	178	278	280
	Z	39	174	436	575
V3_50M_Reclined45_Head-Upright	X	100	199	343	361
	Z	35	154	394	533
V3_50M_Upright_Head-Leaning	X	97	153	215	235
	Z	42	192	464	601
V3_50M_Reclined35_Head-Leaning	X	99	177	289	325
	Z	38	174	430	564
V3_50M_Reclined45_Head-Leaning	X	99	194	352	414
	Z	38	159	391	515
V3_50M_Reclined55_Head-Leaning	X	99	214	387	452
	Z	35	134	355	478
V3_50M_Inclined10_Head-Leaning	X	100	176	288	323
	Z	36	175	431	566
V3_50M_Inclined20_Head-Leaning	X	104	203	352	398
	Z	18	139	376	506
V3_50M_Inclined-Reclined45_Head-Leaning	X	101	199	353	408
	Z	33	154	388	515
V3_50M_Inclined-Reclined55_Head-Leaning	X	104	222	416	496
	Z	20	121	323	438
V1_50F_Upright_Head-Upright	X	102	175	215	186



	Z	34	185	440	551
V1_50F_Reclined35_Head-Upright	X	103	201	292	286
	Z	31	163	405	519
V1_50F_Reclined45_Head-Upright	X	103	222	356	366
	Z	29	139	361	474
V1_50F_Inclined10_Head-Upright	X	104	199	298	292
	Z	28	164	404	518
V2_50F_Swivelled10/20_Head-Upright	X	102	175	221	193
	Z	34	185	439	550
V3_50F_Upright_Head-Upright	X	102	174	215	187
	Z	35	186	441	548
V3_50F_Reclined35_Head-Upright	X	102	198	292	288
	Z	32	166	406	520
V3_50F_Reclined45_Head-Upright	X	103	218	354	361
	Z	30	143	364	478
V3_50F_Upright_Head-Leaning	X	101	168	226	234
	Z	37	190	442	555
V3_50F_Reclined35_Head-Leaning	X	102	195	298	319
	Z	33	168	405	517
V3_50F_Reclined45_Head-Leaning	X	102	213	359	399
	Z	31	148	362	468
V3_50F_Reclined55_Head-Leaning	X	102	230	402	450
	Z	29	125	320	424
V3_50F_Inclined10_Head-Leaning	X	104	193	298	319
	Z	28	169	406	518
V3_50F_Inclined20_Head-Leaning	X	107	222	354	378
	Z	15	137	360	472
V3_50F_Inclined-Reclined45_Head-Leaning	X	105	217	362	398
	Z	25	143	359	467
V3_50F_Inclined-Reclined55_Head-Leaning	X	106	239	418	474
	Z	13	106	294	393

Tables G4-G7 and Figures G3-G7 summarise the results:

Table G4. NIC values and WAD2+ injury risks for BioRID and VIVA+ 50M in comparable configurations of upright seated position using the V1 and V3 seats, respectively.

Seatback 25°		V1 seat	V3 seat
VIVA+ 50M	NIC	31.3	13.9
	WAD2+	96%	39.5%
BioRID	NIC	14.1	9.8
	WAD2+	40.6%	21.4%

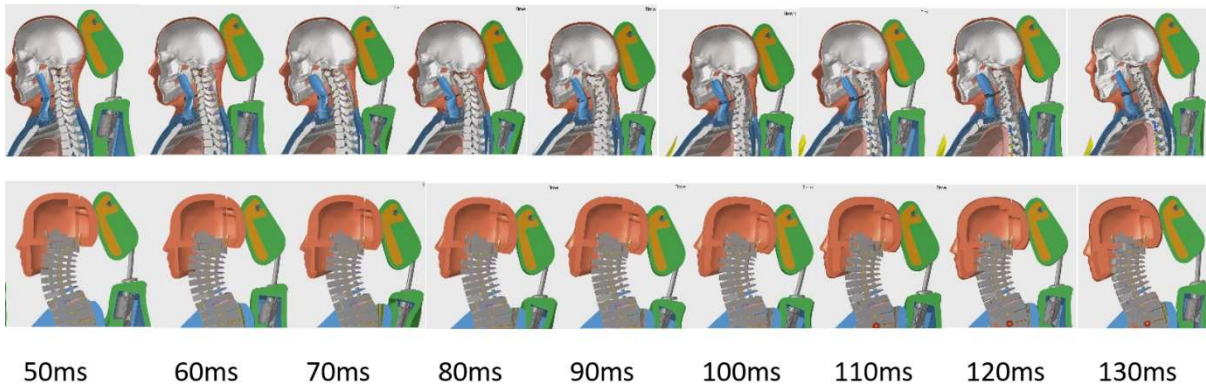


Figure G3 Compares the movement of Viva+ 50M and BioRID in V1 seat at 25° torso angle and head upright.

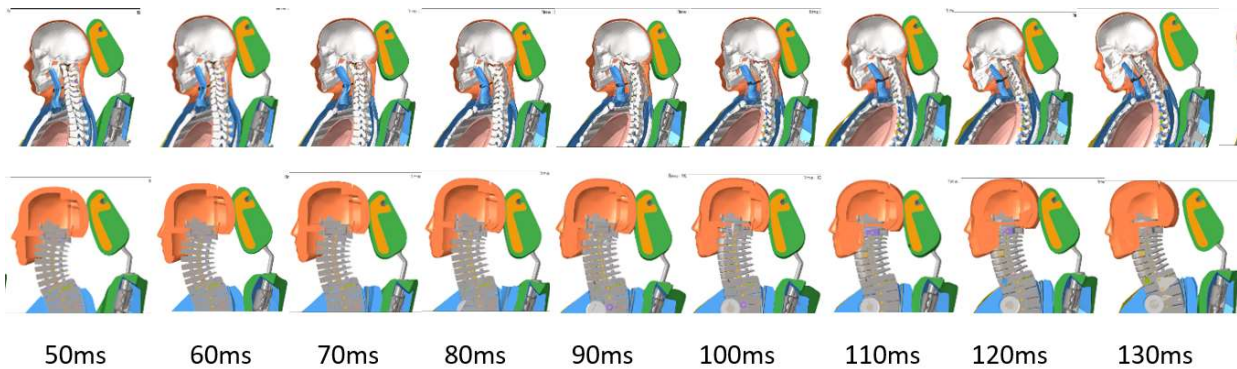


Figure G4 Compares the movement of Viva+ 50M and BioRID in V3 seat at 25° torso angle and head upright.

The neck movements differ between the BioRID and the VIVA+ 50M in several aspects: the movements of the vertebrae differ considerably. The BioRID head shows a slight rearward rotation whereas the head of the 50M head remains horizontal. Only negative values are present when comparing the upper head moments of the 50M in all three seat variants, V1, V2 and V3 (Figure G5), whereas the BioRID measurements show both negative and positive values (Figure G6).

Upper neck My

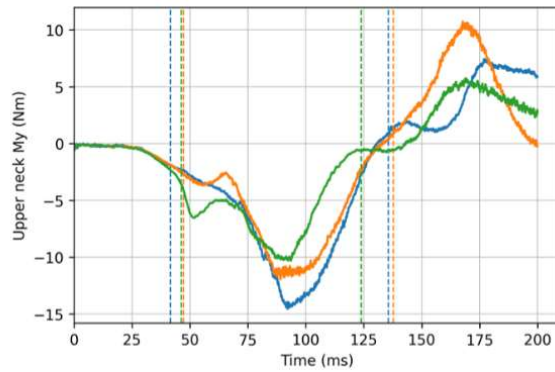


Figure G5 Comparison of the upper neck moments M_y of VIVA+ 50M for V1 (blue), V2 (orange) and V3 (green) in the upright position with the head in the upright position.

BioRID Upper neck V1 seat

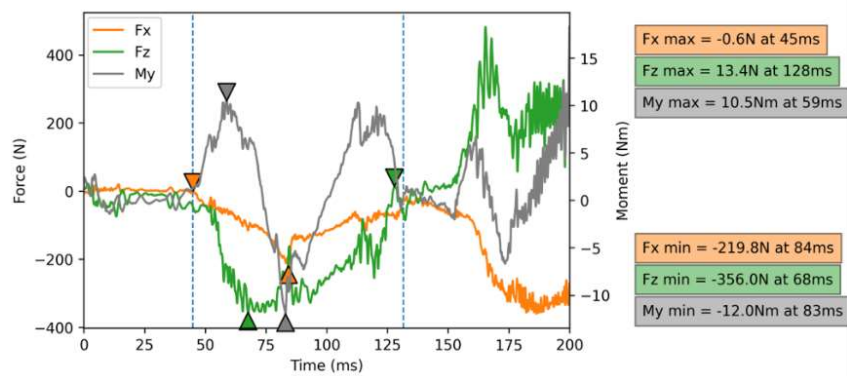


Figure G6 Upper neck moments and forces of the BioRID on V1 seat in the upright position.

Table G5. NIC values and WAD2+ injury risk at different seatback angles on the V3 seat, head upright




V3 seat		Seatback 25°	Seatback 35°	Seatback 45°
				
VIVA+ 50M	NIC	13.9	13.9	18.6
	WAD2+	39.4%	39.5%	63.4%
VIVA+ 50F	NIC	15.9	17	20
	WAD2+	49.6%	55.5%	69.8%

Table G6. NIC values and WAD2+ injury risks at different seatback angles on the V3 seat, nominal cushion position, head leaning on head-restraint.








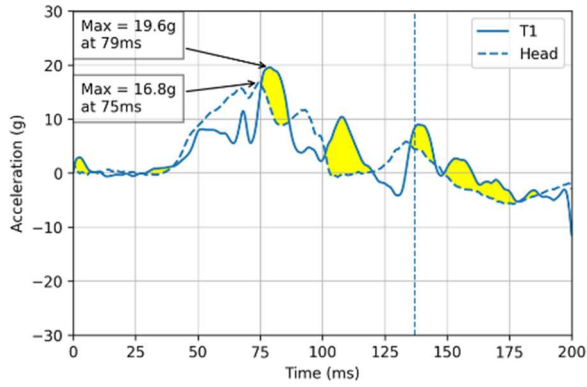
V3 seat		Seatback 25°	Seatback 35°	Seatback 45°	Seatback 55°
					
VIVA+ 50M	NIC	14.1	21.9	26.3	30
	WAD2+	40.2%	77.5%	89.7%	95%
VIVA+ 50F	NIC	16	22,3	21,9	21,7
	WAD2+	50.2%	79.2%	77.8%	76.9%

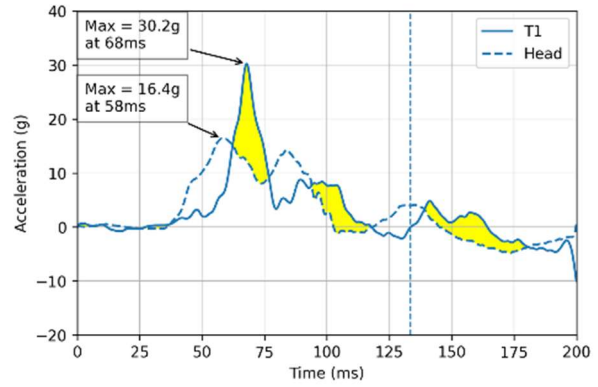
Table G7. NIC values and WAD2+ injury risk at different seatback angles on the V3 seat, in inclined-reclined positions, head leaning on head-restraint

V3 seat		Cushion Inclined 10° Seatback 35°	Cushion Inclined 10° Seatback 45°	Cushion Inclined 10° Seatback 55°
				
VIVA+ 50M	NIC	26.7	36.2	26.2
	WAD2+	90.5%	98.6%	89.6%
VIVA+ 50F	NIC	37.9	41.5	34
	WAD2+	99%	99.5%	97.8%

A more detailed analysis of the VIVA+ 50F kinematics at the same seatback angle, but with different cushion angles, shows that the centre of gravity of the occupant with inclined cushions is positioned higher in z in comparison to the recliner axis of the seat. The crossmember of the frame is therefore less effective and more load is transferred to the upper body and the T1 of the occupant (Figure G7).








Cushion not inclined, seatback 45°

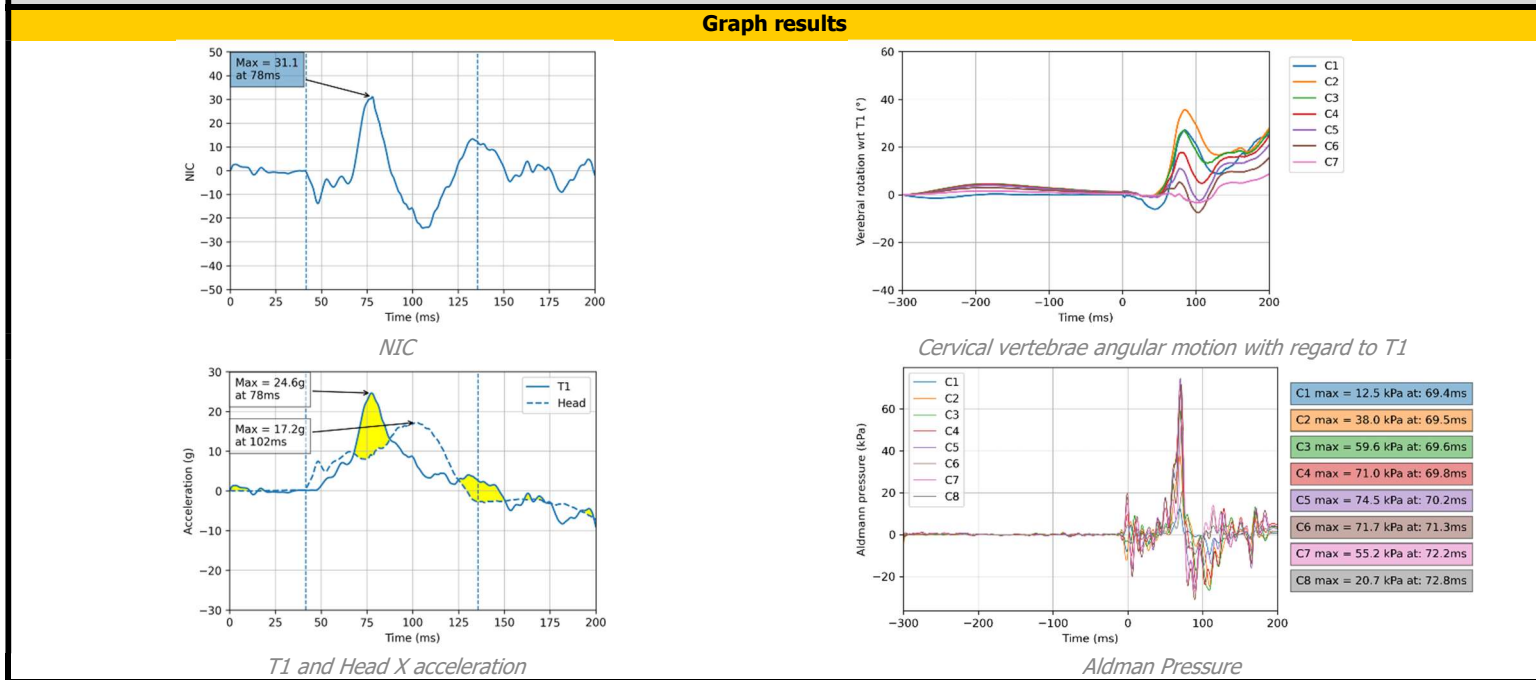


Cushion inclined by 20°, seatback 45°

Figure G7 T1 and Head-X acceleration for VIVA+ 50F in the seatback position of 45°, head leaning on the head-restraint


Simulation case		V1_50M_Upright_Head-Upright		
General description				
Seat used	Variant 1	 		
Seat position	Seatback			25°
	Tracks			Middle
	Height			Middle
	Swivel			0°
	Shoulder			N/A
	Headrest			Middle / Backset = 25mm
Dummy used	VIVA+ 50 th Male			
Crash pulse	IIWPG Medium Whiplash Pulse			
Speed	15,9 km/h			
Load case	Low speed rear crash			

Head kinematics results			Numerical results	
 <p>Time : 42.00 ms</p> <p><i>Head to head-restraint contact</i></p>	 <p>Time : 78.00 ms</p> <p><i>NICmax</i></p>	 <p>Time : 93.00 ms</p> <p><i>Max head rear displacement</i></p>	THRC NICmax WAD2+ risk max Aldman pressure max Head X acceleration max T1 X acceleration max Upper neck Fx max Upper neck Fz max Upper neck My max Lower neck Fx max Lower neck Fz max Lower neck My	41,6ms 31,3 96% 74,5kPa at C5 17,2g 24,6g N/A N/A N/A N/A N/A N/A




Simulation case	V1_50F_Upright_Head-Upright
------------------------	------------------------------------

General description	
Seat used	Variant 1
Seat position	Seatback 25°
	Tracks Middle
	Height Middle
	Swivel 0°
	Shoulder N/A
	Headrest Lowest / Backset = 36mm
Dummy used	VIVA+ 50 th Female
Crash pulse	IIWPG Medium Whiplash Pulse
Speed	15,9 km/h
Load case	Low speed rear crash






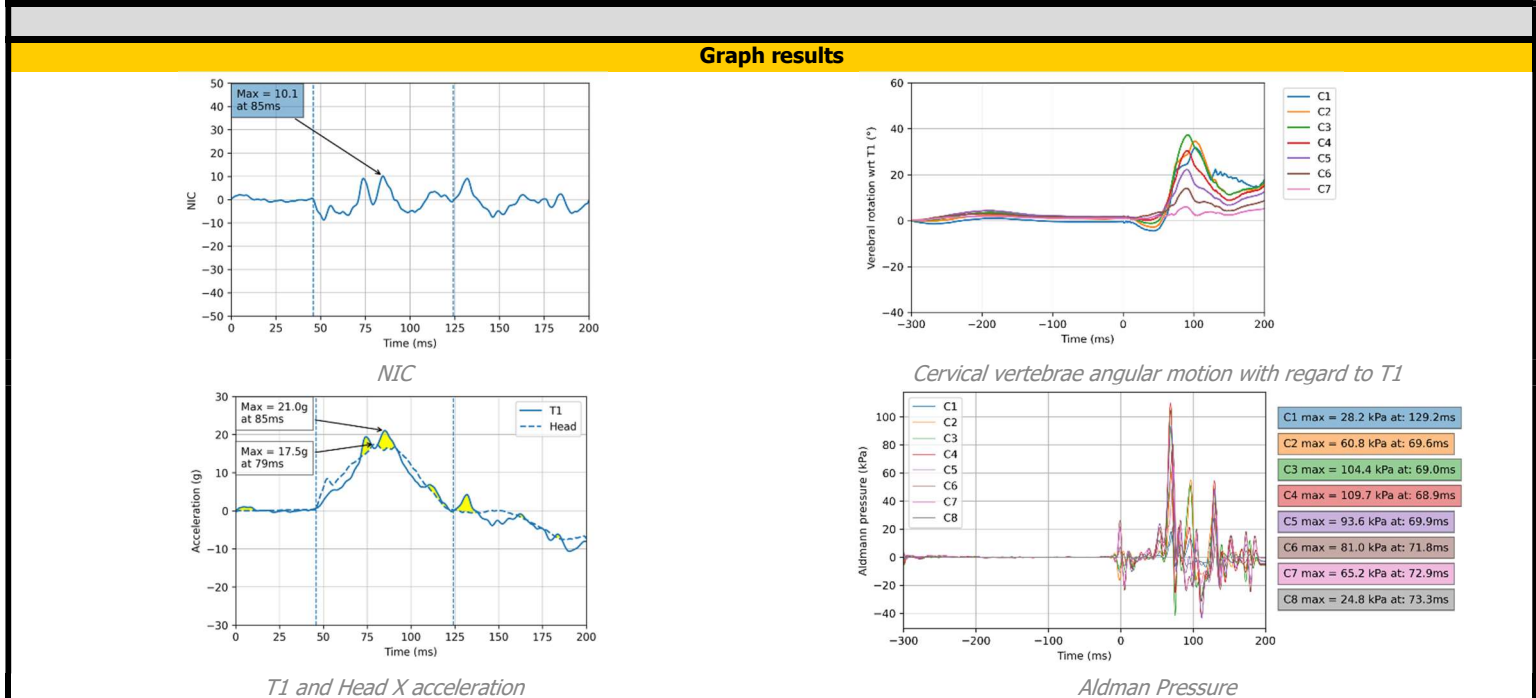
Time : 0.00 ms

Initial vertebrae position



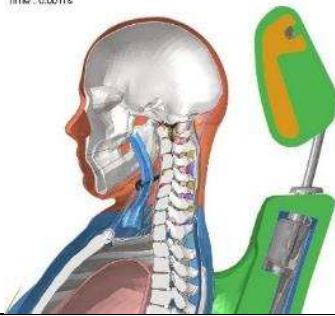
Seat isometric view

Head kinematics results	Numerical results																								
<div style="display: flex; justify-content: space-around;"> <div style="text-align: center;">  <p>Time : 45.00 ms</p> <p><i>Head to head-restraint contact</i></p> </div> <div style="text-align: center;">  <p>Time : 85.00 ms</p> <p><i>Max head rear displacement</i></p> </div> <div style="text-align: center;">  <p>Time : 124.00 ms</p> <p><i>End of head contact</i></p> </div> </div>	<table border="0" style="width:100%;"> <tr> <td>THRC</td> <td style="text-align: right;">45,9ms</td> </tr> <tr> <td>NICmax</td> <td style="text-align: right;">10,1</td> </tr> <tr> <td>WAD2+ risk</td> <td style="text-align: right;">22,8%</td> </tr> <tr> <td>max Aldman Pressure</td> <td style="text-align: right;">109,7kPa at C4</td> </tr> <tr> <td>max Head X acceleration</td> <td style="text-align: right;">17,5g</td> </tr> <tr> <td>max T1 X acceleration</td> <td style="text-align: right;">21g</td> </tr> <tr> <td>max Upper neck Fx</td> <td style="text-align: right;">N/A</td> </tr> <tr> <td>max Upper neck Fz</td> <td style="text-align: right;">N/A</td> </tr> <tr> <td>max Upper neck My</td> <td style="text-align: right;">N/A</td> </tr> <tr> <td>max Lower neck Fx</td> <td style="text-align: right;">N/A</td> </tr> <tr> <td>max Lower neck Fz</td> <td style="text-align: right;">N/A</td> </tr> <tr> <td>max Lower neck My</td> <td style="text-align: right;">N/A</td> </tr> </table>	THRC	45,9ms	NICmax	10,1	WAD2+ risk	22,8%	max Aldman Pressure	109,7kPa at C4	max Head X acceleration	17,5g	max T1 X acceleration	21g	max Upper neck Fx	N/A	max Upper neck Fz	N/A	max Upper neck My	N/A	max Lower neck Fx	N/A	max Lower neck Fz	N/A	max Lower neck My	N/A
THRC	45,9ms																								
NICmax	10,1																								
WAD2+ risk	22,8%																								
max Aldman Pressure	109,7kPa at C4																								
max Head X acceleration	17,5g																								
max T1 X acceleration	21g																								
max Upper neck Fx	N/A																								
max Upper neck Fz	N/A																								
max Upper neck My	N/A																								
max Lower neck Fx	N/A																								
max Lower neck Fz	N/A																								
max Lower neck My	N/A																								




Simulation case	V1_50M_Reclined35_Head-Upright
-----------------	---------------------------------------



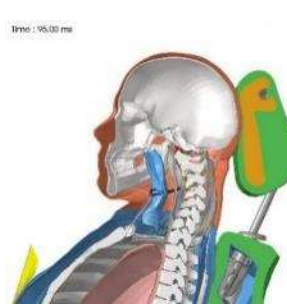
General description		
Seat used	Variant 1	
Seat position	Seatback	35°
	Tracks	Middle
	Height	Middle
	Swivel	0°
	Shoulder	N/A
	Headrest	Middle / Backset = 41mm
Dummy used	VIVA+ 50 th Male	
Crash pulse	IIWPG Medium Whiplash Pulse	
Speed	15,9 km/h	
Load case	Low speed rear crash	

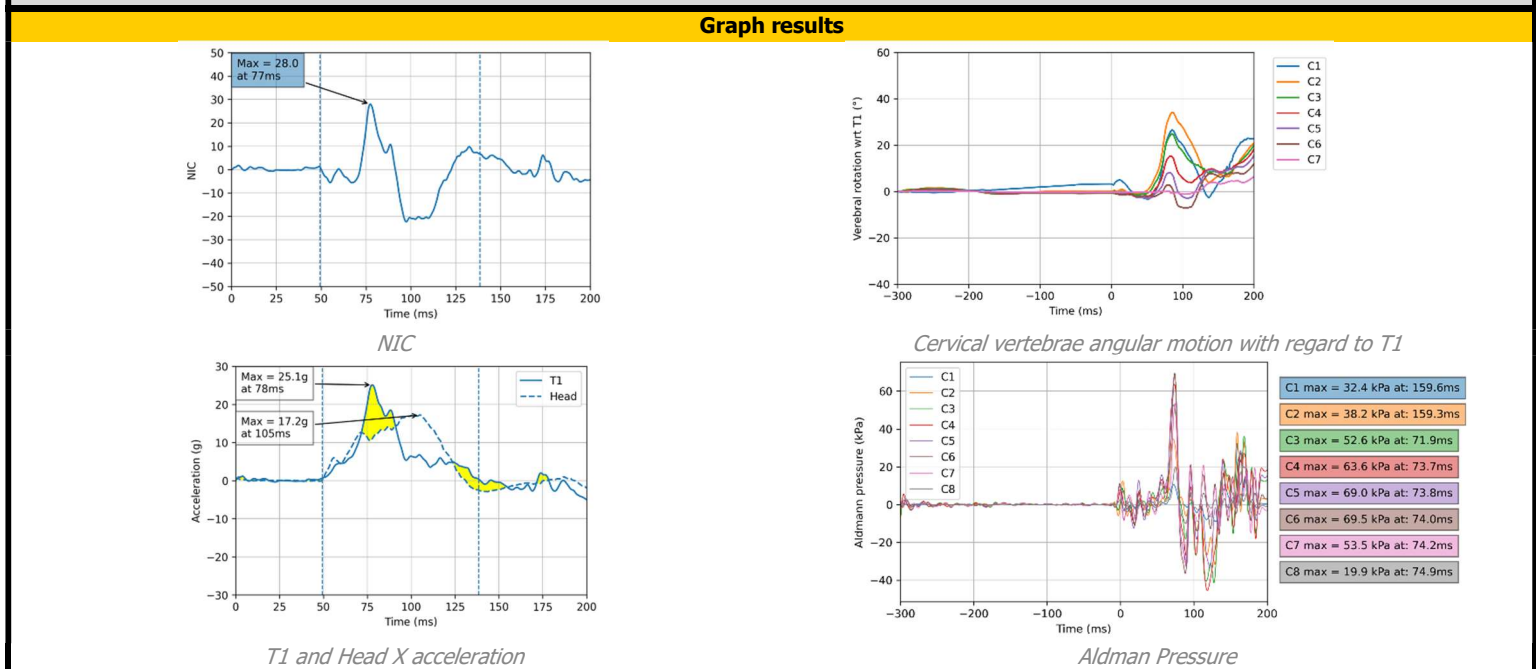


Initial vertebrae position



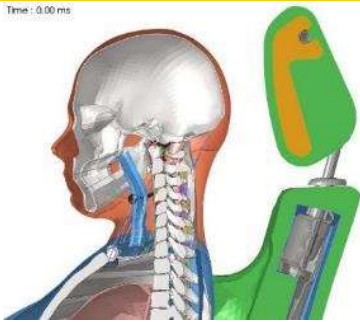
Seat isometric view

Head kinematics results	Numerical results																								
<div style="display: flex; justify-content: space-around;"> <div style="text-align: center;">  <p>Head to head-restraint contact</p> </div> <div style="text-align: center;">  <p>NICmax</p> </div> <div style="text-align: center;">  <p>Max head rear displacement</p> </div> </div>	<table border="0" style="width:100%;"> <tr><td>THRC</td><td style="text-align: right;">49,3ms</td></tr> <tr><td>NICmax</td><td style="text-align: right;">28</td></tr> <tr><td>WAD2+ risk</td><td style="text-align: right;">92,6%</td></tr> <tr><td>max Aldman Pressure</td><td style="text-align: right;">69,5kPa at C6</td></tr> <tr><td>max Head X acceleration</td><td style="text-align: right;">17,2g</td></tr> <tr><td>max T1 X acceleration</td><td style="text-align: right;">25,1g</td></tr> <tr><td>max Upper neck Fx</td><td style="text-align: right;">N/A</td></tr> <tr><td>max Upper neck Fz</td><td style="text-align: right;">N/A</td></tr> <tr><td>max Upper neck My</td><td style="text-align: right;">N/A</td></tr> <tr><td>max Lower neck Fx</td><td style="text-align: right;">N/A</td></tr> <tr><td>max Lower neck Fz</td><td style="text-align: right;">N/A</td></tr> <tr><td>max Lower neck My</td><td style="text-align: right;">N/A</td></tr> </table>	THRC	49,3ms	NICmax	28	WAD2+ risk	92,6%	max Aldman Pressure	69,5kPa at C6	max Head X acceleration	17,2g	max T1 X acceleration	25,1g	max Upper neck Fx	N/A	max Upper neck Fz	N/A	max Upper neck My	N/A	max Lower neck Fx	N/A	max Lower neck Fz	N/A	max Lower neck My	N/A
THRC	49,3ms																								
NICmax	28																								
WAD2+ risk	92,6%																								
max Aldman Pressure	69,5kPa at C6																								
max Head X acceleration	17,2g																								
max T1 X acceleration	25,1g																								
max Upper neck Fx	N/A																								
max Upper neck Fz	N/A																								
max Upper neck My	N/A																								
max Lower neck Fx	N/A																								
max Lower neck Fz	N/A																								
max Lower neck My	N/A																								




Simulation case	V1_50F_Reclined35_Head-Upright	
-----------------	--------------------------------	--

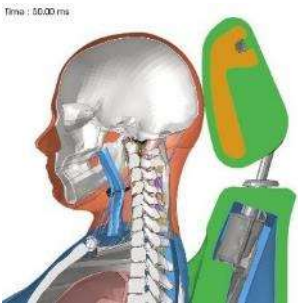
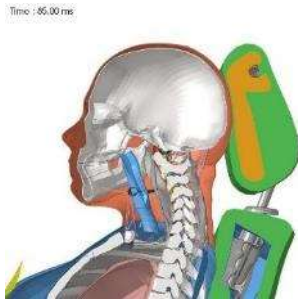
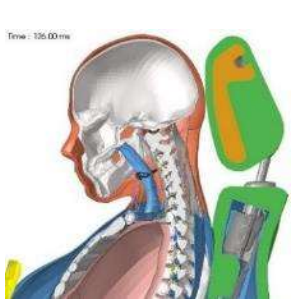
General description		
Seat used	Variant 1	
Seat position	Seatback	35°
	Tracks	Middle
	Height	Middle
	Swivel	0°
	Shoulder	N/A
	Headrest	Lowest / Backset = 43mm
Dummy used	VIVA+ 50 th Female	
Crash pulse	IIWPG Medium Whiplash Pulse	
Speed	15,9 km/h	
Load case	Low speed rear crash	

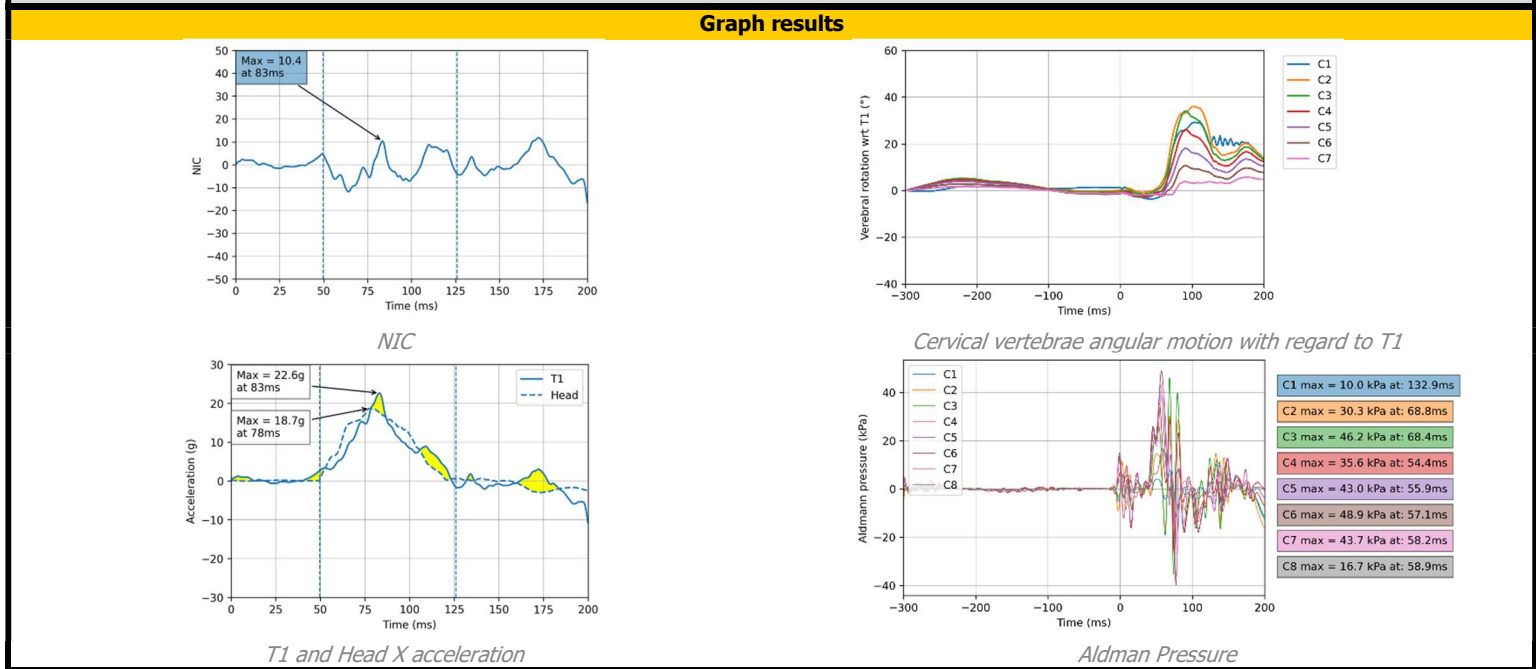


Initial vertebrae position



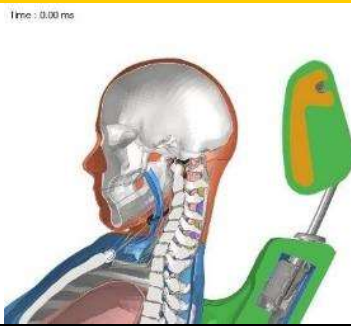
Seat isometric view

Head kinematics results	Numerical results																								
<div style="display: flex; justify-content: space-around;"> <div style="text-align: center;">  <p>Head to head-restraint contact</p> </div> <div style="text-align: center;">  <p>Max head rear displacement</p> </div> <div style="text-align: center;">  <p>End of head contact</p> </div> </div>	<table border="0" style="width:100%;"> <tr><td>THRC</td><td style="text-align: right;">49,6ms</td></tr> <tr><td>NICmax</td><td style="text-align: right;">10,4</td></tr> <tr><td>WAD2+ risk</td><td style="text-align: right;">23,6%</td></tr> <tr><td>max Aldman Pressure</td><td style="text-align: right;">48,9kPa at C6</td></tr> <tr><td>max Head X acceleration</td><td style="text-align: right;">18,7g</td></tr> <tr><td>max T1 X acceleration</td><td style="text-align: right;">22,6g</td></tr> <tr><td>max Upper neck Fx</td><td style="text-align: right;">N/A</td></tr> <tr><td>max Upper neck Fz</td><td style="text-align: right;">N/A</td></tr> <tr><td>max Upper neck My</td><td style="text-align: right;">N/A</td></tr> <tr><td>max Lower neck Fx</td><td style="text-align: right;">N/A</td></tr> <tr><td>max Lower neck Fz</td><td style="text-align: right;">N/A</td></tr> <tr><td>max Lower neck My</td><td style="text-align: right;">N/A</td></tr> </table>	THRC	49,6ms	NICmax	10,4	WAD2+ risk	23,6%	max Aldman Pressure	48,9kPa at C6	max Head X acceleration	18,7g	max T1 X acceleration	22,6g	max Upper neck Fx	N/A	max Upper neck Fz	N/A	max Upper neck My	N/A	max Lower neck Fx	N/A	max Lower neck Fz	N/A	max Lower neck My	N/A
THRC	49,6ms																								
NICmax	10,4																								
WAD2+ risk	23,6%																								
max Aldman Pressure	48,9kPa at C6																								
max Head X acceleration	18,7g																								
max T1 X acceleration	22,6g																								
max Upper neck Fx	N/A																								
max Upper neck Fz	N/A																								
max Upper neck My	N/A																								
max Lower neck Fx	N/A																								
max Lower neck Fz	N/A																								
max Lower neck My	N/A																								




Simulation case	V1_50M_Reclined45_Head-Upright
-----------------	---------------------------------------


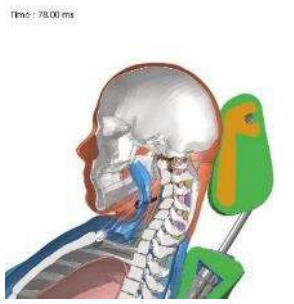
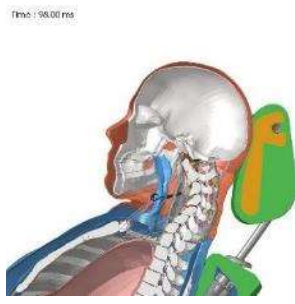
General description	
Seat used	Variant 1
Seat position	Seatback 45°
	Tracks Middle
	Height Middle
	Swivel 0°
	Shoulder N/A
	Headrest Middle / Backset = 62mm
Dummy used	VIVA+ 50 th Male
Crash pulse	IIWPG Medium Whiplash Pulse
Speed	15,9 km/h
Load case	Low speed rear crash

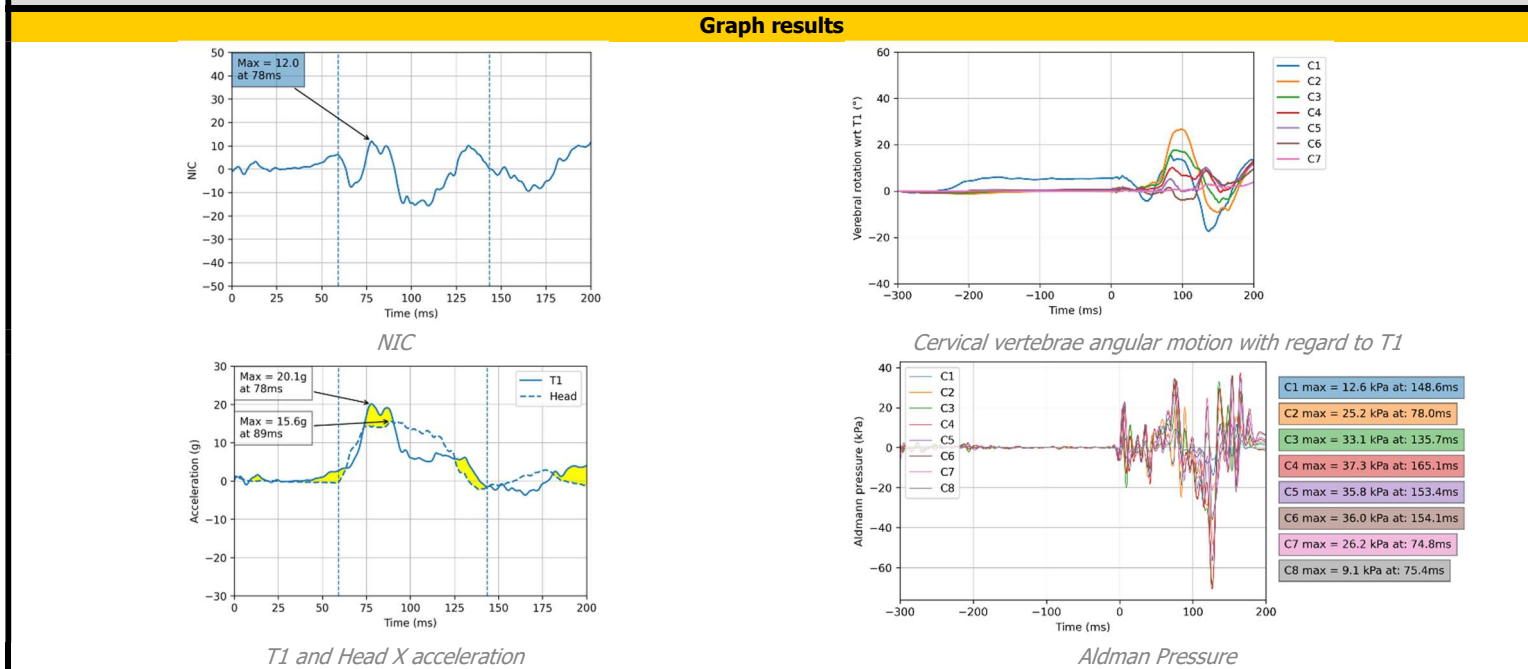


Initial vertebrae position



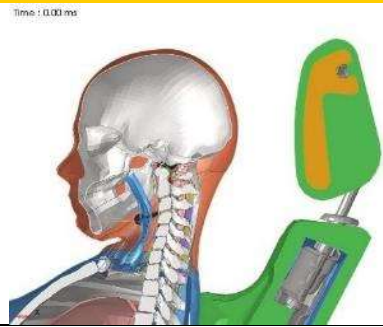
Seat isometric view

Head kinematics results	Numerical results																								
 <p>Head to head-restraint contact</p>	<table style="width:100%; border-collapse: collapse;"> <tr><td>THRC</td><td style="text-align: right;">59,2ms</td></tr> <tr><td>NICmax</td><td style="text-align: right;">12</td></tr> <tr><td>WAD2+ risk</td><td style="text-align: right;">30,2%</td></tr> <tr><td>max Aldman Pressure</td><td style="text-align: right;">37,3kPa at C4</td></tr> <tr><td>max Head X acceleration</td><td style="text-align: right;">15,6g</td></tr> <tr><td>max T1 X acceleration</td><td style="text-align: right;">20,1g</td></tr> <tr><td>max Upper neck Fx</td><td style="text-align: right;">N/A</td></tr> <tr><td>max Upper neck Fz</td><td style="text-align: right;">N/A</td></tr> <tr><td>max Upper neck My</td><td style="text-align: right;">N/A</td></tr> <tr><td>max Lower neck Fx</td><td style="text-align: right;">N/A</td></tr> <tr><td>max Lower neck Fz</td><td style="text-align: right;">N/A</td></tr> <tr><td>max Lower neck My</td><td style="text-align: right;">N/A</td></tr> </table>	THRC	59,2ms	NICmax	12	WAD2+ risk	30,2%	max Aldman Pressure	37,3kPa at C4	max Head X acceleration	15,6g	max T1 X acceleration	20,1g	max Upper neck Fx	N/A	max Upper neck Fz	N/A	max Upper neck My	N/A	max Lower neck Fx	N/A	max Lower neck Fz	N/A	max Lower neck My	N/A
THRC		59,2ms																							
NICmax		12																							
WAD2+ risk		30,2%																							
max Aldman Pressure		37,3kPa at C4																							
max Head X acceleration		15,6g																							
max T1 X acceleration		20,1g																							
max Upper neck Fx		N/A																							
max Upper neck Fz		N/A																							
max Upper neck My		N/A																							
max Lower neck Fx	N/A																								
max Lower neck Fz	N/A																								
max Lower neck My	N/A																								
 <p>NICmax</p>																									
 <p>Max head rear displacement</p>																									




Simulation case	V1_50F_Reclined45_Head-Upright
-----------------	---------------------------------------


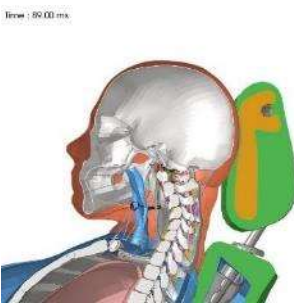
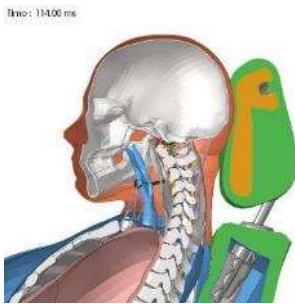
General description	
Seat used	Variant 1
Seat position	Seatback 45°
	Tracks Middle
	Height Middle
	Swivel 0°
	Shoulder N/A
Headrest	Lowest / Backset = 65mm
Dummy used	VIVA+ 50 th Female
Crash pulse	IIWPG Medium Whiplash Pulse
Speed	15,9 km/h
Load case	Low speed rear crash

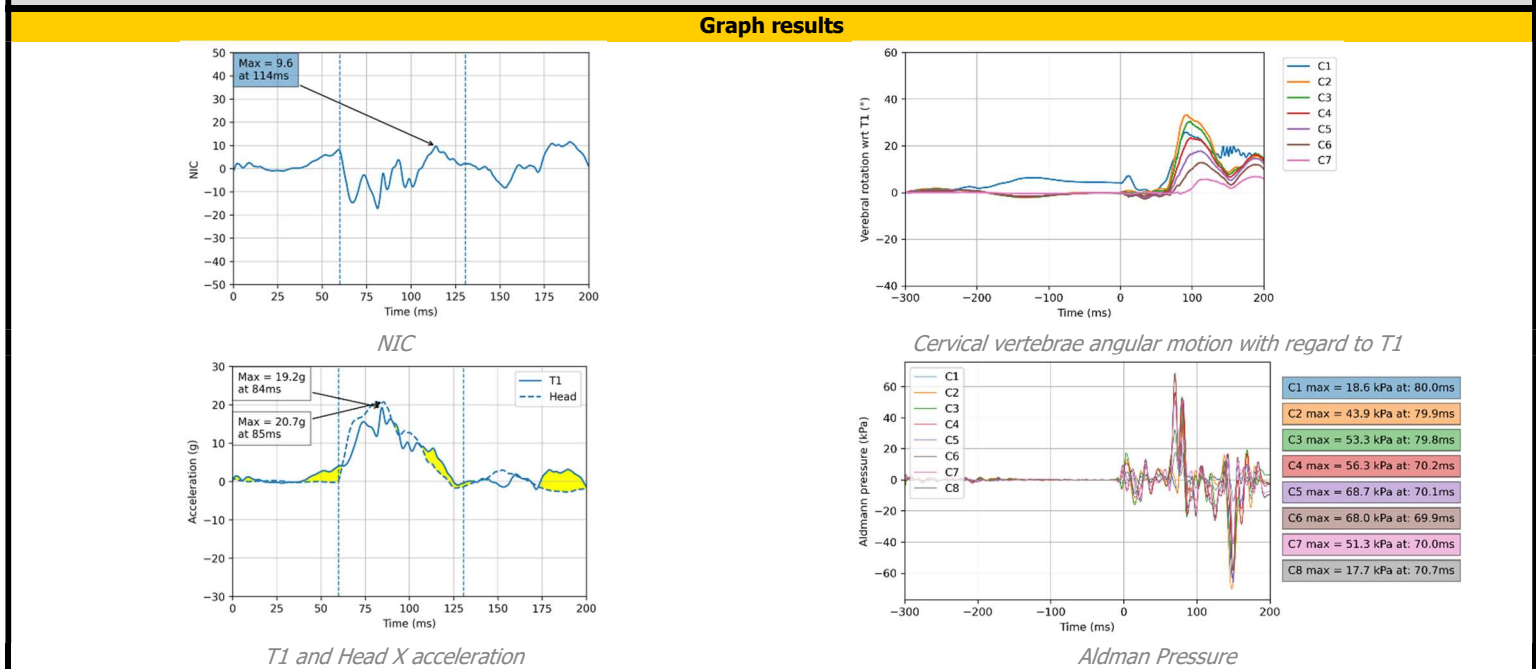


Initial vertebrae position








Seat isometric view

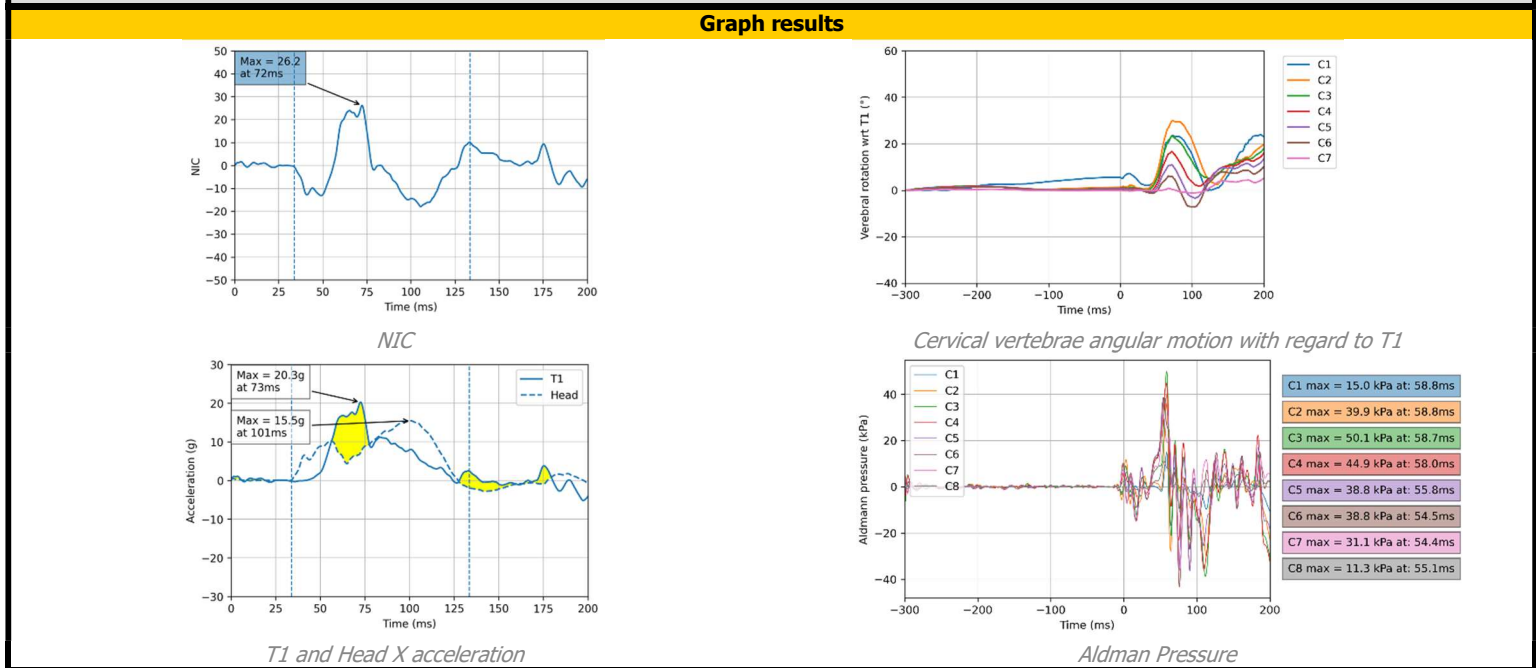
Head kinematics results	Numerical results																								
 <p>Head to head-restraint contact</p>	<table style="width:100%; border-collapse: collapse;"> <tr><td>THRC</td><td style="text-align: right;">59,9ms</td></tr> <tr><td>NICmax</td><td style="text-align: right;">9,6</td></tr> <tr><td>WAD2+ risk</td><td style="text-align: right;">20,9%</td></tr> <tr><td>max Aldman Pressure</td><td style="text-align: right;">68,7kPa at C5</td></tr> <tr><td>max Head X acceleration</td><td style="text-align: right;">20,7g</td></tr> <tr><td>max T1 X acceleration</td><td style="text-align: right;">19,2g</td></tr> <tr><td>max Upper neck Fx</td><td style="text-align: right;">N/A</td></tr> <tr><td>max Upper neck Fz</td><td style="text-align: right;">N/A</td></tr> <tr><td>max Upper neck My</td><td style="text-align: right;">N/A</td></tr> <tr><td>max Lower neck Fx</td><td style="text-align: right;">N/A</td></tr> <tr><td>max Lower neck Fz</td><td style="text-align: right;">N/A</td></tr> <tr><td>max Lower neck My</td><td style="text-align: right;">N/A</td></tr> </table>	THRC	59,9ms	NICmax	9,6	WAD2+ risk	20,9%	max Aldman Pressure	68,7kPa at C5	max Head X acceleration	20,7g	max T1 X acceleration	19,2g	max Upper neck Fx	N/A	max Upper neck Fz	N/A	max Upper neck My	N/A	max Lower neck Fx	N/A	max Lower neck Fz	N/A	max Lower neck My	N/A
THRC		59,9ms																							
NICmax		9,6																							
WAD2+ risk		20,9%																							
max Aldman Pressure		68,7kPa at C5																							
max Head X acceleration		20,7g																							
max T1 X acceleration		19,2g																							
max Upper neck Fx		N/A																							
max Upper neck Fz		N/A																							
max Upper neck My		N/A																							
max Lower neck Fx	N/A																								
max Lower neck Fz	N/A																								
max Lower neck My	N/A																								
 <p>Max head rear displacement</p>																									
 <p>NICmax</p>																									



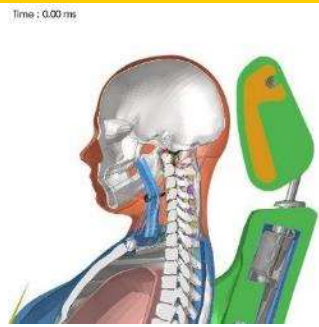

Simulation case	V1_50M_Inclined10_Head-Upright
------------------------	---------------------------------------




General description		
Seat used	Variant 1	 <i>Initial vertebrae position</i>
Seat position	Seatback 35° Tracks Middle / Inclined 10° Height Middle Swivel 0° Shoulder N/A Headrest Middle / Backset = 7mm	
Dummy used	VIVA+ 50 th Male	 <i>Seat isometric view</i>
Crash pulse	IIWPG Medium Whiplash Pulse	
Speed	15,9 km/h	
Load case	Low speed rear crash	

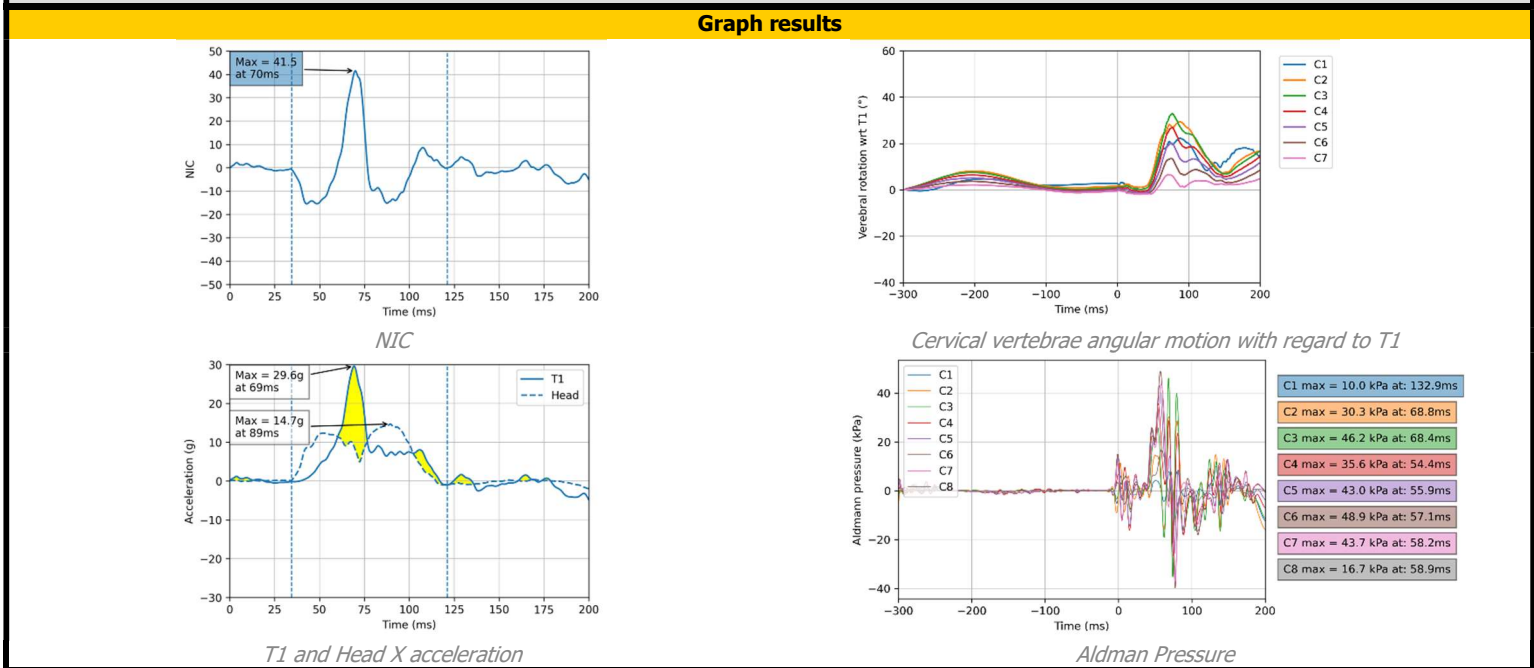
Head kinematics results	Numerical results																								
 <i>Head to head-restraint contact</i>	<table style="width:100%; border-collapse: collapse;"> <tr> <td>THRC</td> <td style="text-align: right;">33,8ms</td> </tr> <tr> <td>NICmax</td> <td style="text-align: right;">26,2</td> </tr> <tr> <td>WAD2+ risk</td> <td style="text-align: right;">89,6%</td> </tr> <tr> <td>max Aldman Pressure</td> <td style="text-align: right;">50,1kPa at C3</td> </tr> <tr> <td>max Head X acceleration</td> <td style="text-align: right;">15,5g</td> </tr> <tr> <td>max T1 X acceleration</td> <td style="text-align: right;">20,3g</td> </tr> <tr> <td>max Upper neck Fx</td> <td style="text-align: right;">N/A</td> </tr> <tr> <td>max Upper neck Fz</td> <td style="text-align: right;">N/A</td> </tr> <tr> <td>max Upper neck My</td> <td style="text-align: right;">N/A</td> </tr> <tr> <td>max Lower neck Fx</td> <td style="text-align: right;">N/A</td> </tr> <tr> <td>max Lower neck Fz</td> <td style="text-align: right;">N/A</td> </tr> <tr> <td>max Lower neck My</td> <td style="text-align: right;">N/A</td> </tr> </table>	THRC	33,8ms	NICmax	26,2	WAD2+ risk	89,6%	max Aldman Pressure	50,1kPa at C3	max Head X acceleration	15,5g	max T1 X acceleration	20,3g	max Upper neck Fx	N/A	max Upper neck Fz	N/A	max Upper neck My	N/A	max Lower neck Fx	N/A	max Lower neck Fz	N/A	max Lower neck My	N/A
THRC		33,8ms																							
NICmax		26,2																							
WAD2+ risk	89,6%																								
max Aldman Pressure	50,1kPa at C3																								
max Head X acceleration	15,5g																								
max T1 X acceleration	20,3g																								
max Upper neck Fx	N/A																								
max Upper neck Fz	N/A																								
max Upper neck My	N/A																								
max Lower neck Fx	N/A																								
max Lower neck Fz	N/A																								
max Lower neck My	N/A																								
 <i>NICmax</i>																									
 <i>Max head rear displacement</i>																									








Simulation case	V1_50F_Inclined10_Head-Upright
-----------------	---------------------------------------

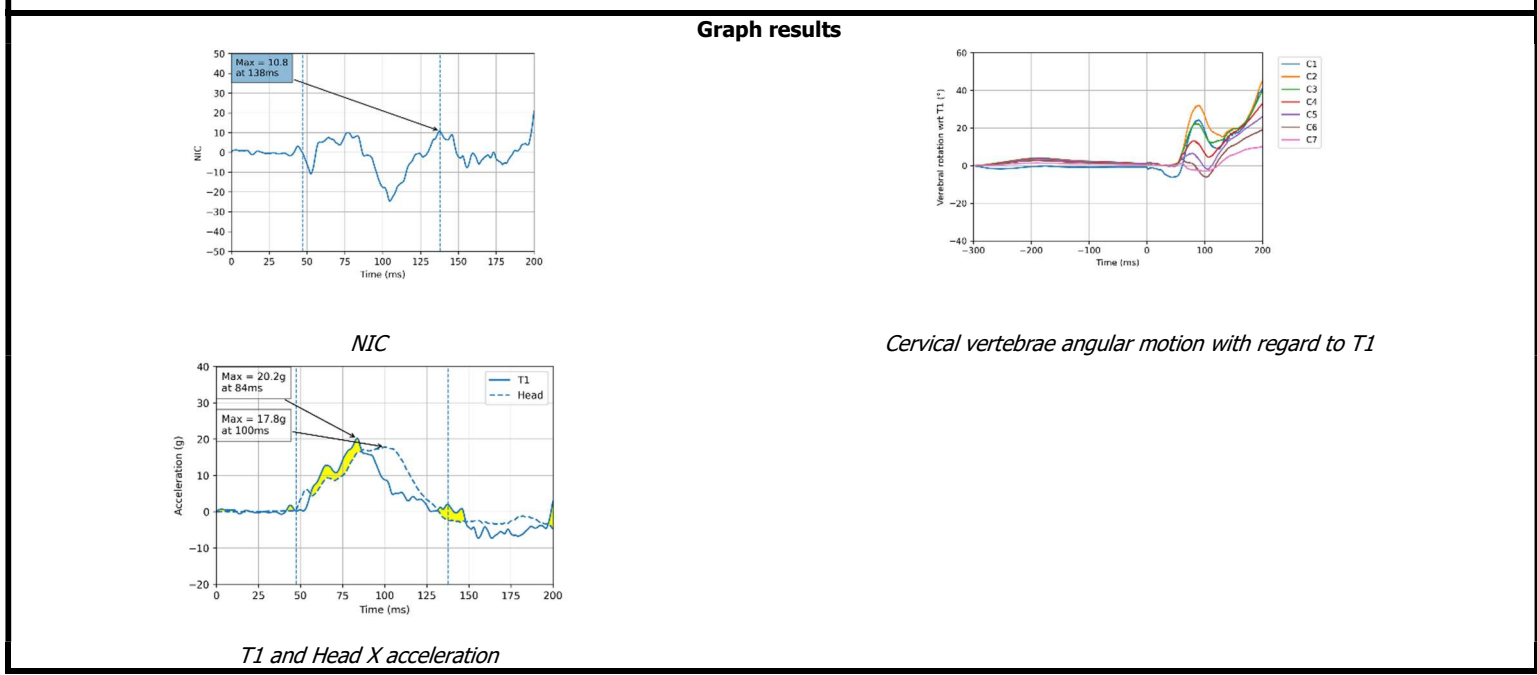
General description		
Seat used	Variant 1	 <i>Initial vertebrae position</i>
Seat position	Seatback 35° Tracks Middle / Inclined 10° Height Middle Swivel 0° Shoulder N/A Headrest Lowest / Backset = 10mm	
Dummy used	VIVA+ 50 th Female	 <i>Seat isometric view</i>
Crash pulse	IIWPG Medium Whiplash Pulse	
Speed	15,9 km/h	
Load case	Low speed rear crash	



Head kinematics results	Numerical results																								
 <i>Head to head-restraint contact</i>	<table style="width:100%; border-collapse: collapse;"> <tr> <td>THRC</td> <td style="text-align: right;">34,4ms</td> </tr> <tr> <td>NICmax</td> <td style="text-align: right;">41,5</td> </tr> <tr> <td>WAD2+ risk</td> <td style="text-align: right;">99,5%</td> </tr> <tr> <td>max Aldman Pressure</td> <td style="text-align: right;">48,9kPa at C6</td> </tr> <tr> <td>max Head X acceleration</td> <td style="text-align: right;">14,7g</td> </tr> <tr> <td>max T1 X acceleration</td> <td style="text-align: right;">29,6g</td> </tr> <tr> <td>max Upper neck Fx</td> <td style="text-align: right;">N/A</td> </tr> <tr> <td>max Upper neck Fz</td> <td style="text-align: right;">N/A</td> </tr> <tr> <td>max Upper neck My</td> <td style="text-align: right;">N/A</td> </tr> <tr> <td>max Lower neck Fx</td> <td style="text-align: right;">N/A</td> </tr> <tr> <td>max Lower neck Fz</td> <td style="text-align: right;">N/A</td> </tr> <tr> <td>max Lower neck My</td> <td style="text-align: right;">N/A</td> </tr> </table>	THRC	34,4ms	NICmax	41,5	WAD2+ risk	99,5%	max Aldman Pressure	48,9kPa at C6	max Head X acceleration	14,7g	max T1 X acceleration	29,6g	max Upper neck Fx	N/A	max Upper neck Fz	N/A	max Upper neck My	N/A	max Lower neck Fx	N/A	max Lower neck Fz	N/A	max Lower neck My	N/A
THRC		34,4ms																							
NICmax		41,5																							
WAD2+ risk	99,5%																								
max Aldman Pressure	48,9kPa at C6																								
max Head X acceleration	14,7g																								
max T1 X acceleration	29,6g																								
max Upper neck Fx	N/A																								
max Upper neck Fz	N/A																								
max Upper neck My	N/A																								
max Lower neck Fx	N/A																								
max Lower neck Fz	N/A																								
max Lower neck My	N/A																								
 <i>NICmax</i>																									
 <i>Max head rear displacement</i>																									

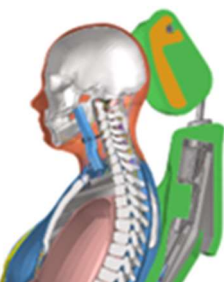
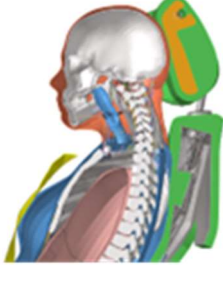



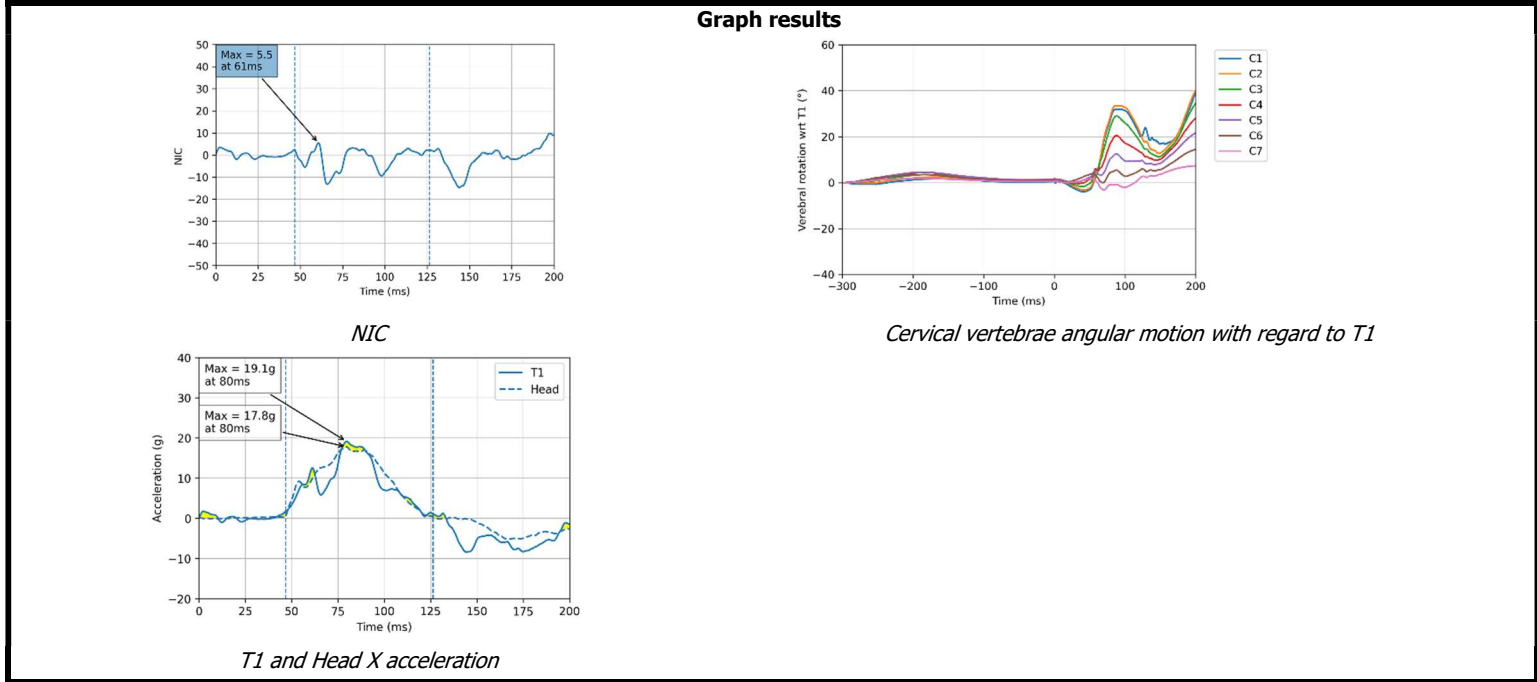
Simulation case		V2_50M_Swiveled0_Head-Upright	
Seat used	Variant 2	General description Time : 0.00 ms  	
Seat position	Seatback 25° Tracks Middle Height Middle Swivel 0° Shoulder N/A Headrest Middle / Backset = 31mm		
Dummy used	VIVA+ 50 th Male		
Crash pulse	IIWPG Medium Whiplash Pulse		
Speed	15,9 km/h		
Load case	Low speed rear crash		

Head kinematics results	Numerical results
  	THRC 48ms NICmax 10,8 WAD2+ risk 25,5% max Aldman Pressure max Head X acceleration 17,8g max T1 X acceleration 20,2g max Upper neck Fx N/A max Upper neck Fz N/A max Upper neck My N/A max Lower neck Fx N/A max Lower neck Fz N/A max Lower neck My N/A
<i>Head to head-restraint contact</i> <i>Max head rear displacement</i> <i>Max T1 acceleration</i>	





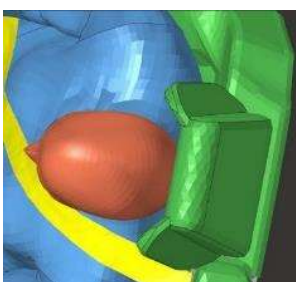
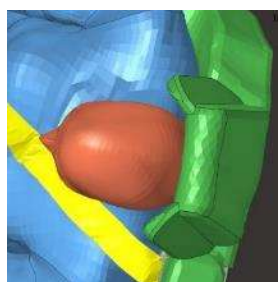
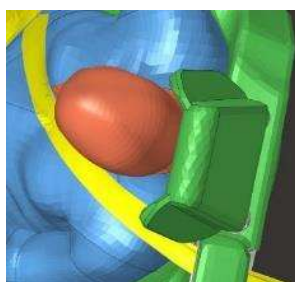
Simulation case		V2_50F_Swiveled0_Head-Upright	
Seat used	Variant 2	General description Time : 0.00 ms.  	
Seat position	Seatback 25° Tracks Middle Height Middle Swivel 0° Shoulder N/A Headrest Lowest / Backset = 31mm		
Dummy used	VIVA+ 50 th Female		
Crash pulse	IIWPG Medium Whiplash Pulse		
Speed	15,9 km/h		
Load case	Low speed rear crash		

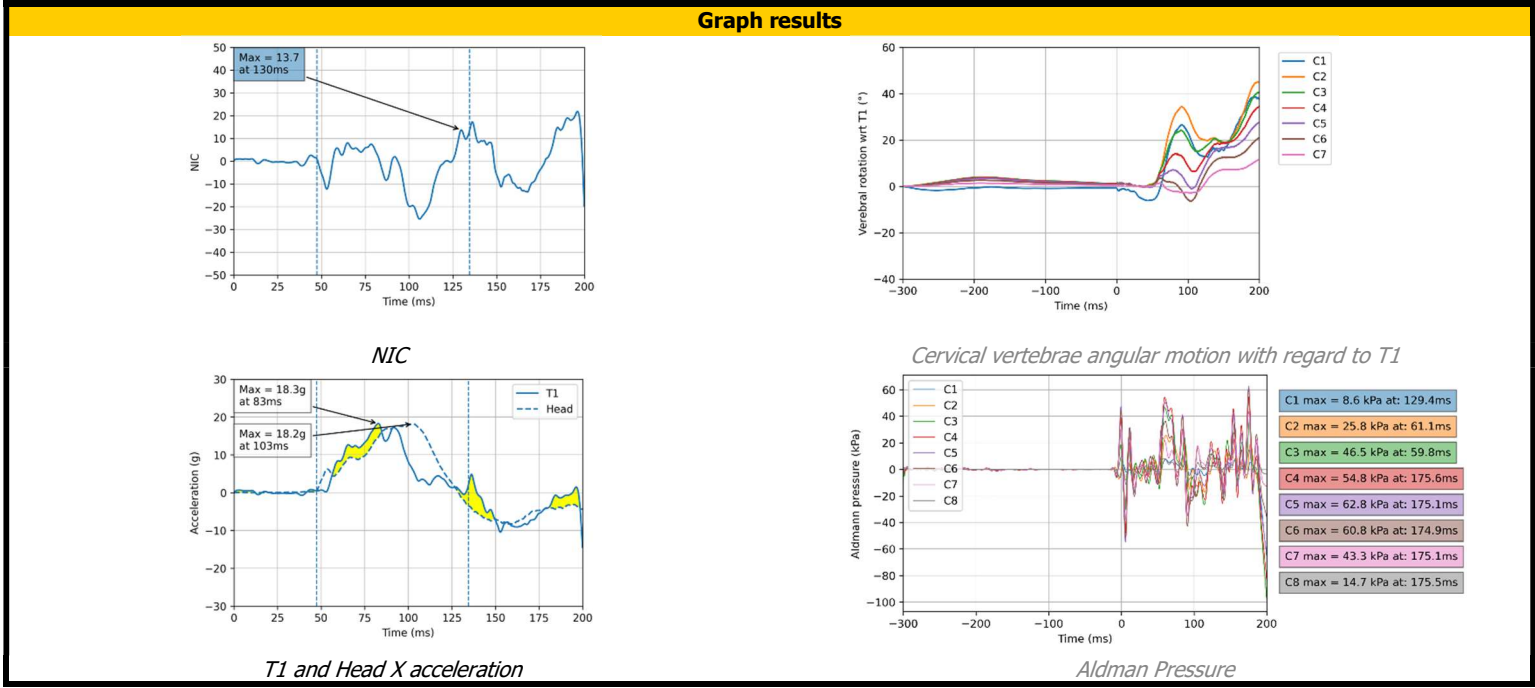
Head kinematics results			Numerical results	
 Time : 47.00 ms <i>Head to head-restraint contact</i>	 Time : 64.90 ms <i>Max head rear displacement</i>	 Time : 80.90 ms <i>Max head Y acceleration</i>	THRC 47ms NICmax 5,5 WAD2+ risk 9,9% max Aldman Pressure max Head X acceleration 17,8g max T1 X acceleration 19,1g max Upper neck Fx N/A max Upper neck Fz N/A max Upper neck My N/A max Lower neck Fx N/A max Lower neck Fz N/A max Lower neck My N/A	

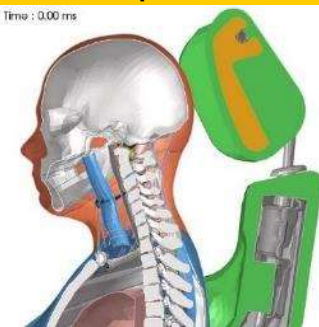



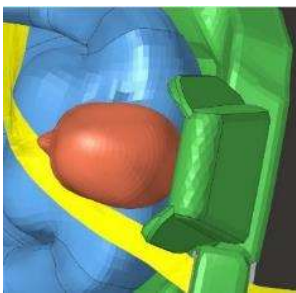
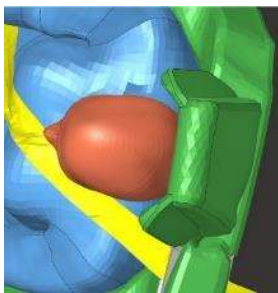
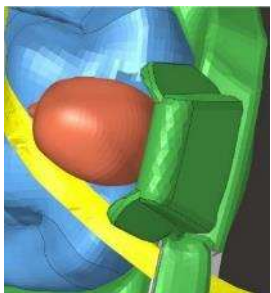
Simulation Case	V2_50M_Swiveled10_Head-Upright
-----------------	---------------------------------------

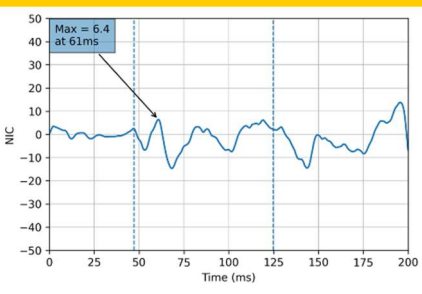
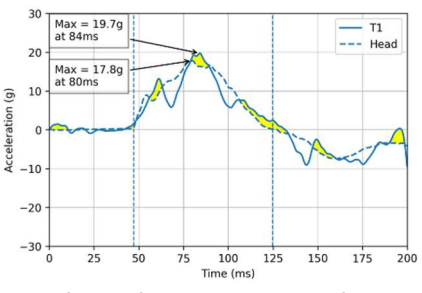
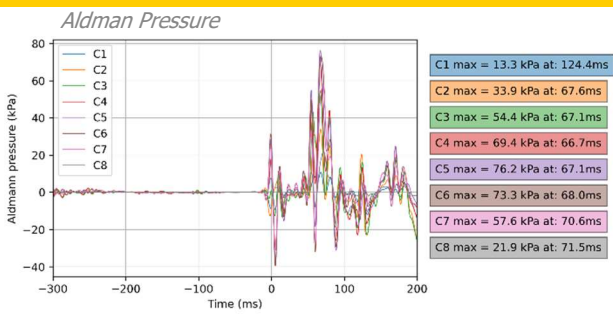
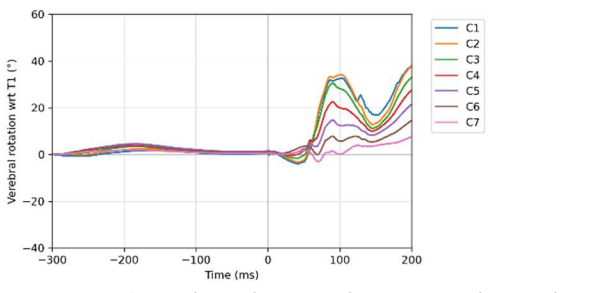
General description		
Seat used	Variant 2	 <i>Initial vertebrae position</i>
Seat position	Seatback: 25° Tracks: Middle Height: Middle Swivel: 10° Shoulder: N/A Headrest: Middle / Backset = 31mm	
Dummy used	VIVA+ 50 th Male	 <i>Seat isometric view</i>
Crash pulse	IIWPG Medium Whiplash Pulse	
Speed	15,9 km/h	
Load case	Low speed rear crash	



Head kinematics results	Numerical results
 <i>Head to head-restraint contact</i>	THRC: 47,5ms NICmax: 13,7 WAD2+ risk: 38,3% max Aldman Pressure: 62,8kPa at C5 max Head X acceleration: 18,2g max Upper neck Fx: N/A max Upper neck Fz: N/A max Upper neck My: N/A max Lower neck Fx: N/A max Lower neck Fz: N/A max Lower neck My: N/A
 <i>Max head rear displacement</i>	
 <i>Max head Y acceleration</i>	

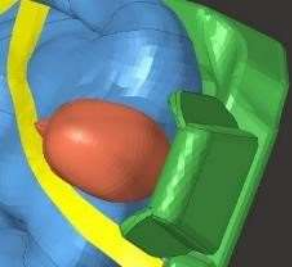
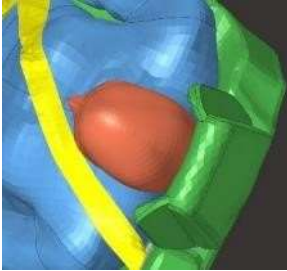
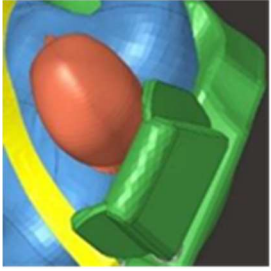


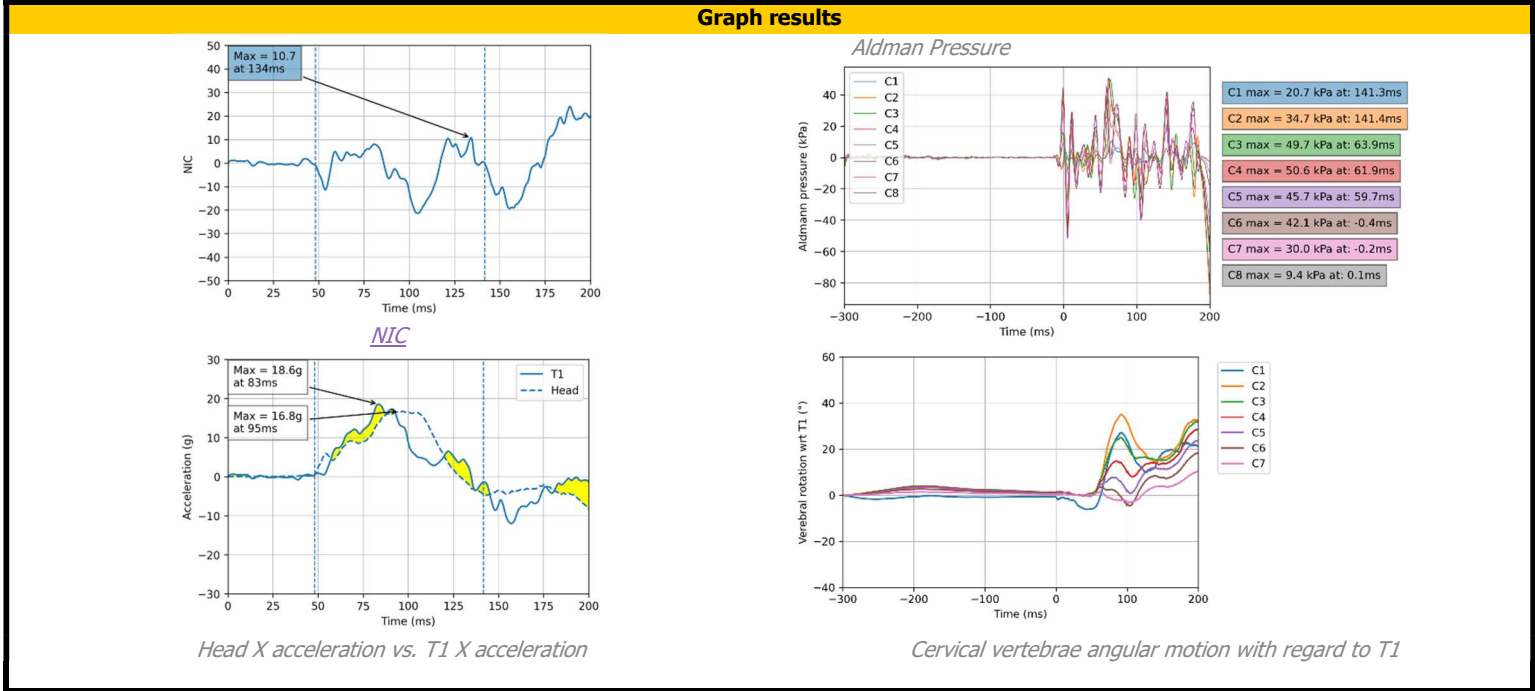
Simulation case		V2_50F_Swiveled10_Head-Upright		
General description				
Seat used	Variant 2	 		
Seat position	Seatback			25°
	Tracks			Middle
	Height			Middle
	Swivel			10°
	Shoulder			N/A
	Headrest	Lowest / Backset = 31mm		
Dummy used	VIVA+ 50 th Female			
Crash pulse	IIWPG Medium Whiplash Pulse			
Speed	15,9 km/h			
Load case	Low speed rear crash			



Head kinematics results	Numerical results																								
  	<table border="0"> <tr><td>THRC</td><td>47,1ms</td></tr> <tr><td>NICmax</td><td>6,4</td></tr> <tr><td>WAD 2+ risk</td><td>11,9%</td></tr> <tr><td>max Aldman Pressure</td><td>76,2kPa at C5</td></tr> <tr><td>max Head X acceleration</td><td>18,2g</td></tr> <tr><td>max T1 X acceleration</td><td>19,0g</td></tr> <tr><td>max Upper neck Fx</td><td>N/A</td></tr> <tr><td>max Upper neck Fz</td><td>N/A</td></tr> <tr><td>max Upper neck My</td><td>N/A</td></tr> <tr><td>max Lower neck Fx</td><td>N/A</td></tr> <tr><td>max Lower neck Fz</td><td>N/A</td></tr> <tr><td>max Lower neck My</td><td>N/A</td></tr> </table>	THRC	47,1ms	NICmax	6,4	WAD 2+ risk	11,9%	max Aldman Pressure	76,2kPa at C5	max Head X acceleration	18,2g	max T1 X acceleration	19,0g	max Upper neck Fx	N/A	max Upper neck Fz	N/A	max Upper neck My	N/A	max Lower neck Fx	N/A	max Lower neck Fz	N/A	max Lower neck My	N/A
THRC	47,1ms																								
NICmax	6,4																								
WAD 2+ risk	11,9%																								
max Aldman Pressure	76,2kPa at C5																								
max Head X acceleration	18,2g																								
max T1 X acceleration	19,0g																								
max Upper neck Fx	N/A																								
max Upper neck Fz	N/A																								
max Upper neck My	N/A																								
max Lower neck Fx	N/A																								
max Lower neck Fz	N/A																								
max Lower neck My	N/A																								
<p><i>Head to head-restraint contact</i> <i>Max head rear displacement</i> <i>Max head Y acceleration</i></p>																									

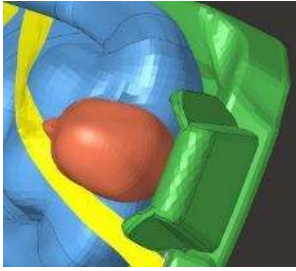
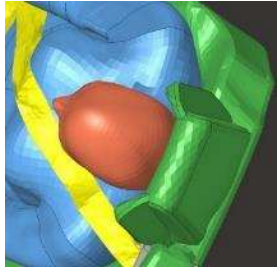
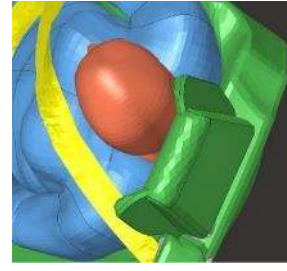
Graph results	
 <p><i>NIC</i></p>  <p><i>Head X acceleration vs. T1 X acceleration</i></p>	 <p><i>Aldman Pressure</i></p>  <p><i>Cervical vertebrae angular motion with regard to T1</i></p>

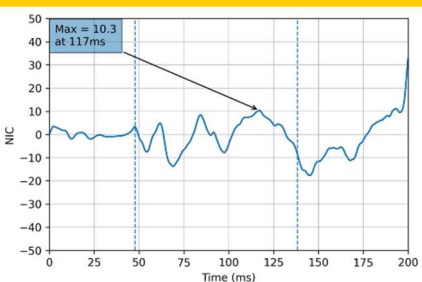
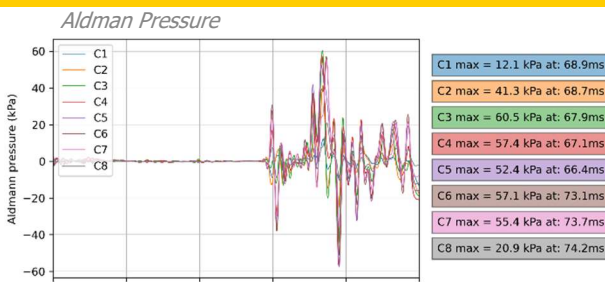
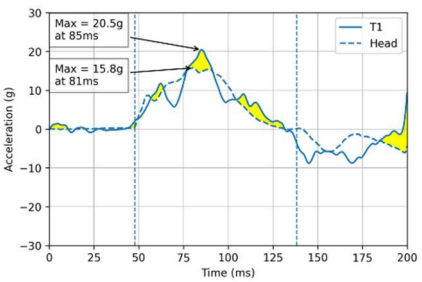
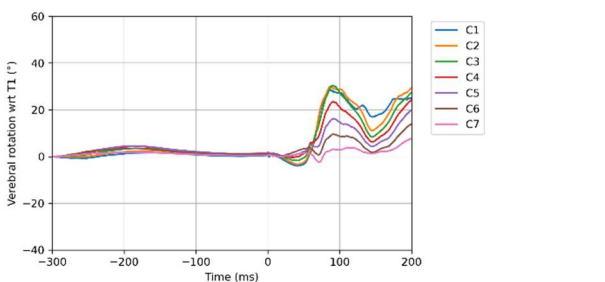
Simulation case		V2_50M_Swiveled20_Head-Upright		
General description				
Seat used	Variant 2	 		
Seat position	Seatback			25°
	Tracks			Middle
	Height			Middle
	Swivel			20°
	Shoulder			N/A
Headrest	Middle / Backset = 31mm			
Dummy used	VIVA+ 50 th Male			
Crash pulse	IIWPG Medium Whiplash Pulse			
Speed	15,9 km/h			
Load case	Low speed rear crash			



Head kinematics results			Numerical results	
			THRC	48,2ms
			NICmax	10,7
			WAD2+ risk	25,1%
			max Aldman Pressure	50,6kPa at C4
			max Head X acceleration	17,1g
			max T1 X acceleration	17,5g
			max Upper neck Fx	N/A
			max Upper neck Fz	N/A
			max Upper neck My	N/A
			max Lower neck Fx	N/A
			max Lower neck Fz	N/A
			max Lower neck My	N/A



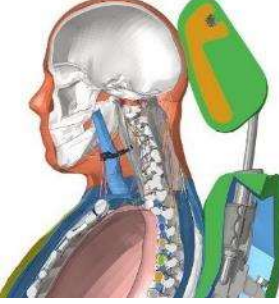


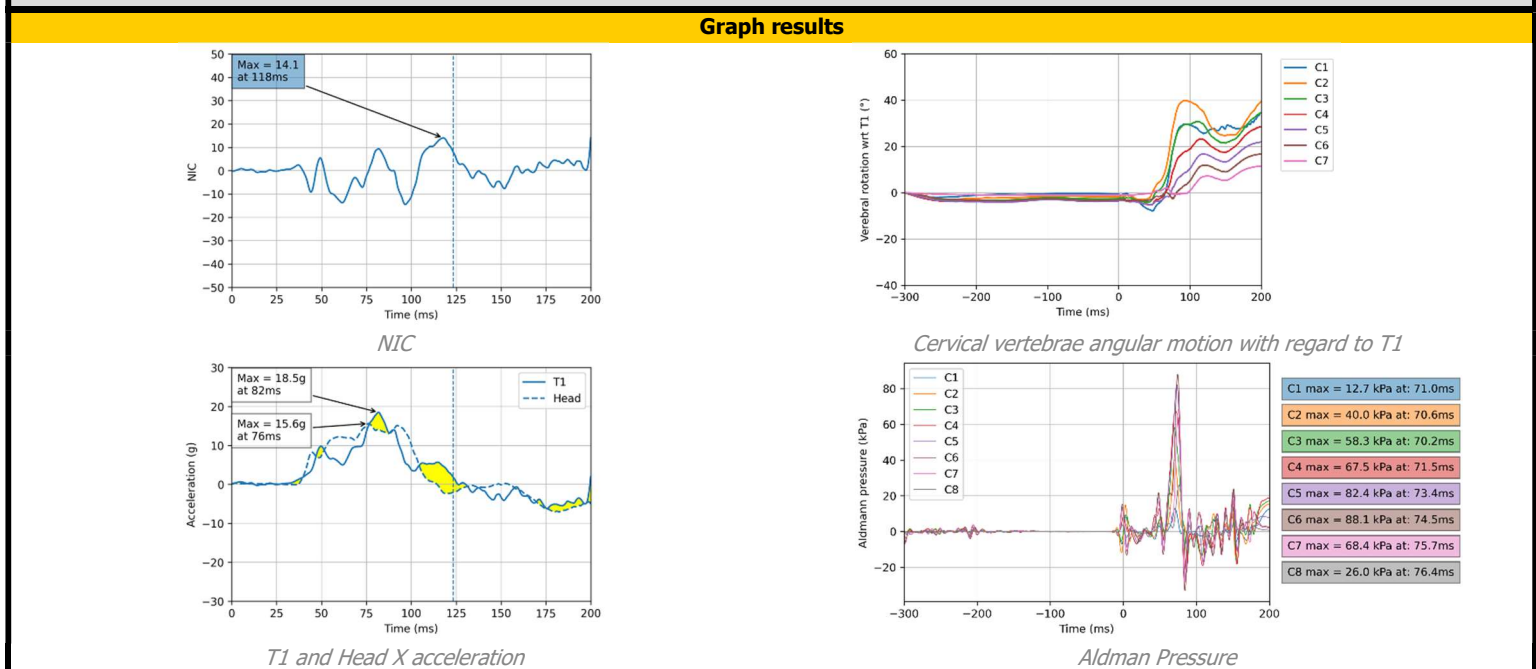
Simulation case		V2_50F_Swiveled20_Head-Upright	
General description			
Seat used	Variant 2		 Time: 0.00 ms
Seat position	Seatback	25°	
	Tracks	Middle	
	Height	Middle	
	Swivel	20°	
	Shoulder	N/A	
	Headrest	Lowest / Backset = 31mm	
Dummy used	VIVA+ 50 th Female		
Crash pulse	IIWPG Medium Whiplash Pulse		
Speed	15,9 km/h		
Load case	Low speed rear crash		<i>Initial vertebrae position</i> <i>Seat isometric view</i>

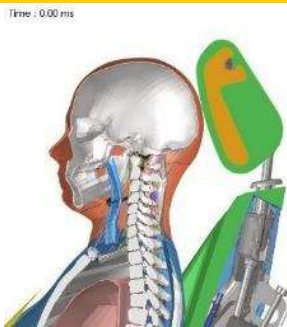

Head kinematics results		Numerical results																									
 <i>Head to head-restraint contact</i>	 <i>Max head rear displacement</i>	 <i>Max head Y acceleration</i>	<table border="0"> <tr><td>THRC</td><td>47,8ms</td></tr> <tr><td>NICmax</td><td>10,3</td></tr> <tr><td>WAD 2+ risk</td><td>23,5%</td></tr> <tr><td>max Head X acceleration</td><td>16,7g</td></tr> <tr><td>max T1 X acceleration</td><td>19,3g</td></tr> <tr><td>max Aldman Pressure</td><td>60,5kPa at C3</td></tr> <tr><td>max Upper neck Fx</td><td>N/A</td></tr> <tr><td>max Upper neck Fz</td><td>N/A</td></tr> <tr><td>max Upper neck My</td><td>N/A</td></tr> <tr><td>max Lower neck Fx</td><td>N/A</td></tr> <tr><td>max Lower neck Fz</td><td>N/A</td></tr> <tr><td>max Lower neck My</td><td>N/A</td></tr> </table>	THRC	47,8ms	NICmax	10,3	WAD 2+ risk	23,5%	max Head X acceleration	16,7g	max T1 X acceleration	19,3g	max Aldman Pressure	60,5kPa at C3	max Upper neck Fx	N/A	max Upper neck Fz	N/A	max Upper neck My	N/A	max Lower neck Fx	N/A	max Lower neck Fz	N/A	max Lower neck My	N/A
THRC	47,8ms																										
NICmax	10,3																										
WAD 2+ risk	23,5%																										
max Head X acceleration	16,7g																										
max T1 X acceleration	19,3g																										
max Aldman Pressure	60,5kPa at C3																										
max Upper neck Fx	N/A																										
max Upper neck Fz	N/A																										
max Upper neck My	N/A																										
max Lower neck Fx	N/A																										
max Lower neck Fz	N/A																										
max Lower neck My	N/A																										




Graph results	
 <i>NIC</i>	 <i>Aldman Pressure</i>
 <i>Head X acceleration vs. T1 X acceleration</i>	 <i>Cervical vertebrae angular motion with regard to T1</i>

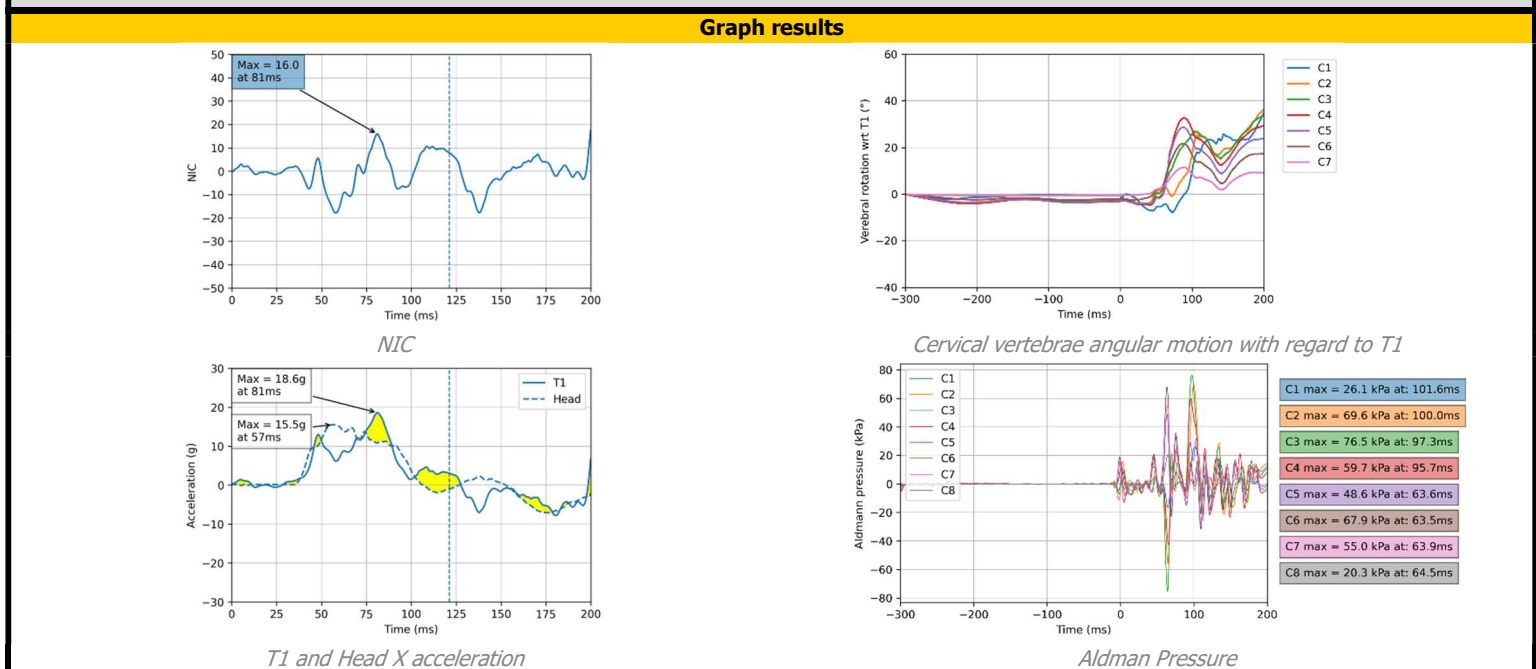
Simulation case		V3_50M_Upright_Head-Leaning	
General description			
Seat used	Variant 3		 Time : 0,00 ms
Seat position	Seatback	25°	
	Tracks	Middle	 <i>Initial vertebrae position</i> <i>Seat isometric view</i>
	Height	Middle	
	Swivel	0°	
	Shoulder	0°	
	Headrest	Middle / Backset = 0mm	
Dummy used	VIVA+ 50 th Male		
Crash pulse	IIWPG Medium Whiplash Pulse		
Speed	15,9 km/h		
Load case	Low speed rear crash		

Head kinematics results			Numerical results	
 Time : 80,00 ms <i>Max head rear displacement</i>	 Time : 86,00 ms <i>Max T1 rear displacement</i>	 Time : 118,00 ms <i>NICmax</i>	THRC NICmax WAD2+ risk max Aldman Pressure max Head X acceleration max T1 X acceleration max Upper neck Fx max Upper neck Fz max Upper neck My max Lower neck Fx max Lower neck Fz max Lower neck My	N/A 14,1 40,2 88,1kPa at C6 15,6g 18,5g N/A N/A N/A N/A N/A N/A



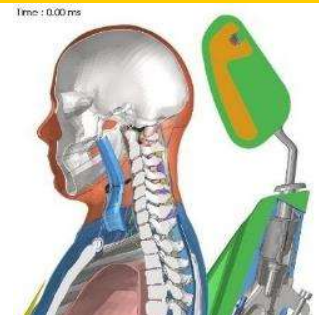
Simulation case		V3_50F_Upright_Head-Leaning		
General description				
Seat used	Variant 3	 		
Seat position	Seatback			25°
	Tracks			Middle
	Height			Middle
	Swivel			0°
	Shoulder			0°
	Headrest			Lowest / Backset = 0mm
Dummy used	VIVA+ 50 th Female			
Crash pulse	IIWPG Medium Whiplash Pulse			
Speed	15,9 km/h			
Load case	Low speed rear crash			

Head kinematics results			Numerical results	
 <p>Time: 63.00 ms</p> <p><i>Beginning of S-shape</i></p>	 <p>Time: 73.00 ms</p> <p><i>Max head rear displacement</i></p>	 <p>Time: 81.00 ms</p> <p><i>NICmax</i></p>	THRC NICmax WAD2+ risk max Aldman Pressure max Head X acceleration max T1 X acceleration max Upper neck Fx max Upper neck Fz max Upper neck My max Lower neck Fx max Lower neck Fz max Lower neck My	N/A 16 50,2% 76,5kPa at C3 15,5g 18,6g N/A N/A N/A N/A N/A N/A




Simulation case	V3_50M_Upright_Head-Upright
------------------------	------------------------------------

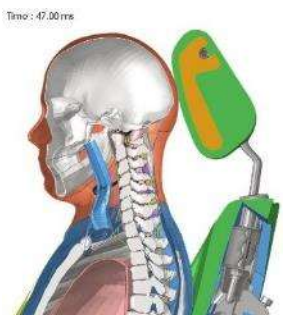
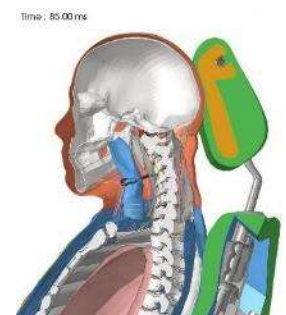
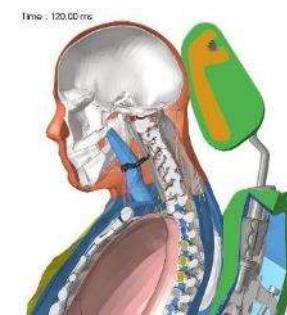
General description	
Seat used	Variant 3
Seat position	Seatback 25°
	Tracks Middle
	Height Middle
	Swivel 0°
	Shoulder 0°
	Headrest Middle / Backset = 26mm
Dummy used	VIVA+ 50 th Male
Crash pulse	IIWPG Medium Whiplash Pulse
Speed	15,9 km/h
Load case	Low speed rear crash

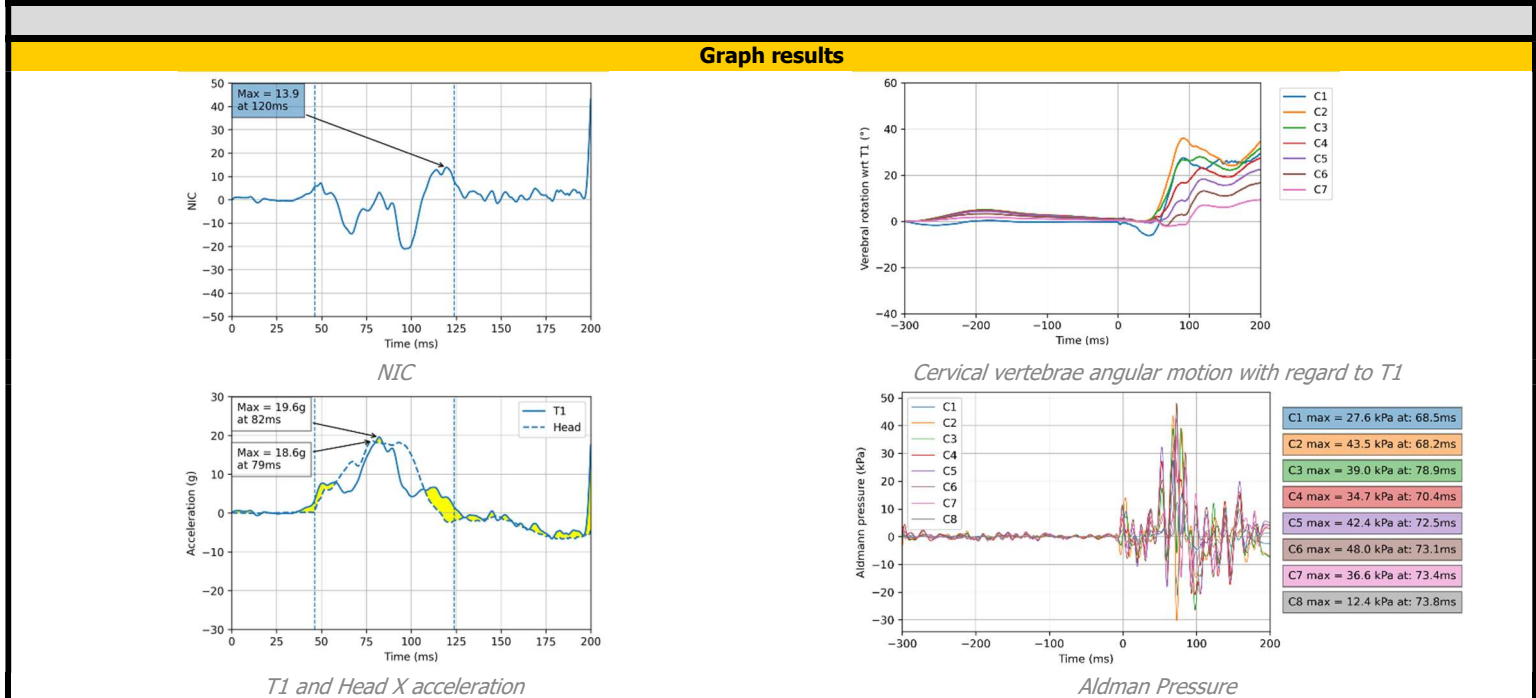


Time : 0,00 ms
Initial vertebrae position




Seat isometric view

Head kinematics results	Numerical results																								
 <p>Time: 47,00 ms <i>Head to head-restraint contact</i></p>	<table style="width:100%; border-collapse: collapse;"> <tr><td>THRC</td><td style="text-align: right;">46,2ms</td></tr> <tr><td>NICmax</td><td style="text-align: right;">13,9</td></tr> <tr><td>WAD2+ risk</td><td style="text-align: right;">39,4%</td></tr> <tr><td>max Aldman Pressure</td><td style="text-align: right;">48kPa at C6</td></tr> <tr><td>max Head X acceleration</td><td style="text-align: right;">18,6g</td></tr> <tr><td>max T1 X acceleration</td><td style="text-align: right;">19,6g</td></tr> <tr><td>max Upper neck Fx</td><td style="text-align: right;">N/A</td></tr> <tr><td>max Upper neck Fz</td><td style="text-align: right;">N/A</td></tr> <tr><td>max Upper neck My</td><td style="text-align: right;">N/A</td></tr> <tr><td>max Lower neck Fx</td><td style="text-align: right;">N/A</td></tr> <tr><td>max Lower neck Fz</td><td style="text-align: right;">N/A</td></tr> <tr><td>max Lower neck My</td><td style="text-align: right;">N/A</td></tr> </table>	THRC	46,2ms	NICmax	13,9	WAD2+ risk	39,4%	max Aldman Pressure	48kPa at C6	max Head X acceleration	18,6g	max T1 X acceleration	19,6g	max Upper neck Fx	N/A	max Upper neck Fz	N/A	max Upper neck My	N/A	max Lower neck Fx	N/A	max Lower neck Fz	N/A	max Lower neck My	N/A
THRC		46,2ms																							
NICmax		13,9																							
WAD2+ risk		39,4%																							
max Aldman Pressure		48kPa at C6																							
max Head X acceleration		18,6g																							
max T1 X acceleration	19,6g																								
max Upper neck Fx	N/A																								
max Upper neck Fz	N/A																								
max Upper neck My	N/A																								
max Lower neck Fx	N/A																								
max Lower neck Fz	N/A																								
max Lower neck My	N/A																								
 <p>Time: 85,00 ms <i>Max head rear displacement</i></p>																									
 <p>Time: 120,00 ms <i>NICmax</i></p>																									




Simulation case	V3_50F_Upright_Head-Upright
-----------------	------------------------------------

General description	
Seat used	Variant 3
Seat position	Seatback 25°
	Tracks Middle
	Height Middle
	Swivel 0°
	Shoulder 0°
	Headrest Lowest / Backset = 32mm
Dummy used	VIVA+ 50 th Female
Crash pulse	IIWPG Medium Whiplash Pulse
Speed	15,9 km/h
Load case	Low speed rear crash






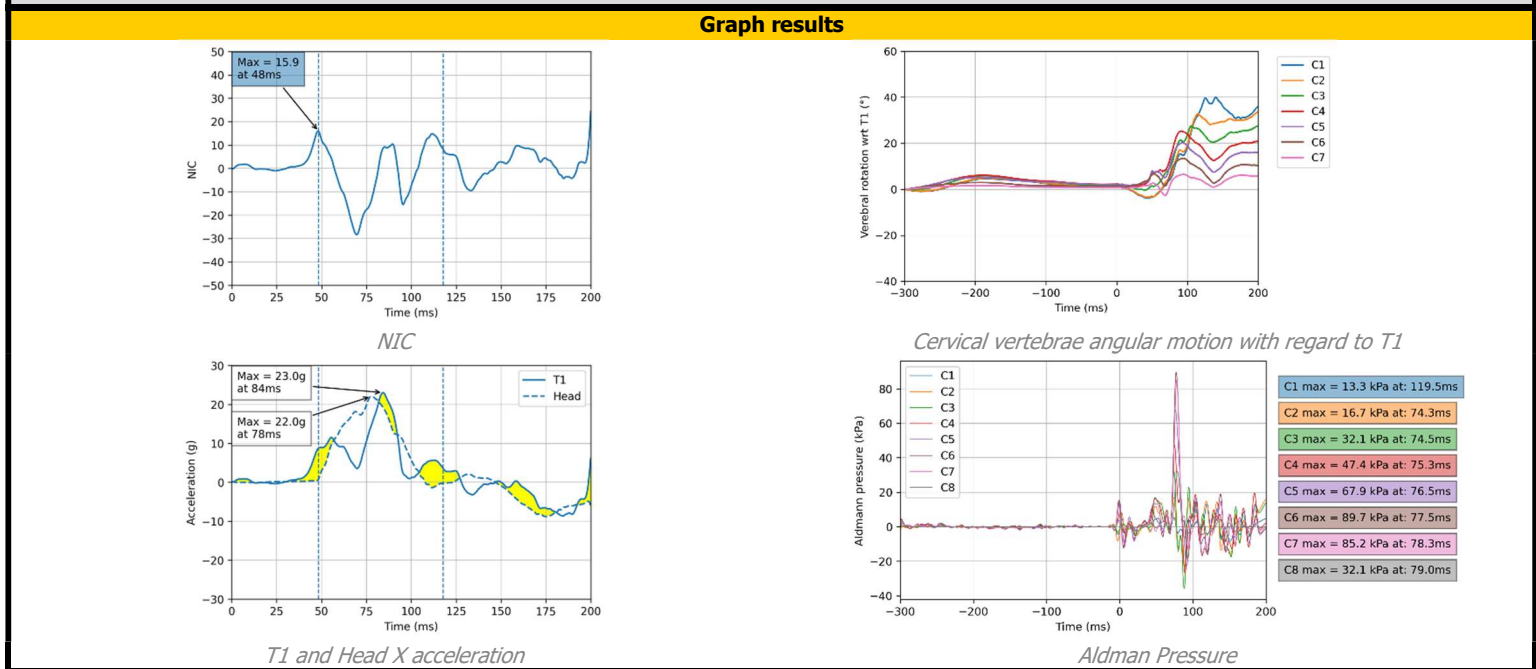
Time : 0,00 ms

Initial vertebrae position

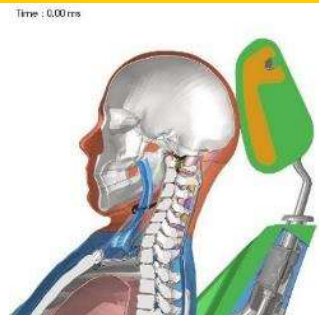



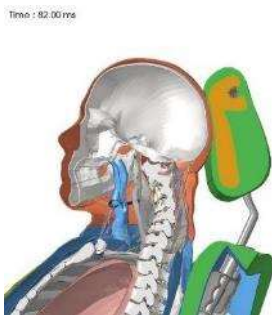
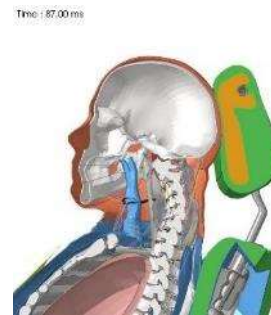
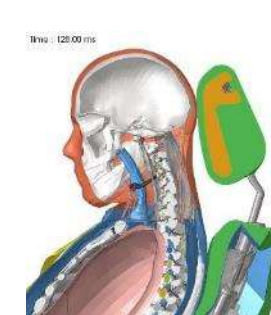
Seat isometric view

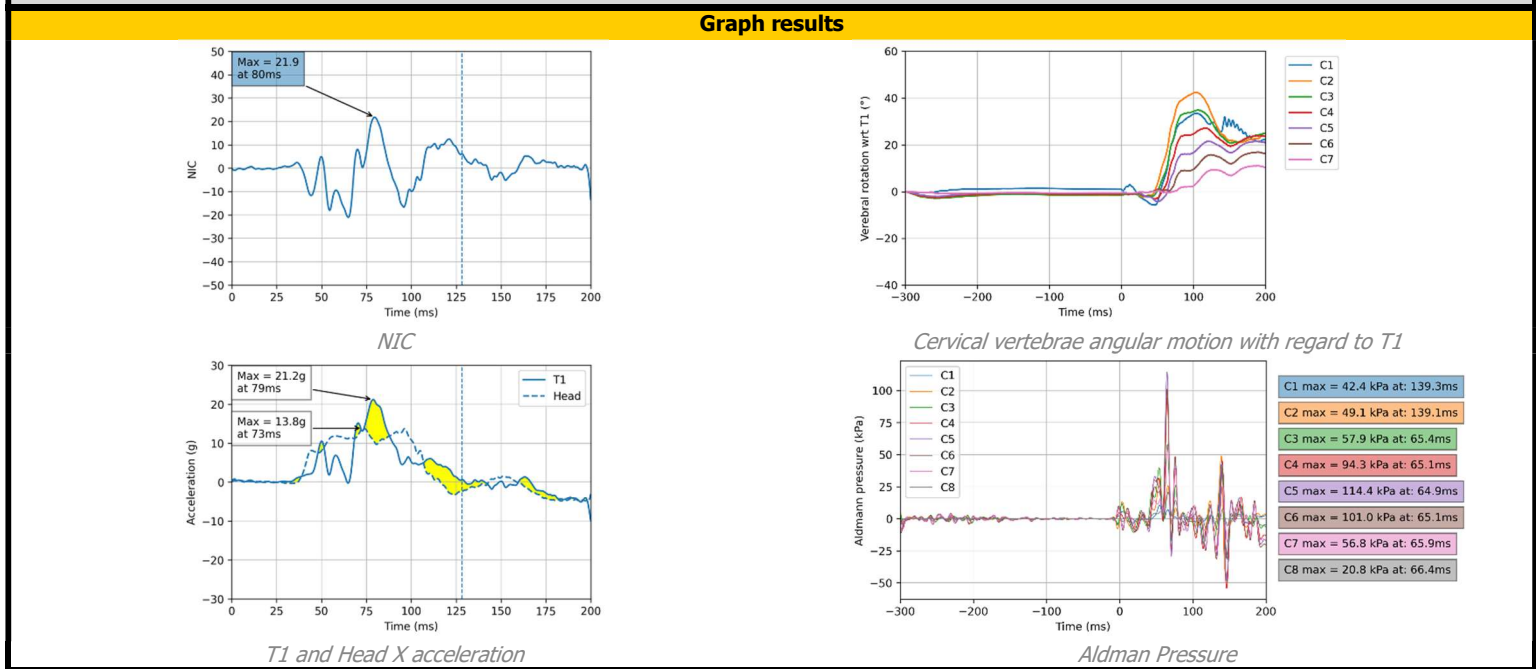
Head kinematics results	Numerical results																								
<div style="display: flex; justify-content: space-around;"> <div style="text-align: center;">  <p>Time : 49,00 ms</p> <p><i>Head to head-restraint contact</i></p> </div> <div style="text-align: center;">  <p>Time : 79,00 ms</p> <p><i>Max head rear displacement</i></p> </div> <div style="text-align: center;">  <p>Time : 86,00 ms</p> <p><i>Max T1 rear displacement</i></p> </div> </div>	<table border="0" style="width:100%;"> <tr><td>THRC</td><td style="text-align: right;">48,3ms</td></tr> <tr><td>NICmax</td><td style="text-align: right;">15,9</td></tr> <tr><td>WAD2+ risk</td><td style="text-align: right;">49,6%</td></tr> <tr><td>max Aldman Pressure</td><td style="text-align: right;">89,7kPa at C6</td></tr> <tr><td>max Head X acceleration</td><td style="text-align: right;">22g</td></tr> <tr><td>max T1 X acceleration</td><td style="text-align: right;">23g</td></tr> <tr><td>max Upper neck Fx</td><td style="text-align: right;">N/A</td></tr> <tr><td>max Upper neck Fz</td><td style="text-align: right;">N/A</td></tr> <tr><td>max Upper neck My</td><td style="text-align: right;">N/A</td></tr> <tr><td>max Lower neck Fx</td><td style="text-align: right;">N/A</td></tr> <tr><td>max Lower neck Fz</td><td style="text-align: right;">N/A</td></tr> <tr><td>max Lower neck My</td><td style="text-align: right;">N/A</td></tr> </table>	THRC	48,3ms	NICmax	15,9	WAD2+ risk	49,6%	max Aldman Pressure	89,7kPa at C6	max Head X acceleration	22g	max T1 X acceleration	23g	max Upper neck Fx	N/A	max Upper neck Fz	N/A	max Upper neck My	N/A	max Lower neck Fx	N/A	max Lower neck Fz	N/A	max Lower neck My	N/A
THRC	48,3ms																								
NICmax	15,9																								
WAD2+ risk	49,6%																								
max Aldman Pressure	89,7kPa at C6																								
max Head X acceleration	22g																								
max T1 X acceleration	23g																								
max Upper neck Fx	N/A																								
max Upper neck Fz	N/A																								
max Upper neck My	N/A																								
max Lower neck Fx	N/A																								
max Lower neck Fz	N/A																								
max Lower neck My	N/A																								

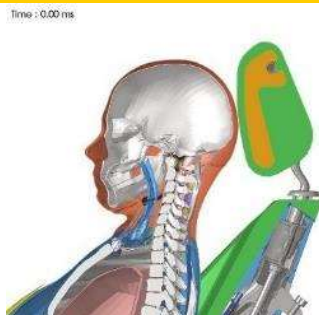



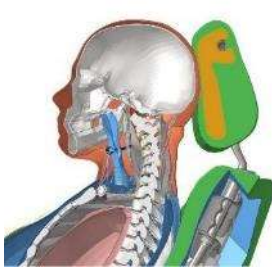


Simulation case	V3_50M_Reclined35_Head-Leaning
------------------------	---------------------------------------

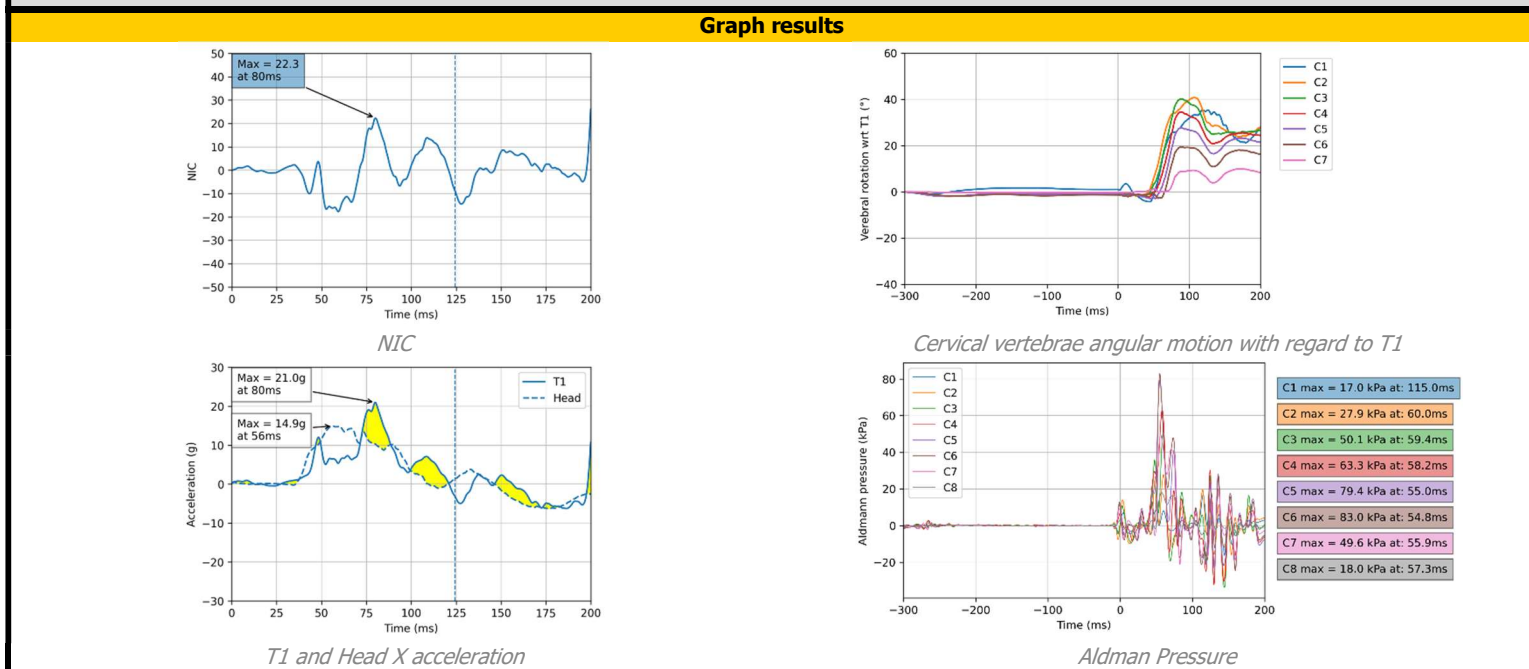
General description		
Seat used	Variant 3	 Time : 0.00 ms
Seat position	Seatback 35° Tracks Middle Height Middle Swivel 0° Shoulder 0° Headrest Middle / Backset = 0mm	
Dummy used	VIVA+ 50 th Male	 <i>Initial vertebrae position</i> <i>Seat isometric view</i>
Crash pulse	IIWPG Medium Whiplash Pulse	
Speed	15,9 km/h	
Load case	Low speed rear crash	



Head kinematics results	Numerical results																								
 Time : 82.00 ms <i>Max head rear displacement</i>	<table style="width:100%; border-collapse: collapse;"> <tr><td>THRC</td><td style="text-align: right;">N/A</td></tr> <tr><td>NICmax</td><td style="text-align: right;">21,9</td></tr> <tr><td>WAD2+ risk</td><td style="text-align: right;">77,5%</td></tr> <tr><td>max Aldman Pressure</td><td style="text-align: right;">114,4kPa at C5</td></tr> <tr><td>max Head X acceleration</td><td style="text-align: right;">13,8g</td></tr> <tr><td>max T1 X acceleration</td><td style="text-align: right;">21,2g</td></tr> <tr><td>max Upper neck Fx</td><td style="text-align: right;">N/A</td></tr> <tr><td>max Upper neck Fz</td><td style="text-align: right;">N/A</td></tr> <tr><td>max Upper neck My</td><td style="text-align: right;">N/A</td></tr> <tr><td>max Lower neck Fx</td><td style="text-align: right;">N/A</td></tr> <tr><td>max Lower neck Fz</td><td style="text-align: right;">N/A</td></tr> <tr><td>max Lower neck My</td><td style="text-align: right;">N/A</td></tr> </table>	THRC	N/A	NICmax	21,9	WAD2+ risk	77,5%	max Aldman Pressure	114,4kPa at C5	max Head X acceleration	13,8g	max T1 X acceleration	21,2g	max Upper neck Fx	N/A	max Upper neck Fz	N/A	max Upper neck My	N/A	max Lower neck Fx	N/A	max Lower neck Fz	N/A	max Lower neck My	N/A
THRC		N/A																							
NICmax		21,9																							
WAD2+ risk	77,5%																								
max Aldman Pressure	114,4kPa at C5																								
max Head X acceleration	13,8g																								
max T1 X acceleration	21,2g																								
max Upper neck Fx	N/A																								
max Upper neck Fz	N/A																								
max Upper neck My	N/A																								
max Lower neck Fx	N/A																								
max Lower neck Fz	N/A																								
max Lower neck My	N/A																								
 Time : 87.00 ms <i>Max T1 rear displacement</i>																									
 Time : 128.00 ms <i>End of head contact</i>																									


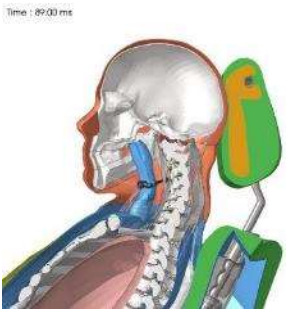
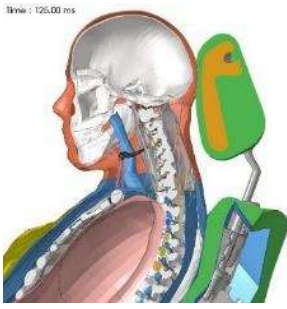


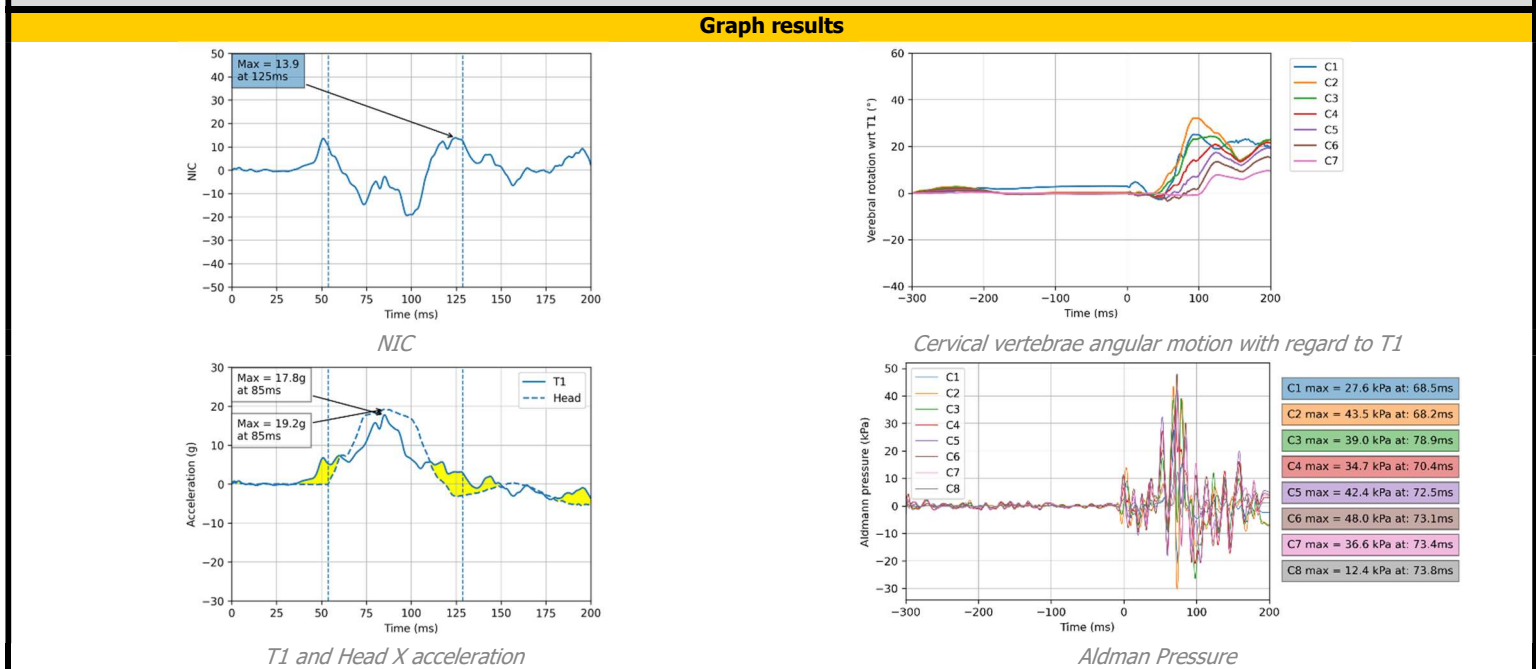
Simulation case		V3_50F_Reclined35_Head-Leaning		
General description				
Seat used	Variant 3	  <p>Time : 0.00 ms</p> <p><i>Initial vertebrae position</i> <i>Seat isometric view</i></p>		
Seat position	Seatback			35°
	Tracks			Middle
	Height			Middle
	Swivel			0°
	Shoulder			0°
Dummy used	Lowest / Backset = 0mm			
Crash pulse	VIVA+ 50 th Female			
Speed	IIWPG Medium Whiplash Pulse			
Load case	15,9 km/h			
	Low speed rear crash			



Head kinematics results			Numerical results	
 <p>Time : 74.00 ms</p> <p><i>Max head rear displacement</i></p>	 <p>Time : 80.00 ms</p> <p><i>Max NIC</i></p>	 <p>Time : 85.00 ms</p> <p><i>Max T1 rear displacement</i></p>	THRC N/A NICmax 22,3 WAD2+ risk 79,2% max Aldman Pressure 83kPa at C6 max Head X acceleration 14,9g max T1 X acceleration 21g max Upper neck Fx N/A max Upper neck Fz N/A max Upper neck My N/A max Lower neck Fx N/A max Lower neck Fz N/A max Lower neck My N/A	

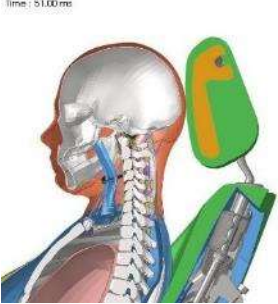

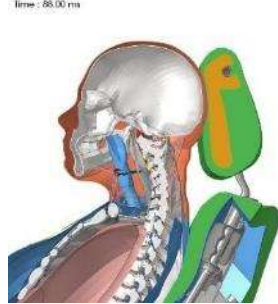


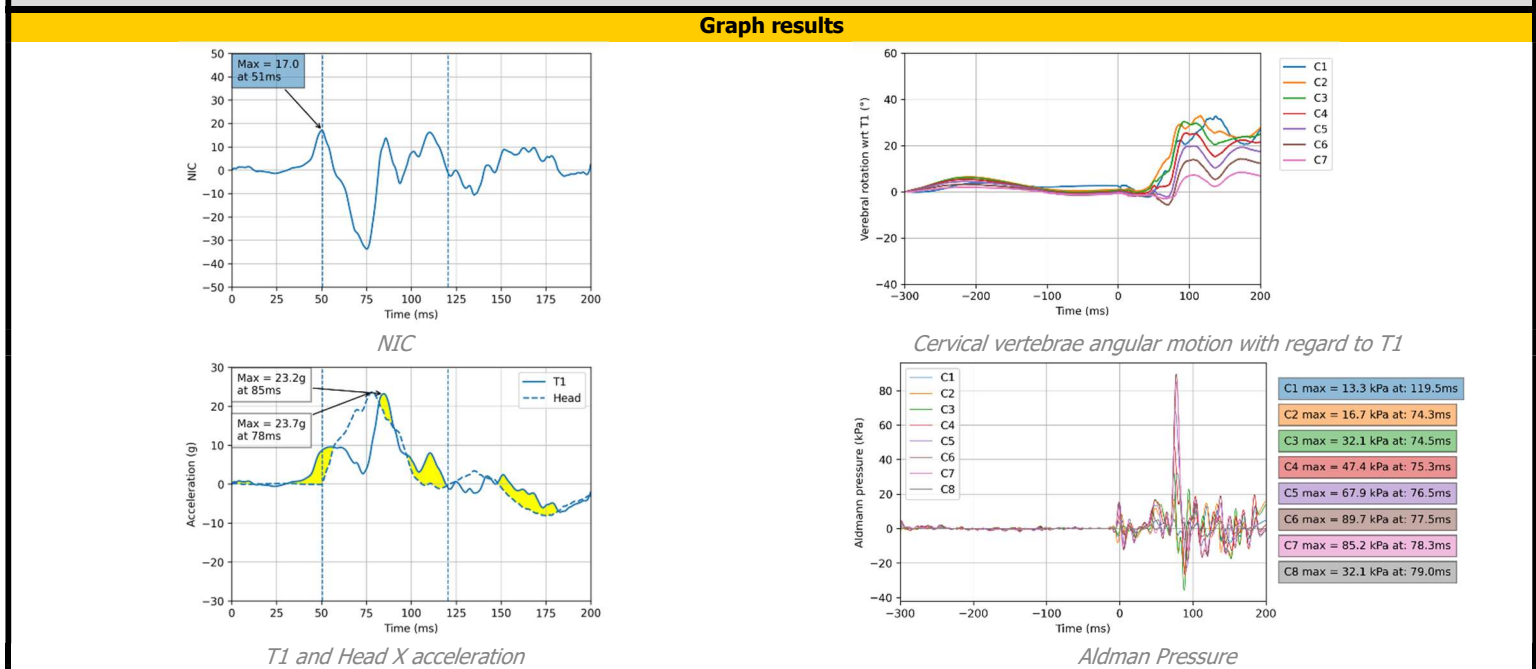
Simulation case		V3_50M_Reclined35_Head-Upright	
General description			
Seat used	Variant 3		 Time : 0.00 ms
Seat position	Seatback	35°	
	Tracks	Middle	 Seat isometric view
	Height	Middle	
	Swivel	0°	
	Shoulder	0°	
	Headrest	Middle / Backset = 43mm	
Dummy used	VIVA+ 50 th Male		
Crash pulse	IIWPG Medium Whiplash Pulse		
Speed	15,9 km/h		
Load case	Low speed rear crash		

Head kinematics results			Numerical results	
 Time : 64.00 ms <i>Head to head-restraint contact</i>	 Time : 89.00 ms <i>Max head rear displacement</i>	 Time : 125.00 ms <i>NICmax</i>	THRC NICmax WAD2+ risk max Aldman Pressure max Head X acceleration max T1 X acceleration max Upper neck Fx max Upper neck Fz max Upper neck My max Lower neck Fx max Lower neck Fz max Lower neck My	53,7ms 13,9 39,5% 48kPa at C6 19,2g 17,8g N/A N/A N/A N/A N/A N/A

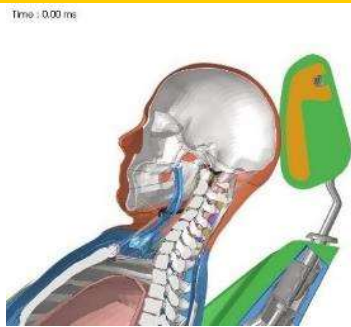




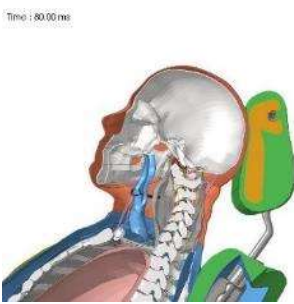
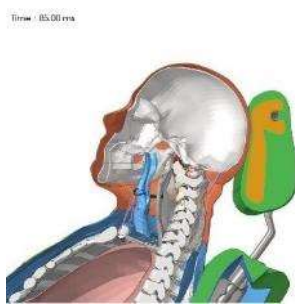
Simulation case		V3_50F_Reclined35_Head-Upright	
General description			
Seat used	Variant 3		 Time : 0.00 ms Initial vertebrae position
Seat position	Seatback	35°	
	Tracks	Middle	
	Height	Middle	
	Swivel	0°	
	Shoulder	0°	
	Headrest	Lowest / Backset = 37mm	
Dummy used	VIVA+ 50 th Female		 Seat isometric view
Crash pulse	IIWPG Medium Whiplash Pulse		
Speed	15,9 km/h		
Load case	Low speed rear crash		

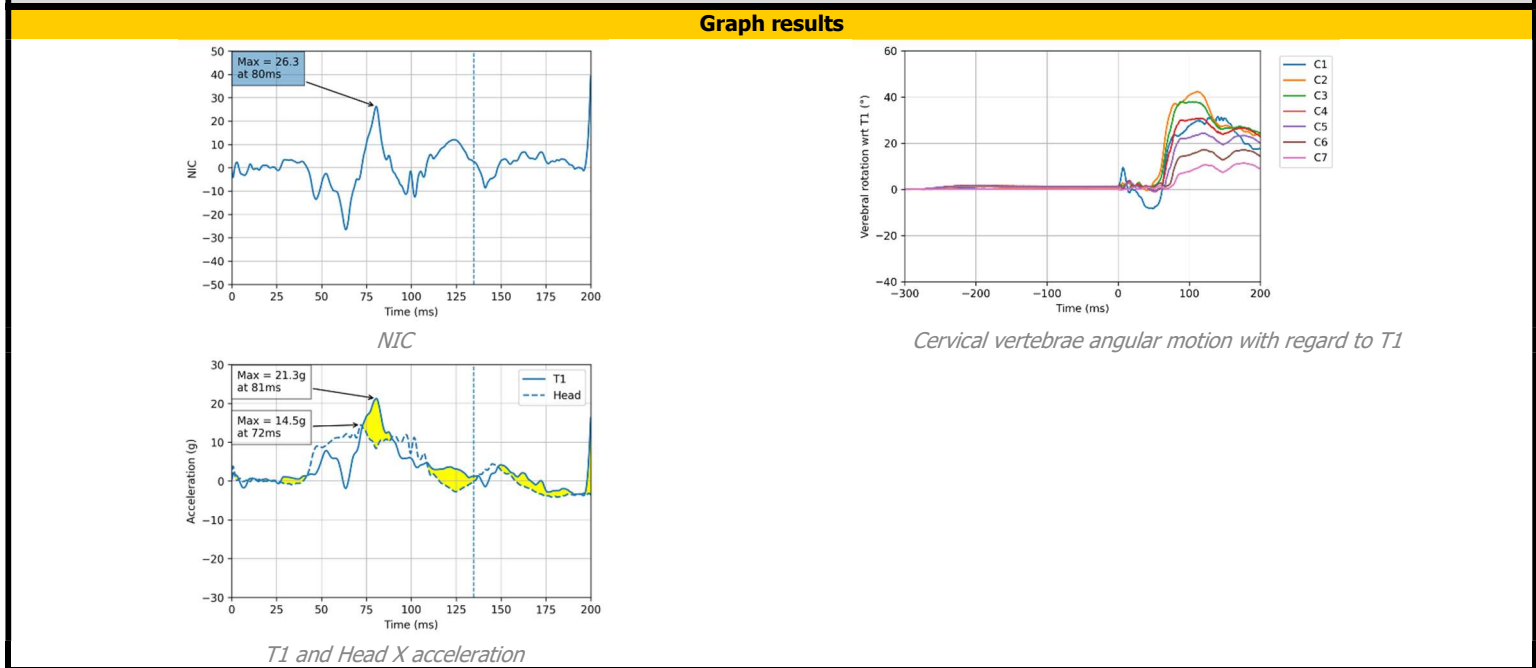
Head kinematics results			Numerical results	
 Time : 51.00 ms Head to head-restraint contact	 Time : 80.00 ms Max head rear displacement	 Time : 88.00 ms Max T1 rear displacement	THRC NICmax WAD2+ risk max Aldman Pressure max Head X acceleration max T1 X acceleration max Upper neck Fx max Upper neck Fz max Upper neck My max Lower neck Fx max Lower neck Fz max Lower neck My	50,5ms 17 55,5% 89,7kPa at C6 23,7g 23,2g N/A N/A N/A N/A N/A N/A



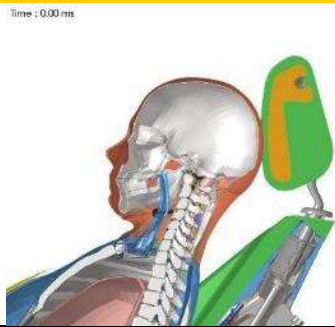

Simulation case	V3_50M_Reclined45_Head-Leaning
------------------------	---------------------------------------

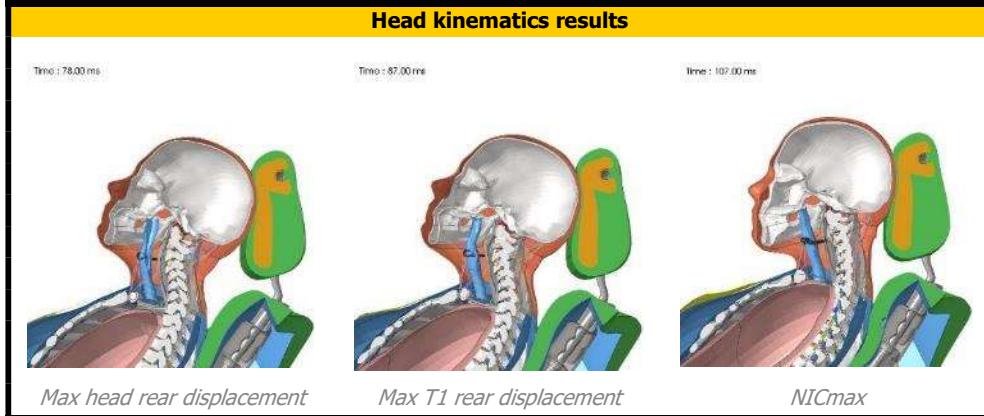
General description		
Seat used	Variant 3	 <i>Initial vertebrae position</i>
Seat position	Seatback 45° Tracks Middle Height Middle Swivel 0° Shoulder 1° Headrest Middle / Backset = 0mm	
Dummy used	VIVA+ 50 th Male	 <i>Seat isometric view</i>
Crash pulse	IIWPG Medium Whiplash Pulse	
Speed	15,9 km/h	
Load case	Low speed rear crash	

Head kinematics results	Numerical results
 <i>S-shape spine</i>	THRC N/A
 <i>NICmax</i>	NICmax 26,3
 <i>Max head rear displacement</i>	WAD2+ risk 89,7%
	max Aldman Pressure
	max Head X acceleration 14,5g
	max T1 X acceleration 21,3g
	max Upper neck Fx N/A
	max Upper neck Fz N/A
	max Upper neck My N/A
	max Lower neck Fx N/A
	max Lower neck Fz N/A
	max Lower neck My N/A



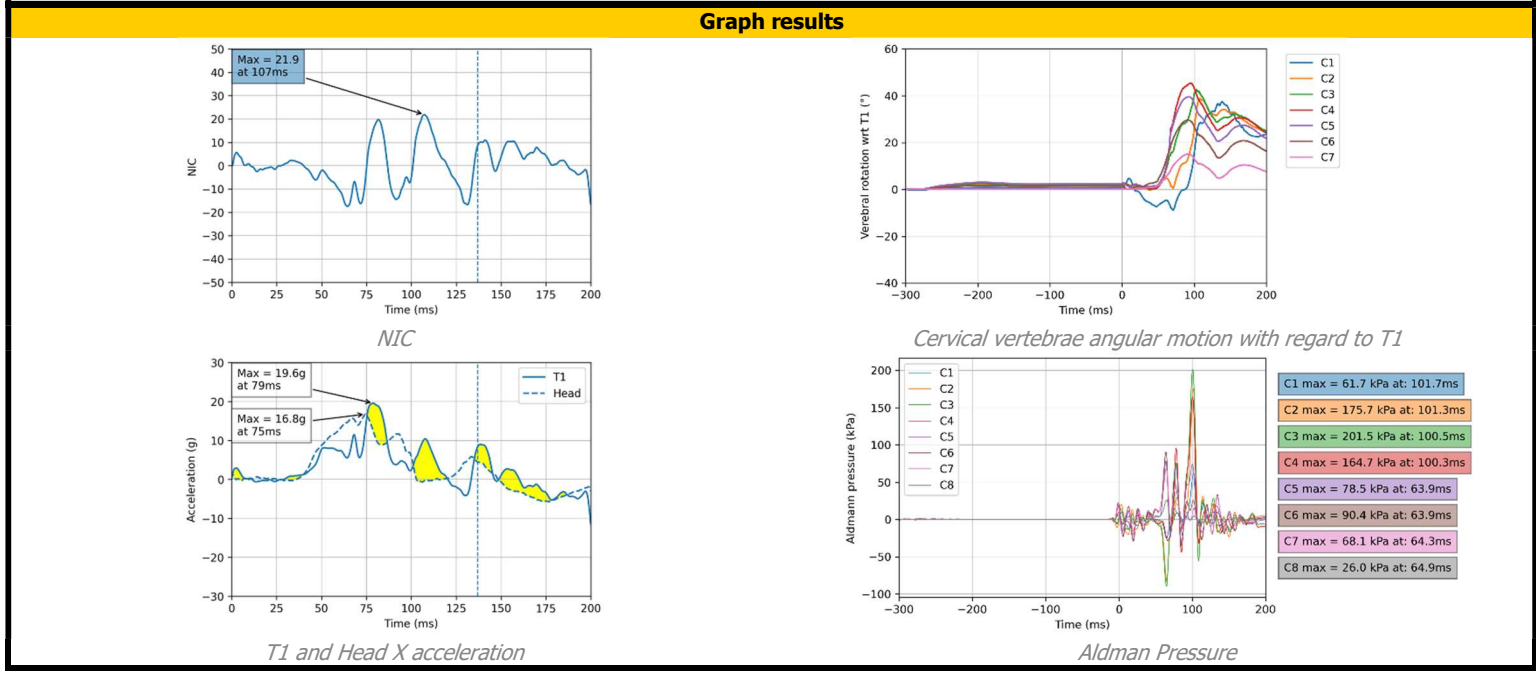
Simulation case	V3_50F_Reclined45_Head-Leaning
-----------------	---------------------------------------

General description		
Seat used	Variant 3	 <i>Initial vertebrae position</i>
Seat position	Seatback 45° Tracks Middle Height Middle Swivel 0° Shoulder 3° Headrest Lowest / Backset = 0mm	
Dummy used	VIVA+ 50 th Female	 <i>Seat isometric view</i>
Crash pulse	IIWPG Medium Whiplash Pulse	
Speed	15,9 km/h	
Load case	Low speed rear crash	



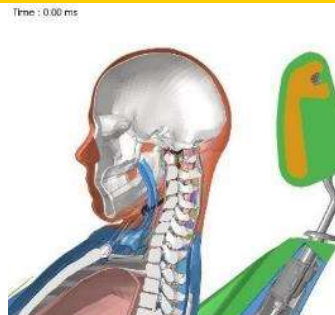
Numerical results

THRC	N/A
NICmax	21,9
WAD2+ risk	77,8%
max Aldman Pressure	201,5kPa at C3
max Head X acceleration	16,8g
max T1 X acceleration	19,6g
max Upper neck Fx	N/A
max Upper neck Fz	N/A
max Upper neck My	N/A
max Lower neck Fx	N/A
max Lower neck Fz	N/A
max Lower neck My	N/A




Simulation case	V3_50M_Reclined45_Head-Upright
-----------------	---------------------------------------

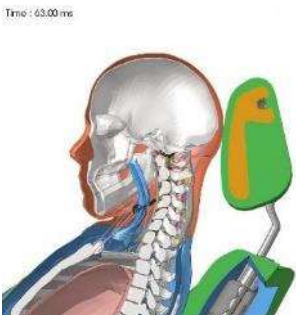
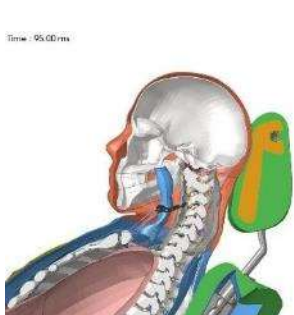
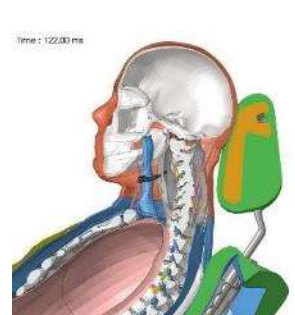
General description	
Seat used	Variant 3
Seat position	Seatback 45°
	Tracks Middle
	Height Middle
	Swivel 0°
	Shoulder 1°
	Headrest Middle / Backset = 63mm
Dummy used	VIVA+ 50 th Male
Crash pulse	IIWPG Medium Whiplash Pulse
Speed	15,9 km/h
Load case	Low speed rear crash

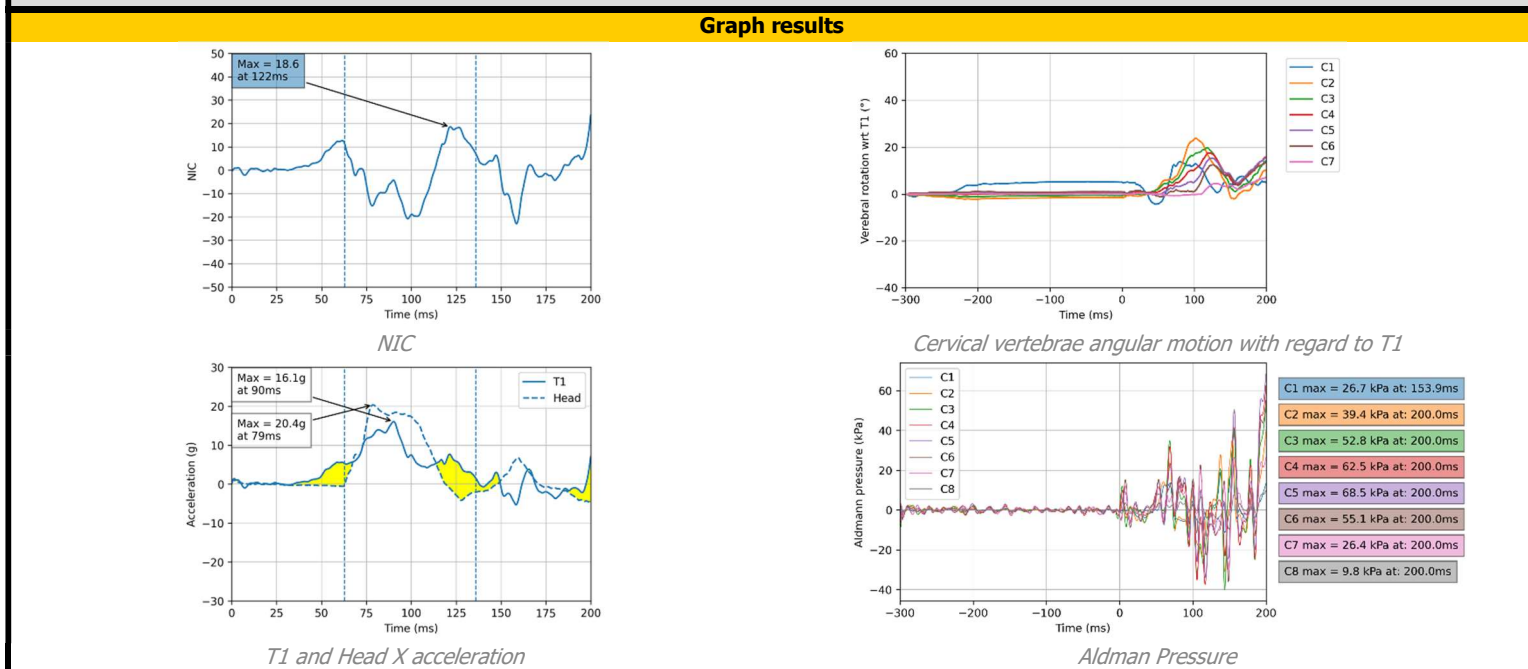


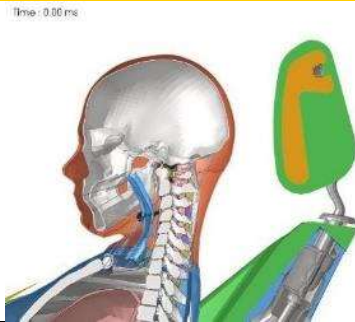

Initial vertebrae position

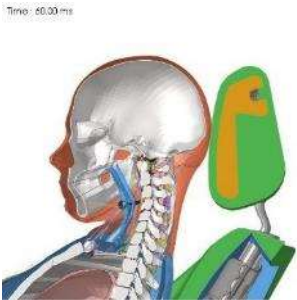
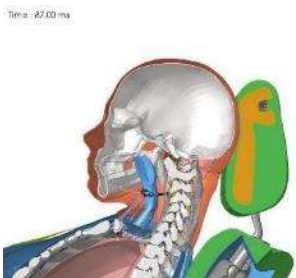
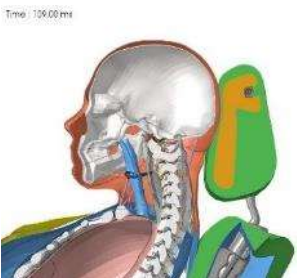


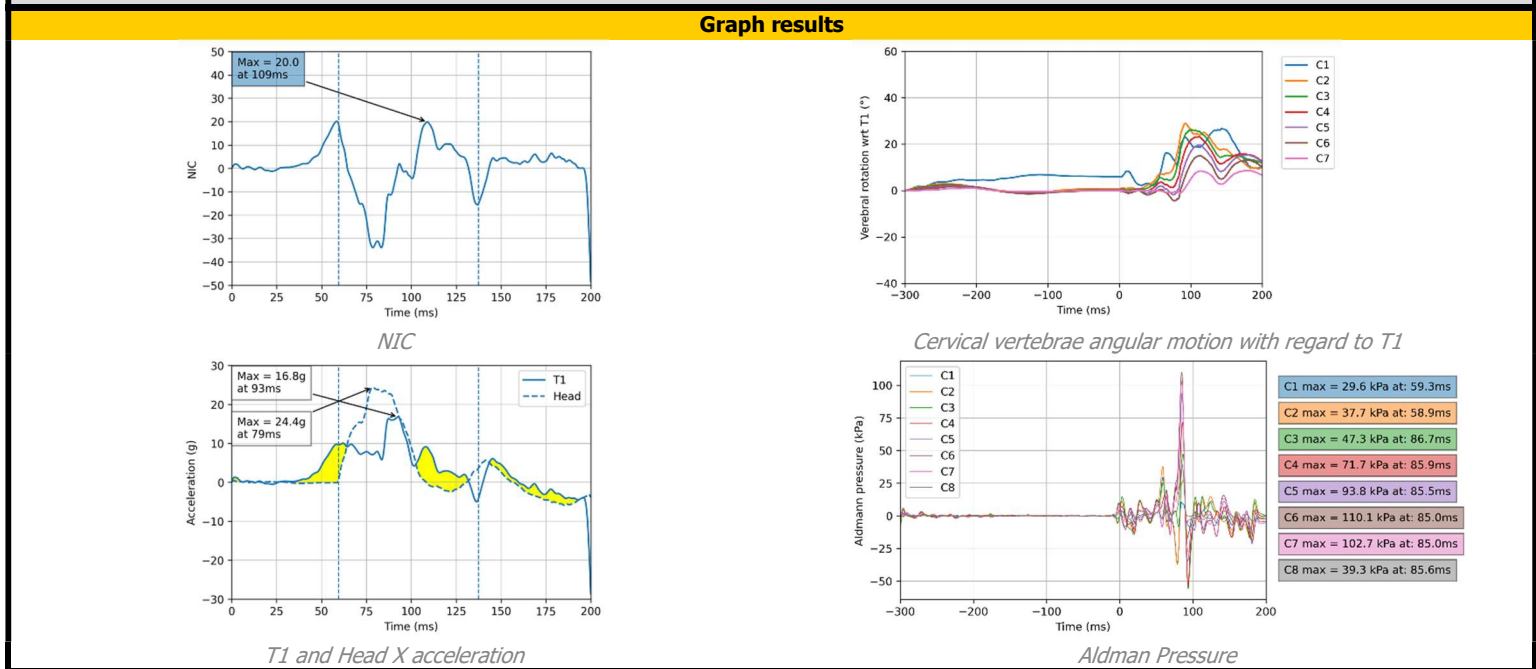
Seat isometric view

Head kinematics results	Numerical results																								
<div style="display: flex; justify-content: space-around;"> <div style="text-align: center;">  <p>Head to head-restraint contact</p> </div> <div style="text-align: center;">  <p>Max head rear displacement</p> </div> <div style="text-align: center;">  <p>NICmax</p> </div> </div>	<table style="width:100%; border-collapse: collapse;"> <tr><td>THRC</td><td style="text-align: right;">62,8ms</td></tr> <tr><td>NICmax</td><td style="text-align: right;">18,6</td></tr> <tr><td>WAD2+ risk</td><td style="text-align: right;">63,4%</td></tr> <tr><td>max Aldman Pressure</td><td style="text-align: right;">68,5kPa at C5</td></tr> <tr><td>max Head X acceleration</td><td style="text-align: right;">20,4g</td></tr> <tr><td>max T1 X acceleration</td><td style="text-align: right;">16,1g</td></tr> <tr><td>max Upper neck Fx</td><td style="text-align: right;">N/A</td></tr> <tr><td>max Upper neck Fz</td><td style="text-align: right;">N/A</td></tr> <tr><td>max Upper neck My</td><td style="text-align: right;">N/A</td></tr> <tr><td>max Lower neck Fx</td><td style="text-align: right;">N/A</td></tr> <tr><td>max Lower neck Fz</td><td style="text-align: right;">N/A</td></tr> <tr><td>max Lower neck My</td><td style="text-align: right;">N/A</td></tr> </table>	THRC	62,8ms	NICmax	18,6	WAD2+ risk	63,4%	max Aldman Pressure	68,5kPa at C5	max Head X acceleration	20,4g	max T1 X acceleration	16,1g	max Upper neck Fx	N/A	max Upper neck Fz	N/A	max Upper neck My	N/A	max Lower neck Fx	N/A	max Lower neck Fz	N/A	max Lower neck My	N/A
THRC	62,8ms																								
NICmax	18,6																								
WAD2+ risk	63,4%																								
max Aldman Pressure	68,5kPa at C5																								
max Head X acceleration	20,4g																								
max T1 X acceleration	16,1g																								
max Upper neck Fx	N/A																								
max Upper neck Fz	N/A																								
max Upper neck My	N/A																								
max Lower neck Fx	N/A																								
max Lower neck Fz	N/A																								
max Lower neck My	N/A																								

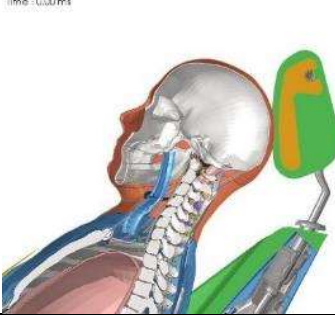



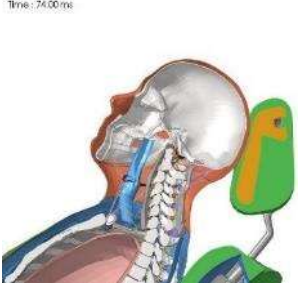
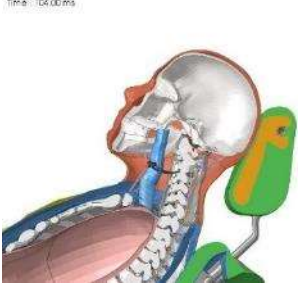
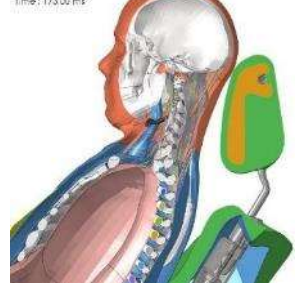
Simulation case		V3_50F_Reclined45_Head-Upright		
General description				
Seat used	Variant 3	 		
Seat position	Seatback			45°
	Tracks			Middle
	Height			Middle
	Swivel			0°
	Shoulder			3°
Headrest	Lowest / Backset = 47mm			
Dummy used	VIVA+ 50 th Female			
Crash pulse	IIWPG Medium Whiplash Pulse			
Speed	15,9 km/h			
Load case	Low speed rear crash			

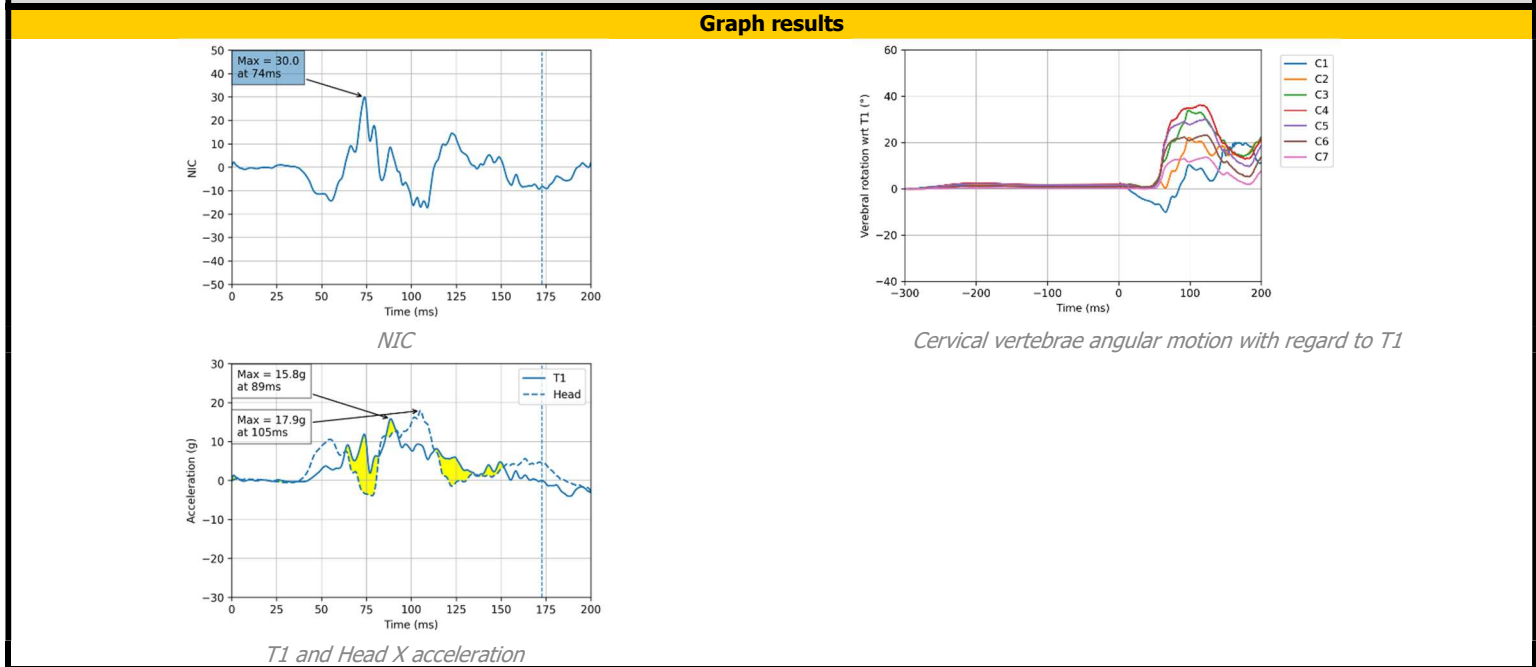
Head kinematics results			Numerical results	
 <p>Time: 60.00 ms</p> <p>Head to head-restraint contact</p>	 <p>Time: 87.00 ms</p> <p>Max head rear displacement</p>	 <p>Time: 109.00 ms</p> <p>NICmax</p>	THRC NICmax WAD2+ risk max Aldman Pressure max Head X acceleration max T1 X acceleration max Upper neck Fx max Upper neck Fz max Upper neck My max Lower neck Fx max Lower neck Fz max Lower neck My	59,5ms 20 69,8% 110,1kPa at C6 24,4g 16,8g N/A N/A N/A N/A N/A N/A

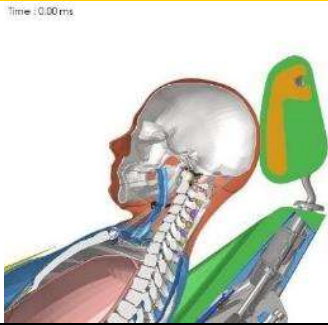



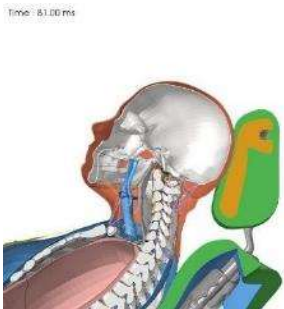
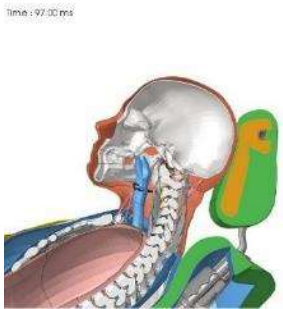
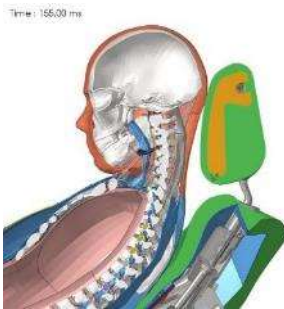
Simulation case	V3_50M_Reclined55_Head-Leaning
-----------------	---------------------------------------

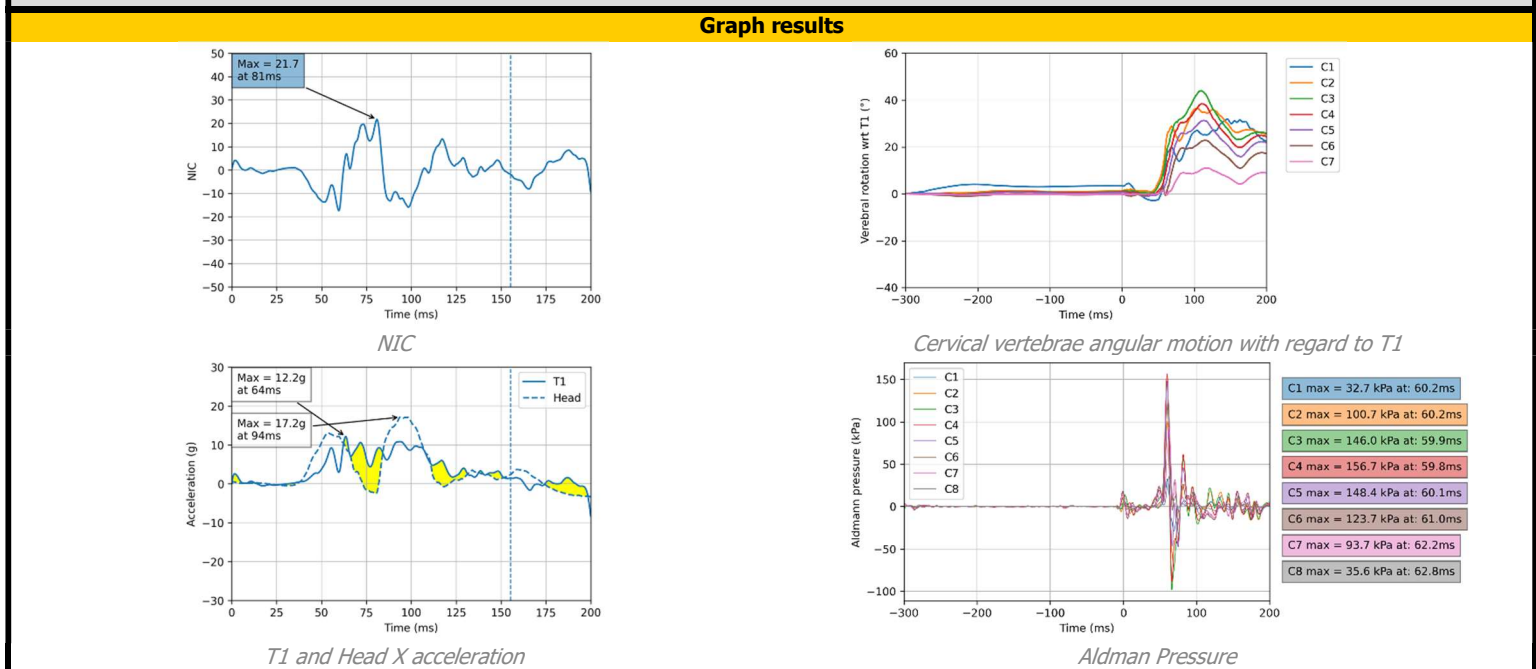
General description		
Seat used	Variant 3	 <i>Initial vertebrae position</i>
Seat position	Seatback 55° Tracks Middle Height Middle Swivel 0° Shoulder 10° Headrest Middle / Backset = 0mm	
Dummy used	VIVA+ 50 th Male	 <i>Seat isometric view</i>
Crash pulse	IIWPG Medium Whiplash Pulse	
Speed	15,9 km/h	
Load case	Low speed rear crash	

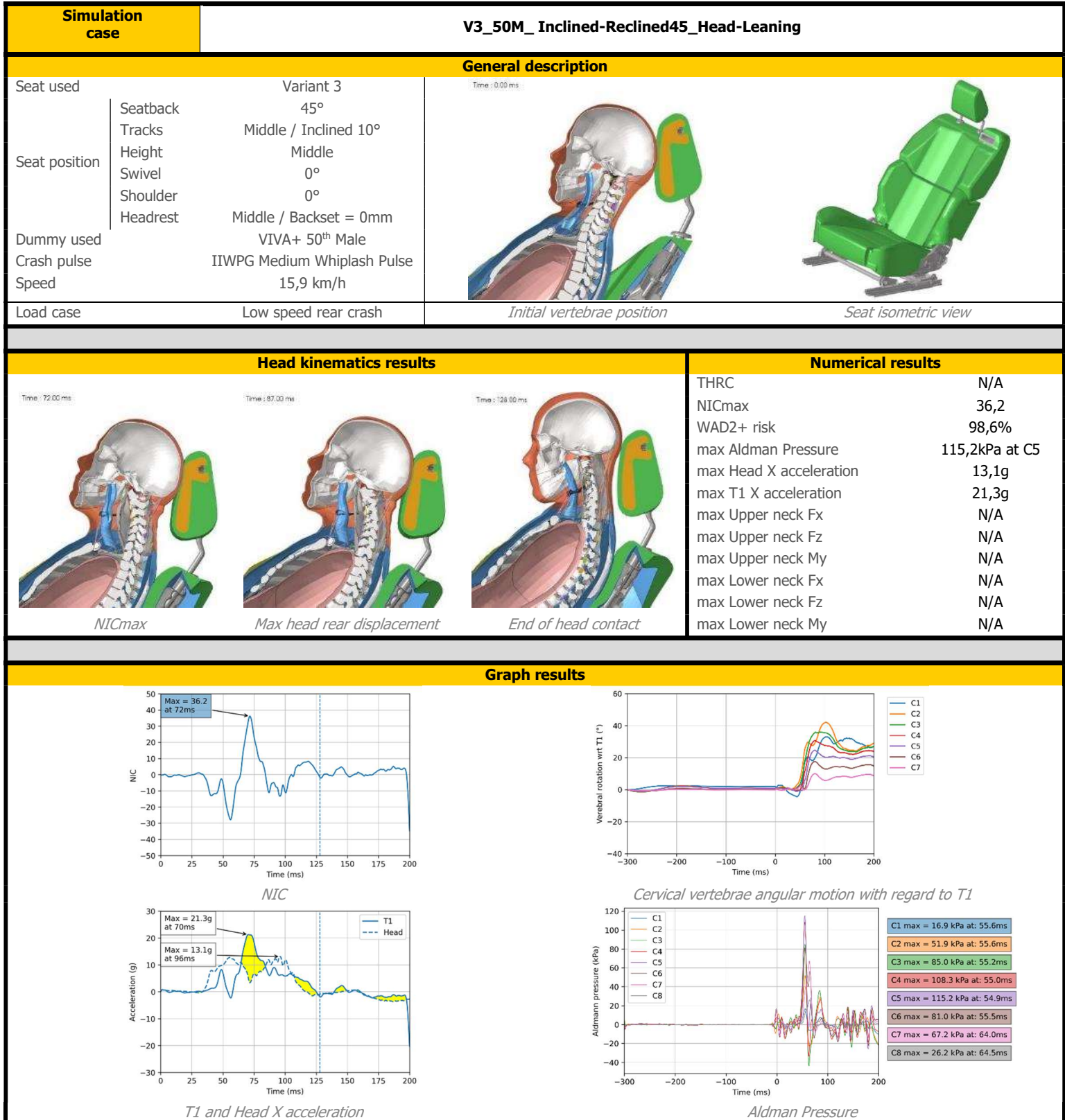
Head kinematics results	Numerical results																								
 <i>NICmax</i>	<table border="0" style="width:100%;"> <tr><td>THRC</td><td style="text-align: right;">N/A</td></tr> <tr><td>NICmax</td><td style="text-align: right;">30</td></tr> <tr><td>WAD2+ risk</td><td style="text-align: right;">95%</td></tr> <tr><td>max Aldman Pressure</td><td></td></tr> <tr><td>max Head X acceleration</td><td style="text-align: right;">17,9g</td></tr> <tr><td>max T1 X acceleration</td><td style="text-align: right;">15,8g</td></tr> <tr><td>max Upper neck Fx</td><td style="text-align: right;">N/A</td></tr> <tr><td>max Upper neck Fz</td><td style="text-align: right;">N/A</td></tr> <tr><td>max Upper neck My</td><td style="text-align: right;">N/A</td></tr> <tr><td>max Lower neck Fx</td><td style="text-align: right;">N/A</td></tr> <tr><td>max Lower neck Fz</td><td style="text-align: right;">N/A</td></tr> <tr><td>max Lower neck My</td><td style="text-align: right;">N/A</td></tr> </table>	THRC	N/A	NICmax	30	WAD2+ risk	95%	max Aldman Pressure		max Head X acceleration	17,9g	max T1 X acceleration	15,8g	max Upper neck Fx	N/A	max Upper neck Fz	N/A	max Upper neck My	N/A	max Lower neck Fx	N/A	max Lower neck Fz	N/A	max Lower neck My	N/A
THRC		N/A																							
NICmax		30																							
WAD2+ risk	95%																								
max Aldman Pressure																									
max Head X acceleration	17,9g																								
max T1 X acceleration	15,8g																								
max Upper neck Fx	N/A																								
max Upper neck Fz	N/A																								
max Upper neck My	N/A																								
max Lower neck Fx	N/A																								
max Lower neck Fz	N/A																								
max Lower neck My	N/A																								
 <i>Max head rear displacement</i>																									
 <i>End of head contact</i>																									



Simulation case		V3_50F_Reclined55_Head-Leaning	
General description			
Seat used	Variant 3	 Time: 0.00ms	
Seat position	Seatback 55° Tracks Middle Height Middle Swivel 0° Shoulder 10° Headrest Lowest / Backset = 0mm		
Dummy used	VIVA+ 50 th Female	 Seat isometric view	
Crash pulse	IIWPG Medium Whiplash Pulse		
Speed	15,9 km/h		
Load case	Low speed rear crash		

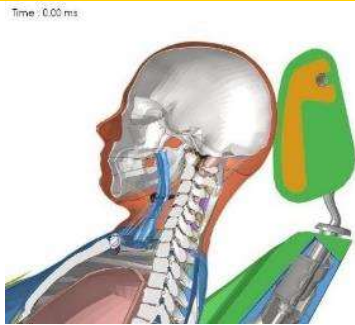
Head kinematics results		Numerical results																									
 Time: 81.00ms <i>Max NIC</i>	 Time: 97.00ms <i>Max head rear displacement</i>	 Time: 166.00ms <i>End of head contact</i>	<table border="0"> <tr><td>THRC</td><td>N/A</td></tr> <tr><td>NICmax</td><td>21,7</td></tr> <tr><td>WAD2+ risk</td><td>76,9%</td></tr> <tr><td>max Aldman Pressure</td><td>156,7kPa at C4</td></tr> <tr><td>max Head X acceleration</td><td>17,2g</td></tr> <tr><td>max T1 X acceleration</td><td>12,2g</td></tr> <tr><td>max Upper neck Fx</td><td>N/A</td></tr> <tr><td>max Upper neck Fz</td><td>N/A</td></tr> <tr><td>max Upper neck My</td><td>N/A</td></tr> <tr><td>max Lower neck Fx</td><td>N/A</td></tr> <tr><td>max Lower neck Fz</td><td>N/A</td></tr> <tr><td>max Lower neck My</td><td>N/A</td></tr> </table>	THRC	N/A	NICmax	21,7	WAD2+ risk	76,9%	max Aldman Pressure	156,7kPa at C4	max Head X acceleration	17,2g	max T1 X acceleration	12,2g	max Upper neck Fx	N/A	max Upper neck Fz	N/A	max Upper neck My	N/A	max Lower neck Fx	N/A	max Lower neck Fz	N/A	max Lower neck My	N/A
THRC	N/A																										
NICmax	21,7																										
WAD2+ risk	76,9%																										
max Aldman Pressure	156,7kPa at C4																										
max Head X acceleration	17,2g																										
max T1 X acceleration	12,2g																										
max Upper neck Fx	N/A																										
max Upper neck Fz	N/A																										
max Upper neck My	N/A																										
max Lower neck Fx	N/A																										
max Lower neck Fz	N/A																										
max Lower neck My	N/A																										






Simulation Case	V3_50F_Inclined-Reclined45_Head-Leaning
-----------------	--

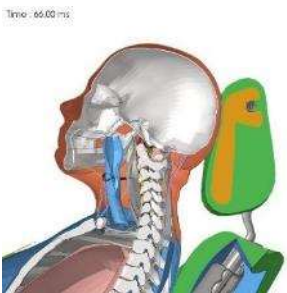
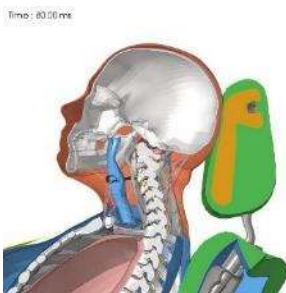
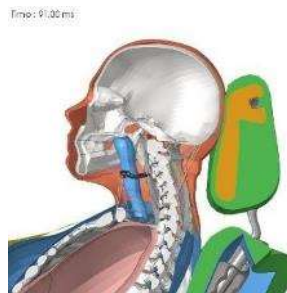
General description	
Seat used	Variant 3
Seat position	Seatback 45°
	Tracks Middle / Inclined 10°
	Height Middle
	Swivel 0°
	Shoulder 0°
	Headrest Lowest / Backset = 0mm
Dummy used	VIVA+ 50 th Female
Crash pulse	IIWPG Medium Whiplash Pulse
Speed	15,9 km/h
Load case	Low speed rear crash

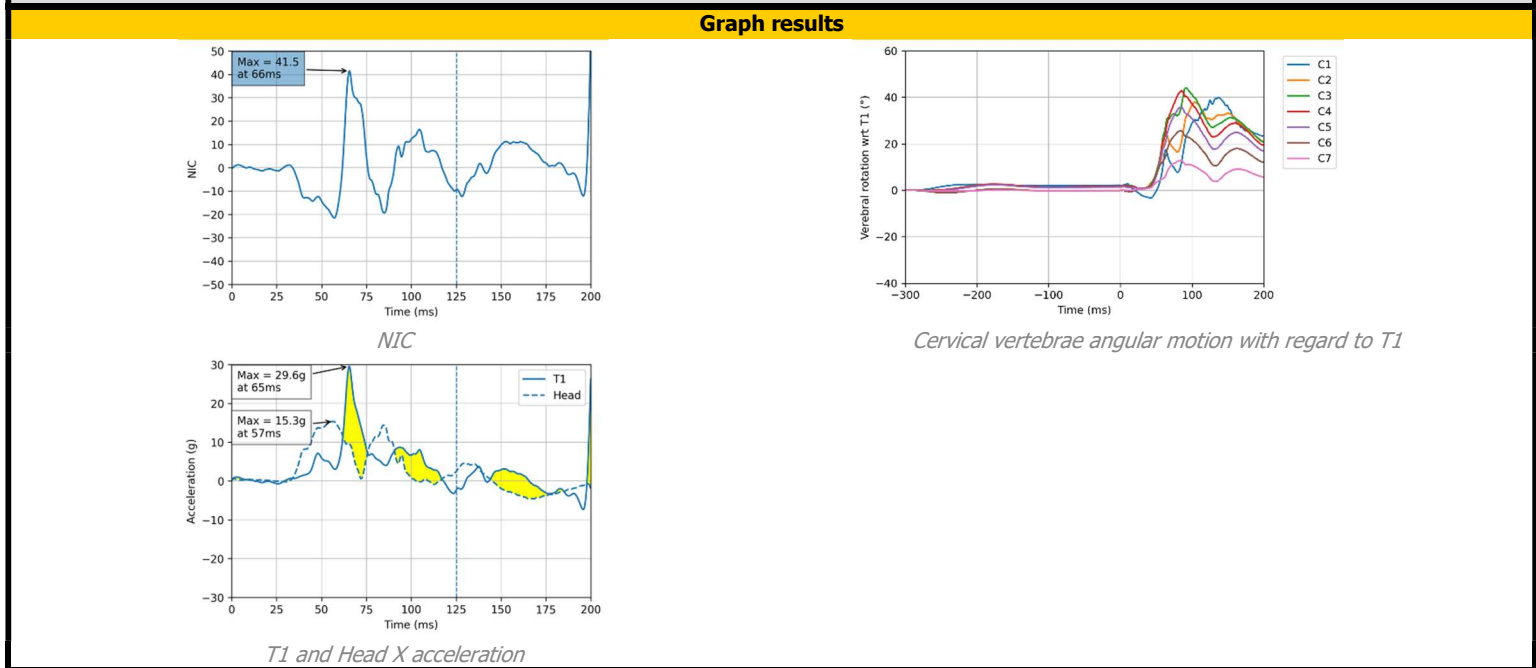


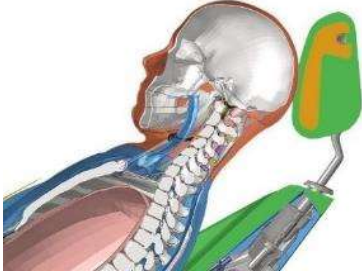

Time: 0,00 ms
Initial vertebrae position

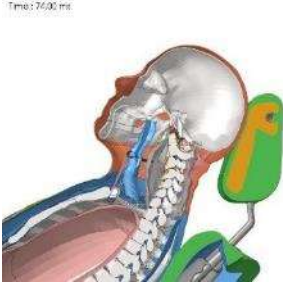
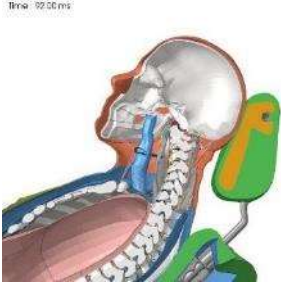
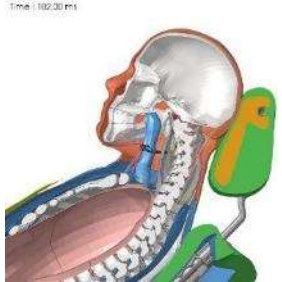


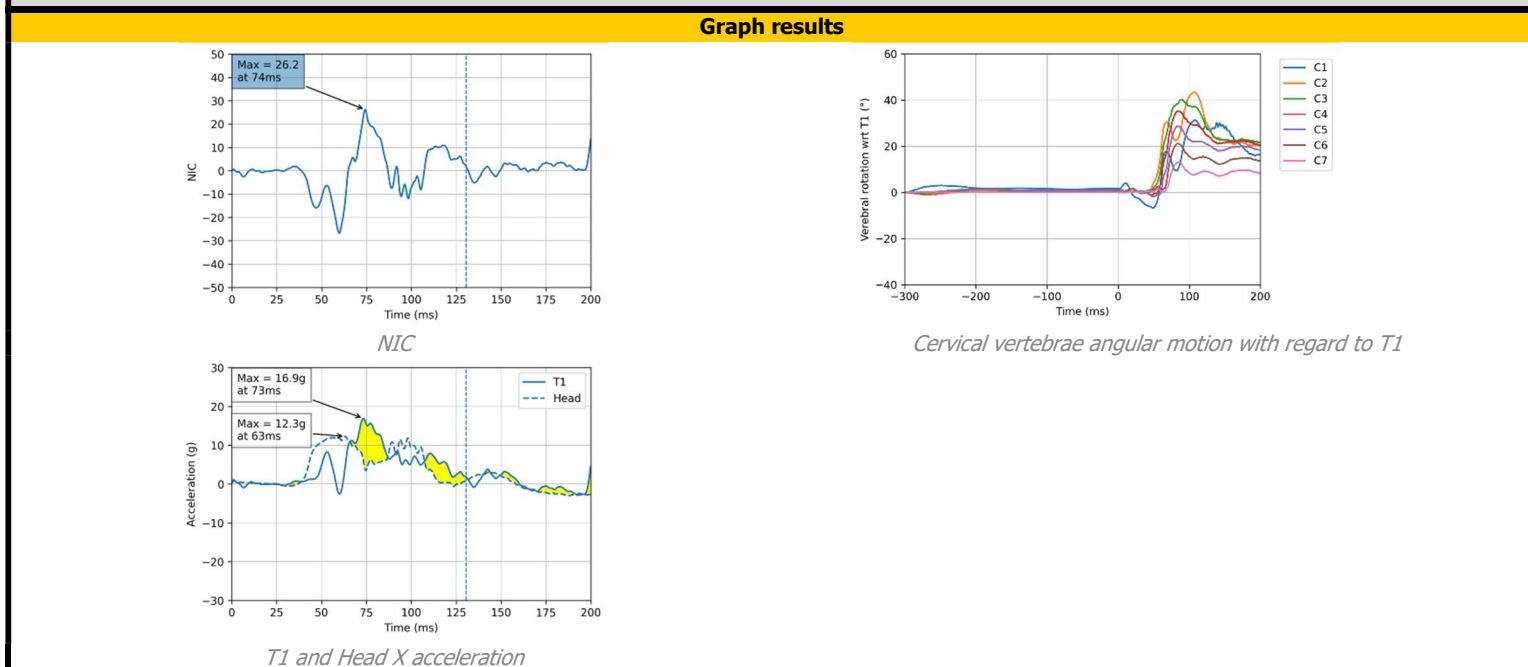
Seat isometric view

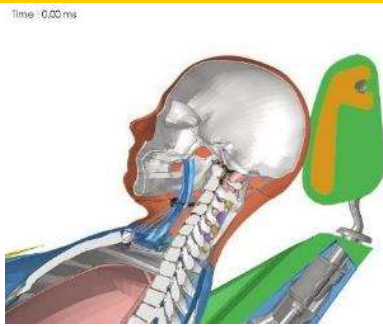

Head kinematics results	Numerical results																								
 <p>Time: 66,60 ms <i>NICmax</i></p>	<table style="width:100%; border-collapse: collapse;"> <tr><td>THRC</td><td style="text-align: right;">N/A</td></tr> <tr><td>NICmax</td><td style="text-align: right;">41,5</td></tr> <tr><td>WAD2+ risk</td><td style="text-align: right;">99,5%</td></tr> <tr><td>max Aldman Pressure</td><td></td></tr> <tr><td>max Head X acceleration</td><td style="text-align: right;">15,3g</td></tr> <tr><td>max T1 X acceleration</td><td style="text-align: right;">29,6g</td></tr> <tr><td>max Upper neck Fx</td><td style="text-align: right;">N/A</td></tr> <tr><td>max Upper neck Fz</td><td style="text-align: right;">N/A</td></tr> <tr><td>max Upper neck My</td><td style="text-align: right;">N/A</td></tr> <tr><td>max Lower neck Fx</td><td style="text-align: right;">N/A</td></tr> <tr><td>max Lower neck Fz</td><td style="text-align: right;">N/A</td></tr> <tr><td>max Lower neck My</td><td style="text-align: right;">N/A</td></tr> </table>	THRC	N/A	NICmax	41,5	WAD2+ risk	99,5%	max Aldman Pressure		max Head X acceleration	15,3g	max T1 X acceleration	29,6g	max Upper neck Fx	N/A	max Upper neck Fz	N/A	max Upper neck My	N/A	max Lower neck Fx	N/A	max Lower neck Fz	N/A	max Lower neck My	N/A
THRC		N/A																							
NICmax		41,5																							
WAD2+ risk		99,5%																							
max Aldman Pressure																									
max Head X acceleration		15,3g																							
max T1 X acceleration		29,6g																							
max Upper neck Fx		N/A																							
max Upper neck Fz		N/A																							
max Upper neck My		N/A																							
max Lower neck Fx	N/A																								
max Lower neck Fz	N/A																								
max Lower neck My	N/A																								
 <p>Time: 80,00 ms <i>Max head rear displacement</i></p>																									
 <p>Time: 91,00 ms <i>Max T1 rear displacement</i></p>																									

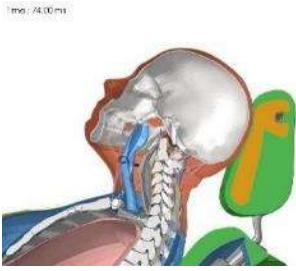




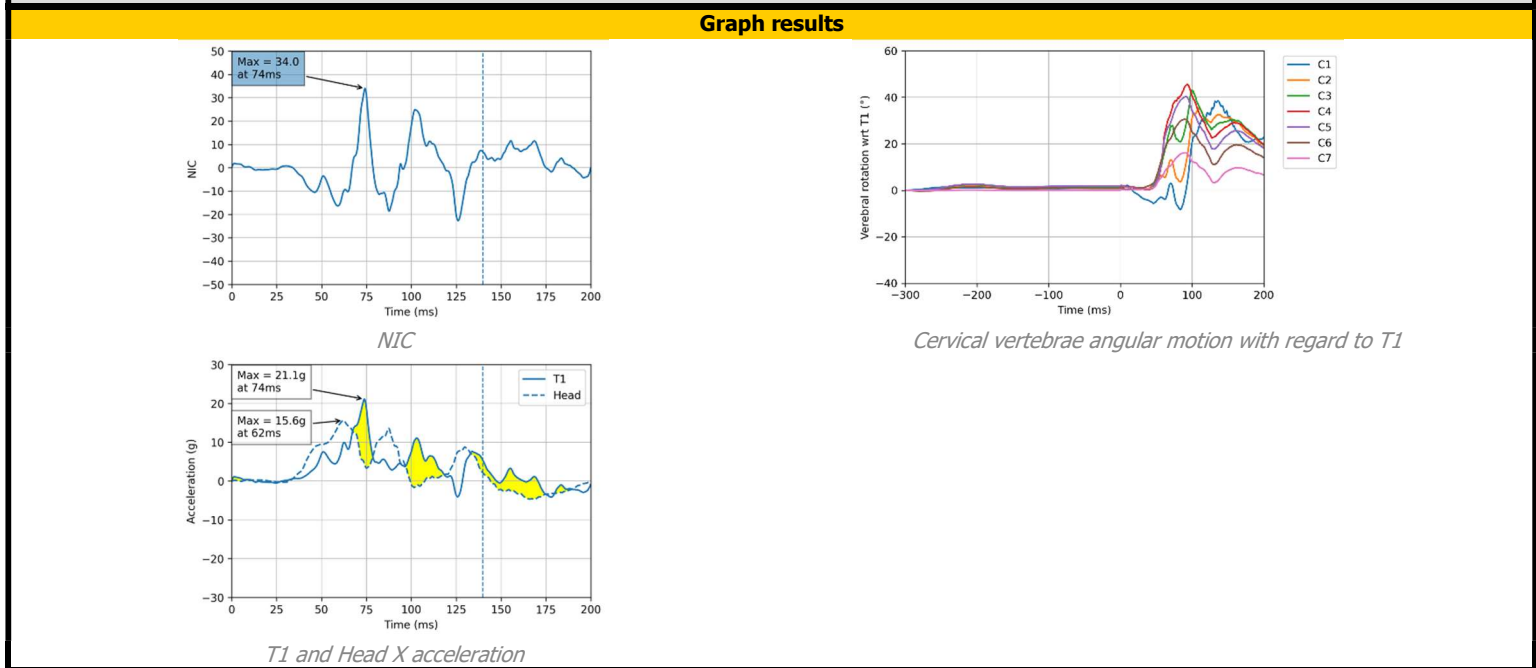
Simulation Case		V3_50M_Inclined-Reclined55_Head-Leaning	
General description			
Seat used	Variant 3		 Initial vertebrae position
Seat position	Seatback	55°	
	Tracks	Middle / Inclined 10°	 Seat isometric view
	Height	Middle	
	Swivel	0°	
	Shoulder	1°	
	Headrest	Middle / Backset = 0mm	
Dummy used	VIVA+ 50 th Male		
Crash pulse	IIWPG Medium Whiplash Pulse		
Speed	15,9 km/h		
Load case	Low speed rear crash		

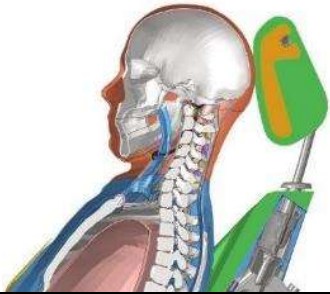

Head kinematics results			Numerical results	
 NICmax	 Max head rear displacement	 Max T1 rear displacement	THRC	N/A
			NICmax	26,2
			WAD2+ risk	89,6%
			max Aldman Pressure	
			max Head X acceleration	12,3g
			max T1 X acceleration	16,9g
			max Upper neck Fx	N/A
			max Upper neck Fz	N/A
			max Upper neck My	N/A
			max Lower neck Fx	N/A
			max Lower neck Fz	N/A
			max Lower neck My	N/A






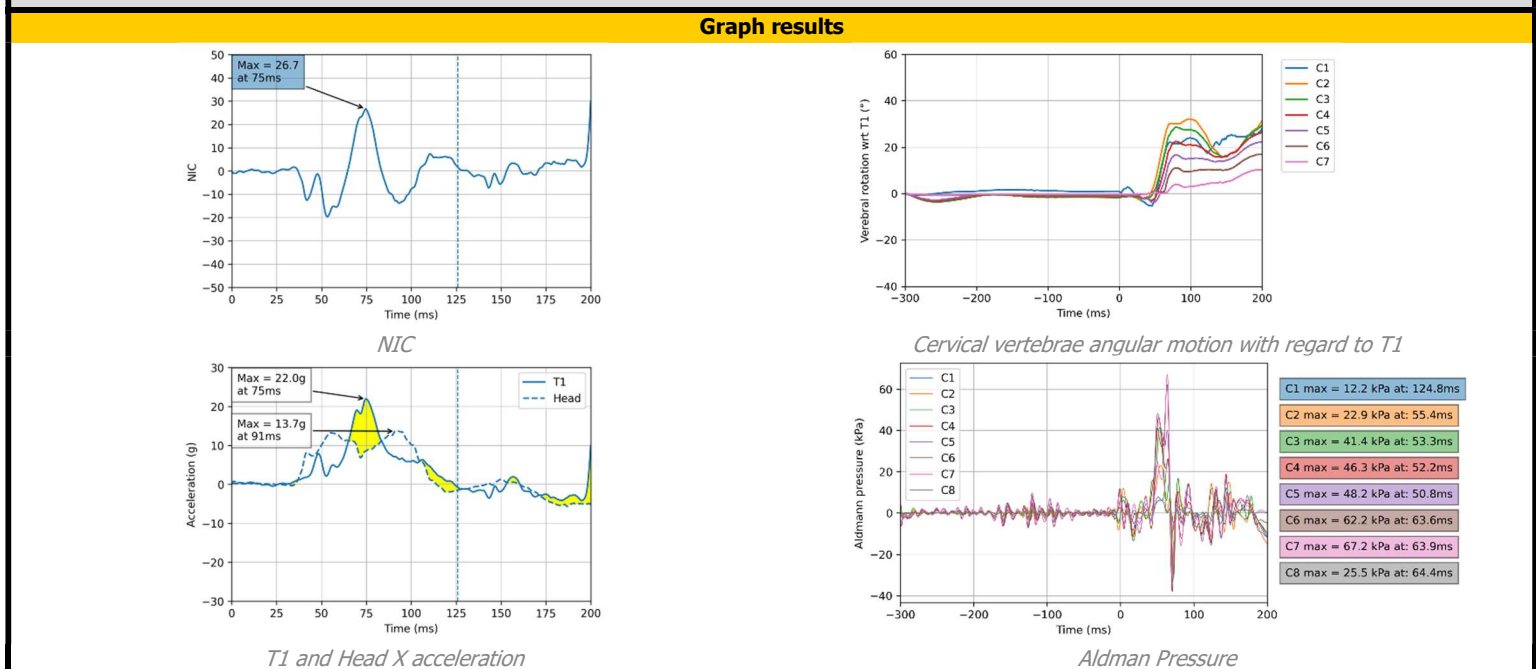
Simulation Case		V3_50F_Inclined-Reclined55_Head-Leaning	
General description			
Seat used	Variant 3		 Time: 0.00 ms
Seat position	Seatback	55°	
	Tracks	Middle / Inclined 10°	
	Height	Middle	
	Swivel	0°	
	Shoulder	3°	
	Headrest	Lowest / Backset = 0mm	
Dummy used	VIVA+ 50 th Female		 Seat isometric view
Crash pulse	IIWPG Medium Whiplash Pulse		
Speed	15,9 km/h		
Load case	Low speed rear crash		

Head kinematics results		Numerical results	
 Time: 74.00 ms NICmax	 Time: 65.00 ms Max head rear displacement	 Time: 103.00 ms Max T1 rear displacement	THRC N/A NICmax 34 WAD2+ risk 97,8% max Aldman Pressure max Head X acceleration 15,6g max T1 X acceleration 21,1g max Upper neck Fx N/A max Upper neck Fz N/A max Upper neck My N/A max Lower neck Fx N/A max Lower neck Fz N/A max Lower neck My N/A



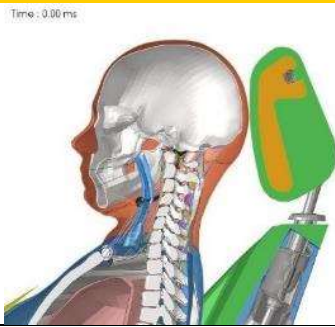
Simulation case		V3_50M_Inclined10_Head-Leaning		
General description				
Seat used	Variant 3	 Time: 0.00 ms  Seat isometric view		
Seat position	Seatback			35°
	Tracks			Middle / Inclined 10°
	Height			Middle
	Swivel			0°
	Shoulder			0°
	Headrest			Middle / Backset = 0mm
Dummy used	VIVA+ 50 th Male			
Crash pulse	IIWPG Medium Whiplash Pulse			
Speed	15,9 km/h			
Load case	Low speed rear crash			

Head kinematics results			Numerical results	
 Time: 60.00 ms <i>Spine S-shape</i>	 Time: 76.00 ms <i>NICmax</i>	 Time: 83.00 ms <i>Max head rear displacement</i>	THRC NICmax WAD2+ risk max Aldman Pressure max Head X acceleration max T1 X acceleration max Upper neck Fx max Upper neck Fz max Upper neck My max Lower neck Fx max Lower neck Fz max Lower neck My	N/A 26,7 90,5% 67,2kPa at C7 13,7g 22g N/A N/A N/A N/A N/A N/A




Simulation case	V3_50F_Inclined10_Head-Leaning
------------------------	---------------------------------------

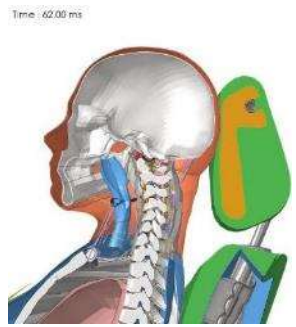

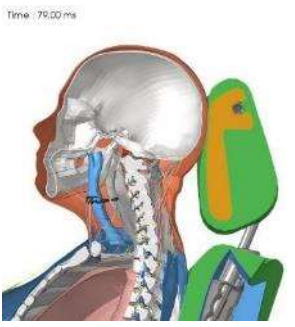
General description	
Seat used	Variant 3
Seat position	Seatback 35°
	Tracks Middle / Inclined 10°
	Height Middle
	Swivel 0°
	Shoulder 0°
	Headrest Lowest / Backset = 0mm
Dummy used	VIVA+ 50 th Female
Crash pulse	IIWPG Medium Whiplash Pulse
Speed	15,9 km/h
Load case	Low speed rear crash

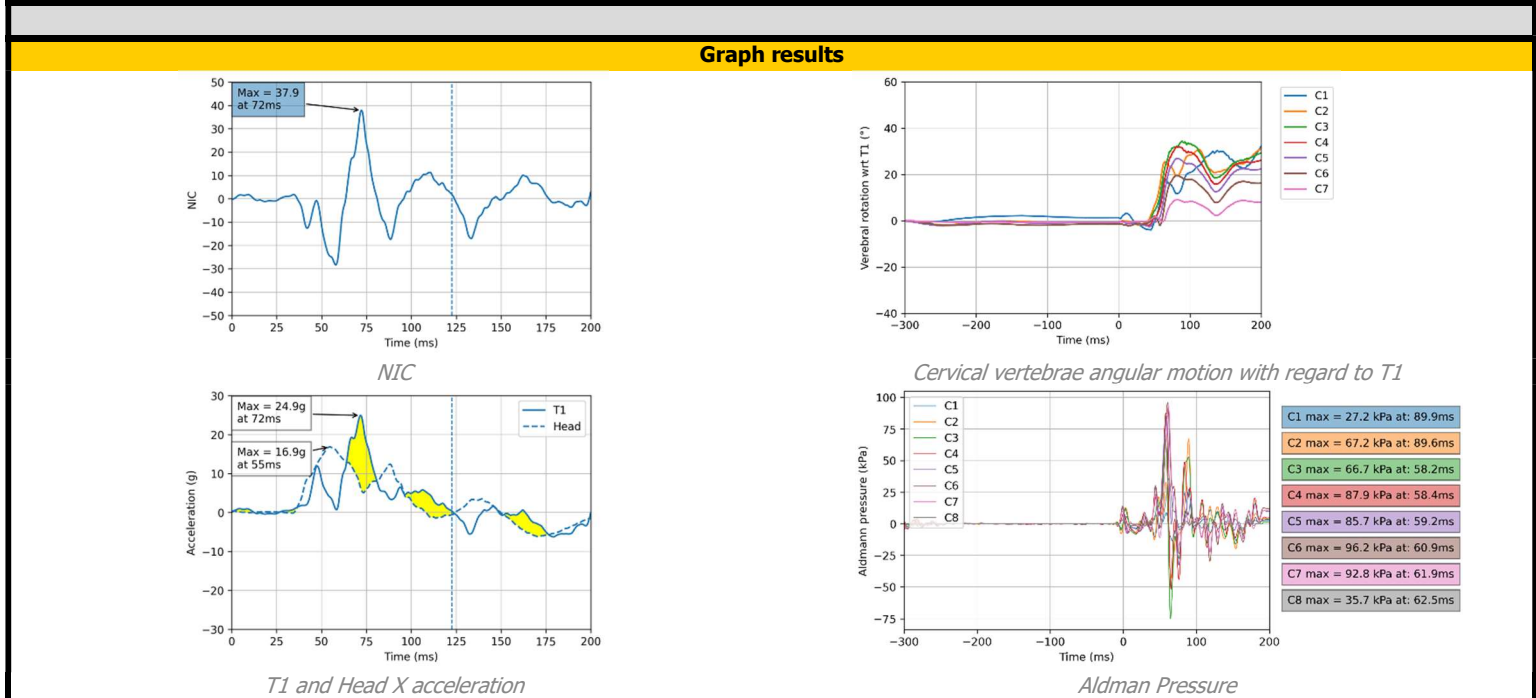


Initial vertebrae position





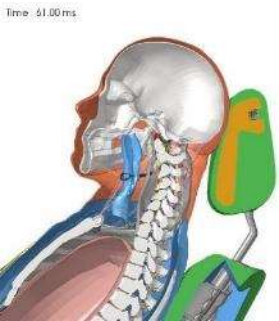
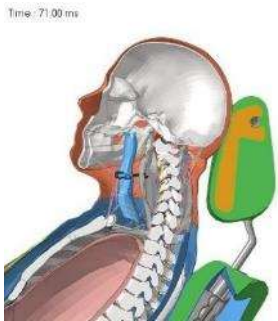
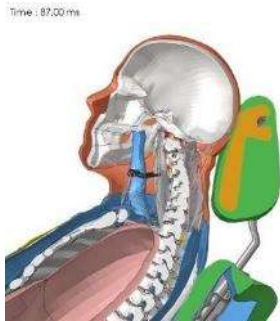
Seat isometric view

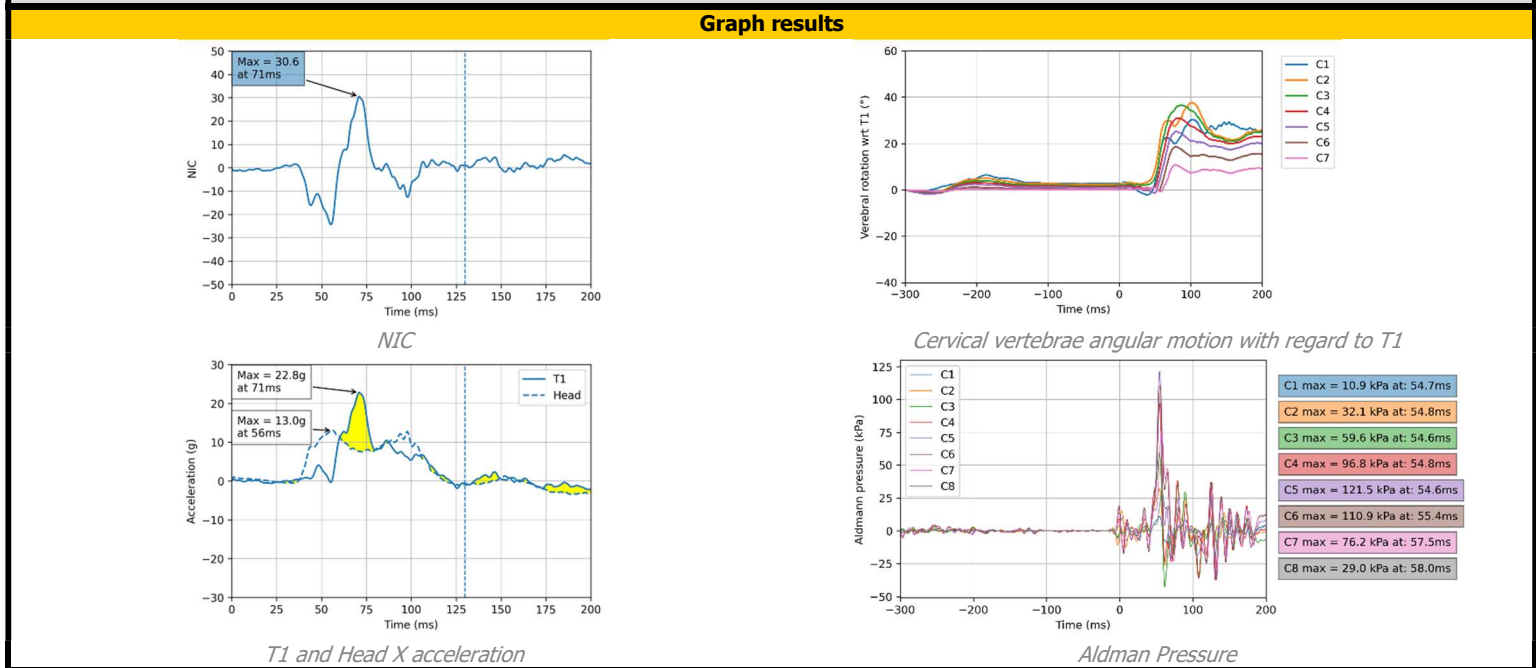
Head kinematics results	Numerical results																								
 <p>Spine S-shape</p>	<table style="width:100%; border-collapse: collapse;"> <tr><td>THRC</td><td style="text-align: right;">N/A</td></tr> <tr><td>NICmax</td><td style="text-align: right;">37,9</td></tr> <tr><td>WAD2+ risk</td><td style="text-align: right;">99%</td></tr> <tr><td>max Aldman Pressure</td><td style="text-align: right;">96,2kPa at C6</td></tr> <tr><td>max Head X acceleration</td><td style="text-align: right;">16,9g</td></tr> <tr><td>max T1 X acceleration</td><td style="text-align: right;">24,9g</td></tr> <tr><td>max Upper neck Fx</td><td style="text-align: right;">N/A</td></tr> <tr><td>max Upper neck Fz</td><td style="text-align: right;">N/A</td></tr> <tr><td>max Upper neck My</td><td style="text-align: right;">N/A</td></tr> <tr><td>max Lower neck Fx</td><td style="text-align: right;">N/A</td></tr> <tr><td>max Lower neck Fz</td><td style="text-align: right;">N/A</td></tr> <tr><td>max Lower neck My</td><td style="text-align: right;">N/A</td></tr> </table>	THRC	N/A	NICmax	37,9	WAD2+ risk	99%	max Aldman Pressure	96,2kPa at C6	max Head X acceleration	16,9g	max T1 X acceleration	24,9g	max Upper neck Fx	N/A	max Upper neck Fz	N/A	max Upper neck My	N/A	max Lower neck Fx	N/A	max Lower neck Fz	N/A	max Lower neck My	N/A
THRC		N/A																							
NICmax		37,9																							
WAD2+ risk		99%																							
max Aldman Pressure		96,2kPa at C6																							
max Head X acceleration		16,9g																							
max T1 X acceleration		24,9g																							
max Upper neck Fx		N/A																							
max Upper neck Fz		N/A																							
max Upper neck My		N/A																							
max Lower neck Fx	N/A																								
max Lower neck Fz	N/A																								
max Lower neck My	N/A																								
 <p>NICmax</p>																									
 <p>Max T1 rear displacement</p>																									





Simulation case	V3_50M_Inclined20_Head-Leaning
-----------------	---------------------------------------

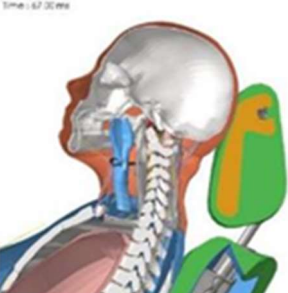
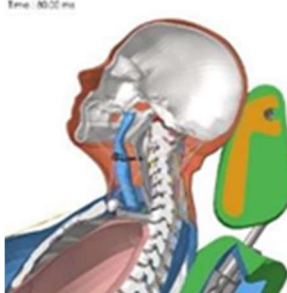
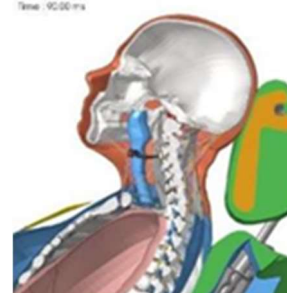
General description		
Seat used	Variant 3	 <i>Initial vertebrae position</i>
Seat position	Seatback 45° Tracks Middle / Inclined 20° Height Middle Swivel 0° Shoulder 1° Headrest Middle / Backset = 0mm	
Dummy used	VIVA+ 50 th Male	 <i>Seat isometric view</i>
Crash pulse	IIWPG Medium Whiplash Pulse	
Speed	15,9 km/h	
Load case	Low speed rear crash	

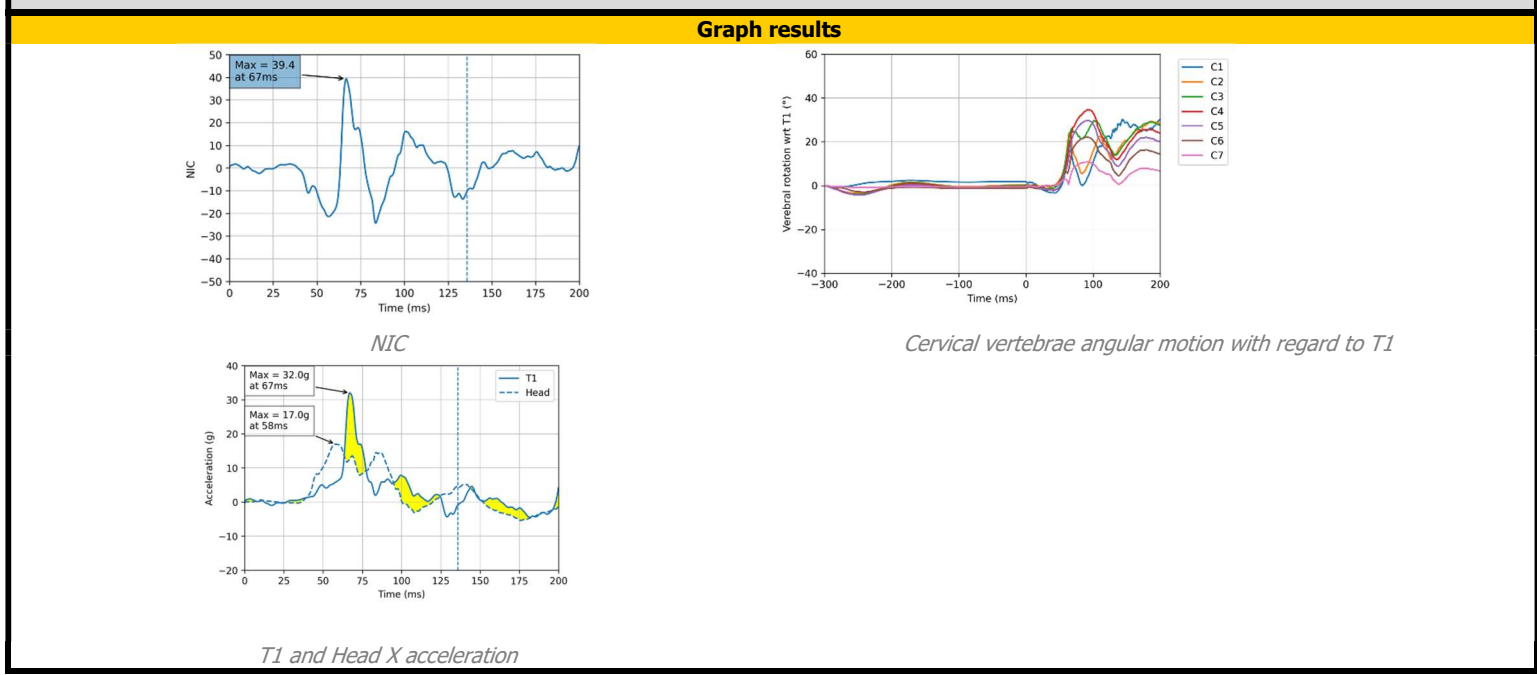
Head kinematics results	Numerical results																								
 <i>Spine S-shape</i>	<table border="0" style="width:100%;"> <tr><td>THRC</td><td style="text-align: right;">N/A</td></tr> <tr><td>NICmax</td><td style="text-align: right;">30,6</td></tr> <tr><td>WAD2+ risk</td><td style="text-align: right;">95,6%</td></tr> <tr><td>max Aldman Pressure</td><td style="text-align: right;">121,5kPa at C5</td></tr> <tr><td>max Head X acceleration</td><td style="text-align: right;">13g</td></tr> <tr><td>max T1 X acceleration</td><td style="text-align: right;">22,8g</td></tr> <tr><td>max Upper neck Fx</td><td style="text-align: right;">N/A</td></tr> <tr><td>max Upper neck Fz</td><td style="text-align: right;">N/A</td></tr> <tr><td>max Upper neck My</td><td style="text-align: right;">N/A</td></tr> <tr><td>max Lower neck Fx</td><td style="text-align: right;">N/A</td></tr> <tr><td>max Lower neck Fz</td><td style="text-align: right;">N/A</td></tr> <tr><td>max Lower neck My</td><td style="text-align: right;">N/A</td></tr> </table>	THRC	N/A	NICmax	30,6	WAD2+ risk	95,6%	max Aldman Pressure	121,5kPa at C5	max Head X acceleration	13g	max T1 X acceleration	22,8g	max Upper neck Fx	N/A	max Upper neck Fz	N/A	max Upper neck My	N/A	max Lower neck Fx	N/A	max Lower neck Fz	N/A	max Lower neck My	N/A
THRC		N/A																							
NICmax		30,6																							
WAD2+ risk	95,6%																								
max Aldman Pressure	121,5kPa at C5																								
max Head X acceleration	13g																								
max T1 X acceleration	22,8g																								
max Upper neck Fx	N/A																								
max Upper neck Fz	N/A																								
max Upper neck My	N/A																								
max Lower neck Fx	N/A																								
max Lower neck Fz	N/A																								
max Lower neck My	N/A																								
 <i>NICmax</i>																									
 <i>Max head rear displacement</i>																									

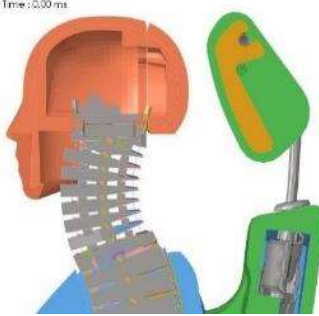



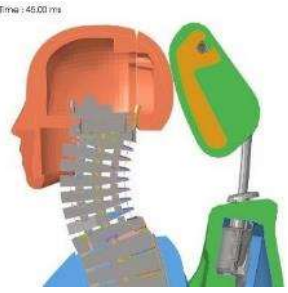
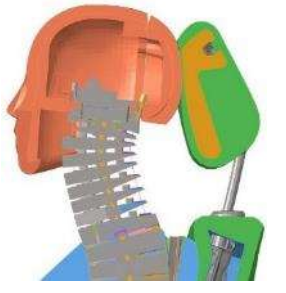
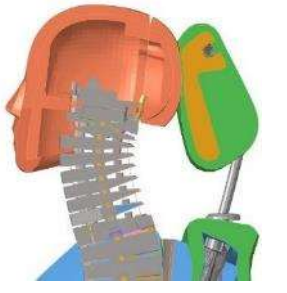
Simulation case **V3_50F_Inclined20_Head-Leaning**

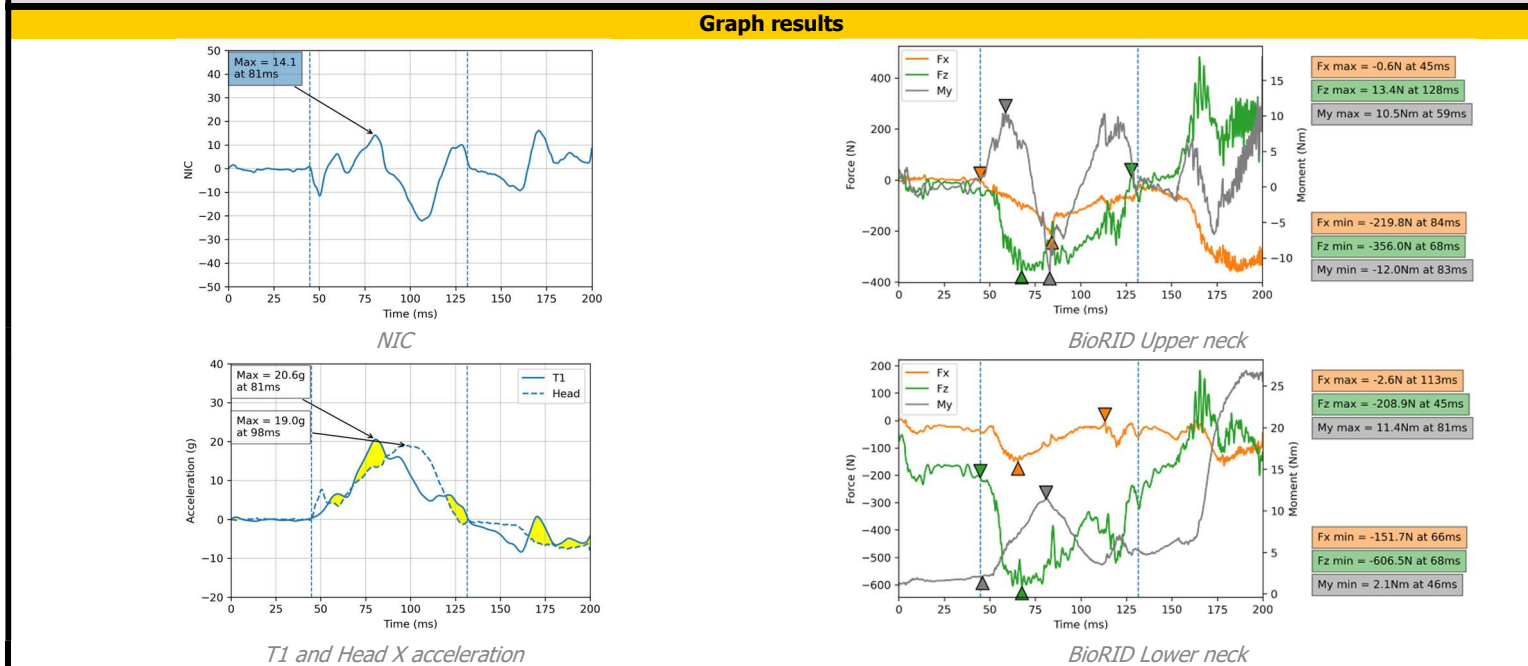
General description		
Seat used	Variant 3	 <i>Initial vertebrae position</i>
Seat position	Seatback 45° Tracks Middle / Inclined 20° Height Middle Swivel 0° Shoulder 3° Headrest Lowest / Backset = 0mm	
Dummy used	VIVA+ 50 th Female	 <i>Seat isometric view</i>
Crash pulse	IIWPG Medium Whiplash Pulse	
Speed	15,9 km/h	
Load case	Low speed rear crash	

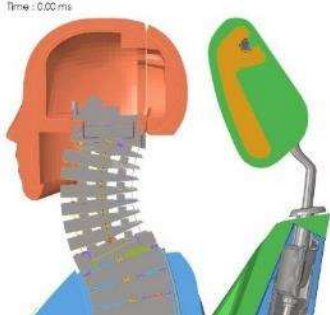

Head kinematics results	Numerical results
 <i>Max NIC</i>	THRC N/A
 <i>Max head rear displacement</i>	NICmax 36,4
 <i>Spine Compression</i>	WAD2+ risk 98,6%
	max Aldman pressure
	max Head X acc 16,4g
	max T1 X acc 30,2g
	max Upper neck Fx N/A
	max Upper neck Fz N/A
	max Upper neck My N/A
	max Lower neck Fx N/A
	max Lower neck Fz N/A
	max Lower neck My N/A

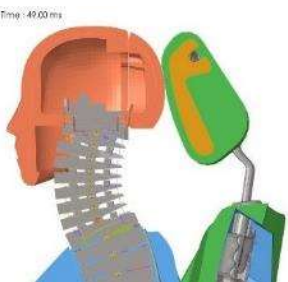
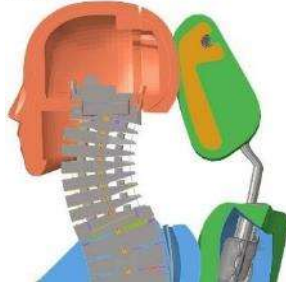
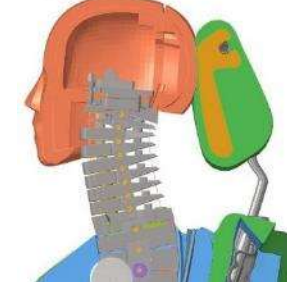


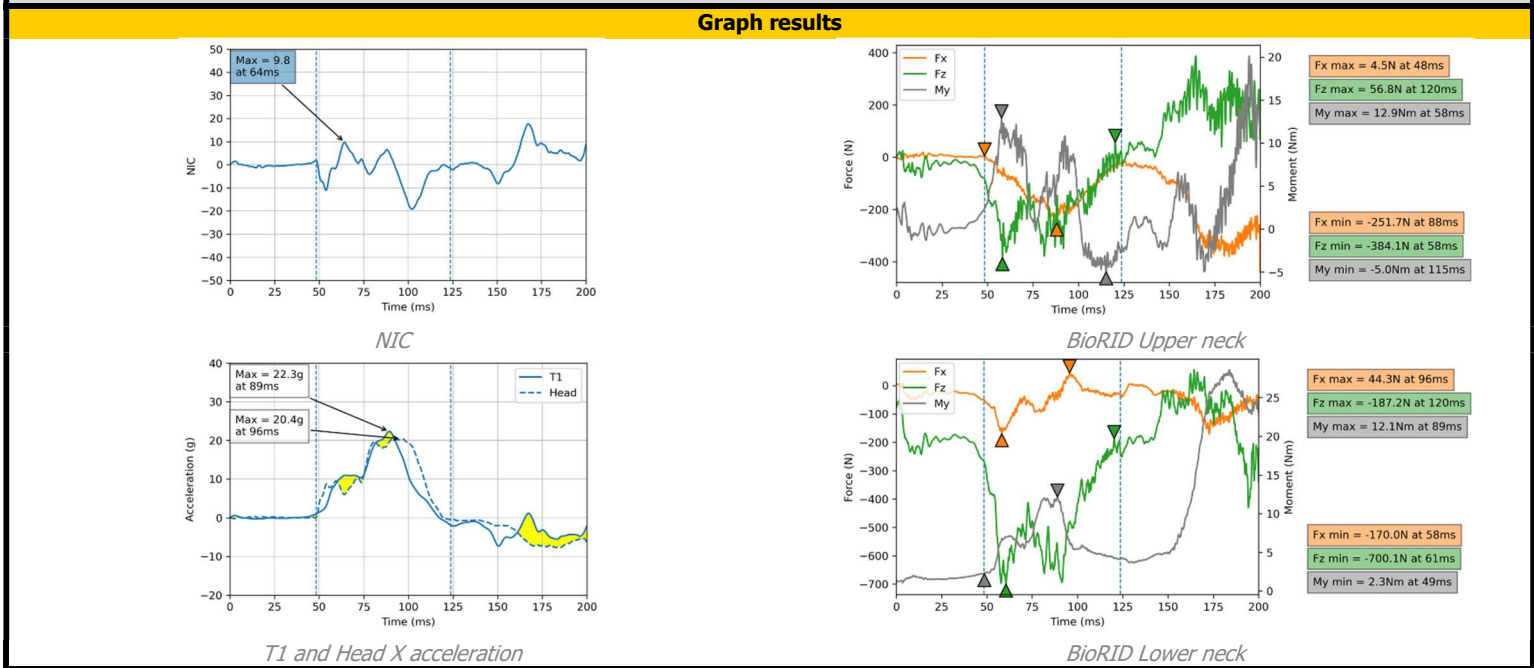
Simulation Case		V1_BioRID_Upright_Head-Upright		
General description				
Seat used	Variant 1	 		
Seat position	Seatback			25°
	Tracks			Middle
	Height			Middle
	Swivel			0°
	Shoulder			0°
	Headrest	Middle / Backset = 34mm		
Dummy used	BioRID			
Crash pulse	IIWPG Medium Whiplash Pulse			
Speed	15,9 km/h			
Load case	Low speed rear crash	<i>Initial vertebrae position</i> <i>Seat isometric view</i>		

Head kinematics results			Numerical results	
 <p><i>Head to head-restraint contact</i></p>	 <p><i>NICmax</i></p>	 <p><i>Max head rear displacement</i></p>	THRC NICmax WAD2+ risk max Aldman Pressure max Head X acceleration max T1 X acceleration max Upper neck Fx max Upper neck Fz max Upper neck My max Lower neck Fx max Lower neck Fz max Lower neck My	44,8ms 14,1 40,6% N/A 19g 20,6g -0,6N 13,4N 10,5Nm -2,6N -208,9N 11,4Nm



Simulation Case		V3_BioRID_Upright_Head-Upright		
General description				
Seat used	Variant 3	 		
Seat position	Seatback			25°
	Tracks			Middle
	Height			Middle
	Swivel			0°
	Shoulder			0°
	Headrest	Middle / Backset = 34mm		
Dummy used	BioRID			
Crash pulse	IIWPG Medium Whiplash Pulse			
Speed	15,9 km/h			
Load case	Low speed rear crash	Initial vertebrae position Seat isometric view		

Head kinematics results			Numerical results	
 <p>Time: 49.00 ms</p> <p>Head to head-restraint contact</p>	 <p>Time: 64.00 ms</p> <p>NICmax</p>	 <p>Time: 89.00 ms</p> <p>Max head rear displacement</p>	THRC 48,4ms NICmax 9,8 WAD2+ risk 21,4% max Aldman Pressure N/A max Head X acceleration 20,4g max T1 X acceleration 22,3g max Upper neck Fx 4,5N max Upper neck Fz 56,8N max Upper neck My 12,9Nm max Lower neck Fx 44,3N max Lower neck Fz -187,2N max Lower neck My 12,1Nm	



Appendix H Rearward-Facing VIVA+ 50F in Vehicle Interior Environment

Authors: Alexandros Leledakis ^{a, b}, Jonas Östh ^{a, b}, Lotta Jakobsson ^{a, b}, Linus Wågström ^a

^a Volvo Cars, Gothenburg, Sweden

^b Chalmers University of Technology, Gothenburg, Sweden

This is the Appendix for Chapter 3.2.2.1.

This first step sub-study included frontal impacts for one type of novel seated positions, as part of work carried out in WP3 to demonstrate a VT protocol for seated passenger car occupants. The VIVA+ 50F was positioned in a rearward-facing vehicle front passenger seat and exposed to frontal impacts. The aim was to investigate the sensibility of the model, when seated in a rearward-facing front passenger vehicle seat (Figure H1), representing a potential novel seated position, varying the seatback angle and two frontal impact crash pulses. An additional aim was to integrate the VIVA+ 50F in a vehicle environment, a first of its kind.

1. Methods

In total four simulations were performed, varying the crash pulses and the sitting posture by adjusting the seatback angle. The two sitting postures were nominal, with a seatback angle of 25°, and semi-reclined, with an angle of 30° (Figure H1). The nominal seat configuration in this study, except facing rearward, corresponds to the seat position as specified in the EuroNCAP Whiplash Assessment Protocol (EuroNCAP, 2019). The two seat configurations resulted in head to head-restraint distances of 51 mm and 61 mm, respectively, after applying the positioning procedure.

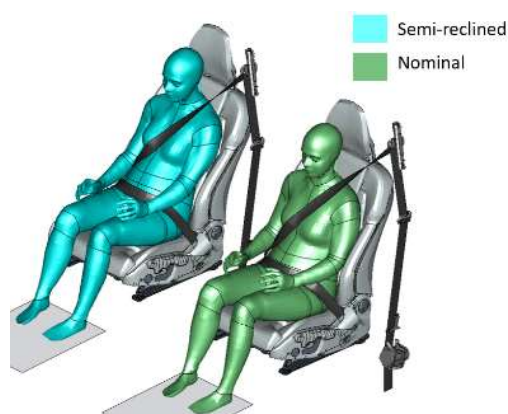


Figure H1. VIVA+ 50F is seated in a production vehicle seat environment in nominal (25° seatback angle) and semi-reclined (30° seatback angle) configurations. The seat is placed rearward-facing in the vehicle, while exposed to frontal impacts.

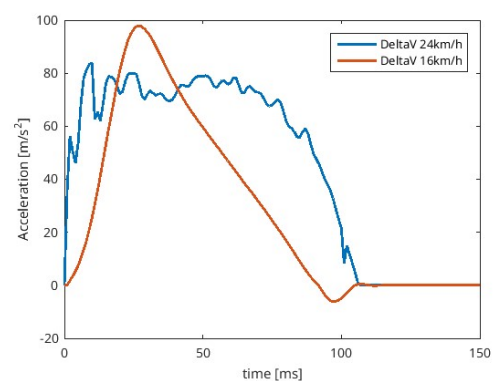


Figure H2. Frontal impact crash pulses; 'deltaV 24 km/h' with a mean acceleration of 63 m/s², and 'deltaV 16km/h' with a mean acceleration of 48 m/s².

Two different crash pulses were used, shown in Figure H2. The mean acceleration of the 'deltaV 24km/h' crash pulse was at 63 m/s², while the mean acceleration of the 'deltaV 16 km/h' was at 48 m/s², although

higher maximum acceleration. They are comparable in shape and magnitude with two of the rear-end impact crash pulses used in EuroNCAP Whiplash Assessment Protocol (EuroNCAP, 2019).

In the target posture, VIVA+ 50F was positioned with the feet parallel to the vehicle floor. The torso was in contact with the seatback and was centred on the seat. The arms were adjacent to the torso and the hands rested on the side of the thighs. The backset, defined as the distance between the rearmost point of the head and the front surface of the head-restraint, was targetted to be 50 mm for the nominal posture and 60 mm for the semi-reclined posture, which is comparable with the backset observed for females while driving (Jonsson et al., 2008). The additional 10 mm in the backset target for the semi-reclined posture was chosen to keep the Frankfort plane of the head parallel to the horizon. Figure H3 shows a side view of the two seat configurations.

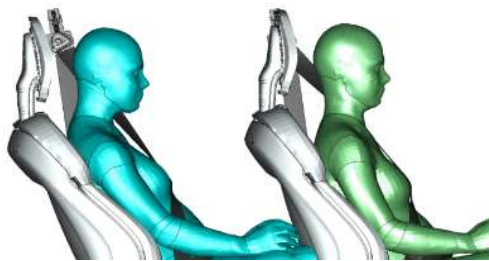


Figure H3. Side view of the VIVA+ 50F in nominal (25° seatback angle) and semi-reclined (30° seatback angle) configurations. The seat was placed rearward-facing in the vehicle, while exposed to frontal impacts.

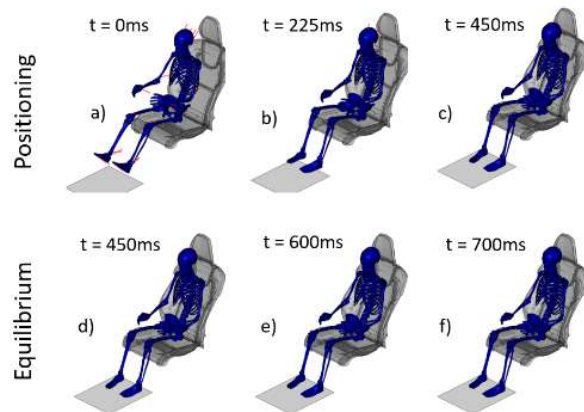


Figure H4. The two positioning stages of VIVA+ 50F. From 0-450ms (a-c), force was applied to selected landmarks on the VIVA+ 50F's skeleton. From 450-700ms (d-f), the force was set to 0 and the VIVA+ 50F was allowed to reach equilibrium with the vehicle interior.

VIVA+ 50F was positioned in the target postures by pre-simulation using the marionette method (Poulard et al., 2015). One-dimensional elements were used to pull selected body landmarks to the desired position. The duration of the positioning simulation was 700ms and comprised two stages. First, forces between 70-350N were applied using the one-dimensional elements for 450ms, Figure H4a-c. Simultaneously as the pulling of the occupant landmarks into position, the geometrical constraints for the occupant posture were also moved into position. The vehicle surfaces that came into contact with the VIVA+ 50F (in this case the seat and the floor), started 100mm below and behind the VIVA+ 50F and were moved into their original position. In the second stage Figure H4 d-f), after 450ms, the force of the elements was set to 0N and VIVA+ 50F was allowed to reach equilibrium with the seat. Gravity was enabled throughout the entire simulation to generate the appropriate contact forces and squash the seat. The simulations were run using the explicit FE solver LS-DYNA MPP s R9.3.0 (LSTC, Livermore, CA, USA).

With the purpose of evaluating the sensitivity of the model to discriminate the two posture configurations for each of the crash pulses, the analysis focused mainly on kinematics. This was done by visual comparison and analysing the head to head-restraint contact. As occupant response, Head and T1 relative velocity and acceleration in the x-direction were in focus. NIC_{max}, using the procedure described in the EuroNCAP protocol (EuroNCAP, 2019), was calculated based on these responses and compared between the four simulations. Although not developed for the mid-sized female HBM, the injury risk function for NIC_{max} by Ono et al (2009) was used to provide some further insights into the sensitivity when using a potential injury criterion.

2. Results

The VIVA+ 50F kinematics in the nominal and semi-reclined configurations are shown in Figures H5 and H6, for the 'deltaV 16km/h' and 'deltaV 24km/h' pulses, respectively. The times for initial head to head-restraint contact as well as the start of the rebound are summarised in Table H1.

Similar kinematics is seen between the simulations providing indication that the positioning procedure when reclining the occupant seems relevant. The time of head to head-restraint contact follows the trends in backset, increasing the time for increased backset. This correlation trend was seen in both crash pulses.

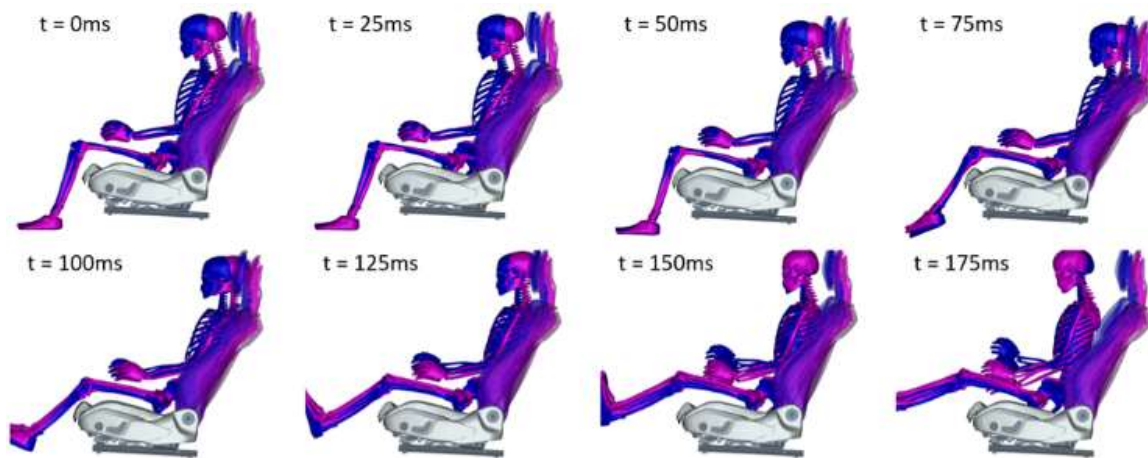


Figure H5. VIVA+ 50F kinematics in the nominal (blue) and semi-reclined posture (magenta) for the 'deltaV 16km/h' pulse.

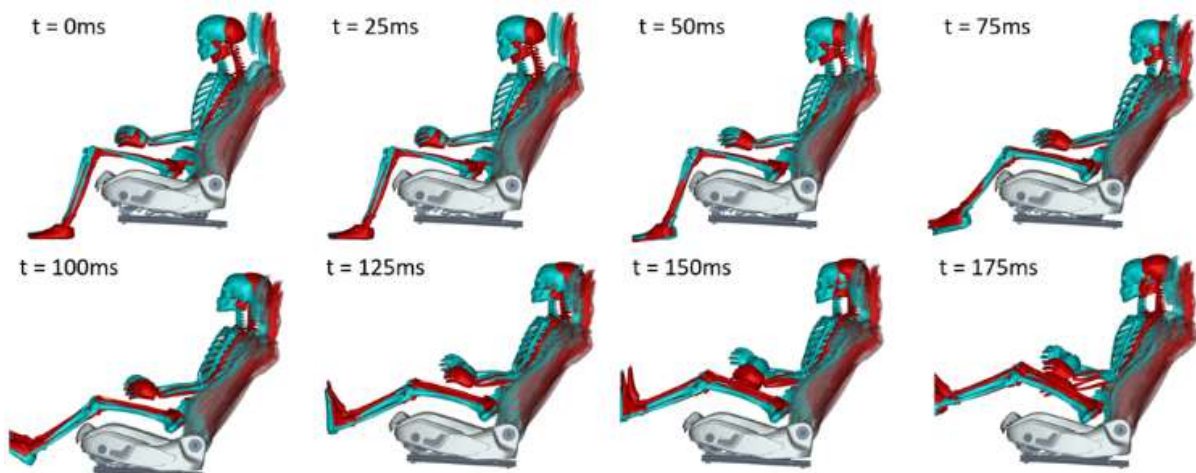


Figure H6. VIVA+ 50F kinematics in the nominal (cyan) and semi-reclined posture (red) for the 'deltaV 24km/h' pulse.

NIC over time is presented in Figures H7 and H8, for the 'deltaV 16km/h' and 'deltaV 24km/h' pulses, respectively, together with the components used for its calculation; head and T1 relative acceleration and velocity in the x-direction (direction of the pulse).

Table H1. Initial backset (head to head-restraint distance), head to head-restraint contact time and start of rebound for the four simulations.

	'deltaV 16km/h'		'deltaV 24km/h'	
	Nominal	Semi-reclined	Nominal	Semi-reclined
Backset	51mm	61mm	51mm	61mm
Head to head-restraint contact time	55ms	60ms	48ms	54ms
Rebound start	136ms	130ms	159ms	164ms

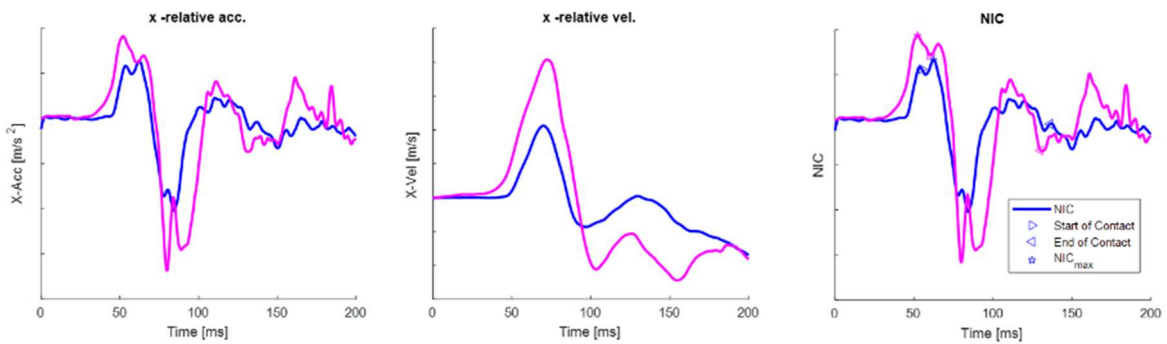


Figure H7. NIC, head and T1 relative velocity and acceleration in the x-direction for the VIVA+ 50F in the nominal (blue) and semi-reclined (magenta) configurations in 'deltaV 16km/h' pulse.

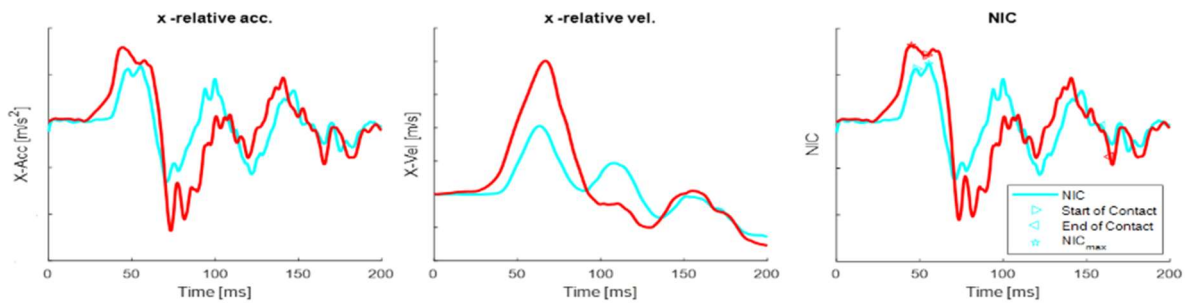


Figure H8. NIC, head and T1 relative velocity and acceleration in the x-direction for the occupant in the nominal (cyan) and semi-reclined (red) configurations in 'deltaV 24km/h' pulse.

The head to T1 relative responses show a consistent trend for being influenced by the seatback angle, irrespective frontal impact crash pulse, see Figures H7 and H8. Higher peak head and T1 relative acceleration and velocities were seen for the semi-reclined configuration. This applies for NIC_{max} as well, which corresponds to the first peak of the NIC function. Applying the injury risk function for NIC_{max} by Ono et al. (2009), the relative estimated risk differences were approximately 20%; ranging from approximately 16% in the 'deltaV 24km/h' to 23% in the 'deltaV 16km/h' configurations. The NIC_{max} responses only slightly deviated between the two crash pulses with somewhat higher values in the 'deltaV 16km/h' pulse. The deviation was driven by the relatively higher contribution of the acceleration-based component in that pulse configuration.

3. Discussions and Conclusions

This sub-study is a first step in investigating novel seated positions in frontal impacts, using the ViVA+ models. The ViVA+ 50F was successfully integrated in the vehicle interior model and was possible to position in the target postures using common positioning techniques. The model was sensitive to change in posture between the nominal and the semi-reclined seat positions, as well as the different crash pulses applied.

While the HBM was found sensitive to changes in the two posture configurations in the study, the degree of sensitivity and to what degree the kinematics and amplitude of the response differences replicate the situation for a mid-sized female occupant in corresponding real-world situations, cannot be judged based on this study. The trend of increased occupant responses with increased backset, caused by the semi-reclined seat position, replicates what would be expected from earlier test or simulation experiences in rear-end impacts for forward-facing occupants. Increased backset has been shown related to increased injury risk in real-world follow-up crash data studies (Jakobsson et al., 2008). However, the influence of the seatback angle, as such, creating the backset is not known as a separate variable from real-world follow-up studies in rear-end impacts. For frontal impacts with rearward-facing seats the influence of backset, as well as the relative importance of whiplash injury risks remain to be understood. In frontal impacts, an increased likelihood of higher severity pulses is expected, which likely will pose additional challenges regarding the vehicle seat integrity when rearward-facing. In addition, the space available behind a front row rearward-facing seat is likely less than when the seat is forward-facing. Hence, there are several seat design parameters that could influence the seatback movements, as well as possibilities for seatback adjustments, when positioned rearward-facing in a vehicle.

The test matrix in this study cannot distinguish the influence of the reclined seatback angle from the influence of increased backset. In order to understand them separately, additional simulations isolating those factors are needed. Thereby, at this stage, it is essential not to draw conclusions based on one or the other factor.

Which injuries and injury mechanisms to focus on for a rearward-facing occupant in frontal impacts is not evident, especially at higher impact severities. As presented by Kang et al. (2020), a large variety of injury types were seen. It also became clear that the design of the seatback, including the seatbelt attachments, in addition to the seatback strength and support, influenced the injury outcome. In the present study, the choice was to focus on kinematics, and to include some results in-line with the injury responses evaluated in the study on ViVA+ 50F in the Chalmers lab seat (Chapter 3.1.3.1.) However, due to all the uncertainties with respect to the novel HBM used, in addition to the novel seated position and the limitations in the setup as such, the calculated injury prediction should be treated with great caution. They can be used for relative comparison with respect to whiplash injury assessment, but will likely not reflect true injury risk, nor provide an overall injury assessment relevant for a rearward-facing occupant exposed to a frontal impact.

7. References

- Euro NCAP (2019). The dynamic assessment of car seats for neck injury protection testing protocol. Version 4.1 November 2019 <https://cdn.euroncap.com/media/57828/euro-ncap-whiplash-test-protocol-v41.pdf>
- Kang YS, Stammen J, Ramachandra R, Agnew AM, Hagedorn A, Thomas C, Kwon HJ, Moorhouse K, BolteIV JH (2020) Biomechanical responses and injury assessment of post mortem human subjects in various rear-facing seating configurations. *Stapp Car Crash Journal*, pp155-212
- Jakobsson L, Isaksson-Hellman I, Lindman M (2008). WHIPS (Volvo Cars' Whiplash Protection System) – The Development and Real-World Performance. *Traffic Injury Prevention* 9:6, 600-605
- Jonsson B, Stenlund H, Björnstig U (2008). Backset—Stationary and During Car Driving, *Traffic Injury Prevention*, 9:6, 568-573, DOI: 10.1080/15389580802308312
- Ono K, Ejima S, Yamazaki K, Sato F, Pramudita JA, Kaneoka K, Ujihashi S (2009). Evaluation criteria for the reduction of minor neck injuries during rear-end impacts based on human volunteer experiments and accident reconstruction using human FE model simulations. *IRCOBI Conf.* York, UK
- Poulard D, Subit D, Donlon J-P, Kent RW (2015). Development of a computational framework to adjust the pre-impact spine posture of a whole-body model based on cadaver tests data. *J. Biomech.* 48(4), 636–643. doi:10.1016/j.jbiomech.2014.12.050

Appendix I Forward-Facing VIVA+ 50M and 50F Simulations in a Variety of Seated Positions, Frontal and Side Impacts

Authors: Alexandros Leledakis ^{a,b}, Jonas Östh ^{a,b}, Lotta Jakobsson ^{a,b}

^a Chalmers University of Technology, Gothenburg, Sweden

^b Volvo Car Corporation, Gothenburg, Sweden

This is the Appendix for Chapter 3.2.2.2.

1. Introduction

One of the main goals of the VIRTUAL project is to enhance the robustness of safety assessment by taking into account the real-world variability. One step towards achieving that goal involved the development of the VIVA+ 50F and 50M HBMs, representing average-sized females and males. Another step towards greater robustness is creating simulation setups including a range of parameter variations, i.e., real-world safety deals comprising more than one size of occupant, in one seat position exposed to one impact type, including significant parameter variability, such as different occupants, seated positions and crash configurations.

The objectives of this study include examining the numerical stability of the models and investigating the sensitivity of the VIVA+ 50F and 50M HBMs to altered seat positions while exposed to frontal and side impacts. Additionally, the simulations were compared to corresponding simulations with similar size SAFER HBMs from Leledakis et al. (2022).



Figure I1. VIVA+ 50F (left) and 50M (right) HBM seated in a front passenger seat in a vehicle interior model in the nominal seat adjustment (25° seatback angle and 40% of the fore-aft travel).

2. Methods

A simulation series using the VIVA+ 50F and 50M HBM in the front passenger seat of a vehicle interior model was performed (Figure I1). The simulations were compared to corresponding simulations with similar size SAFER HBMs from Leledakis et al. (2022). The HBM was positioned in six seat adjustments, comprising two seatback angles and three seat fore-aft positions. Four crash configurations were included, resulting in a total of 48 crash simulations.

2.1. Numerical models

The passenger compartment sled was modelled using a rigid body-in-white with a deformable interior (Leledakis et al., 2021), while the VIVA+ 50F and 50M HBMs were used as occupant models, representing a 50th percentile female and male, respectively. The main anthropometric characteristics of the VIVA+ HBMs, as well as the corresponding SAFER HBMs, can be seen in Table I1.

Table I1. Anthropometric measurements of the VIVA+ 50F and 50M, and morphed SAFER HBM v9

Anthropometry					
	Stature	BMI	Age	Mass	Head Mass
VIVA+ 50F	1.616	24	50	62	3.74
SAFER HBM v9 (morphed 50F)	1.617	28	40	73	4.43
VIVA+ 50M	1.753	25	50	77	4.39
SAFER HBM v9 (morphed 50M)	1.758	28	40	86	4.89

Six different seat adjustments were used in this study. The seat was always set to mid-height and low-tilt, while the fore/aft position was adjusted in three steps (full-forward, mid-travel, and full-backwards). The seatback angle was set to 25° for an upright and 30° for a semi-reclined position.

The occupant restraint systems consisted of a three-point pyrotechnically-pretensioned load-limited seatbelt, a frontal passenger airbag deploying from the dashboard and, for the side impacts, a seat-mounted torso airbag and an inflatable curtain (Figure I2). All simulations were performed using the explicit FE solver LS-DYNA MPP s R9.3.0 (ANSYS/LST, Livermore, CA, USA) using 140 CPUs.

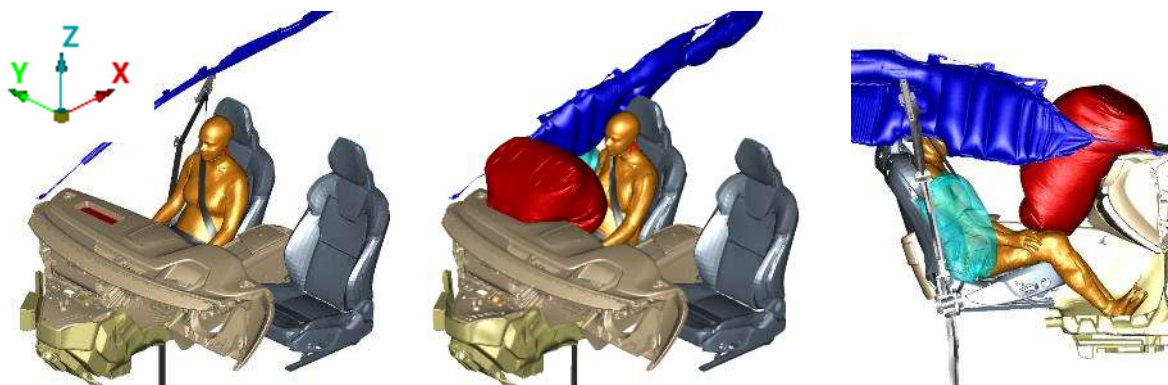


Figure I2. The VIVA+ 50M HBM is positioned in the passenger compartment. The deployed passenger frontal airbag is visible in red, the side airbag is visible in cyan, and the inflatable curtain can be seen in blue.

2.2. Occupant positioning

The occupant posture can have an influence on the occupant kinematics (Leledakis et al., 2021). In order to compare occupant responses for multiple seat positions, an automated occupant positioning

method was used. The method involved rigid body rotations to optimise a set of predefined criteria, as seen in Table I2, to define the target postures of the occupants.

Table I2. Occupant positioning steps

Body Region	Action
H-Point	Move the HBM H-point to H-Point Manikin location.
Torso	Rotate around the H-Point until the back is in contact with the seatback.
Lower extremities	Rotate thigh, calf, and foot around the y-axis until:
	Thighs are in contact with the seat base.
	Feet are as low and forward as possible while in contact with the carpet.
Upper extremities	Rotate shoulder around y until arm contacts seatback.
	Rotate elbow around y until hand contacts the thigh.

The occupant was positioned in the target postures by pre-simulation using the marionette method (Poulard et al., 2015). One-dimensional elements were used to pull selected body landmarks to the target posture. The positioning simulation had a duration of 1000ms comprising two stages. First, a force 150-400N was applied using the one-dimensional elements for 450ms (Figure I3). Simultaneously as pulling the occupant landmarks into position, the geometrical constraints for the occupant posture were also moved into position. The vehicle surfaces that came into contact with the occupant (in this case, the seat and the floor), started 150mm below and behind the occupant and were moved into their original position. In the second stage (Figure I3) after 450ms, the force of the elements was set to 0N, and the occupant was allowed to reach equilibrium with the seat. Gravity was applied throughout the entire simulation to generate the appropriate contact forces and deform the seat cushion.

The seat fore-aft position was adjusted along the full fore-aft travel length of 260 mm. Three fore-aft positions were used; a nominal position (defined as 40% of the fore-aft travel), a full-backwards position (100% of the fore-aft travel position), and a full-forward position in which the seat was moved as forward as possible while ensuring no contact between the occupant’s lower extremities and the vehicle interior. The fore-aft positions used for the male and female HBMs, as well as the resulting knee-to-vehicle-interior longitudinal distance, can be seen in Tables I3 and I4, respectively.

Table I3. Seat adjustments

Seat Adjustment – Fore-aft travel			
	Forward	Nominal	Backward
Female	0%	40%	100%
Male	20%	40%	100%

Table I4. HBM knee to vehicle interior longitudinal distance for all seat adjustments

Knees to Instrument Panel longitudinal distance						
	25°- forward	25°- nominal	25°- backward	30°- forward	30°- nominal	30°- backward
Female	20.9	85.5	212.3	19.9	87.6	214.2
Male	13.5	46.6	167	14.4	48.4	166.5

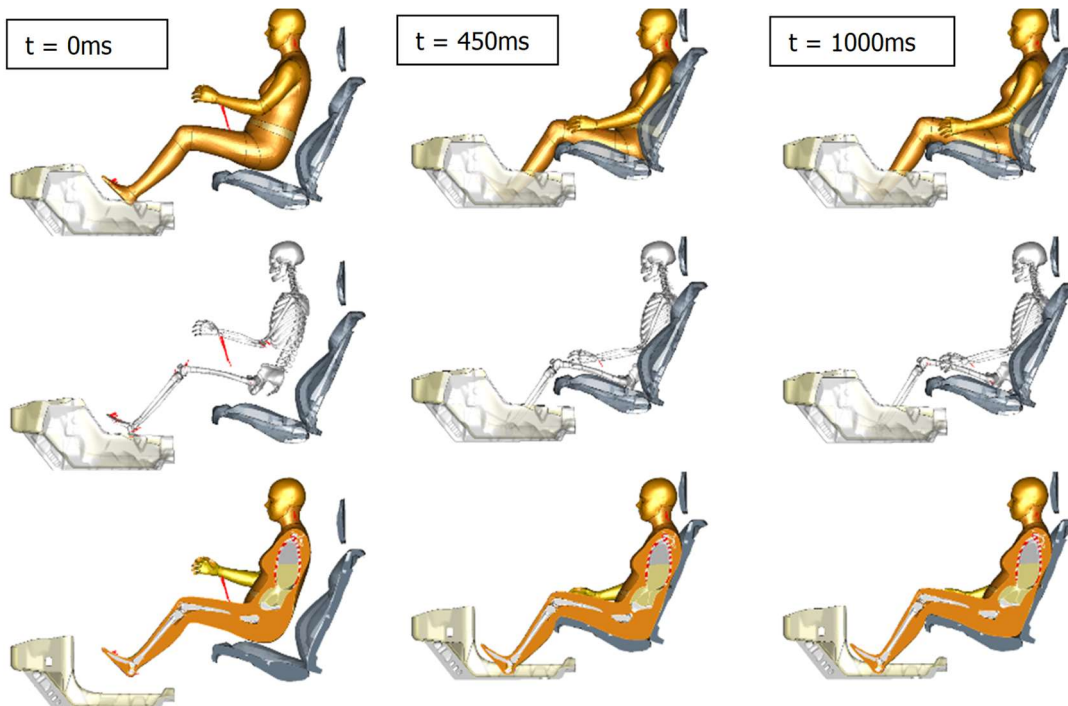


Figure I3. The two positioning stages of the HBM. From 0-450ms, force was applied to selected landmarks on the occupant skeleton. From 450-1000ms, the force of the cables was set to 0, and the occupant was allowed to reach equilibrium with the vehicle interior.

The validity of the seat-squashing was controlled by ensuring that the contact force between the occupant and the vehicle interior (Figure I4) was approximately equal to the occupant's mass. For all positioning simulations, the contact force between the occupant and the vehicle was within 112% - 125% of the occupant's weight. The stresses, produced during the positioning stage, were not retained for the HBM, but were reinitialised for the foam of the seat (using the INITIAL_FOAM_REFERENCE option of LS-DYNA).

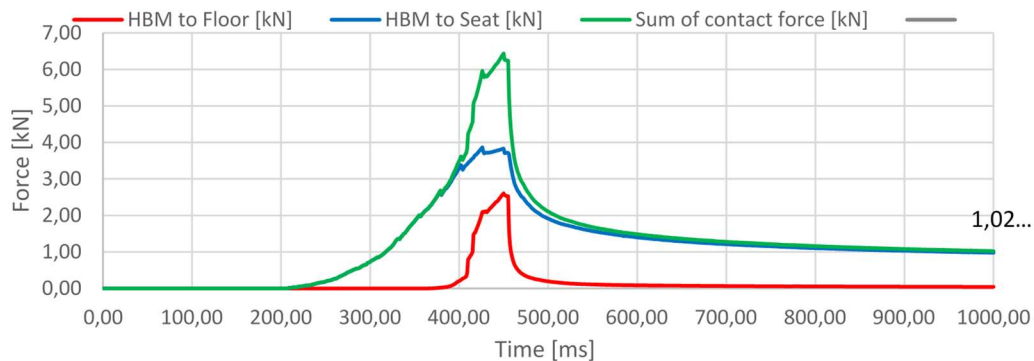


Figure I4. Positioning simulation of the VIVA+ 50M HBM. The contact force, in z-direction, between the HBM and the vehicle environment was 1.023kN at the final timestep, which is equivalent to 114% of the occupant's weight.

2.3. Crash configurations

Four crash configurations were included in this study (Figure I5). Three of the configurations were used in a prior study and described in Leledakis et al., (2021) as representative of potential future intersection crashes. They include two side impacts, a *Near-Side* impact to the front right corner and a *Far-Side* impact to the front left corner, and a *Frontal (intersection)* impact with approximately 50% overlap from the left. In addition, a car-to-car frontal crash, with approximately 50% overlap and initial velocity of 50km/h for both vehicles, was used to represent a high-severity frontal impact, *Frontal (oncoming)*. The crash pulses were generated from car-to-car impact simulations, as described in Leledakis et al. (2021). The crash pulses from the intersection crash configurations can be categorised as relatively low-severity impacts, while the *Frontal (oncoming)* is a high severity impact. The crash configurations and the in-crash vehicle motions are illustrated in Figure I5.

The occupant in-crash simulations were performed by applying the motion from the car-to-car impacts to the compartment model using prescribed rigid-body DOF translational and rotational velocities.

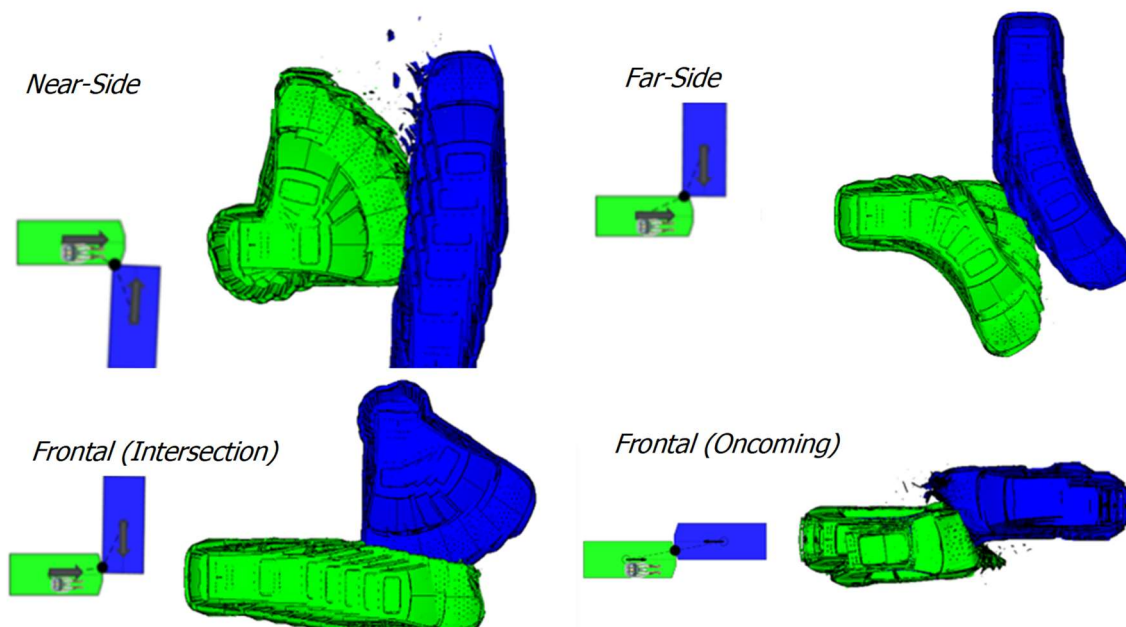


Figure I5. Crash configurations and vehicle kinematics during the crash.

3. Results

3.1. Numerical stability

In total, 12 positioning and 48 crash simulations were performed. Six seat adjustments were used, and four crash configurations were evaluated using the 50F and 50M VIVA+ HBMs. All simulations terminated normally, and no numerical instabilities were observed.

The simulations were performed with mass scaling enabled and minimum timestep set to 0.00049ms. It should be noted that the recommendation for the minimum timestep with the VIVA+ model is 0.00036ms. As a result, the added mass to the VIVA+ during the positioning simulations reached approximately 3.8kg. The added mass was mainly distributed in the skeleton of the HBM, with approximately 2kg being concentrated on the lower extremities. The mass increase was approximately 6% and 5% for the female and male HBM, respectively. The ten (10) parts with the most added mass can be seen in Table I5.

Table I5. Added mass during the positioning simulations per body region

Body Region	Female (50F)	Male (50M)
LX-Bone-Fibula-shaft-Cortical-L	0.428	0.458
LX-Bone-Fibula-shaft-Cortical-R	0.428	0.458
LX-Bone-Tibia-shaft-Cortical-R	0.276	0.261
LX-Bone-Tibia-shaft-Cortical-L	0.276	0.261
LX-Bone-Femur-shaft-middle-Cortical-R	0.175	0.185
LX-Bone-Femur-shaft-middle-Cortical-L	0.175	0.185
LX-Bone-Femur-shaft-distal-Cortical-R	0.105	0.107
LX-Bone-Femur-shaft-distal-Cortical-L	0.105	0.107
PE-Pelvis-joints-SI-joint-L	0.080	0.100
PE-Pelvis-joints-SI-joint-R	0.080	0.100
Sum of top 10	2.126	2.222
Total added mass	3.743	3.785

A small pre-study (Figure I6) was performed to determine the model scaling performance by running simulations on the same cluster using 140 to 980 CPUs.

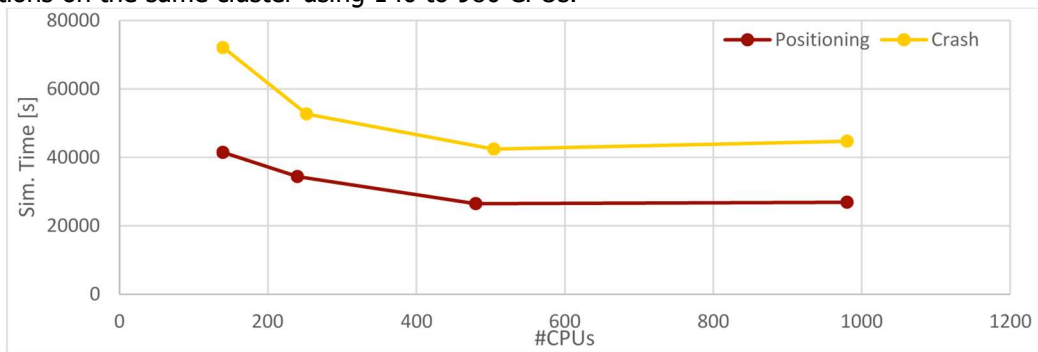


Figure I6. Simulation model scaling performance.

3.2. Influence of seat adjustment

A qualitative kinematic analysis was performed, comparing each occupant's response to the different seat adjustments. The occupants are coloured according to the seat adjustments, as seen in Figure I7, consistently for all animations presented.

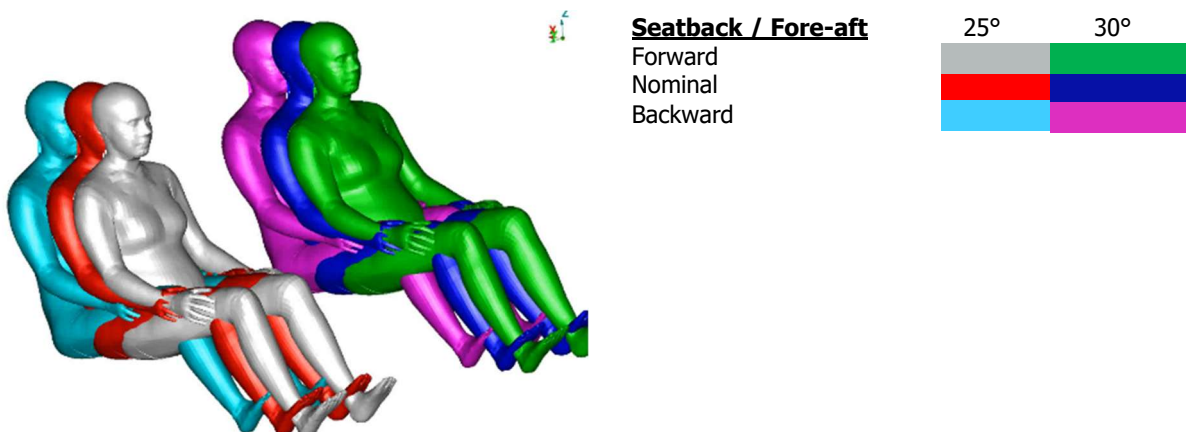


Figure I7. VIVA+ 50F, coloured for the specific seat adjustments.

3.2.1. Near-Side side impact

In the *Near-Side* configuration, no major differences were observed in the occupant kinematics for neither the 50F (Figure I8) nor the 50M (Figure I9) models. In the forward seated position, a slight increase in head rotation was observed for the full-forward seated occupant, as compared to occupants seated in the nominal seat fore-aft travel. The occupant kinematics present a similar pattern between the 50F and 50M.

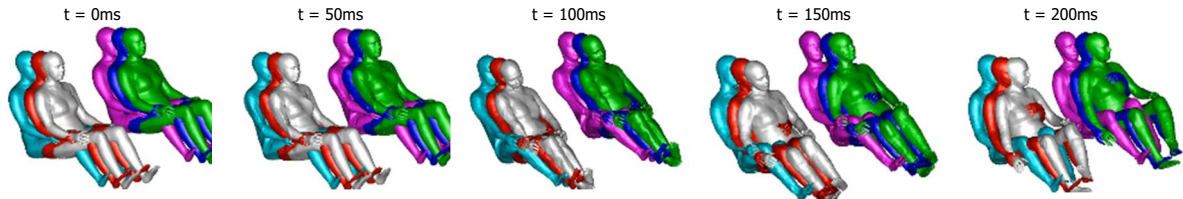


Figure I8. Kinematics of the VIVA+ 50F during the *Near-Side* configuration.

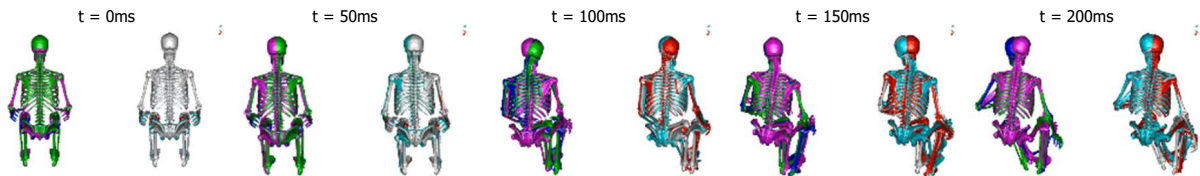


Figure I9. Kinematics of the VIVA+ 50M during the *Near-Side* configuration.

3.2.2. Far-Side

In the *Far-Side* configuration, the torso and head kinematics were influenced by the fore-aft position of the seat. The HBM's torso moved further inboard, and the head reached a more downward position, late in the loading phase (approximately at 200ms), when the occupant was in the full-backwards positioned seat. No evident influence of the seatback angle adjustment was visible, while the female (Figure I10) and male (Figure I11) models had similar kinematics patterns.

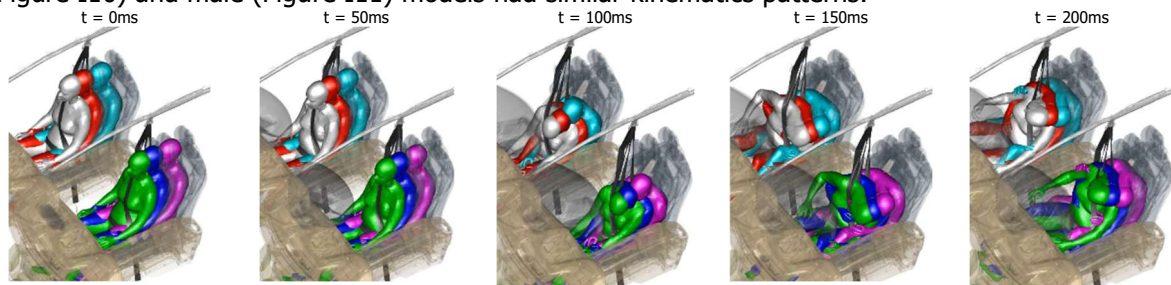


Figure I10. Kinematics of the VIVA+ 50F during the *Far-Side* configuration.

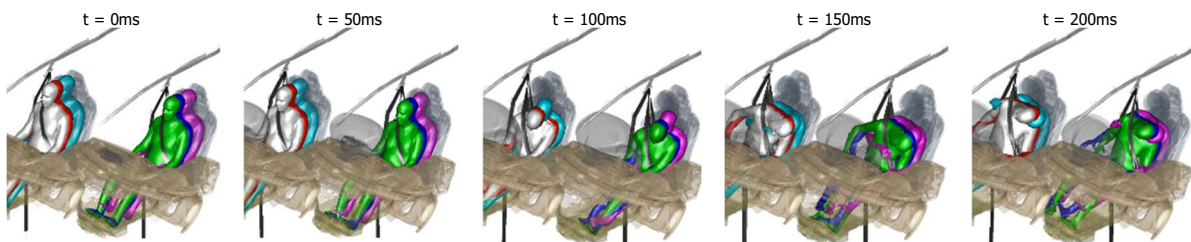


Figure I11. Kinematics of the VIVA+ 50M during the *Far-Side* configuration

3.2.3. Frontal (intersection)

In the *Frontal (intersection)* configuration, the lower extremities of the VIVA+ 50F and 50M were restrained by the contact with the instrument panel (IP) when seated in the full-forward position (Figure I12) and in the nominal position for the VIVA+ 50M (Figure I15). That can be explained by the increased initial distance between the knees and the instrument panel (Table I4), which led to altered lower extremity kinematics for the occupants that did not contact the IP. Despite the lack of support by the IP, no submarining was observed in any of the simulations.

Additionally, the fore-aft position affected the torso and head longitudinal motion (Figure I13). Specifically, when seated fully backwards, the head moved more upwards. In this low-severity frontal impact, the occupant never engaged with the passenger airbag when seated fully backwards. Finally, semi-reclining to 30° had a minor influence on the kinematics, with the occupants reaching approximately the same end position at maximum excursion (Figure I14). The trends observed were valid both for the VIVA+ 50F as well as the VIVA+ 50M.

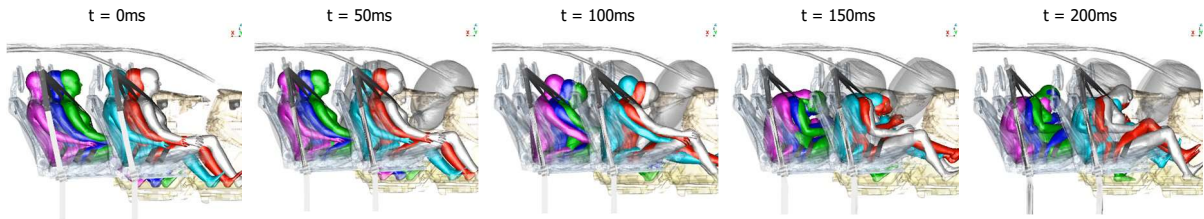


Figure I12. Kinematics of the VIVA+ 50F HBM during the *Frontal (intersection)* configuration.

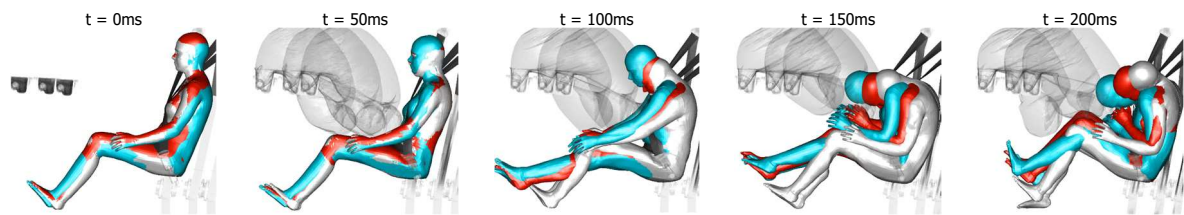


Figure I13. Kinematics of the VIVA+ 50F HBM during the *Frontal (intersection)* configuration. The effect of the fore-aft position is highlighted by overlaying the models with different fore-aft positions.

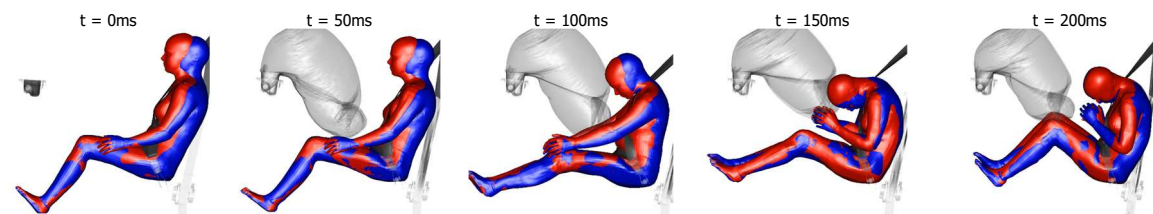


Figure I14. Kinematics of the VIVA+ 50F HBM during the *Frontal (intersection)* configuration. The HBMs seated in the 25° and 30° backrest angles are overlaid.

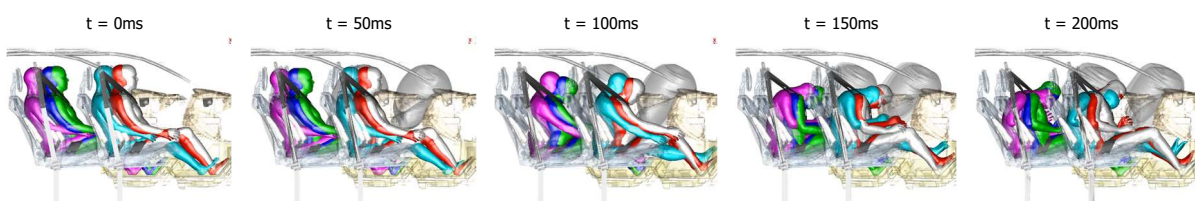


Figure I15. Kinematics of the VIVA+ 50M HBM during the *Frontal (intersection)* configuration.

3.2.4. Frontal (oncoming)

The observations from the *Frontal (intersection)* configuration with regard to knee contact are valid in *Frontal (oncoming)* impact, in which no submarining occurred for any seat adjustment, even in the situations with lack of contact with the IP.

The fore-aft position had a substantial influence over torso and head kinematics. When the occupant was in the full-backwards position, the head relative speed was higher. The cervical spine was compliant and allowed the head to rotate inboard and move downward, which was more pronounced for the female model (Figures I16-I17), compared to the male model (Figure I19).

The semi-reclined posture had a minor influence on the kinematics of the head for the 50F HBM (after 150ms, Figure I18). The 50M HBM was not influenced by the seatback angle, as it followed a similar trajectory for both the 25° and 30° seatback angles (Figure I20).

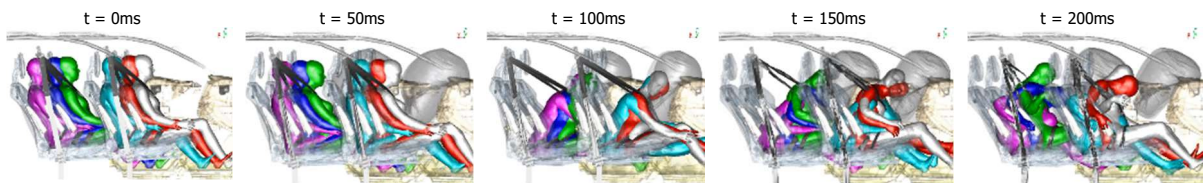


Figure I16. Kinematics of the VIVA+ 50F during the *Frontal (oncoming)* configuration.

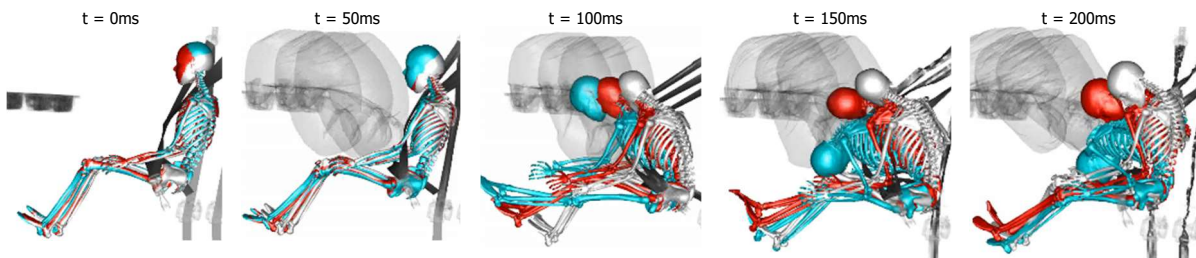


Figure I17. Kinematics of the VIVA+ 50F HBM during the *Frontal (oncoming)* configuration. The effect of the fore-aft position is highlighted by overlaying the models with different fore-aft positions.

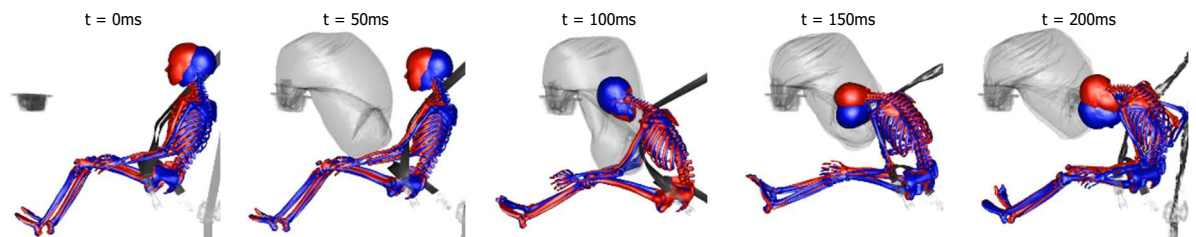


Figure I18. Kinematics of the VIVA+ 50F HBM during the *Frontal (oncoming)* configuration. The HBMs seated in the 25° and 30° backrest angles are overlaid.

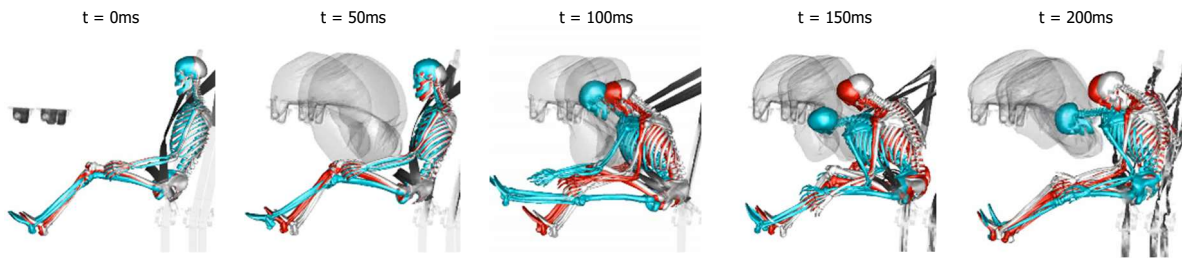


Figure I19. Kinematics of the VIVA+ 50M HBM during the *Frontal (oncoming)* configuration. The effect of the fore-aft position is highlighted by overlaying the models with different fore-aft positions.

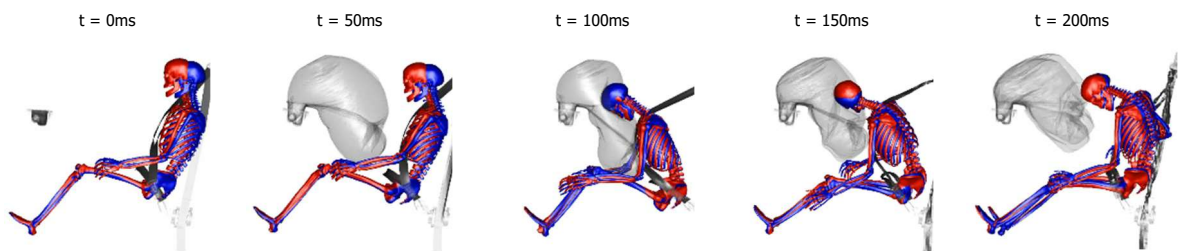


Figure I20. Kinematics of the VIVA+ 50M HBM during the *Frontal (oncoming)* configuration. The HBMs seated in the 25° and 30° backrest angles are overlaid.

3.3. Comparison with SAFER HBM

3.3.1. Near-Side

In the *Near-Side* configuration, the VIVA+ showed overall similar kinematics with the SAFER HBM. The VIVA+ shoulder moved up and compressed during the loading phase. Furthermore, differences in the kinematics of the upper extremities were observed. The SAFER HBM's upper extremities were more flexible and moved more during the crash phase. The outboards upper extremity of the SAFER HBM moved away from the seat (Figure I21) compared to the upper outboards extremity of the VIVA+ which stayed in place. The altered upper extremity position could affect the interaction with the side airbag and alter the occupant injury prediction.

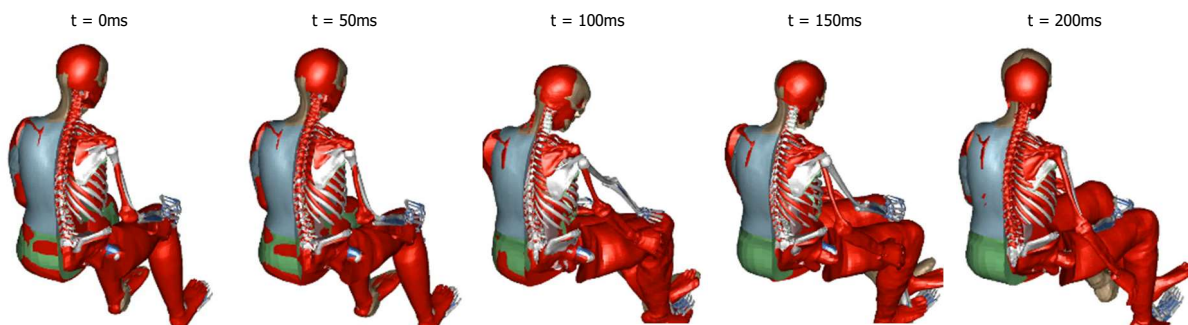


Figure I21. Kinematics of the VIVA+ 50F in red and the corresponding SAFER HBM in white, in the *Near-Side* configuration

3.3.2. Far-Side

In the same manner as the *Near-Side* configuration, the VIVA+ showed overall similar kinematics with the SAFER HBM during the *Far-Side* configuration. The VIVA+ shoulder moved up and compressed during the loading phase. The VIVA+ showed similar kinematics up to 100ms (Figure I22). However, the cervical spine was more flexible and allowed the head to move further downward. The VIVA+ started the rebound phase earlier.

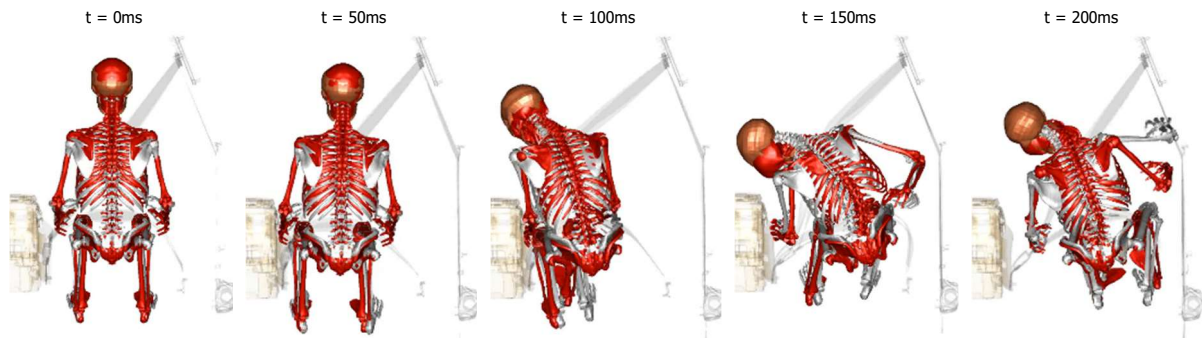


Figure I22. Kinematics of the VIVA+ 50F in red and the corresponding SAFER HBM in white, in the *Far-Side* configuration.

3.3.3. Frontal (intersection)

In the *Frontal (intersection)* configuration, the kinematics of the extremities and torso looked similar for the VIVA+ and SAFER HBM v9 HBMs (Figures I23 and I24). Differences were observed in the cervical spine, with the VIVA+ ending up with a higher flexion angle and rotated inboard during the crash, especially for the female model (Figure I23).

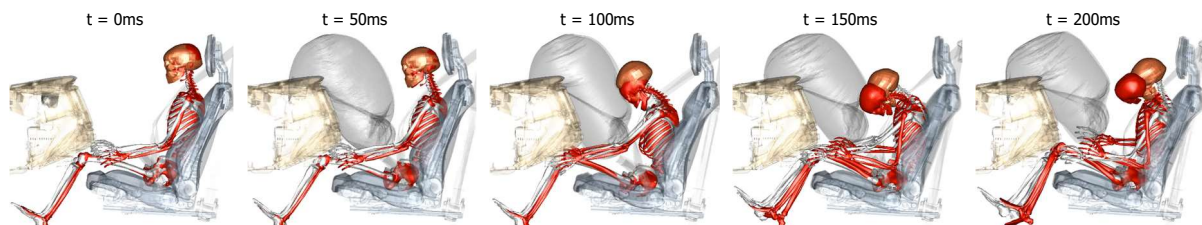


Figure I23. Kinematics of the VIVA+ 50F HBM in red and SAFER HBM v9 in white, in the *Frontal (intersection)* configuration.

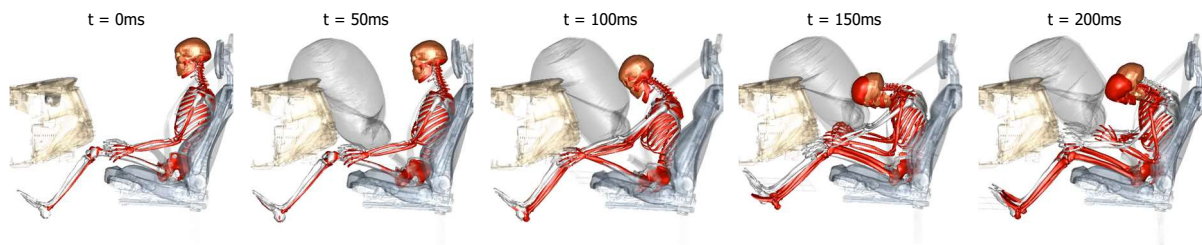


Figure I24. Kinematics of the VIVA+ 50M HBM in red and SAFER HBM v9 in white, in the *Frontal (intersection)* configuration.

3.3.4. Frontal (oncoming)

In the *Frontal (oncoming)* configuration, similar kinematics were observed for the corresponding VIVA+ and SAFER HBM when the occupant was seated in the full-forward or nominal position (Figure I25). The full-backwards position resulted in altered kinematics. The VIVA+ model interacted with the frontal airbag differently to the SAFER HBM. The initial contact point between the SAFER and VIVA+ was similar. However, the cervical spine of the VIVA+ model is more flexible, which allowed the head to move further inboard. The inertia of the head then took over and pulled the torso of the HBM downward. This behaviour was observed with both models (VIVA+ 50M and 50F); However, it was more pronounced with the 50F model (Figure I26).

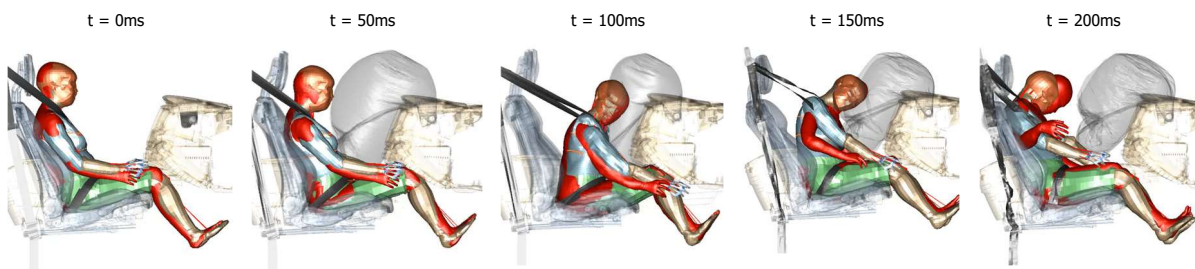


Figure I25. Kinematics of the VIVA+ 50F HBM in red and SAFER HBM v9 in the *Frontal (oncoming)* configuration. The seat is adjusted in the full-forwards position at 25° of backrest angle.

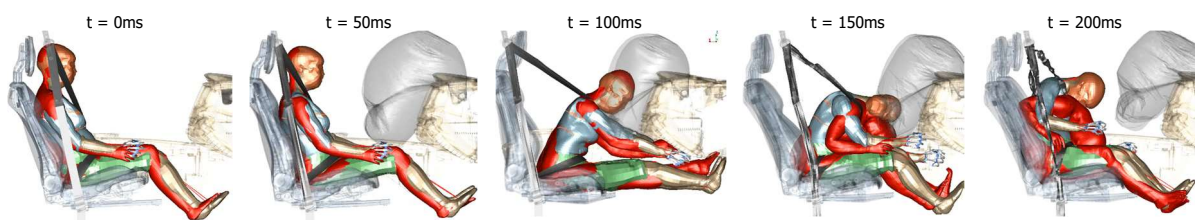


Figure I26. Kinematics of the VIVA+ 50F HBM in red and SAFER HBM v9 in the *Frontal (oncoming)* configuration. The seat is adjusted in the full-backwards position at 25° of backrest angle.

4. Discussion and Conclusion

This is the first study comprising both the VIVA+ 50F and 50M HBMs in a detailed vehicle interior model, including a state-of-the-art seat and restraints. The HBMs were successfully integrated in the vehicle interior model and were positioned into the target postures using common techniques for positioning other HBMs and ATD models. The positioned HBMs were simulated in a diverse set of frontal and side impacts and no numerical error leading to premature termination were encountered during any of the simulations. Hence, the HBMs are suitable for use in production vehicle environments.

In the *Near-Side* configuration, there were slightly higher head rotations when the HBMs were in the full-forward position. In the *Far-Side* configuration, the torso of the HBM moved further inboard, and the head reached a more downward position, when the occupant was in the full-backwards position. In the frontal impacts, the lower extremities of the 50F and 50M HBMs were restrained by the contact with the IP when the occupants were seated in the full-forward position. Hence, the kinematics of the lower extremities were altered when the seat was adjusted in the fore-aft position. No submarining occurred for any seat adjustment; However, the torso and head kinematics were altered. Furthermore, semi-reclining to 30° had no clear influence on the occupants' kinematics for all tested crash and seat adjustments. Overall, similar kinematic trends were observed between the female (50F) and male (50M)



VIVA+ HBMs. As a summary, the VIVA+ HBM was found sensitive to changes in the fore-aft position of the seat, while the seatback angle had only a minor influence on occupant kinematics.

When comparing the kinematics of the VIVA+ models with the similar size SAFER HBM models from the study in Chapter 3.2.2.3 (Leledakis et al., 2022), overall similar trends were observed. However, some differences between the models were observed. In the side impacts, the shoulder of the VIVA+ HBMs moved up and compressed during the loading phase, which also influenced the kinematics of the upper extremities. In the frontal impacts, the cervical spine of the VIVA+ models was more compliant than the SAFER HBMs, which altered the motion of the head and torso. The divergence was more pronounced for the female models compared to the male models. Although there have been several biofidelity evaluations of the SAFER HBM, the morphed HBMs used in this comparison have not been evaluated. Nonetheless, the similarity of the kinematics response of the two models corroborates the observed kinematics trends.

This study contributes to enhanced understanding of including occupant heterogeneity and novel seating aspects into virtual testing, in line with the overall goals of project VIRTUAL.

5. References

- Leledakis, A., Östh, J., Davidsson, J., Jakobsson, L. (2021). The influence of car passengers' sitting postures in intersection crashes. *Accid. Anal. Prev.* 157, 106170. doi:10.1016/j.aap.2021.106170
- Poulard, D., Subit, D., Donlon, J.-P., Kent, R.W. (2015). Development of a computational framework to adjust the pre-impact spine posture of a whole-body model based on cadaver tests data. *J. Biomech.* 48 4, 636–643. doi:10.1016/j.jbiomech.2014.12.050
- Leledakis A, Östh J, Iraeus J, Davidsson J, Jakobsson L (2022). The influence of occupant's size and shape in frontal and side impacts for varying seat positions, *IRCOBI Conf.*, Porto, Portugal

Appendix J HIII6y in a Rearward-Facing Vehicle Seat

This Appendix contains complementary material for Chapter 4.1.1. HIII6y in a Rearward-Facing-Vehicle Seat; Sled Tests and Simulations

1. Methods

Figure J1 shows the simulation pulses for the two frontal impact crash pulses used. For the 30 km/h pulse, the average pulse from all corresponding sled tests were averaged and then shifted to align with the origin. For the 50 km/h pulse, all sled tests are averaged and shifted.

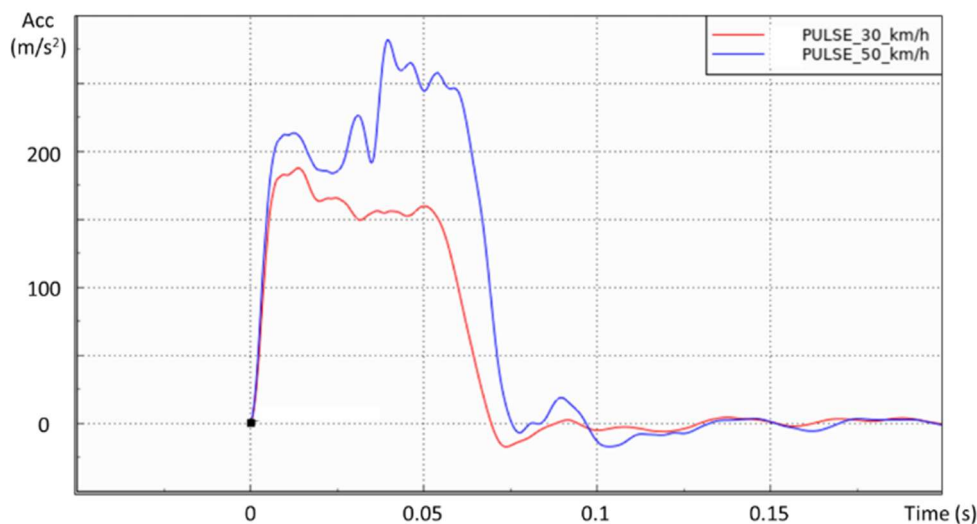


Figure J1. The two frontal impact crash pulses (acceleration versus time) used in the sub-study. The plots represent the pulses used in the simulations, derived from the average pulses in the corresponding sled tests.

Table J1 shows the test matrix for the 13 sled tests performed within the study. The varied parameters include the two different crash pulses and the three configurations of booster seat headrest positions: mid-, low- and high-position. In addition, a second booster seat was tested in some configurations. The headrest of booster seat version 2 was closer to the ATDs head in the lateral position as compared to booster seat version 1, otherwise no other design differences were observed. This difference does not substantially influence this particular test situation, in which the seatback angle of the vehicle seat was adjusted to 20°. A total of six vehicle seats were used. For each 30 km/h test, except one, a new vehicle seat was used. This vehicle seat was then also exposed to a subsequent 50 km/h test, as shown in Table J1. The exception is Test T12 (30km/h test), for which the seat from Test T11 was used again. This seat was then exposed to a subsequent 50km/h test (T13). The booster seats were factory new and replaced for each test. To test the repeatability, each configuration was tested two times, except the 50km/h test for the headrest high position, as well as for the two tests with the booster seat version 2.



Table J1. Test matrix for sled tests of the rearward-facing vehicle seat sub-study.

Test no.	Pulse	Booster seat version	Booster seat headrest position	Vehicle seat head-restraint	Vehicle seat No.
T01	30km/h	1	mid	No	Seat_1
T02	50km/h	1	mid	No	Seat_1 after test T01
T03 (repeat of T01)	30km/h	1	mid	No	Seat_2
T04 (repeat of T02)	50km/h	1	mid	No	Seat_2 after test T03
T05	30km/h	1	low	No	Seat_3
T06	50km/h	1	low	No	Seat_3 after test T05
T07 (repeat of T05)	30km/h	1	low	No	Seat_4
T08 (repeat of T06)	50km/h	1	low	No	Seat04 after test T07
T09	30km/h	2	mid	No	Seat_5
T10	50km/h	2	mid	No	Seat_5 after test T09
T11	30km/h	1	high	No	Seat_6
T12 (repeat of T11)	30km/h	1	high	Yes	Seat_6 after test T11
T13	50km/h	1	high	Yes	Seat_6 after test T12

The models assembled and used in the simulation of the sled tests are presented in Table J2. Apart from the proprietary HIII6y ATD model, all used models were either public domain or subject to different OS licenses.

Table J2. Simulation models used for the rearward-facing vehicle seat sub-study.

Simulation model	Reference	Issuer
Vehicle Seat	OS vehicle seat model	VIRTUAL project
Booster seat	OS booster seat model, (Booster Seat CAE model, 21/10/2019, Version 1)	VIRTUAL project
Belt system	Parts from NHTSA Honda Accord	NHTSA
ATD	LSTC HIII 6-year-old 150202_V.0.104.BETA	Ansys LST
PIPER HBM	PIPER_child_v1.0.0_release	PIPER project

The HIII6y model was positioned primarily matching the head marker of the physical HIII6y ATD, followed by the chest contour. A similar approach was applied for positioning the PIPER HBM model. However, the geometries of the two models are slightly different (see Figure 4-3). For example, the legs of the PIPER HBM are straighter and the sitting posture slightly more reclined as compared to the HIII6y model when positioned as in the tests.

When positioned, the child occupant model was pulled into the targetted posture for pre-simulation using springs and dampers, a method sometimes referred to as the marionette method. The booster seat model was then squashed by the pre-simulated occupant model, after which the seat model was squashed with the combined booster seat and occupant model. Finally, the belt was routed around the occupant and the booster seat model using the pre-processor Primer. The result of the pre-simulation is shown in Figure 3-4. Good agreement was obtained in most models. However, the configuration with

the booster seat headrest in low-position was tilted slightly more rearward in the simulation model. This is caused by the headrest of the booster seat model being slightly narrower than the physical seat, so in the lowest position the shoulders of the ATD interfere with the headrest (which was not the case in the physical test). Thus, the entire seatback of the booster seat was tilted rearward to achieve the same position of the head marker.

The vehicle seatback angle was adapted to replicate the tested seats, taking into account a slight deviation between the 50km/h and the 30km/h sled tests identified in the footage of the physical tests. The 50km/h tests started with the seatback approximately 2° more reclined compared to the preceding 30km/h test. This difference is likely due to plastic deformation of the seat structure caused by the 30km/h test. Because of this, three additional models were developed to represent the more reclined seats in the 50km/h simulations. The booster backrest angle at the start of simulation was at 21° for the 30km/h and 23° for the 50km/h crash pulse. The six simulation models with reference to corresponding sled test setup configurations are shown in Table J3. The following sled tests were used as reference for model positioning and pre-simulations; T07, T08, T09, T10, T11 and T13, highlighted as bold in Table J3

Table J3. The six simulation models corresponding to sled test configurations. Bold tests are the reference for the positioning of simulation models.

Simulation model	Pulse	Booster seat headrest position	Vehicle seat head-restraint	Corresponding tests
S01 (run_30kmh_15)	30km/h	Mid	no	T01, T03, T09
S02 (run_50kmh_15)	50km/h	Mid	no	T02, T04, T10
S03 (run_30kmh_16)	30km/h	Low	no	T05, T07
S04 (run_50kmh_16)	50km/h	Low	no	T06, T08
S05 (run_30kmh_17)	30km/h	High	yes	T11 , T12
S06 (run_50kmh_17)	50km/h	High	yes	T13

The adjustments of the vehicle seat model had been made to adapt to the kinematics of the physical seat, including the stiffness of the torsion springs at the recliner of the vehicle seat model, which was scaled up to give better correlation to seatback rotation. The vehicle seat model is height adjustable, while the physical seats used in tests are not height adjustable and were more rigid in rotations. In addition, attachments were added to the upper and lower rails of the seat model.

The vehicle seat model was positioned to match four chosen hard points on the seat structure of the physical seat setup, as indicated in Figure J2. Due to the geometrical differences in the simulation model as compared to the physical seat, a perfect match could not be achieved. Point "1" in the front seat structure was prioritised, followed by Point "2"- "4".

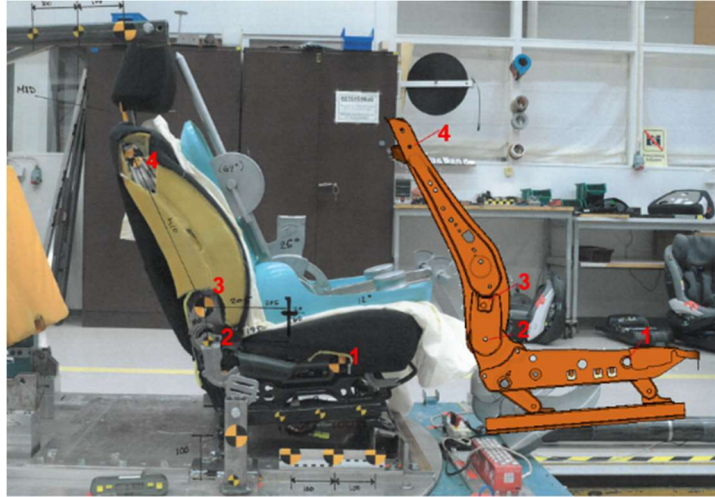


Figure J2. Vehicle seat model setup compared to the sled test. The numbers indicate the four hard points used in the creation of the vehicle seat model setup labelled "1" - "4".

Since neither cushion nor clothing are included in the OS booster seat model (except foams on bolsters and headrest), the coefficient of friction between the booster seat model and the surrounding components was tuned to generate the effect of clothing. The booster seat model was updated regarding contact definition, part definition and similar, to ensure good model representation also when moving the headrest to the low- and high-positions. The booster seat model was positioned onto the vehicle seat model by matching the contour of the physical seat. The shoulder belt outlet was positioned to match the seatbelt in the sled tests, using the B-pillar of NHTSA Honda Accord model, to keep it in position.

2. Results

Figures J3-J5 show snapshots from the sled tests at the time of maximum vehicle seatback deformation, for headrest mid-, low- and high-position, respectively.

Please note that in some of the tests with the highest head extension, unintended interaction and detachment of the rubber part of the ATD's detachable lid at the back of the head occurred. The detachment influenced the head acceleration for those tests, which therefore cannot be fully trusted.



Figure J3. Snapshots of maximum vehicle seatback deformation for the booster seat in the headrest mid-position. Left to right. Top row, left to right: crash pulse 30km/h, T01 and T03 (booster seat version1), and T09 (booster seat version2). Bottom row, left to right: 50km/h, T02 and T04 (booster seat version1), and T10 (booster seat version2).



Figure J4. Snapshots of maximum vehicle seatback deformation for the booster seat in the **headrest low-position**. Left to right, crash pulse 30km/h (T05 and T07) and 50km/h (T06 and T08). An unintentional deformation of the rubber parts of the cap of the ATD's back head occurred, also resulting in a detachment in T06.



Figure J5. Snapshots of maximum vehicle seatback deformation for the booster seat in the **headrest high-position**. Left to right, crash pulse 30km/h (T11 and T12) and 50km/h (T13).

Table J4 presents the maximum resultant acceleration (3ms) for the head, pelvis and chest, for each test categorised by configuration and crash pulse. Plots of the acceleration components are shown in Figures J6-J12.

Table J4. Head, chest and pelvis resultant acceleration (3ms) from the sled tests. * tests with booster version 2.
 ** unsure value due to unintended interaction and detachment of the rubber part of the ATD's back of head lid.

Configuration	Test no.	Head acc, 3ms [g]	Chest acc, 3ms [g]	Pelvis acc, 3ms [g]
Booster headrest in mid-position, no vehicle seat head-restraint, 30km/h	T01	52	38	36
	T03	62	45	32
	T09*	75	39	36
Booster headrest in mid-position, no vehicle seat head-restraint, 50km/h	T02	67	60	56
	T04	66	58	55
	T10*	79	48	53
Booster headrest in low-position, no vehicle seat head-restraint, 30km/h	T05	54**	43	30
	T07	77**	41	39
Booster headrest in low-position, no vehicle seat head-restraint, 50km/h	T06	68**	58	48
	T08	92**	51	58
Booster headrest in high-position, 30km/h	T11	48	31	35
	T12	66	44	49
Booster headrest in high-position, 50km/h	T13	64	65	59

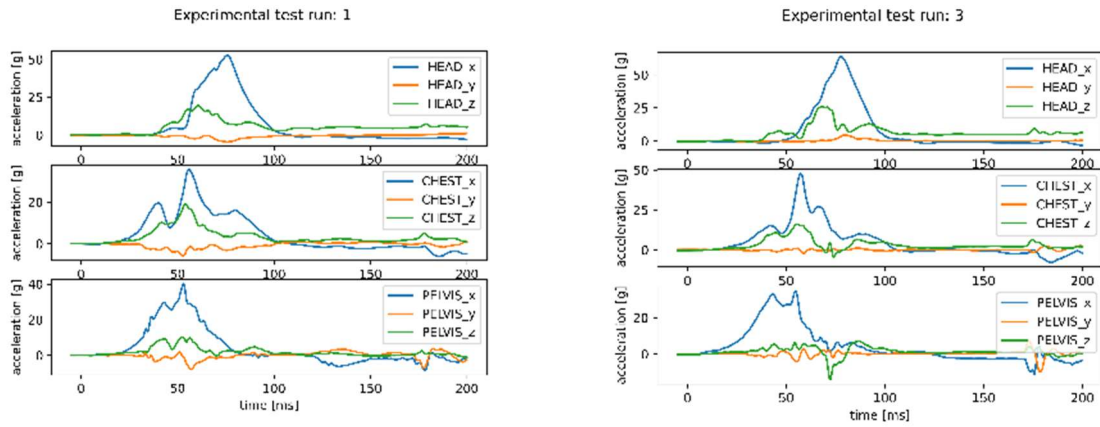


Figure J6. Configuration 'mid-position' in 30km/h, tests T01 (left) and T03 (right).

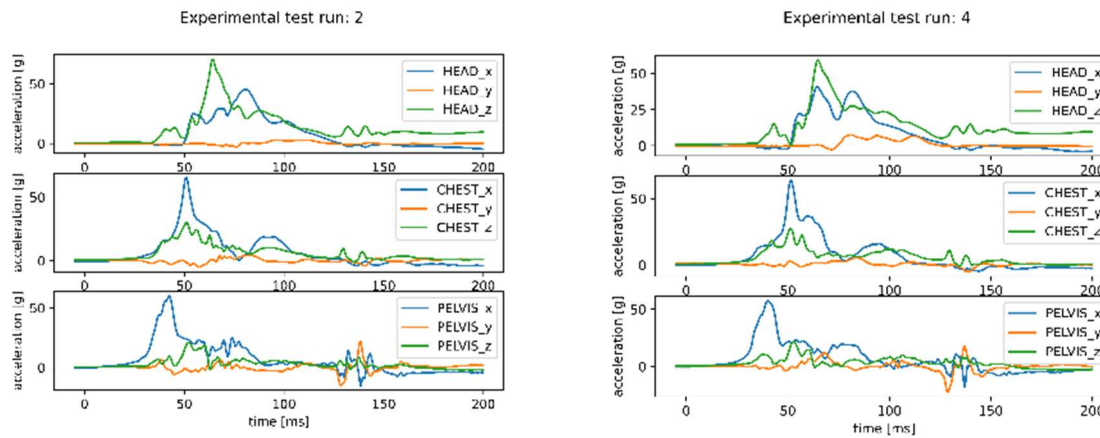


Figure J7. Configuration 'mid-position' in 50km/h, tests T02 (left) and T04 (right).

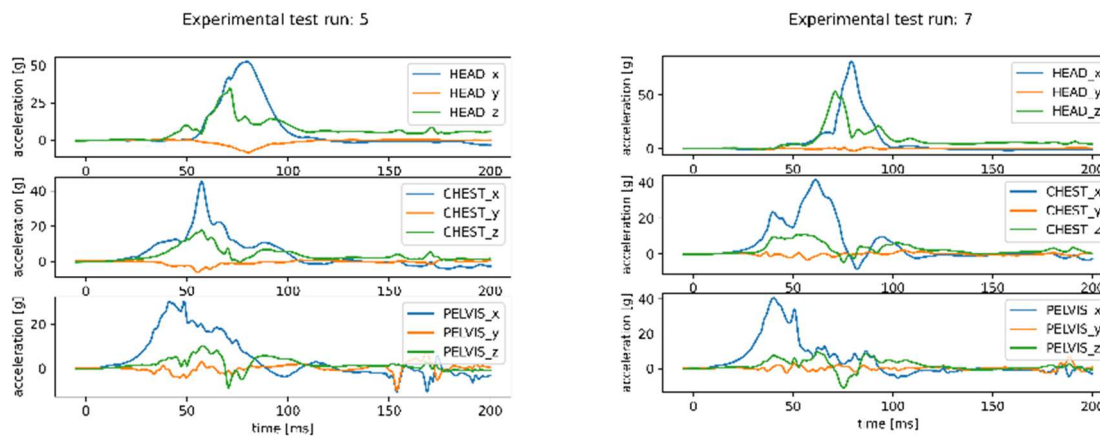


Figure J8. Configuration 'low-position' in 30km/h, tests T05 (left) and T07 (right).

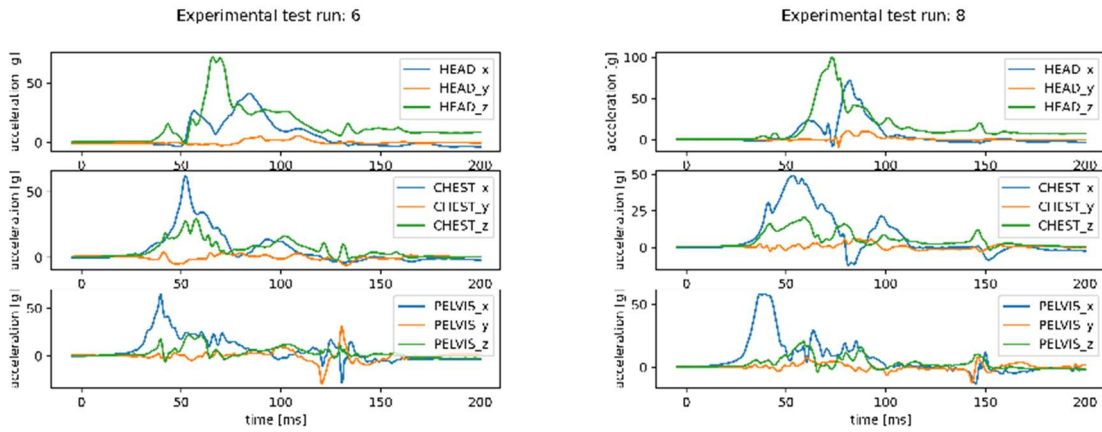


Figure J9. Configuration 'low-position' in 50km/h, tests T06 (left) and T08 (right).

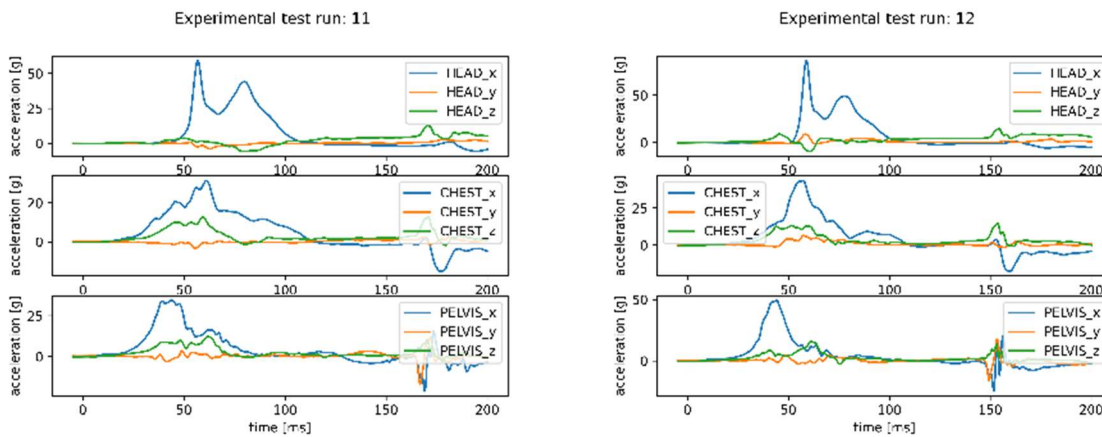


Figure J10. Configuration 'high-position' in 30km/h, tests T11 (left) and T12 (right).

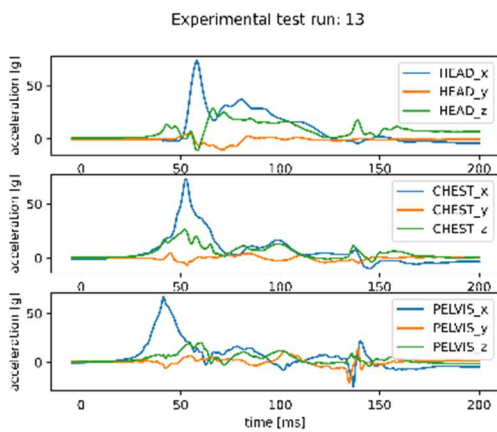


Figure J11. Configuration 'high-position' in 50km/h, tests T13.

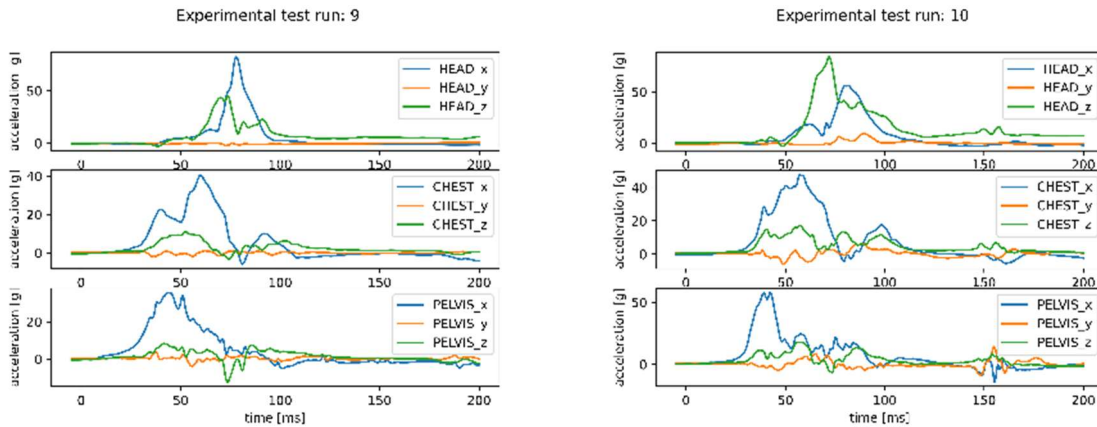


Figure J12. Configuration 'mid-position' with booster seat version 2, in 30km/h, tests T09 (left) and 50km/h T10 (right).

Tables J5 and J6 provide summaries of the resultant head acceleration (3ms) for the simulations using the HIII6y ATD model and the PIPER model, respectively.

Table J5. Head resultant acceleration responses for all six simulated configurations using HIII6y. * - S03 terminated due to unresolved numerical issues in the neck area (HIII6y model not validated for this loading)

Simulation model	Head acceleration 3ms [g]	HIC15
S01 (mid-position, 30km/h)	74	595
S03 (low-position, 30km/h)*	>76*	>343*
S05 (high-position, 30km/h)	46	196
S02 (mid-position, 50km/h)	71	494
S04 (low-position, 50km/h)	83	791
S06 (high-position, 50km/h)	57	364

Table J6. Head resultant acceleration responses for all six simulated configurations using PIPER

Simulation model	Head acceleration 3ms [g]	HIC15
S01P (mid-position, 30km/h)	42	170
S03P (low-position, 30km/h)	49	209
S05P (high-position, 30km/h)	32	69
S02P (mid-position, 50km/h)	42	184
S04P (low-position, 50km/h)	56	279
S06P (high-position, 50km/h)	39	123

Appendix K PIPER HBM in Forward-Facing Concept Vehicle Seat Models

This Appendix contains complementary material for Chapter 4.1.2 – PIPER HBM in forward-facing concept vehicle seats

1. Methods

Table K1 shows the simulation matrix with the configurations simulated using PIPER HBM, specifying which booster was used in which concept seat variant and seated position. The configurations have been selected as examples of how children in boosters can be seated in novel seated positions in current and future vehicles. The three variants (V1, V2 and V3) of the Faurecia concept seat models, presented in Chapter 2.2.1 and Appendix C, were used. The seats were positioned in the mid-track position and the mid-position of the height adjuster.

Table K1. Simulation matrix; combinations of HBM seated positions, seat model and booster type

	V1 seat (standard)	V2 seat (belt-guide)	V3 seat (split seatback)
Upright position	Booster cushion	Booster cushion	Booster cushion
Reclined position	Booster cushion	Booster cushion	Booster cushion
Articulated position	-	-	Booster cushion
Inclined position	-	-	Booster seat

The frontal impact crash pulse used in the study is shown in Figure K1. The pulse represents a generic small car in a United States New Car Assessment Program (USNCAP) 56 km/h frontal impact. The pulse was retrieved from the NHTSA’s website and created using an occupant Madymo model in a Toyota Yaris vehicle. Delta V for this pulse is approximately 57 km/h.

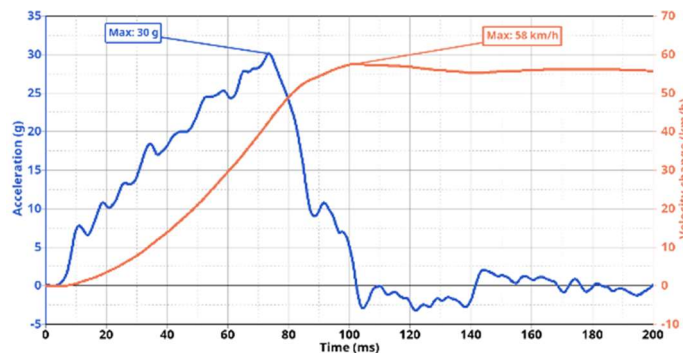


Figure K1. Frontal impact crash pulse used in the sub-study with forward-facing concept vehicle seats.

2. Results

Figures K2 and K3 show head excursion (x displacement vs time), head and pelvis trajectory (x and z displacement) and head resultant acceleration for the three simulations in the upright seated position.

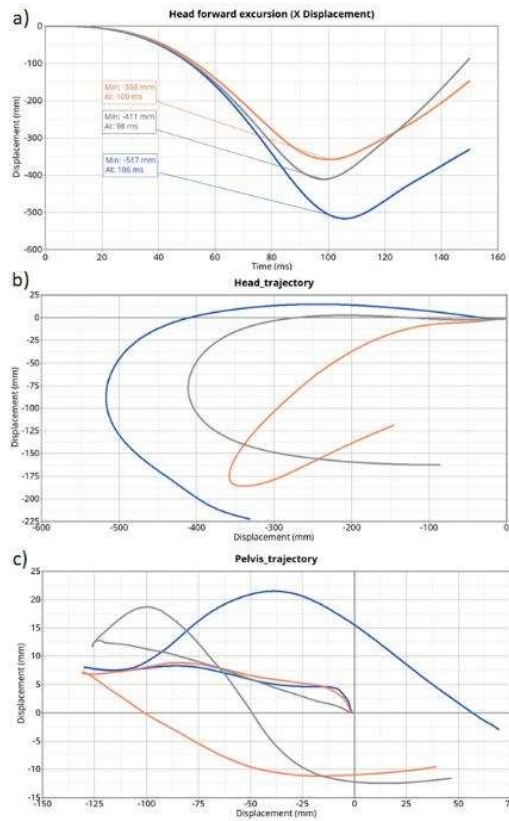


Figure K2. PIPER kinematics for the upright position and booster cushion a) Head excursion, b) Head trajectory, c) Pelvis trajectory. Blue-V1 seat, Orange - V2 seat, Grey - V3 seat.

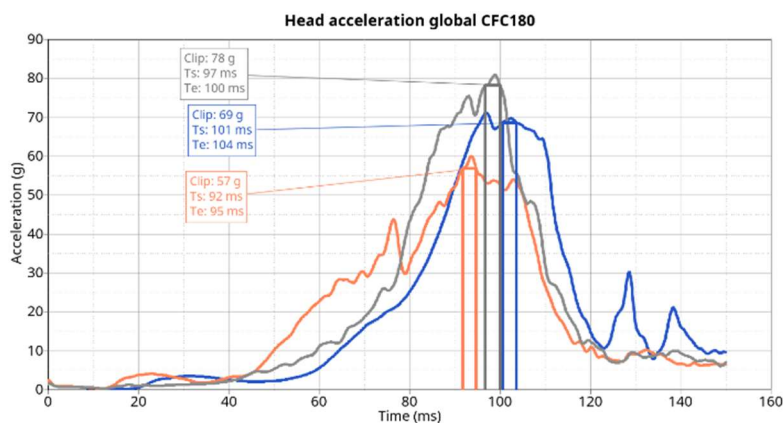


Figure K3. Head resultant acceleration for the **upright position and booster cushion**. Blue-V1 seat, Orange - V2 seat, Grey - V3 seat.

Top views of the belt-guide on top of the seatback for the V2 seat are shown in Figure K, for the upright and reclined position, respectively.

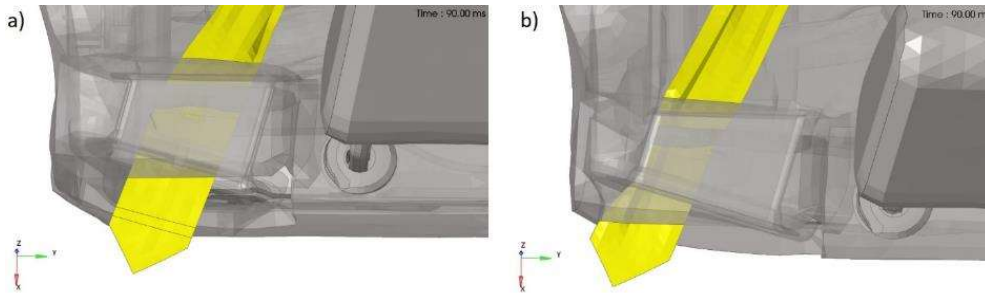


Figure K4. Top view of seatbelt routing inside the belt-guide of the V2 seat in a) Upright position, b) Reclined position.

Figures K5 and K6 show head excursion (x displacement vs time), head and pelvis trajectory (x and z displacement) and head resultant acceleration for the three simulations in the reclined seated position.

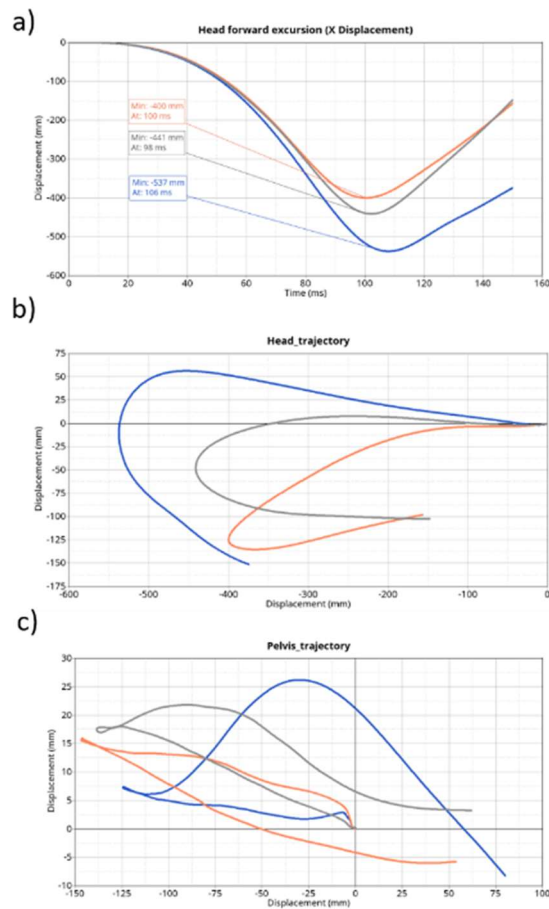


Figure K5. PIPER kinematics for the **reclined position and booster cushion** a) Head excursion, b) Head trajectory, c) Pelvis trajectory. Blue-V1 seat, Orange - V2 seat, Grey - V3 seat.

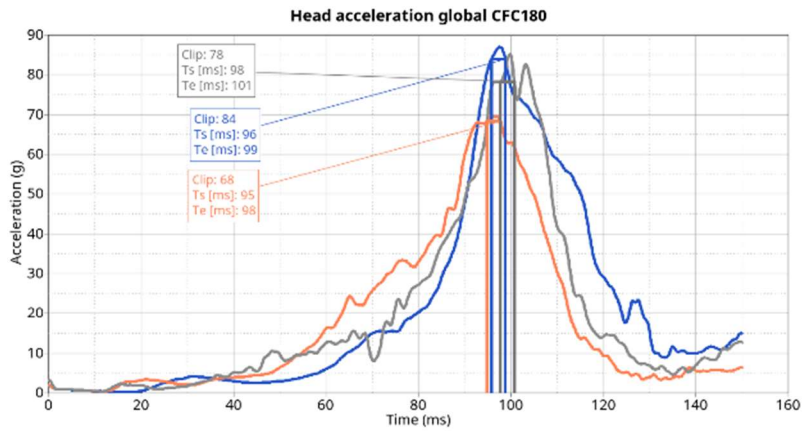


Figure K6. Head resultant acceleration for the **reclined position and booster cushion**. Blue-V1 seat, Orange - V2 seat, Grey - V3 seat

Figures K9 and K10 show head excursion (x displacement vs time), head and pelvis trajectory (x and z displacement) for the V3 seat in the articulated position and booster cushion, and in the inclined position and booster seat, respectively. The head resultant acceleration for those two positions are shown in Figures K7 and K8.

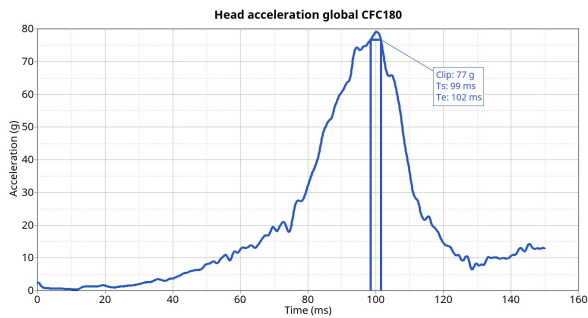


Figure K7. Head resultant acceleration for the **articulated position and booster cushion**.

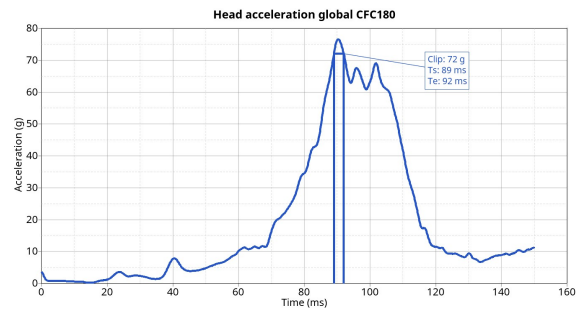


Figure K8. Head resultant acceleration for the **inclined position and booster seat**.

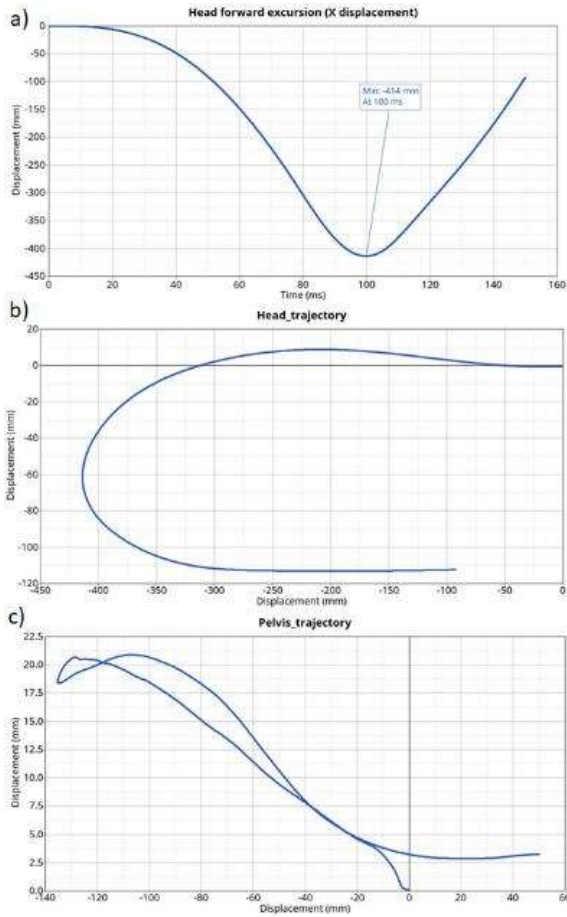


Figure K9. PIPER kinematics for the **articulated position and booster cushion**, a) Head excursion, b) Head trajectory, c) Pelvis trajectory.

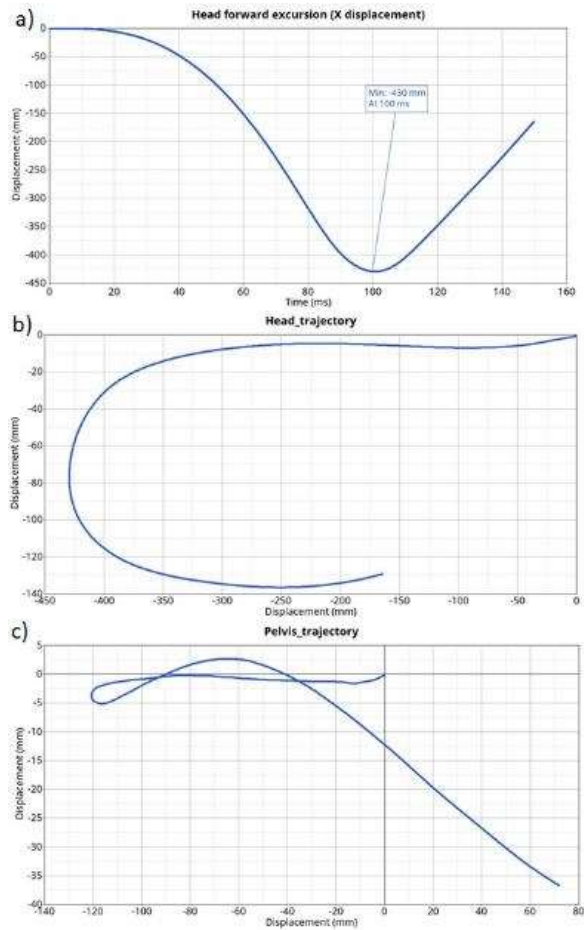


Figure K10. PIPER kinematics for the **inclined position and booster seat**, a) Head excursion, b) Head trajectory, c) Pelvis trajectory.

Table K2 and Figure K11 compare the head forward excursion and head resultant acceleration for the 6 year-old child installed on a booster cushion in different seated positions of the V3 seat which has been equipped with an integrated seatbelt.

Table K2. Head forward excursion and head resultant acceleration values, comparing upright, reclined and articulated positions with the booster cushion, for the V3 seat

V3 seat (split seatback)	Head forward excursion [mm]	Head a3ms [g]
Upright position	-411	78
Reclined position	-441	78
Articulated	-414	77

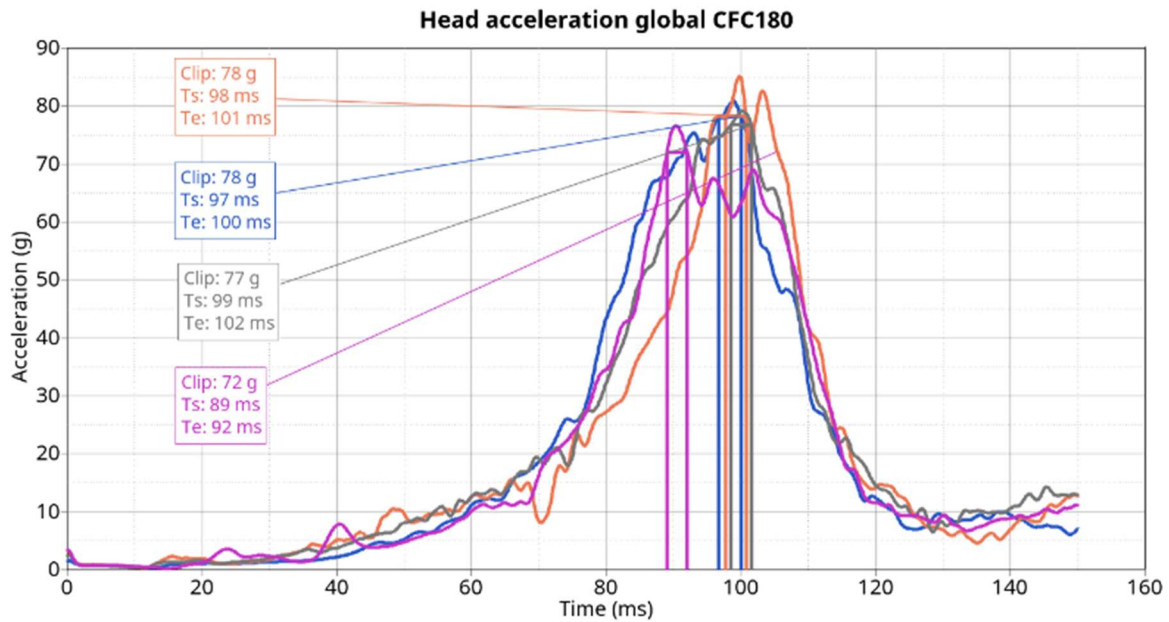


Figure K11. Head resultant acceleration for the four seated positions in the V3 seat. Upright, reclined and articulated positions with booster cushion, and inclined position with booster seat. Orange - Reclined, Blue - Upright, Grey – Articulated, Pink – Inclined.

Tables K3 and K4 show the head forward excursion and head resultant acceleration, respectively.

Table K3. Head forward excursion (mm) for all configurations

	V1 seat (standard)	V2 seat (belt deviator)	V3 seat (split seatback)
Upright position	-517	-358	-411
Reclined position	-537	-400	-441
Articulated position	-	-	-414
Inclined position	-	-	-427

Table K4. Head resultant acceleration, a3ms(g) for all configurations.

	V1 seat (standard)	V2 seat (belt deviator)	V3 seat (split seatback)
Upright position	69	57	78
Reclined position	84	68	78
Articulated position	-	-	77
Inclined position	-	-	72

Tables K5 and K6 summarise the 99th percentile 1st principal Green-Lagrange strains and the tissue-based brain injury criterion, respectively, for all configurations.

Table K5. 99th percentile 1st principal Green-Lagrange strain results

	V1 seat (standard)	V2 seat (belt .guide)	V3 seat (split seatback)
Upright position	0,35	0,36	0,24
Reclined position	0,53	0,42	0,29
Articulated position	-	-	0,23
Inclined position	-	-	0,37

Table K6. Probability/risk (%) for concussion using the tissue-based brain injury criterion

	Variant 1 seat (standard)	Variant 2 seat (belt-guide)	Variant 3 seat (split seatback)
Upright position	77,1%	82,8%	30,4%
Reclined position	99,9%	95,4%	50,9%
Articulated position	-	-	28%
Inclined position	-	-	84,1%

Figures K12 to K18 show additional responses from PIPER, including chest and pelvis acceleration, chest deflection at upper, middle and lower sternum (CFC180 filter), and upper neck forces in tension/compression (Fz) and fore-aft shear (Fx) (CFC180 filter).

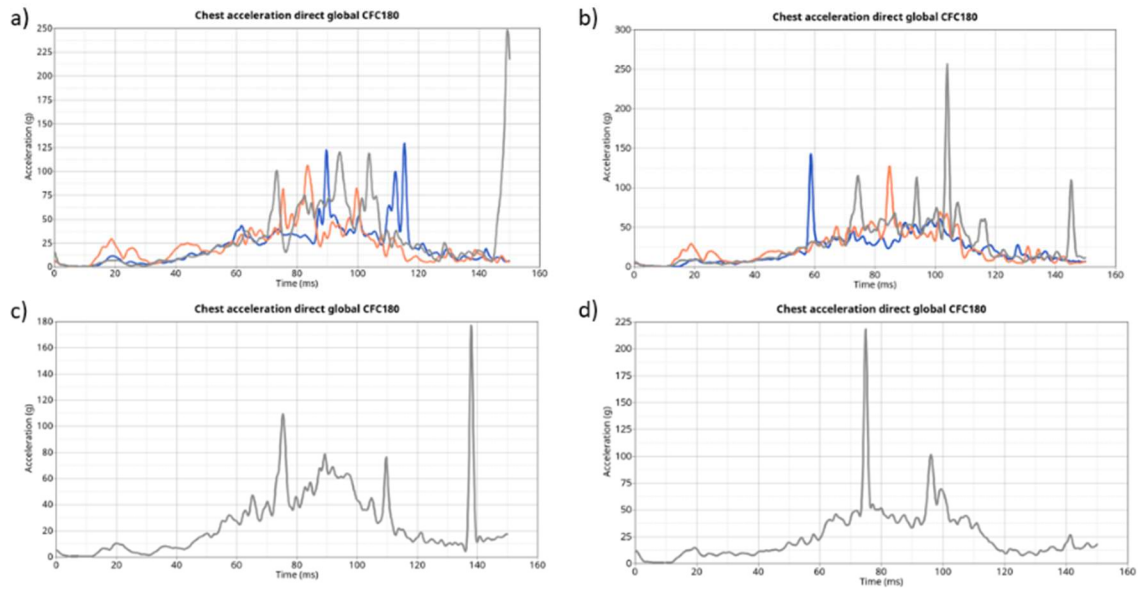


Figure K12. **Chest resultant acceleration**, a) Upright position (booster cushion), b) Reclined position (booster cushion), c) Articulated position (booster cushion), d) Inclined position (booster seat). Blue-V1 seat, Orange - V2 seat, Grey - V3 seat. The highest chest acceleration values (peaks) for the V3 seat shall not be taken into consideration– due to issues with the seat design.

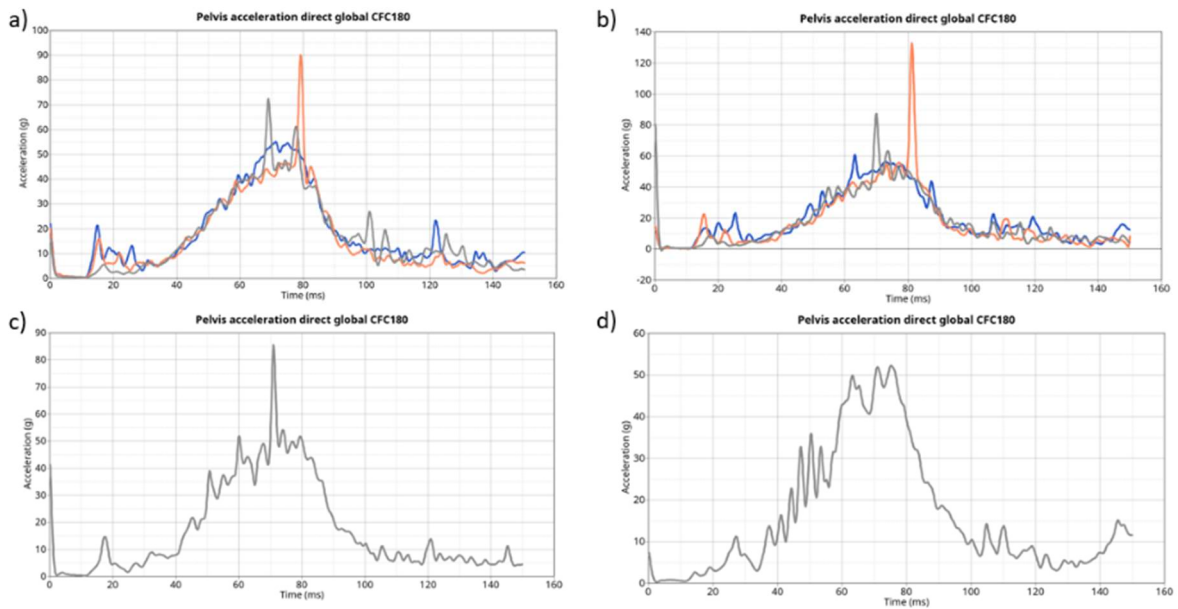


Figure K13. **Pelvis resultant acceleration**, a) Upright position (booster cushion), b) Reclined position (booster cushion), c) Articulated position (booster cushion), d) Inclined position (booster seat). Blue-V1 seat, Orange - V2 seat, Grey - V3 seat.

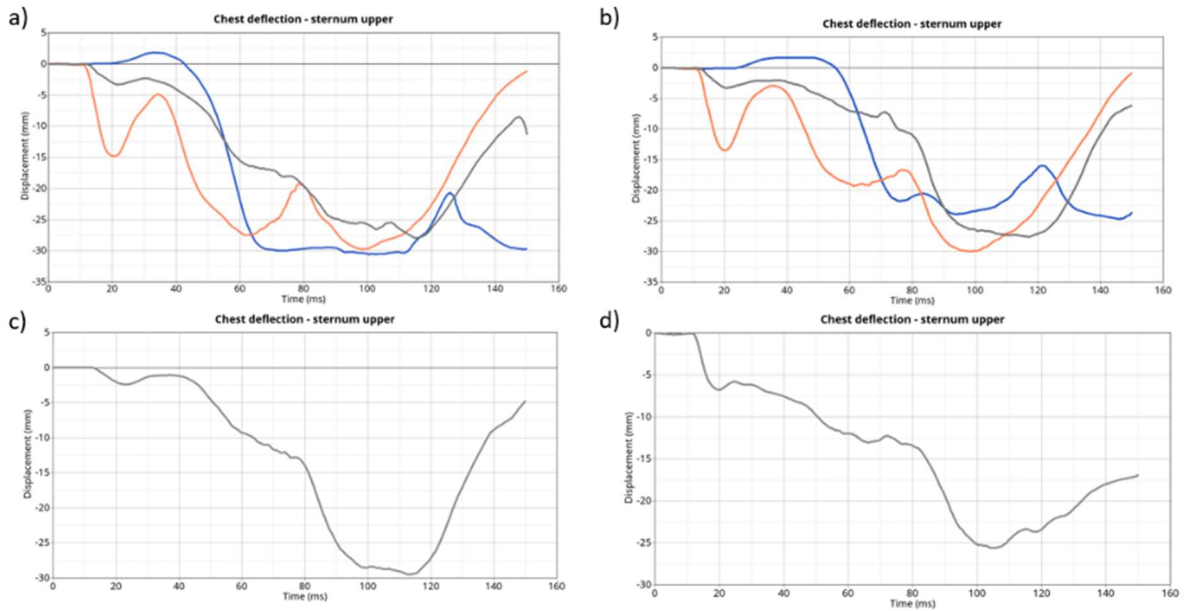


Figure K14. **Chest deflection – sternum upper**, a) Upright position (booster cushion), b) Reclined position (booster cushion), c) Articulated position (booster cushion), d) Inclined position (booster seat). Blue-V1 seat, Orange - V2 seat, Grey - V3 seat.

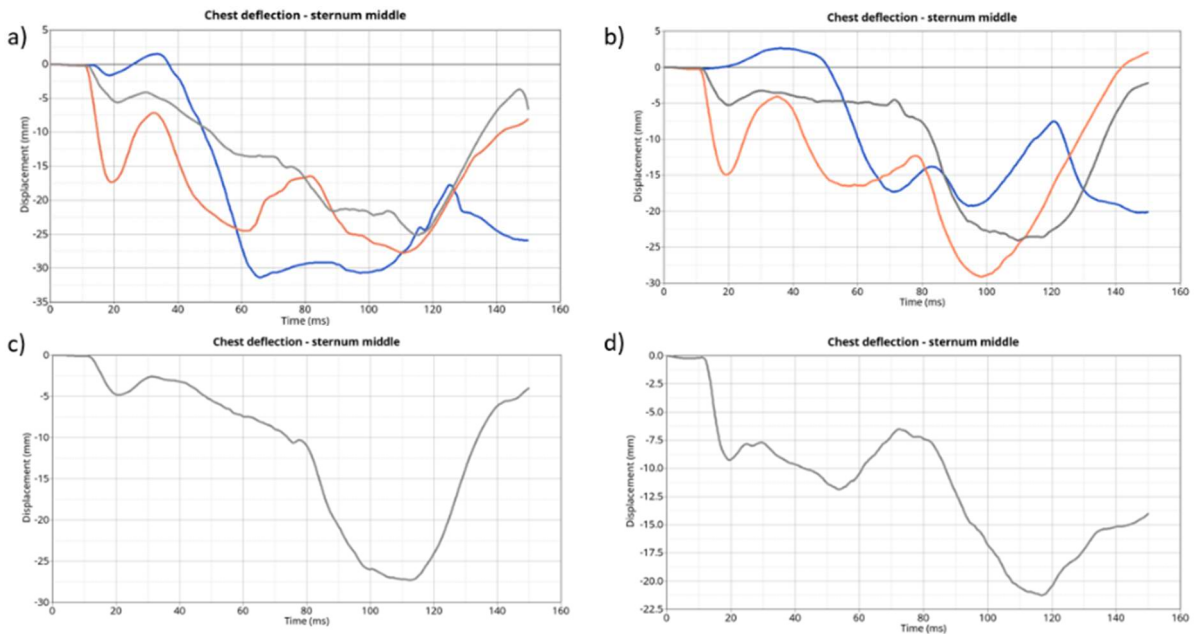


Figure K15. **Chest deflection – sternum middle**, a) Upright position (booster cushion), b) Reclined position (booster cushion), c) Articulated position (booster cushion), d) Inclined position (booster seat). Blue-V1 seat, Orange - V2 seat, Grey - V3 seat.

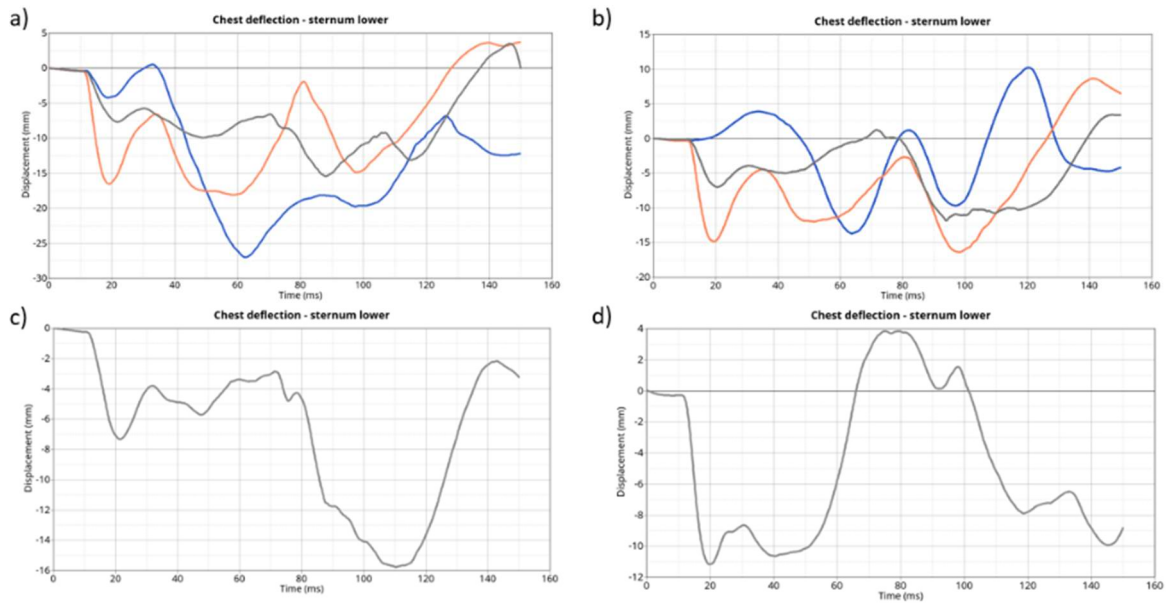


Figure K16. **Chest deflection – sternum lower**, a) Upright position (booster cushion), b) Reclined position (booster cushion), c) Articulated position (booster cushion), d) Inclined position (booster seat) Blue-V1 seat, Orange - V2 seat, Grey - V3 seat.

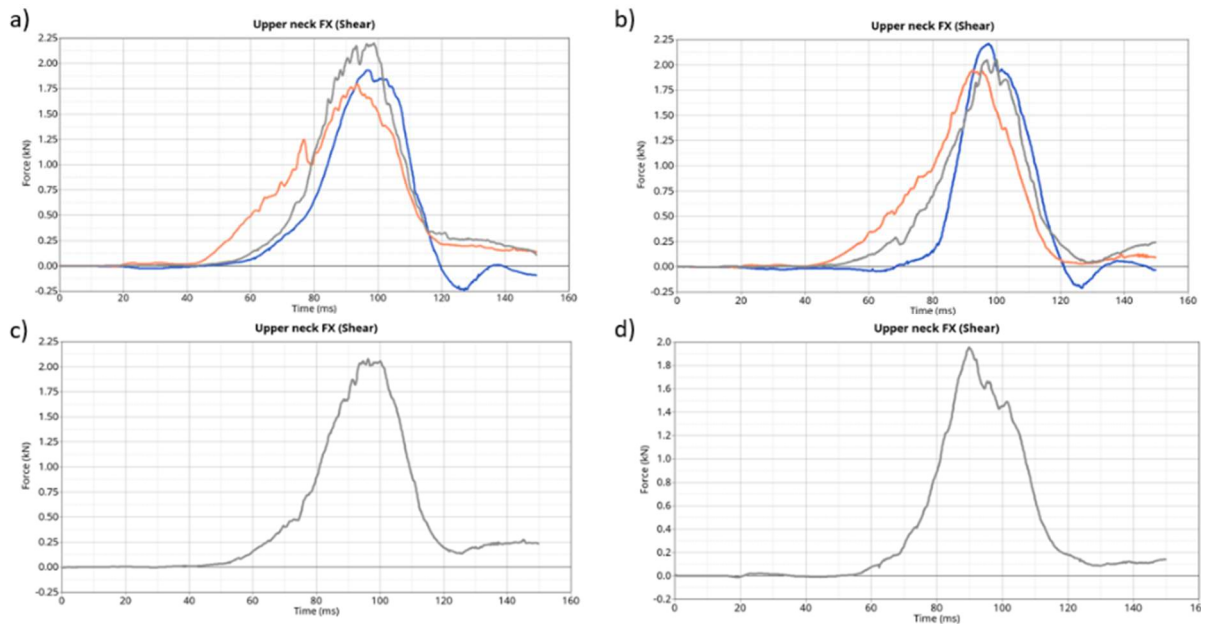


Figure K17. **Upper neck fore-aft shear force (Fx)**, a) Upright position (booster cushion), b) Reclined position (booster cushion), c) Articulated position (booster cushion), d) Inclined position (booster seat). Blue-V1 seat, Orange - V2 seat, Grey - V3 seat.

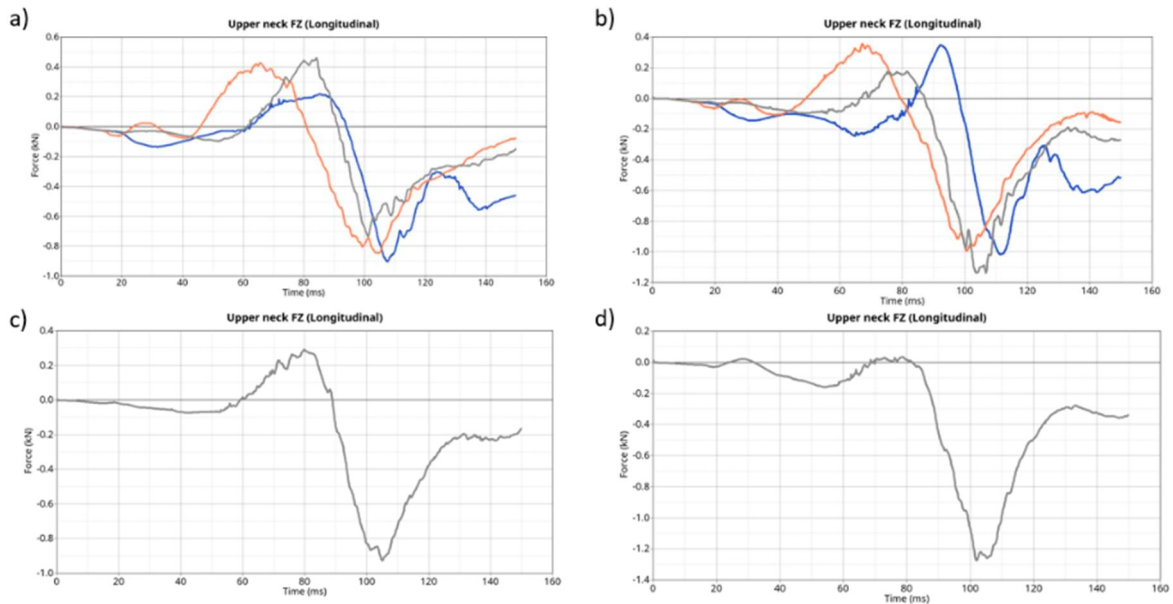


Figure K18. **Upper neck tension/compression force (Fz)**, a) Upright position (booster cushion), b) Reclined position (booster cushion), c) Articulated position (booster cushion), d) Inclined position (booster seat). Blue-V1 seat, Orange - V2 seat, Grey - V3 seat.